UNIVERSITEIT VAN PRETORIA
UNIVERSITY OF PRETORIA
YUNIBESITHI YA PRETORIA

Kinetic studies of the dimerization, alkylation and enzyme kinetic isotope effects of adenine.

by

Dominique Marie-Jeanne Solange Buyens

Submitted in partial fulfilment of the requirements for the degree

Doctor of Philosophy (Chemistry)

in the

Department of Chemistry

Faculty of Natural and Agricultural Sciences

UNIVERSITY OF PRETORIA

December 2021

© University of Pretoria

SUMMARY

Kinetic studies of the dimerization, alkylation and enzyme kinetic isotope effects of adenine.

by

Dominique Marie-Jeanne Solange Buyens

Supervisor: Professor L. A. Pilcher

Co-supervisor: Professor Emil Roduner

Co-supervisor: Professor Ignacy Cukrowski

Department: Department of Chemistry

University: University of Pretoria

Degree: Doctor of Philosophy (Chemistry)

Keywords: Adenine, adeninate, nucleobases, ion-pairs, aggregation, hydrogen bonding, alkylation, regio-selectivity, REP-FAMSEC, Mass spectroscopy, shikimate kinase, kinetic isotope effect

Tautomeric and anionic forms of nucleic acids are potentially involved in mutations and replication and translational errors; however, research into the chemistry of deprotonated nucleobases is limited. This research focused on the ion-pairing and self-aggregation ability of the adeninate anion in DMSO. Through ^{1}H NMR and UV spectroscopy and theoretical studies using IQA and REP-FAMSEC, it was shown that ion pairs of sodium and potassium salts of adenine exist in solution with cation coordination sites at the N3 and N9 atoms of the purine ring. Self-aggregation of these ion-pairs is governed by π-π stacking followed by higher order aggregation governed by coordination to metal cations. Our study provides insight into the interactions of the molecule and provides a building block for future studies on the adeninate system.

Much research has been dedicated to understanding the site preference for the alkylation of the adeninate ion as it yields mixtures of regio-isomers during the synthesis of biologically active compounds, yet no kinetic data have been obtained to understand the thermodynamics governing the reaction. The thermodynamic control of the regio-selectivity of benzylation of the adeninate ion was investigated. Through dynamic ^{1}H NMR spectroscopy and theoretical modelling, it was shown

© University of Pretoria

that benzylation occurs via an S_N2 mechanism in which the enthalpy of formation for N9-benzyladenine is higher than for the N3 isomer. However, this increase in the barrier height is compensated for by the increase in the entropy resulting in a looser transition state structure than that of the N3 isomer which experiences an entropic bottleneck. The derived thermodynamic properties of the adeninate anion will enable reaction conditions to be optimized for better control of synthesis at research and industrial level.

A primary KIE from ATP deuterated at the C8 position (C8D-ATP) on several kinase enzymes has been reported, potentially providing new insight for drug design towards *Mycobacterium tuberculosis*. However, the KIE on the V and V/K were not obtained. This research aimed to develop a high resolution mass spectroscopy method to study the KIE of C8D-ATP on *Mycobacterium tuberculosis* shikimate kinase. To this end, a high resolution MS method was developed which showed high sensitivity, precision and specificity. A KIE on V and V/K of 1.5 and 1.4, respectively, were observed for *Mycobacterium tuberculosis* shikimate kinase showing a secondary isotope effect. The MS method can be used for quantitative data collection of enzyme kinetics without sample modification. Our study implies that the adenine moiety in ATP facilitates molecular recognition only and that the C8–H bond of ATP is not involved in bond cleavage during phosphorylation.

© University of Pretoria

NUCLEOBASE NUMBERING SYSTEM

The standard numbering of guanine (**1**), adenine (**2**), cytosine (**3**) and thymine (**4**) is shown in **Figure 1** and has been followed in this thesis.

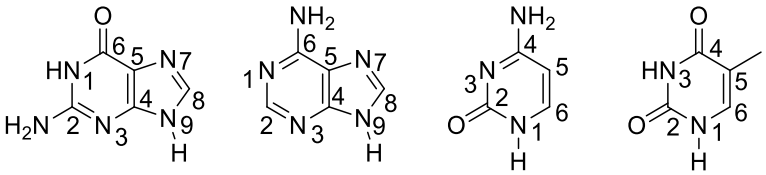

1 **2** **3** **4**

Figure 1: Chemical structures and numbering of guanine, adenine, cytosine and thymine.

© University of Pretoria

DECLARATION

I, Dominique Marie-Jeanne Solange Buyens, declare that the thesis, which I hereby submit for the degree Philosophiae Doctor in Chemistry at the University of Pretoria, is my own work and has not previously been submitted by me for a degree at this or any other tertiary institution.

Signature: 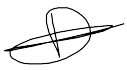

Student name: Dominique Marie-Jeanne Solange Buyens

Month Year: December 2021

© University of Pretoria

ACKNOWLEDGEMENTS

This research could not have been completed without the assistance of my supervisors, Professor Lynne Pilcher, Professor Emil Roduner and Professor Ignacy Cukrowski. I am extremely grateful for their invaluable advice, support, encouragement and patience throughout the years of my PhD. I would also like to thank Doctor Mamoalosi Selepe and Doctor Shankara Radhakrishnan for allowing me to work extended hours on the NMR and UV spectroscopy machines, and Doctor Frikkie Malan, for performing the XRD analyses. Additionally, I want to thank Doctor Madelien Wooding for her support, technical assistance and advice on Mass spectroscopy. I also thank the University of Pretoria and the department of chemistry for providing me with the opportunity to undertake my studies here. I'd like to extend my thanks to my family, friends and lab colleagues who have supported me through my studies.

I also want to thank the National Research Foundation for the funding of the research and the Scarce Skills Doctoral Scholarship awarded to me (grant number 97879).

© University of Pretoria

LIST OF ABBREVIATIONS

15C5	15-crown-5 ether
18C6	18-crown-6 ether
Ade^-	Free adeninate anion
ADP	Adenosine diphosphate
ATP	Adenosine triphosphate
BnCl	Benzyl chloride
CV	Coefficient of variation
DBDB	N,N'-dibenzyl-1,4-diaminobutane
DBU	1,8-Diazabicyclo(5.4.0)undec-7-ene
DFT	Density functional theory
DMSO	Dimethyl sulfoxide
DMSO-d_6	Deuterated DMSO
DMF	Dimethylformamide
ESI	Electrospray ionisation
FIA	Flow injection analysis
FAMSEC	Critical thermal maximum
HDMS	High definition mass spectrometry
HG	Hoogsteen
HIV	Human immunodeficiency virus
HMBC	Heteronuclear Multiple Bond Correlation
HPLC	High-performance liquid chromatography
HSQC	Heteronuclear Single Quantum Correlation
IQA	Interacting Quantum Atoms
IRC	Intrinsic reaction coordinate
K-Ade	Potassium adeninate complex
KIE	Kinetic isotope effect
LC	Liquid chromatography
LG	Leaving group

© University of Pretoria

LOD	Limit of detection
LOQ	Limit of quantification
LVF	Low vibrational frequencies
REP-FAMSEC	Reaction Energy Profile Fragment Attributed Molecular System Energy Change
MALDI	Matrix-assisted laser desorption/ionization
Mt-SK	*Mycobacterium tuberculosis* shikimate kinase
MS	Mass spectroscopy
Na-Ade	Sodium adeninate complex
NAD	Oxidized β-Nicotinamide adenine dinucleotide
NADH	Reduced β-Nicotinamide adenine dinucleotide
NMR	Nuclear Magnetic Resonance
Nu	Nucleophile
PEP	Phosphoenolpyruvate
PDE	Phosphodiesterase
QTOF	Quadrupole-time-of-flight
S3P	Shikimate-3-phosphate
TEA	Trimethylamine
TRIS	Trisaminomethane
TS	Transition state
UPLC	Ultra-performance liquid chromatography
UV	Ultraviolet–visible
WC	Watson-Crick
XRD	X-ray diffraction

© University of Pretoria

Table of Contents

Chapter 1 Introduction 1

1.1 Overview of the thesis 1

1.2 Background 3

1.3 Overview of the methodology 4

1.4 Discussion of the findings 5

1.5 Layout of the thesis 6

1.6 References 7

Chapter 2 Towards a molecular understanding of cation–anion interactions and self-aggregation of adeninate salts in DMSO by NMR and UV spectroscopy and crystallography 10

2.1 Introduction 10

2.1.1 Hydrogen bonding and π–π stacking interactions of nucleic acids 10

2.1.2 Metal coordination of nucleic acids and their bases 11

2.1.3 Studying aggregation through ^{1}H NMR spectroscopy 12

2.1.4 The adeninate anion 16

2.2 Experimental details 17

2.3 Results and discussion 19

2.3.1 Ion pairing of the adeninate anion with Na^{+} and K^{+} 19

2.3.2 Coordination sites of Na^{+} and K^{+} with the adeninate anion 21

2.3.3 Concentration dependent ^{1}H NMR chemical shifts of Na-Ade, K-Ade, Na-Ade(15C5) and K-Ade(18C6) 26

2.3.4 ^{1}H NMR temperature coefficient of Na-Ade, K-Ade, Na-Ade(15C5) and K-Ade(18C6) 28

2.3.5 Aggregation by π-π stacking and in-plane dimerization 30

2.3.6 Higher order aggregates 33

2.3.7 Thermodynamics of the self-aggregation 34

2.4 Conclusion 36

2.5 References 38

Chapter 3 Towards a molecular understanding of the preferential site of coordination of sodium and potassium ions to the adeninate anion in DMSO by quantum chemical studies 44

© University of Pretoria

3.1 Introduction 44

3.2 Metal ion coordination to dominant tautomeric forms of nucleobases 45

3.2.1 Alkali metal ions 45

3.2.2 Alkaline earth metals 47

3.2.3 Tautomeric forms of alkali and alkaline earth metal ion complexes 47

3.2.4 Transition metals 48

3.2.5 The role of the NH_2 group in metal ion binding 50

3.2.6 Cation-π complexes 51

3.3 Computational Methods 52

3.4 Results and Discussion 52

3.4.1 Relative stability of Na- and K-Ade ionic complexes 53

3.4.2 Preferential coordination sites between Na^+ and K^+ and the adeninate anion from IQA and REP-FAMSEC methods 55

3.4.3 Understanding Na^+ and K^+ complexation trends with the adeninate anion 56

3.4.4 Influence of complexation on covalent and long-distance intramolecular interactions of adeninate anion 59

3.4.5 Effect of the solvent environment on the Na^+ and K^+ coordination site of the adeninate anion 70

3.4.6 Na- and K-Ade isomers in the presence of explicit DMSO solvent molecules 71

3.4.7 Influence on the interaction between counter ion and the adeninate anion in the presence of explicit DMSO solvent molecules 73

3.5 Conclusion 74

3.6 References 76

Chapter 4 Experimental and theoretical investigation into the reaction kinetics of the benzylation of sodium complexed adeninate anion in anhydrous DMSO 79

4.1 Introduction 79

4.1.1 Alkylation sites of nucleic acids in DNA and RNA, free nucleobases and their anions 79

4.1.2 Factors governing the site of alkylation of nucleic acids, nucleobases and the adeninate anion 81

© University of Pretoria

4.1.3 The benzylation of the adeninate anion 87
4.2 Experimental details 89
4.3 Results and discussion 91
4.3.1 The effect of the structure of benzyl halide derivatives on the N9 and N7 product ratio . 91
4.3.2 Identification of the side reaction occurring during the benzylation of the adeninate anion 93
4.3.3 The effect of the counter ion present on the N9 and N7 product ratio 94
4.3.4 Reaction order of the benzylation of Na-Ade in anhydrous DMSO 96
4.3.5 Thermodynamic data for the formation N9- and N3-benzyladenine in anhydrous DMSO 100
4.3.6 Theoretical studies on the benzylation of the adeninate anion 105
4.4 Conclusion 115
4.5 References 116
Chapter 5 The study of the kinetic isotope effect of ATP-C8D on shikimate kinase through high resolution mass spectrometry 121
5.1 Introduction 121
5.1.1 The shikimate pathway and shikimate kinase 121
5.1.2 The role of the adenyl moiety in molecular recognition 122
5.1.3 Kinetic isotope effects in enzymatic reactions 123
5.1.4 Measuring KIEs on enzymatic reactions 125
5.1.5 The scope of this research 130
5.2 Experimental details 130
5.3 Results and discussion 132
5.3.1 Experimental design 132
5.3.2 Determination of *Mt*-SK kinetics and KIEs by high resolution mass spectroscopy 134
5.4 Conclusion 137
5.5 References 138
Chapter 6 Thesis Summary and Conclusion 142

© University of Pretoria

6.1 Overall findings of this research 142

6.2 Contribution made to the field 143

6.3 Limitations of the study 144

6.4 Future work 145

List of Figures.....146

List of Tables.....152

Appendix 1

Appendix 2: Supporting Information 1 – 4

© University of Pretoria

Chapter 1 Introduction

1.1 Overview of the thesis

Adenine is one of the most important biological molecules with many studies dedicated to its neutral and protonated forms. However, very little is known about its equally important anionic form, the adeninate anion, which is the central theme of the research described in this thesis. The main aim was to investigate and understand the ion-pairing and self-aggregation ability and the regio-selectivity towards alkylation of the adeninate anion. The research on the adeninate anion stemmed from another research section addressed in this thesis, the kinetic isotope effect (KIE) of deuterated adenosine triphosphate at the C8 position of the adenyl moiety (C8D-ATP) on *Mycobacterium tuberculosis* shikimate kinase (*Mt*-SK). This brings us to the second aim: to develop a high resolution mass spectroscopy (MS) method to study the KIE of C8D-ATP on *Mt*-SK.

The adeninate anion, which is synthesized by deprotonation of adenine by a base, should possess different chemical behaviour to the neutral adenine form due to the increase in electron density. Therefore, we developed the following research questions to address the main aim:

i) Does ion-pairing occur between the adeninate anion and the base cationic counter ion, sodium and potassium?
ii) Where is the most likely site for the ion coordination to the adeninate anion?
iii) Does the adeninate anion or its ion pairs form dimers and higher order aggregates in solution?
iv) How do the non-covalent interactions (such as hydrogen bonding and π–π stacking) in these aggregates differ from those of neutral adenine aggregates?

Furthermore, as the adeninate anion has four nucleophilic nitrogen atoms, the N1, N3, N7 and N9 nitrogen atoms of the purine ring, it is of particular interest to know:

v) Which thermodynamic properties control the reactivity of alkylation at these sites?

Studying the enzyme kinetics of *Mt*-SK by high resolution MS, which is regarded as a sensitive, rapid and accurate analytical technique, left us with two important research questions to address the second aim:

vi) Is the method developed sufficiently sensitive and reproducible to give reliable results?
vii) Does a KIE by C8D-ATP exist on the maximal velocity V and on the specificity constant V/K of *Mt*-SK?

The anionic forms of nucleic acids are potentially involved in mutations and replication and translational errors,[1–4] provide scaffolds for metal organic frameworks,[5–9] and are often the starting point for the synthesis of biologically active *N*-alkylated nucleobase derivatives.[10–12] There is a lack of information surrounding anionic forms of nucleobases[2,13] especially involving the chemical properties of the free adeninate anion and its interactions with monovalent alkali metals. This research provides novel insight into the reactivity of the adeninate anion and can be extrapolated into biological systems or provide a good comparative point between the isolated anionic form and the biologically active anionic form. The enzyme reaction of *Mt*-SK converts shikimic acid and ATP to

© University of Pretoria

shikimate-3-phosphate and ADP via the transfer of a phosphate group. Previous research showed the KIE of C8D-ATP on the overall rate of *Mt*-SK but did not measure the KIE on V and V/K.[14,15] In this research, apart from providing a high-resolution MS method for studying the kinetics of *Mt*-SK, we report the KIE on V and V/K for the first time.

The above aims and research questions were achieved by the following objectives:

1) To observe the presence of possible ion-pairs and the self-aggregation thereof, concentration and temperature dependent properties of adeninate anion in the presence of the Na^+ and K^+ cations in anhydrous DMSO were investigated. In order to gain an understanding of the interactions between adenine and the counter ions, the experiments were conducted in DMSO solvent which allowed for the solubility of adenine and the adeninate salt and allowed for potential ion-pairing. In addition, studies conducted on the regio-selectivity of the adeninate salt require the use of DMSO. Therefore, to keep identical reaction environments, the solvent is kept constant between the studies.
2) The above Na^+ and K^+ adeninate systems were studied in the presence of 15-crown-5 ether and 18-crown-6 ether, respectively, and water in order to confirm the presence of ion-pairs. In addition, any deviation in the dimer formation would confirm the influence of the counter ions present on self-aggregation.
3) The possible sites of the Na^+ and K^+ ion coordination on the purine ring of the adeninate anion were further investigated using computational chemistry. Several isomers were investigated in which the position of the counter ion was varied i.e. either positioned i) in-plane and coordinated in a unidentate fashion to the N1, N3, N7 and N9 nitrogen atoms or via a bidentate fashion bridged between the N3 and the N9, and ii) out-of-plane to form the cation-π complex or interact with the exo-cyclic amino group. The interactions between the counter ion and the adeninate anion were studied using Interacting Quantum Atoms (IQA) and the Reaction Energy Profile Fragment Attributed Molecular System Energy Change method (REP-FAMSEC) protocol which allows for the partitioning of the interaction energies between diatomic atoms or molecular fragments.
4) The alkylation of the adeninate anion was studied in anhydrous DMSO using several benzyl halides which differed in structure i.e. benzyl bromide, (1-bromoethyl)benzene and pentafluorobenzyl bromide. The alternative structures are used to influence the transition state structure making it tighter or looser which in turn could influence the product ratio.
5) The thermodynamic properties for the alkylation of the adeninate anion were studied using benzyl chloride in which concentration and temperature dependent studies were carried out to confirm the S_N2 reaction mechanism and obtain the thermodynamic parameters for the alkylation reaction for the observed formation of products, i.e. the N1-, N3-, N7-, and N9-benzyladenines.
6) Theoretical studies were carried out to further investigate the energetics of the reaction pathways leading to the N1-, N3-, N7-, and N9-benzyladenines in which transition state theory was employed. Relationships were drawn between the experimentally and theoretically obtained thermodynamic parameters.
7) The KIE of C8D-ATP on Mt-SK was studied by firstly finding an MS appropriate buffer for the enzyme reaction to prevent additional sample preparation prior to injection. The production of ADP and C8D-ADP were used to calculate the KIE when ATP or C8D-ATP, respectively, were used as a substrate in the enzyme reaction. A standard curve was developed from the

© University of Pretoria

instrument's response to ADP at various concentrations. The ADP standard stock samples were prepared under identical enzyme assay conditions to eliminate the matrix effect when analysing the enzyme reaction samples.

8) The non-competitive enzyme assay method was used as it was the only method to yield the KIE on V in addition to V/K.

The findings of the research conducted in this thesis provide evidence for the existence of ion-pairs of the adeninate anion with Na^+ and K^+ in DMSO with the preferred sites of alkali metal coordination at the N3 and N9 nitrogen atoms. Self-aggregation of adeninate ion-pairs occur in solution via π–π stacking and coordination via the counter ion. The thermodynamic properties for the alkylation of the adeninate ion provide evidence for an entropic bottleneck governing the regio-selectivity of the alkylation of the adeninate anion. And lastly, we found a secondary KIE on the V and V/K of *Mt*-SK by ATP deuterated at the C8 position. The high resolution MS method developed allows for quantitative data to be obtained in order to study enzyme kinetics.

1.2 Background

The overall topic of the thesis falls within the study of adenine, both the investigation of the adeninate anion and the KIE of C8D-ATP surrounding the adenine molecule and its importance in the biological world.[16] Since Watson and Crick (1953) proposed the structure of DNA scientists have striven to understand the factors governing non-covalent interactions for the aggregation of isolated nucleobases[17–25] in order to gain a greater understanding of their role in the structure, function and stability of DNA.[24,26–30] In addition to these interactions, understanding the coordination of metal ions to nucleobases has also gained momentum as the excess binding of alkali metal ions such as Na^+ and K^+ to nucleotides influences the structural integrity of DNA by interfering with hydrogen bonding and stacking interactions between base pairs.[31–33]

While the above studies focus mainly on the neutral forms of nucleobases, research into their rare tautomeric and anionic forms is growing steadily. This is due to research revealing that the presence of rare tautomeric and anionic forms of nucleic acids can form Watson-Crick mispairs that are involved in mutations and replication and translational errors,[1–4] as well as playing a role in nucleic acid catalysis[34] and RNA-ligand recognition.[35] As the understanding of the stabilization, aggregation and metal complexation of rare tautomeric forms grows via experimental and computational studies, research into deprotonated nucleobases is limited.

The research conducted in this thesis provides the perfect opportunity to add some understanding into the Na^+ and K^+ complexation with the deprotonated form of adenine. As Na^+ and K^+ are biologically important counter ions and are complexed to nucleotides in DNA, the ion-pairing of Na^+ and K^+ with adeninate could provide insight into how the coordination of these metals differ from that of adenine and how they stabilize the deprotonated form. Furthermore, the ability of these ion-pairs to form aggregates and the mode of aggregation can provide further insight into how the hydrogen bonding and π–π stacking of nucleobases can be disrupted by the presence of deprotonated adenine.

A great amount of research has been dedicated to understanding the site preference of alkylation of the nucleophilic atoms of nucleic acids in DNA and RNA as the oxygen and nitrogen atoms are available for alkylation by carcinogens and chemotherapy drugs.[36–40] An interplay between

© University of Pretoria

thermodynamic, steric and charge control is believed to govern the site preference for the alkylation of nucleotides and their bases[41–50] in which alkylating reagents react via an S_N2 mechanism predominantly at the purine ring nitrogen atoms. The direct alkylation of the anions of nucleobases, generally for the synthesis of biologically active compounds, has long presented the problem of yielding complicated mixtures of regio-isomers i.e. deprotonated adenine reacts predominantly at the N9 atom followed by the N3 and N7 via an S_N2 mechanism.[51,52] Purines and their derivatives, with adenine and guanine being key players, have been used to treat a wide variety of diseases.[53,54] Thus understanding the chemistry of these molecules and their anionic forms can help to resolve some of the regio-selectivity problems faced during synthesis alongside understanding their reactivity in general.

Although there have been extensive investigations into the role of the factors in governing the regio-selectivity of the alkylation of the adeninate anion, no real-time ^{1}H NMR analysis, rate constants and thermodynamic data have been obtained experimentally. Our research reports for the first time the thermodynamic properties for the alkylation of the adeninate anion. This not only adds new insight into the chemical behaviour of the adeninate anion but alongside the ion-pairing studies, consistently points towards the reactivity of the N3 and N9 nitrogen atoms.

The study of the adeninate anion began from the synthesis of adenine derivatives intending to study their inhibition of *Mt*-SK. This work fell within the study of the KIE of C8D-ATP. The need for new effective drugs towards multi-resistant (MDR) and extensively drug-resistant (XDR) tuberculosis has been ongoing as MDR and XDR tuberculosis continue to be a global threat.[55,56] A KIE from C8D-ATP of between 2 to 7 on the overall rate of several kinase and synthetase enzymes has been reported.[14,15,57] The research potentially provided new insight into how these enzymes work and therefore the possibility for new drug design, especially towards tuberculosis as *Mt*-SK which was investigated in the study.[15] However, the KIE on the V and V/K were not obtained and generally this is the standard for reporting KIEs. Hence, we aimed, with the use of high resolution MS, to report the isotope effect of C8D-ATP on the V and V/K.

1.3 Overview of the methodology

Various techniques were employed throughout the study to achieve the aims and address the research questions above. In order to experimentally study the ion-pairing and aggregate formation of the adeninate anion, the change in observable physical properties such as ^{1}H and ^{13}C NMR chemical shifts and UV spectroscopy were utilized. In addition, single crystal X-ray diffraction is used as an additional tool to gain further insight into the sites of coordination and mode of aggregation. Although the latter provides information about the solid state, it can provide some guidance into the possible structures in solution. Computational studies were conducted to theoretically model the ion-pair formation of the Na^+ and K^+ adeninate complexes in which various coordination sites were investigated. This was completed by performing Gaussian optimizations on the structures of interest and analysing the interaction energies with the use of IQA and REP-FAMSEC. REP-FAMSEC[58] is a recent protocol developed in our research group based on the parent FAMSEC[59] method. REP-FAMSEC allows for the study of the change in intra- and inter-molecular interaction energies of a molecular system (diatomic for whole molecular fragments) relative to a reference state due to changes in the immediate or distant molecular environment.[60] This protocol served as a tool to

© University of Pretoria

extract the information of energy changes experienced by the free adeninate anion upon Na^+ and K^+ complexation and to compare the different sites of ion coordination.

The investigation into the regio-selectivity of the adeninate anion towards alkylation was completed using dynamic ^1H NMR spectroscopy in which the reaction was monitored in real time. Various benzylated halides were used to study the influence of reagent structure of the overall product ratio i.e. the ratio between the N1-, N3-, N7- and N9-benzylated adenine products. Concentration and temperature dependent studies were carried out in order to determine the order of reaction as well as the thermodynamic parameters. This was followed by theoretically modelling of the reaction pathway leading to each of the four possible alkylated adenine products in Gaussian. In each case the reactant, transition state and product complexes were obtained. The predicted thermodynamic parameters were used to evaluate the conclusion drawn from the experimental section.

The study of the KIE of C8D-ATP on *Mt*-SK was performed on an Ultra Performance Liquid Chromatography system hyphenated to a quadrupole-time-of-flight (QTOF) instrument. The instrument's response to the amount of ADP in solution was used to construct a standard curve in which the method was validated by the limit of detection, the limit of quantification, and precision under repeatability through triplicate injections of the same sample and reproducibility via interday analysis of independently prepared samples. The incorporation of deuterium at the C8 position of ADP does not alter the ionization properties relative to ADP. The KIE on V and V/K was obtained through the non-competitive method whereby separate reactions were performed for ATP and C8D-ATP. The enzyme assays were studied via the discontinuous method in which the reactions were terminated at a set time such that the enzyme converted less than 10% of the substrate.

1.4 Discussion of the findings

From the research conducted and presented in this thesis we show that the adeninate anion doesn't exist as a free anion in DMSO solution but rather as an ion-pair with the Na^+ and K^+ counter ion. The K^+ ion is most likely coordinated in a bidentate fashion at the N3 and N9 nitrogen atoms of the purine ring. The Na^+ ion, being smaller in size than K^+, can coordinate in a bidentate or unidentate fashion at the N3 and N9 nitrogen atoms. The coordination of the counter ions at the N3 and N9 nitrogen atoms results in charge polarization of the adeninate anion, significantly altering the electron density distribution compared to the free adeninate anion. The Na^+ and K^+ counter ions were not successfully removed from complexation to the adeninate anion by the addition of 15-crown-5 and 18-crown-6 ether. It is proposed that the addition of 18-crown-6 ether results in complex formation with the K-Ade. Self-aggregation of these Na^+ and K^+ adeninate ion-pairs occurs in solution with dimer formation governed by π–π stacking proposed to occur at low concentrations. With increasing concentration, higher order aggregates are formed by the coordination through the counter ion of the neighbouring molecule and are dependent on the counter ion present.

The preference for the site of alkylation of the adeninate anion is independent of the structure of the benzyl halides investigated. Furthermore, the presence of the Na^+ or K^+ ion doesn't alter the product ratio observed. A side reaction was identified which depletes the adeninate starting material through protonation leading to neutral adenine. This side reaction is proposed to be the Kornblum oxidation reaction and is counteracted by performing the alkylation reactions in the presence of a mop-up base. The thermodynamic parameters for the alkylation of the adeninate anion are reported for the first time. The benzylation of adeninate ion occurs via an S_N2 mechanism

© University of Pretoria

leading to N9- and N3-benzyladenine as the major and minor products, respectively, in which the enthalpy of formation of N9-benzyladenine is higher than the one of the N3 isomer. However, this increase in the barrier height is largely compensated for by the increase in the entropy at the transition state resulting in a looser transition state structure than that of the N3 isomer. This leads to the overall Gibbs free energy of N9-Bn being 2.3 kJ mol^{-1} lower than for N3-Bn which experiences an entropic bottleneck.

The high resolution MS method developed in this research showed high sensitivity, precision and specificity and therefore can be used for quantitative data collection of enzyme assays without sample modification. A KIE on V and V/K of 1.5 and 1.4, respectively, were observed showing a secondary isotope effect.

1.5 Layout of the thesis

The research covered in this thesis is divided into separate chapters. Each chapter is a lone standing chapter that contains an introduction with an in-depth review of the literature on the topic covered, experimental methods, results and discussion, conclusion and reference sections. As each chapter included a detailed literature section, to avoid repetition, a separate literature review chapter is not given.

The chapters flow in the following order: Chapter 2 covers the experimental research into the ion-pairing and dimer formation of the adeninate anion. Chapter 3 describes the theoretical investigation into the ion-pairing of the adeninate anion with Na^+ and K^+. Chapter 4 presents the experimental and theoretical research into the alkylation of the adeninate anion and lastly, chapter 5 covers the analytical high resolution MS method development and the KIE of C8D-ATP on *Mt*-SK.

Appendix 1 is the published article from the thesis.

Appendix 2 contains the Supporting Information for chapters 2 to 5.

© University of Pretoria

1.6 References

[1] K. Bebenek, L. C. Pedersen, T. A. Kunkel, *Proc. Natl. Acad. Sci. U. S. A.* **2011**, *108*, 1862–1867.

[2] I. J. Kimsey, K. Petzold, B. Sathyamoorthy, Z. W. Stein, H. M. Al-Hashimi, *Nature* **2015**, *519*, 315–320.

[3] W. Wang, H. W. Hellinga, L. S. Beese, *Proc. Natl. Acad. Sci.* **2011**, *108*, 17644–17648.

[4] C. Tamm, P. Strazewski, *Angew. Chemie Int. Ed. English* **1990**, *29*, 36–57.

[5] G. Beobide, O. Castillo, J. Cepeda, A. Luque, S. Pérez-Yáñez, P. Román, J. Thomas-Gipson, *Coord. Chem. Rev.* **2013**, *257*, 2716–2736.

[6] S. L. Anderson, K. C. Stylianou, *Coord. Chem. Rev.* **2017**, *349*, 102–128.

[7] J. An, S. J. Geib, N. L. Rosi, *J. Am. Chem. Soc.* **2009**, *131*, 8376–8377.

[8] H. Cai, M. Li, X.-R. Lin, W. Chen, G.-H. Chen, X.-C. Huang, D. Li, *Angew. Chemie Int. Ed.* **2015**, *54*, 10454–10459.

[9] A. Gładysiak, T. N. Nguyen, S. L. Anderson, P. G. Boyd, R. G. Palgrave, J. Bacsa, B. Smit, M. J. Rosseinsky, K. C. Stylianou, *Inorg. Chem.* **2018**, *57*, 1888–1900.

[10] T. J. Torphy, *Am. J. Respir. Crit. Care Med.* **1998**, *157*, 351–370.

[11] E. Boichot, J. L. Wallace, N. Germain, M. Corbel, C. Lugnier, V. Lagente, J. J. Bourguignon, *J. Pharmacol. Exp. Ther.* **2000**, *292*, 647–53.

[12] B. Bielekova, A. Lincoln, H. McFarland, R. Martin, *J. Immunol.* **2000**, *164*, 1117–1124.

[13] M. K. Mishra, S. P. Kelley, V. Smetana, D. A. Dixon, A. S. McNeill, A.-V. Mudring, R. D. Rogers, *Proc. Natl. Acad. Sci.* **2020**, *117*, 18224–18230.

[14] C. P. Kenyon, R. L. Roth, *BMC Biochem.* **2012**, *13*, 15.

[15] C. P. Kenyon, A. Steyn, R. L. Roth, P. A. Steenkamp, T. C. Nkosi, L. C. Oldfield, *BMC Biochem.* **2011**, *12*, 36.

[16] Y. Li, J. Liu, *Analyst* **2020**, *145*, 6753–6768.

[17] M. Dey, J. Grotemeyer, E. W. Schlag, *Zeitschrift für Naturforsch. A* **1994**, *49*, 776–784.

[18] I. K. Yanson, A. B. Teplitsky, L. F. Sukhodub, *Biopolymers* **1979**, *18*, 1149–1170.

[19] E. Nir, C. Janzen, P. Imhof, K. Kleinermanns, M. S. de Vries, *Phys. Chem. Chem. Phys.* **2002**, *4*, 732–739.

[20] M. Dey, F. Moritz, J. Grotemeyer, E. W. Schlag, *J. Am. Chem. Soc.* **1994**, *116*, 9211–9215.

[21] Y. Kyogoku, R. C. Lord, A. Rich, *J. Am. Chem. Soc.* **1967**, *89*, 496–504.

[22] G. J. Thomas, Jr., Y. Kyogoku, *J. Am. Chem. Soc.* **1967**, *89*, 4170–4175.

[23] N. G. Williams, L. D. Williams, B. R. Shaw, *J. Am. Chem. Soc.* **1989**, *111*, 7205–7209.

[24] L. Katz, *J. Mol. Biol.* **1969**, *44*, 279–296.

© University of Pretoria

[25] T. N. Solie, J. A. Schellman, *J. Mol. Biol.* **1968**, *33*, 61–77.

[26] Y. Kyogoku, R. C. Lord, A. Rich, *Proc. Natl. Acad. Sci.* **1967**, *57*, 250–257.

[27] A. Dunger, H.-H. Limbach, K. Weisz, *J. Am. Chem. Soc.* **2000**, *122*, 10109–10114.

[28] C. Giessner-Prettre, B. Pullman, *J. Theor. Biol.* **1970**, *27*, 87–95.

[29] J. D. Engel, P. H. Von Hippel, *Biochemistry* **1974**, *13*, 4143–4158.

[30] E. M. Basílio Janke, K. Weisz, *J. Phys. Chem. B* **2013**, *117*, 4853–4859.

[31] M. T. Rodgers, P. B. Armentrout, *J. Am. Chem. Soc.* **2000**, *122*, 8548–8558.

[32] B. A. Cerda, C. Wesdemiotis, *J. Am. Chem. Soc.* **1996**, *118*, 11884–11892.

[33] N. Russo, M. Toscano, A. Grand, *J. Am. Chem. Soc.* **2001**, *123*, 10272–10279.

[34] P. C. Bevilacqua, R. Yajima, *Curr. Opin. Chem. Biol.* **2006**, *10*, 455–464.

[35] V. Singh, C. S. Peng, D. Li, K. Mitra, K. J. Silvestre, A. Tokmakoff, J. M. Essigmann, *ACS Chem. Biol.* **2014**, *9*, 227–236.

[36] G. P. Ford, J. D. Scribner, *Chem. Res. Toxicol.* **1990**, *3*, 219–230.

[37] K. W. Kohn, J. A. Hartley, W. B. Mattes, *Nucleic Acids Res.* **1987**, *15*, 10531–10549.

[38] R. Bonaccorsi, A. Pullman, E. Scrocco, J. Tomasi, *Theor. Chim. Acta* **1972**, *24*, 51–60.

[39] W. A. Denny, *Expert Opin. Ther. Pat.* **2000**, *10*, 459–474.

[40] P. Lawley, P. Brookes, *Biochem. J.* **1963**, *89*, 127–138.

[41] I. Mahadevan, M. Rasmussen, *Tetrahedron* **1993**, *49*, 7337–7352.

[42] M. Rasmussen, J. Hope, *Aust. J. Chem.* **1982**, *35*, 525.

[43] A. Beasley, M. Rasmussen, *Aust. J. Chem.* **1981**, *34*, 1107.

[44] M. Rasmussen, J. Hope, *Aust. J. Chem.* **1982**, *35*, 535.

[45] N. M. Chung, H. Tieckelmann, *J. Org. Chem.* **1970**, *35*, 2517–2520.

[46] G. Hopkins, J. Jonak, H. Minnemeyer, H. Tieckelmann, *J. Org. Chem.* **1967**, *32*, 4040–4044.

[47] N. P. Ramzaeva, I. N. Goncharova, M. Y. Lidak, Y. S. Gol'dberg, M. V. Shimanskaya, *Chem. Heterocycl. Compd.* **1987**, *23*, 93–98.

[48] M. Rasmussen, J. Chan, *Aust. J. Chem.* **1975**, *28*, 1031.

[49] J. Kjellberg, N. G. Johansson, *Nucleosides and Nucleotides* **1989**, *8*, 225–256.

[50] M. R. Haque, M. Rasmussen, *Tetrahedron* **1994**, *50*, 5535–5554.

[51] D. M.-J. S. Buyens, Alkylation of Adenine: A Synthetic and Computational Study of the Reaction Mechanism, **2015**.

[52] D. M. S. Buyens, P. Mangondo, I. Cukrowski, L. A. Pilcher, *J. Heterocycl. Chem.* **2017**, *54*,

© University of Pretoria

2946–2950.

[53] Y. Wang, H. Xu, H. Wang, Z. Zheng, Z. Meng, Z. Xu, J. Li, M. Xue, *ACS Omega* **2021**, *6*, 4386–4394.

[54] E. Doleželová, T. Klejch, P. Špaček, M. Slapničková, L. Guddat, D. Hocková, A. Zíková, *Sci. Rep.* **2021**, *11*, 13317.

[55] T. Schön, P. Miotto, C. U. Köser, M. Viveiros, E. Böttger, E. Cambau, *Clin. Microbiol. Infect.* **2017**, *23*, 154–160.

[56] X. Chen, G. He, S. Wang, S. Lin, J. Chen, W. Zhang, *Front. Microbiol.* **2019**, *10*, 1–10.

[57] C. P. Kenyon, R. L. Roth, C. W. van der Westhuyzen, C. J. Parkinson, *BMC Res. Notes* **2012**, *5*, 131.

[58] I. Cukrowski, G. Dhimba, D. L. Riley, *Phys. Chem. Chem. Phys.* **2019**, *21*, 16694–16705.

[59] I. Cukrowski, *Comput. Theor. Chem.* **2015**, *1066*, 62–75.

[60] I. Cukrowski, *WIREs Comput. Mol. Sci.* **2021**, 1–19.

© University of Pretoria

Chapter 2 Towards a molecular understanding of cation–anion interactions and self-aggregation of adeninate salts in DMSO by NMR and UV spectroscopy and crystallography

2.1 Introduction

2.1.1 Hydrogen bonding and π–π stacking interactions of nucleic acids

The non-covalent interactions between two or more molecules is a combination of several effects such as i) Van der Waals interactions, ii) electrostatic interactions, iii) induction energy, iv) charge transfer and v) desolvation (before complexation can occur between two molecules, solute-solvent interactions must break).[1–3] Van der Waals interactions are the sum of dispersion and repulsion energies between two molecules and depend on the contact surface area.[1,2] Electrostatic interactions involve the molecular charge distribution whereas induction interactions involve the charge distribution of one molecule with the induced charge distribution on the neighbouring molecule.[1] These interactions play a critical role in molecular recognition, having electrostatic and Van der Waals interactions along with desolvation the most important.[1,4] Solvent molecules that interact via the same non-covalent interactions can compete for interaction sites and destabilize dimers or higher order aggregates. Other solvents may, however, stabilize complex formation between two or more molecules.[1]

Non-covalent interactions governing the aggregation of isolated purine bases have been investigated in order to gain a greater understanding of their role in structure, function and stability since Watson and Crick (1953) proposed the structure of DNA. Two strands of DNA are held together via in-plane hydrogen bonding of a purine with a pyrimidine base, adenine with thymine and guanine with cytosine. In addition to hydrogen bonding, the importance of π-π stacking interactions in the stability of DNA was revealed.[5,6] It is well known that adenine is involved in Watson-Crick type hydrogen bonding[7,8] along with reversed Watson-Crick,[9] Hoogsteen[10] and reversed Hoogsteen[11] type hydrogen bonding, Figure 2.1. In crystalline form and in solution, the hydrogen bonding between base pairs might not resemble that in DNA or RNA, e.g. N9-substituted adenine has shown Hoogsteen type hydrogen bonding with uracil derivatives in crystal form instead of the common Watson-Crick type bonding.[12,13] The self-[14–16] and hetero-association of adenine and adenine derivatives with other nucleobases[14,15,17–19] and carboxylic acids[20–22] as well as the effect of substituents[14,18,23,24] have been investigated extensively. Most studies of hydrogen bonding[17,25–28] and stacking[8,29–32] were investigated in chloroform and aqueous solutions, respectively. This is due non-polar solvents such as chloroform allowing for hydrogen bonding to take place between nucleic acid bases, whereas water forms hydrogen bonds itself with purines in solution and therefore promotes π-π stacking. The formation of the nucleobase hetero-dimers in gas phase is governed by hydrogen bonding with little to no stacking.[33,34] The association constants for nucleic acids involved in hydrogen bonding are largest for purine-pyrimidine interactions, decreasing for pyrimidine-pyrimidine and purine-purine[14] interactions. The π-π stacking association constants show decreasing order for purine-purine > purine-pyrimidine > pyrimidine-pyrimidine.[30,35]

© University of Pretoria

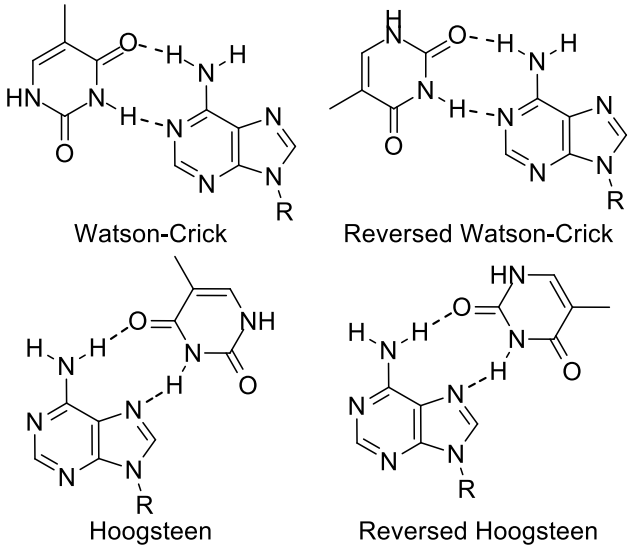

Figure 2.1: The configuration of the adenyl group involved in Watson-Crick, reversed Watson-Crick, Hoogsteen and reversed Hoogsteen bonding with thymine.

2.1.2 Metal coordination of nucleic acids and their bases

The binding of alkali metal ions such as Na^+ and K^+ to nucleobases influences the structural integrity of DNA and plays a role in synthesis, replication, recognition and cleavage of DNA and RNA.[36,37] Binding of metal ions can interfere with hydrogen bonding and stacking interactions between base pairs and compromise the structural stability of DNA.[38] Experimentally, the affinity for alkali metals increase in the order guanine > cytosine > adenine > thymine > uracil, following the trend of proton affinity in nucleobases.[36,39] The preferred binding sites of metal ions are the N7 in adenine, the N7 and O6 atoms in guanine, the N3 and O2 atoms in cytosine and the O4 in thymine and uracil.[36] The three dimensional folding adopted by nucleic acid repeat sequences show ion dependency[40,41] which further highlights the role and importance of monovalent metal ions in DNA structure.

The multi-site coordination and ability of nucleobases to interact non-covalently have rendered them desirable ligands in the synthesis of stable bio-metal-organic frameworks that can have structural flexibility.[42–45] Metal complexes of adenine can have mono- or bidentate coordination through different combinations of N3, N7 and N9 nitrogen atoms. The deprotonated form of adenine (adeninate anion) has four sites for metal coordination, Figure 2.2, in which di, tri- or tetradentate coordination can occur, having varying coordinate combinations through the N1, N3, N7 and N9 atoms.[43,46]

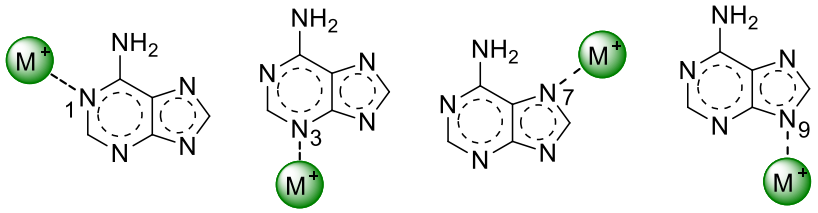

Figure 2.2: Metal coordination (M = metal ion) via the N1, N3, N9 and N7 (left to right) nitrogen atoms of the adeninate anion. IUPAC numbering of adenine purine ring shown on the first structure.

© University of Pretoria

2.1.3 Studying aggregation through ^{1}H NMR spectroscopy

The self-association or complex formation of molecules is studied by observing the change in a physical property of the system such as ^{1}H NMR chemical shift or UV absorbance when varying the concentration or temperature.[47–50] In ^{1}H NMR spectroscopy, the observed chemical shift, δ_{obs}, is the weighted average between the concentrations of the two or more species in solution, e.g. chemical shifts of the monomer, δ_M, and dimer, δ_D, can be assigned from experimental data if concentration-independent shifts are observed,[23,35,51–53]

$$\delta_{obs} = x_M\delta_M + x_D\delta_D \quad (2.1)$$

whereby x_M and x_D represent the molar fraction of monomer and dimer forms,

$$x_m = \frac{[A]}{[A]_0} \quad (2.2)$$

and

$$x_D = \frac{[A_2]}{[A]_0} = 1 - x_m \quad (2.3)$$

2.1.3.1 Aggregation via hydrogen bonding

Generally, a hydrogen bond, X–H···Y, is a weak interaction between a hydrogen atom covalently bonded to an electronegative atom X (hydrogen donor) and the lone pair of electrons of an acceptor atom Y, generally a heteroatom.[54,55] The interaction is dominated by the electrostatic interaction between the partial positive charge on the hydrogen atom and the partial negative charge on the acceptor atom. In ^{1}H NMR spectroscopy, a proton involved in the hydrogen bond will experience a shift downfield (become deshielded) relative to its position in the non-hydrogen bonded form.[17,56–58] This deshielding of the proton is associated with the loss of electron density of the hydrogen atom.[54,59,60] Upon increasing concentration or decreasing temperature, the protons become more deshielded as equilibrium shifts towards the formation of hydrogen-bond associated complexes. Decreasing the concentration or increasing the temperature leads to dissociation of the hydrogen bonded complex, increasing the shielding of the formerly hydrogen bonded protons.

The self- and hetero-association of nucleobases have been studied via ^{1}H NMR spectroscopy by monitoring the deshielding of the NH_2 protons.[17] The type of bonding patterns, Watson-Crick and Hoogsteen, have been assigned to certain dimer formations based on the chemical shift of the C2-H and C8-H protons.[61,62] The proton on the atom adjacent to the heteroatom that is participating in

© University of Pretoria

hydrogen bonding becomes deshielded and migrates downfield[17,18,61] i.e. for Watson-Crick and Hoogsteen hydrogen bonding patterns the C2-H and C8-H, respectively, become deshielded. The hydrogen-bond π-polarization model[61] was proposed to explain the C2-H upfield shift with Watson-Crick hydrogen bonding between 9-*N*-butyladenine and the aliphatic carboxylic acids. In the model, the N1 purine nitrogen atom has an induced partial negative charge and therefore shields the adjacent C2-H proton, resulting in an upfield shift (Figure 2.3a). However, with adenine-uracil complexes hydrogen bonded via Watson-Crick pairing, the position of the uracil oxygen and its interaction with the C2-H withdraws electron density, causing a downfield shift of the proton (Figure 2.3b).[15,17,18] Furthermore, the model explains the downfield shift of the C8-H proton for Hoogsteen type hydrogen bonding in that no π-polarization occurs to create a partial negative charge on the N7 which in turn would shield the C8-H (Figure 2.3c).

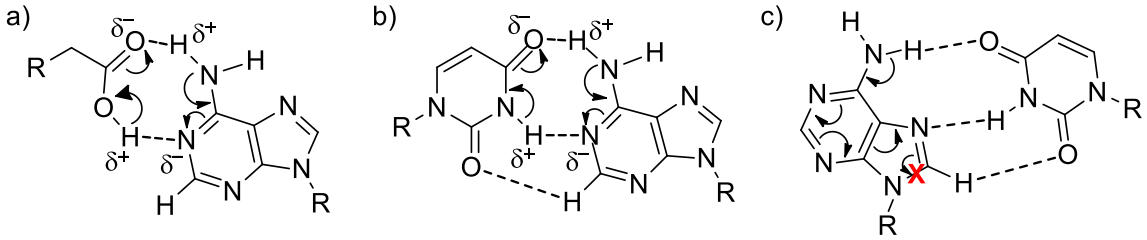

Figure 2.3: Hydrogen-bond π-polarization model for (a, b) Watson-Crick hydrogen bonding between adenine with a carboxylic acid and uracil, respectively and c) Hoogsteen type hydrogen bonding with uracil. Partial negative (δ-) and positive (δ+) charges are shown.

The hetero-association of nucleobases beyond dimer formation has been observed via ^{1}H NMR spectroscopy.[21,22] Trimer formation such as 1:2 and 2:1 complex formation between adenine with benzoic acid and 2-iodobenzoic acid were identified by an initial upfield shift of the C2-H at low concentrations of the acids, ascribed to Watson-Crick bonding, to a downfield shift with higher concentrations as the Hoogsteen site is occupied by a second acid molecule.[21] The hydrogen-bond π-polarization effect is masked by the overall polarization of the adenyl moiety. A mixture of adenosine:acetic acid at 113 K in a Freon mixture forms trimolecular complexes. The 1:2 and 2:1 complexation occurs in equal ratios in which the 2:1 complexation had the two adenyl moieties predominantly in the Hoogsteen type hydrogen bonding pattern.[22] The effect of temperature on the preference of hydrogen bonding patterns has also been observed. The hetero-association of di-O-acetylated 2'-deoxyadenosine with 2'-deoxyuridine has the preferred Watson-Crick type hydrogen bonding at low temperatures whereas at temperatures of 293 K the probability was about equal between Watson-Crick and Hoogsteen.[15]

Aggregate formation, however, extends past the simple one dimensional monomer-dimer formation and is driven by a range of non-covalent interactions such as electrostatic interactions (hydrogen bonding and cation-π[63]), dispersion (such as π-π stacking[64]) and hydrophobic interactions,[65] resulting in complex ^{1}H NMR chemical shift behaviour. An increase in the dissociation energy of hydrogen bonds results in a decrease in the dependence of the chemical shift on temperature as a larger amount of energy is needed to distort the bond.[47]

© University of Pretoria

A change in temperature can cause a change in chemical shifts of the protons involved in the hydrogen-bonded complex without having the complex dissociate.[66] This is due to the effect of temperature on the low frequency and anharmonicity of the hydrogen-bond stretching vibration. Increasing the temperature leads to increasing the populations of higher excited vibrational levels of the hydrogen bond, and hence the distance between the hydrogen and the hydrogen acceptor atom increases, increasing the shielding of the proton. Temperature also influences the solvent electric field.[67] This effect was used to explain the deshielding of the hydrogen bonded proton between chloroacetic acid and hydrochloric acid with pyridine with an increase in temperature. Solvent molecules that have an electric dipole moment create an electric field at the solute-solvent interface. The disorder amongst the solvent molecules (disorder amongst the dipoles) determines the strength of the experienced electric field. High temperatures increase the disorder among the solvent molecules resulting in a weak electric field. Reducing the temperature leads to a more ordered system and consequently the solute experiences a stronger electric field. This electric field induces an enhanced dipole moment of the hydrogen bond resulting in a decrease in hydrogen bond length and hence deshielding of the proton.

The dissociation of hydrogen bonds can also be examined using the temperature coefficient, $\Delta\delta/\Delta T$.[68–71] A plot of the change in chemical shift of a proton with the change in temperature gives a straight line with a slope defined as the temperature coefficient. Increasing the temperature of a solution increases the distance between molecules.[72] The protons which originally shifted downfield due to hydrogen bonding will move upfield upon the increase in temperature as the length of the hydrogen bond is increased. Protons that are hydrogen bonded with solvent will move upfield to a larger extent than those that are sheltered away from solvent due to hydrogen bonding with molecules other than the solvent. Slow exchange amide protons with corresponding temperature coefficients smaller (more positive) than -4.5 ppb/K reflect hydrogen bonded protons, amide protons with fast exchange rates and temperature coefficients larger (more negative) than -4.5 ppb/K indicate non-hydrogen bonded protons.[71,72]

2.1.3.2 Aggregation via π–π stacking

Besides hydrogen bonding, π-π stacking is another common interaction responsible for the aggregation of aromatic systems, ranging from small molecules to large biological systems.[4] The aromatic π–π stacking interaction plays a critical role in base-pair stacking,[5,73,74] protein stabilization,[75,76] drug intercalation with DNA[77–79] and molecular recognition in biological and artificial systems.[79,80]

The π-system is composed of a positively charged σ-framework (electron deficient periphery) surrounded by a negatively charged π-electron cloud (electron rich centre) above and below the plane of the aromatic system, Figure 2.4a.[1,81,82] The π–π stacking interaction is dominated by an attractive π–σ electrostatic interaction between two aromatic systems that outweighs π–π electronic repulsion.[3] Various configurations of stacking occur such as parallel face–to–face, parallel-displaced and edge to face stacking, also known as “T-shaped” stacking (Figure 2.4b).[83] The T-shaped configuration is a C–H···π interaction. The face–to–face stacking arrangement results in the largest electrostatic π–π repulsion.[1] The distance between the two centroids of the stacked molecules ranges from 3-4 Å and 4.5-5 Å for parallel[16,83,84] and T-shaped stacked [85],[3] complexes, respectively. Parallel geometries are dominant in stacked nucleobases in DNA with a parallel

© University of Pretoria

displaced configuration which is complementary to the twist of the DNA helix.[86] The most stable stacking arrangement for heteroaromatic systems is anti-parallel-displaced such as that for pyridine, Figure 2.4c.[87,88] This is due to heteroatoms perturbing the electron density of the aromatic system resulting in partial atomic charges and a permanent dipole moment.[89] This in turn leads to electrostatic dipole-dipole interactions.

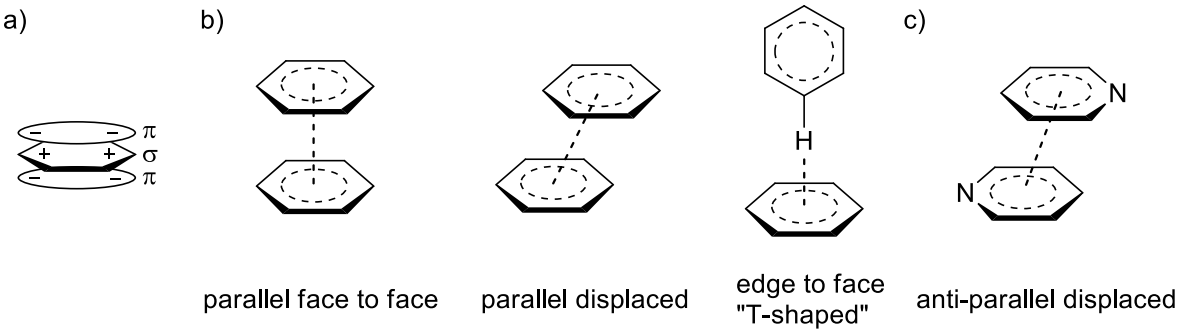

Figure 2.4: π-π stacking geometry of aromatic systems.

Aromatic stacking interactions become more favourable with an increase in the size of aromatic systems.[87,90] The strength of stacking increases with the addition of electron withdrawing groups or heteroatoms as the repulsive π–π interaction is decreased due to reduced electron density in the ring.[2,82,84,91] Hydrogen-bonding between molecules can influence the ability to stack as electron-density is redistributed with the formation of hydrogen bonds.[84] Heterocyclic aromatic molecules which act as hydrogen bond acceptors have enhanced π-π stacking interactions.

For stacking aggregation, the influence of the ring current of one molecule, A, results in shielding of the protons of the neighbouring molecule B which are located above or below the aromatic system of the associated molecule A.[16,92,93] It is predicted for parallel stacked dimers that all protons experience a shielding effect, having the protons closest to the neighbouring aromatic ring undergo the largest shift.[94] For the T-shaped configuration, the proton of molecule A interacting with the π system of the aromatic ring of the neighbouring molecule B undergoes a substantial shielding effect compared to its neighbouring protons whereas the protons of the aromatic ring of B undergo a deshielding effect.[94] For parallel stacked dimers an increase in concentration or decrease in temperature will result in a shift in the equilibrium towards stacked dimers causing a shielding effect on the protons.[95] Upon dilution or increase in temperature, the protons experience a deshielding effect as the stacked dimers dissociate. The magnitude of the shift depends on the type of aromatic system involved and the position of the proton being shielded by the ring current.[16,96] The position of the proton above or below the aromatic plane of a neighbouring molecule depends on the distance between the two centroids of the molecules involved (parallel displacement), and the distance and angle of the planes of the two molecules.[84]

The stacking of nucleobases has been observed in ^{1}H NMR spectroscopy whereby shielding of the purine protons occurs.[16,17,97] The stacking of two adenine molecules has the calculated average change in chemical shift (Δδ) reported as 0.2 and 0.37 ppm for the C8-H and C2-H protons,

© University of Pretoria

respectively, of the purine ring.[16] The temperature coefficient has also been used to study stacking interactions.[98] An increase in temperature results in the downfield shifting of the purine protons due to the disturbance of the stacking arrangement. For purines, the temperature coefficient is different for each proton in the stacked conformation i.e. The imidazole proton (C8-H) is affected the least compared to the pyrimidine proton (C2-H). Two possible explanations were proposed for the effect on the C8-H proton, 1) the stacking arrangement resulted in an equal shielding-deshielding pattern that eliminates the overall effect on the C8-H or 2) that the imidazole proton was positioned away from the effect of the ring current effects of associated molecules. The effect of the alkyl group on ordered stacking was highlighted in the temperature coefficient difference between the C8-H of purine vs alkyl substituted purines, where the $\Delta\delta/\Delta T$ of the latter is far less than that of the purine.[98]

In absorption spectroscopy, the formation of dimers is indicated by hypochromic shifts of the absorption maxima for stacked dimers and hypochromic or hyperchromic shift for hydrogen bonded dimers. [8,14,26,99] For π-π stacking, the interaction between dipole moments on neighbouring oscillators which originate from different electronic transitions, is predicted to give large hypochromic shifts.[99] For hydrogen-bonding the model of resonance interaction is predicted to give the largest hypochromic shifts, whereby the induced electric dipole moment from neighbouring oscillators adds to the electric field of a given molecule. UV spectroscopy has been used to study hydrogen bond dimer formation between purine with pyrimidine[14] and 9-ethyladenine with 1-cyclohexyluracil.[100]

2.1.4 The adeninate anion

The presence of disfavoured tautomeric and anionic forms of nucleic acids can form WC-like mispairs (i.e. guanine-thymine, adenine-cytosine and guanine-uracil) that are involved in mutations and replication and translational errors.[101–104] These forms of nucleic acids are also believed to play a role in nucleic acid catalysis[105] and RNA-ligand recognition.[106] The anion forms can be readily generated by dissociative electron attachment[107] have featured in investigations of the photostability of nucleic acids in DNA.[108,109] The adeninate anion deprotonated at the N9 position (the pK_a value of N9 is 9.8) is commonly used in the synthesis of N9-substituted adenines, which have important biological roles such as anti-asthmatic [110] and anti-inflammatory activity,[111] activity against diseases such as multiple sclerosis and autoimmune disease.[112] There is a lack of information surrounding anionic forms of nucleobases and is a topic being addressed currently.[102,113] However, studies of the chemical properties of the free adeninate anion and its interactions with monovalent alkali metals are limited. Hence, gaining insight into the chemical behaviour of this anion is important to better understand the systems in which it is involved.

During an independent kinetic study of the regio-selectivity of the adeninate anion towards alkylation (chapter 4) in DMSO-d_6, a dependence of the ^{1}H NMR chemical shifts of the purine protons on the concentration of the adeninate anion was observed prompting an investigation into the origin of these shifts. In this chapter, the ion-pair formation of the adeninate anion with monovalent metals, Na^+ (Na-Ade) and K^+ (K-Ade), and the self-aggregation of these ionic complexes in DMSO are investigated using NMR and UV spectroscopy as well as XRD of crystal structures. In addition, we have studied the influence of the 15-crown-5 (15C5) and 18-crown-6 (18C6) ether on the spectroscopic and crystal structures of Na-Ade and K-Ade. To this end, we show that ion-pair

© University of Pretoria

formation exists between the adeninate anion and the counter ions even at extremely dilute concentrations and that self-aggregation of these complexes is highly influenced by the counter ion present. Furthermore, there is a possibility of complex formation between K-Ade and the 18-crown-6 ether.

2.2 Experimental details

General: ^{1}H NMR, Heteronuclear Multiple Bond Correlation (HMBC) and Heteronuclear Single Quantum Correlation (HSQC) spectra were recorded at 400.13 MHz with a Bruker 400 AVANCE ultrashield +. The ^{13}C NMR spectra were recorded at 101 MHz using the Bruker 400 AVANCE ultrashield +. The ^{13}C NMR spectra were calibrated using the DMSO-d_6 solvent peak at 39.5 ppm. X-ray diffraction analyses were performed on a Bruker D8 Venture (copper radiation). Adenine, sodium and potassium hydride (purified from 60% in dispersion mineral oil by hexane), and DMSO-d_6 were purchased from Sigma-Aldrich. The sodium and potassium hydride are used as bases to avoid introduction of water into the reactions. The anhydrous DMSO-d_6 was prepared as follows: Powdered 4 Å molecular sieves were heated at 200 °C under vacuum for 4 days and placed inside a glovebox. The sieves were added to DMSO-d_6 and left for 24 hours. The solvent was checked via ^{1}H NMR to confirm the absence of water. The molecular sieves were removed by passing the solvent through a 25 mm hydrophilic polyamide syringe filter. Stock solutions of Na-Ade, K-Ade and Na-Ade(15C5) and K-Ade(18C6) were prepared within the glovebox using the anhydrous DMSO-d_6. Details for stock concentrations and dilutions are given in the SI. All NMR samples were prepared and sealed within the glovebox. The UV absorbance spectra were measured using Varian Cary 300 UV–Vis spectrophotometer scanning from 200 to 800 nm. Samples were run in a 1 mm quartz cuvette for DMSO samples with DMSO as a blank sample, and a 4 mm quartz cuvette for anhydrous DMSO samples (prepared and sealed in a glove box) with anhydrous DMSO as the blank sample.

Refer to Supporting Information 1 for the experimental details of the ^{1}H NMR and UV spectroscopy study and for the X-ray crystallography study.

Self-aggregation studies: The ^{1}H NMR spectra were recorded at 300 MHz with a Bruker 300 AVANCE ultrashield + for a series of concentrations at 5 different temperatures (300/305, 320, 340, 360 and 380 K). Chemical shifts of ^{1}H NMR spectra were calibrated using residual non-deuterated solvent peaks of DMSO-d_6 according to temperature adjustments reported by Hoffman and Becker.[114] All analyses were performed in triplicate. The experimental ^{1}H NMR data were normalized as described in the SI. Aggregation between monomers (A) is considered in terms of dimer (A_2, eqn (2.4)), trimer (A_3, eqn (2.5)) or *n*-mer (A_n, eqn(2.6)) formation.

$$2\mathrm{A} \rightleftharpoons \mathrm{A_2} \qquad K_2 = \frac{[\mathrm{A_2}]}{[\mathrm{A}]^2} \tag{2.4}$$

$$3\mathrm{A} \rightleftharpoons \mathrm{A_3} \qquad K_3 = \frac{[\mathrm{A_3}]}{[\mathrm{A}]^3} \tag{2.5}$$

$$n\mathrm{A} \rightleftharpoons \mathrm{A_n} \qquad K_n = \frac{[\mathrm{A_n}]}{[\mathrm{A}]^n} \tag{2.6}$$

© University of Pretoria

To quantitatively analyse and interpret thermodynamic and kinetic data of aggregation, two mathematical models are used to describe aggregation, the isodesmic (eqn (2.7)) and trimer model, eqn (2.8):

$$\delta_N = \delta_m + (\delta_a - \delta_m)\left(1 + \frac{1-\sqrt{4K_{agg}C_t+1}}{2K_{agg}C_t}\right) \quad (2.7)$$

Where $K_{agg} = K_2 = K_3 = K_n$,

$$\delta_N = \delta_m + 3C_t^2K_3(\delta_t - \delta_m) \quad (2.8)$$

where $K_3 = \frac{[A_3]}{[A]^3}$

where δ_N is the normalized observed chemical shift, δ_M and δ_a (or δ_t) is the chemical shifts of the monomer and aggregate (or trimer) forms, K_{agg} and K_3 are the aggregate and trimer formation constants and C_t is the total concentration of the ionic compound. The isodesmic model is the simplest aggregation model used to study the aggregation of small molecules. The models were used to fit the normalized observed chemical shifts (δ_N). Nonlinear regression analyses for the above models were fitted in OrginPro 8.5 to obtain K_{agg}, K_3, δ_M, δ_a, and δ_t for each proton, i.e. C2-H, C8-H and NH_2. The average over the three protons was used to plot the van't Hoff plot of lnK (where K is K_{agg} or K_3) vs 1/T and the trend line was fitted using linear regression in OrginPro 8.5. The thermodynamic data was obtained from the slope (slope = $-\Delta H/R$) and the intercept (intercept = $\Delta S/R$) and ΔG using eqn (2.9)

$$\Delta G = \Delta H - T\Delta S \quad (2.9)$$

The same procedure described above was performed for the guest-host model for the complexation of Na-Ade and 15C5. The concentration dependent ^{1}H NMR data of Na-Ade(15C5) at the various temperatures were fitted using nonlinear regression to the guest-host model, assuming 1:1 complexation, eqn (2.10), in OriginPro 8.5.

$$\delta_N = \frac{\delta_0 + \delta_{AB}K_1C_{Na+}}{1+K_1C_{Na+}} \quad (2.10)$$

© University of Pretoria

where δ_N and δ_{AB} is the chemical shift of the uncomplexed and complexed 15C5, K_1 is the association constant of 1:1 complexation between 15C5 and Na^+ and C_{Na^+} is the concentration of Na^+.

2.3 Results and discussion

2.3.1 Ion pairing of the adeninate anion with Na^+ and K^+

The use of organic solvents such as DMSO, DMF, methanol etc., has an effect on the non-covalent interactions (such as hydrogen bonding, π-π stacking and cation binding) of nucleic acids[115] and therefore on the interactions of nucleobases as well. However, many thermodynamic properties of nucleobases are reported in organic solvents or co-solvents of water and organic solvents in order to enhance the chemical property being studied or to understand the effect of solvent.[116] It is important to note that often nucleobase derivatives are used in aqueous media due to the low solubility of free nucleobases in organic solvents.[30] In order to gain an understanding of the interactions between adenine and the counter ion, the experiments were conducted in a solvent which allowed for the solubility of adenine and the adeninate salt and allows for potential ion-pairing. DMSO, which acts as a hydrogen bond acceptor only, will not form hydrogen bonds at nitrogen sites of adenine rendering these sites available for metal ion coordination. Moreover, further studies conducted of the regio-selectivity of the adeninate salt (chapter 4) require the use of DMSO and hence, to maintain a common solvent, DMSO was used to perform these studies.

The UV studies performed (refer to SI 1 for experimental details) showed a significant dependence on the counter ion present indicating that ion pairs exist between the adeninate anion and the Na^+/K^+ counter ion. The normalized UV absorption profiles of Na-Ade and K-Ade in DMSO/H_2O and anhydrous DMSO are shown in Figure 2.5 (UV absorbance spectra, Figure S1.16). The λ_{max} and shoulder bands observed are reported in Table 2.1.

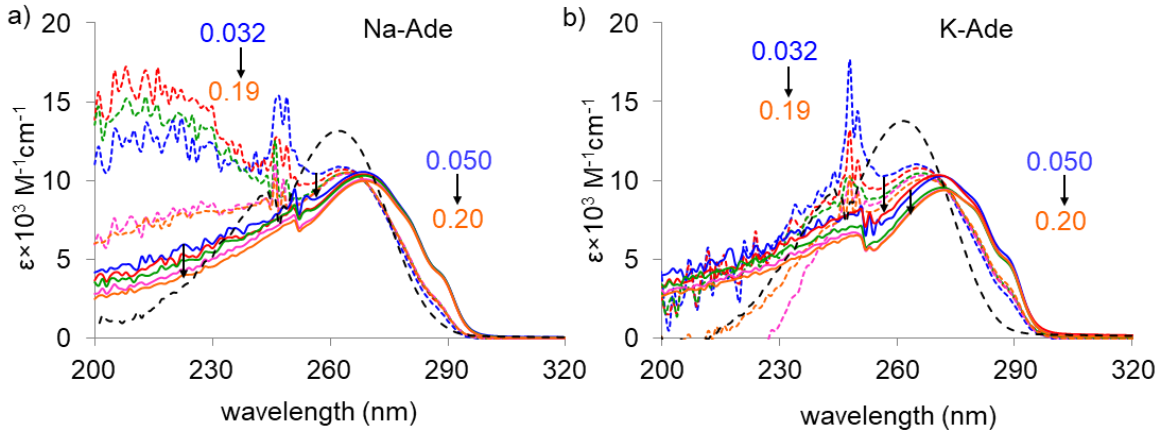

Figure 2.5: Concentration dependent UV absorption profile of a) Na-Ade and b) K-Ade in DMSO/H_2O (dotted lines) and anhydrous DMSO (solid lines) for the concentration range (0.05 – blue, 0.075 – red, 0.10 – green, 0.15 – pink, 0.20 – orange, in mM) and in the presence of a large excess of 15C5 (126 eq) and 18C6 (117 eq) ether, respectively (dashed black lines) are shown. Shoulder bands are indicated by red arrows.

© University of Pretoria

The blueshift of the λ_{max} from K-Ade (272 nm) to Na-Ade (269 nm) in DMSO is associated with the larger stabilization of the ground state of the anion by the Na^+ counter ion which has a stronger cationic field strength due to its smaller ionic radius compared to K^+.[117,118] Water molecules facilitate the dissociation of the counter ion from the adeninate ion pair. Studying the system with a small amount of water present (5.2% v/v H_2O) provided insight into i) how the Na- and K-Ade complexes responded to interactions with water and ii) how the M-Ade concentration dependent characteristics of the bands changed. The blueshift from DMSO to DMSO/H_2O for both ionic complexes is due to the hydrogen bonding of water stabilizing the ground state of the anion. Conversely, the solvation of the adeninate anion by polar solvents stabilizes the π* orbital, resulting in a redshift of the λ_{max} with increasing polarity and hydrogen-acceptor properties of the solvent i.e the λ_{max} shifts from 262 nm in water, methanol and ethanol to 266 and 270 nm in DMSO and DMF, respectively.[119] However, the blueshift observed from anhydrous DMSO to DMSO/H_2O is only partly due to the formation of hydrogen bonds between water and Na-/K-Ade. Peripheral solvation of the cation by polar aprotic solvents would shield the positive charge, reducing the magnitude of the cationic field and would result in a redshift of λ_{max} in anhydrous DMSO. The hypochromic shift is ascribed to π-π stacking interactions of the Na^+ and K^+ complexed adeninate dimer.[120]

Table 2.1: The λ_{max} and (shoulder) bands (nm) in the UV absorption spectrum of Na- and K-Ade, Na-Ade(15C5) and K-Ade(18C6) in DMSO/H_2O and anhydrous DMSO

solvent	λ_{max}
DMSO/H_2O + NaH	246, 250, 264→265 (278, 287)
DMSO/H_2O + KH	248, 250, 264→269 (278, 287)
Anhydrous DMSO + NaH	251, 254, 269 (278, 287)
Anhydrous DMSO + KH	251, 253, 272 (278, 287)
DMSO/H_2O +NaH+15C5	245, 262
DMSO/H_2O +KH+18C6	245, 262

A metal-Ade concentration dependent redshift is observed in DMSO/H_2O, having the Na-Ade shift from 262 to 265 nm and K-Ade shift from 264 to 269 nm, accompanied by the increase in shoulder band intensity at 278 and 287 nm, which are attributed to the presence of the cationic and anionic species.[119] These shoulder bands decrease in intensity as the concentration of Na- and K-Ade decreases as the presence of water molecules assists the dissociation of ion-pairs. In DMSO, the concentration-dependent redshift of the band around 265 nm for Na- and K-Ade is absent and the band intensity at 278 and 287 nm is larger in magnitude than in DMSO/H_2O, indicating the ion-pairs are the predominate species.

The UV spectroscopy study of Na^+ and K^+ ion complexation to the adeninate anion was conducted alongside the studies in the presence of 15C5 and 18C6 (Figure 2.5, dashed), respectively, in order to confirm the presence of ion-pairs. In the presence of the large excess of 15C5 and 18C6, the shoulder profile is absent and the λ_{max} blueshifts to 262 nm for both Na- and K-Ade as the free adeninate anion is formed, thus confirming that ion-pairs exist in the absence of the crown ethers. Narrow finger like bands around the 245-250 nm region in the DMSO/H_2O spectra are ascribed to DMSO-water-metal counter ion complexes as they also appear in the cation-DMSO solutions in the

© University of Pretoria

absence of the adeninate anion, see Supporting Information 1 Figure S1.17. Solvated metal atoms do not have molecular vibrational states and hence display narrow absorption bands. In addition, the intensity of the band grows as the solutions of Na-Ade and K-Ade are diluted, leading to the separation of the ion-pair increasing the concentration of the free cation for interaction with DMSO and water molecules. These bands are significantly less prominent in anhydrous DMSO due to fewer free ions, and are absent in the presence of the 15C5 and 18C6 crown ether, indicating the dependence on the cation. In the Na-Ade DMSO/H_2O UV spectra, a broad band lying below 235 nm is observed and is largely suppressed in DMSO and in the presence of 15C5 and is attributed to the population of higher lying bright $^1\pi\pi^*$ state(s) of the adeninate anion by the excitation at 220 nm.[121]

2.3.2 Coordination sites of Na^+ and K^+ with the adeninate anion

The ^{1}H NMR spectra of the ionic compounds, Na-Ade, K-Ade and K-Ade(18C6) are shown in Figure 2.6 at dilute (Figure 2.6a) and saturated concentrations (Figure 2.6b) in anhydrous DMSO-d_6 and the ^{13}C NMR spectra at saturation concentrations are shown in Figure 2.6c.

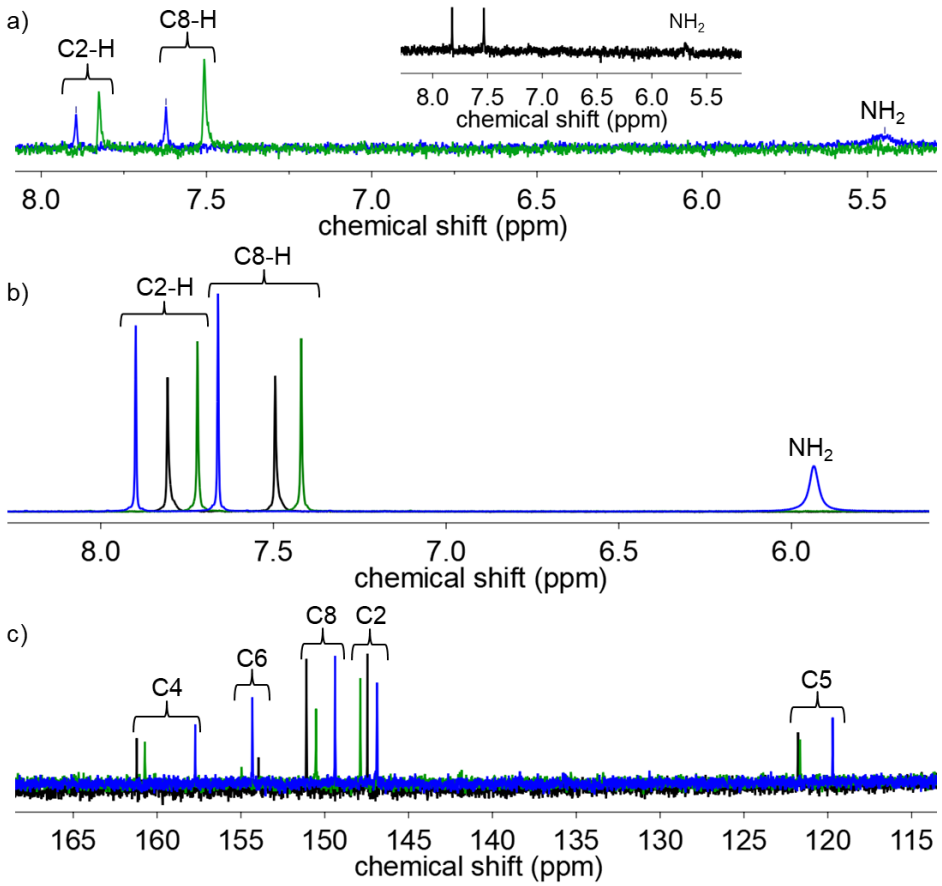

Figure 2.6: Superimposed ^{1}H NMR spectra of Na-Ade (blue), K-Ade (green) and K-Ade(18C6) (black) at a) dilute concentrations of 1.44, 2.11 and 0.489 mM, respectively, with data for K-Ade(18C6) shown in the insert b) Saturated concentrations of 52.2, 84.8 and 78.7 mM, respectively, and c) ^{1}H decoupled ^{13}C NMR at the saturated concentrations, in DMSO-d_6.

© University of Pretoria

The spectra reveal a dependence of chemical shift on both the concentration and the counter ion. Comparing the spectral data at saturated conditions, three differences are noted: Firstly, the NH_2 peak of K-Ade is absent in the ^1H NMR spectrum whereas the Na-Ade has the peak occur at 6.07 ppm integrating for 2 protons. Upon dilution of the K-Ade, the NH_2 peak is never observed, Figure 2.6a. Secondly, all the ^{13}C nuclei are more deshielded for K-Ade than Na-Ade and the K-Ade C6 chemical shift is suppressed to a large extent. Thirdly, upon addition of the 18C6 to K-Ade, the C2-H and C8-H become deshielded relative to the K-Ade peaks, and the NH_2 peak is not observed at saturated concentrations but becomes slightly visible at very dilute concentrations, ≤ 2 mM, at 5.7 ppm (Figure 2.6a insert).

The addition of base, NaH/KH, to adenine in DMSO-d_6 results in deprotonation, shielding all the purine protons relative to the peaks of adenine as electron density is gained in the purine ring, Table 2.2. The formation of an ionic bond between the adeninate anion and the counter ion leads to an extent of shared electron density between the two involved ions, withdrawing electron density from the anion. The Na^+ counter ion, with the larger charge-to-radius ratio, has stronger ion and ion-induced dipole interactions with the adeninate anion, and this is reflected in the larger deshielding of the C2–H and C8–H protons relative to K-Ade (Δδ of 0.11 and 0.17 ppm at dilute and 0.18 and 0.24 at saturated concentrations). The larger shielding of the C8-H is ascribed to the ring current effect (Figure S1.4). The gained negative charge from deprotonation of adenine is shared on all five nitrogen atoms of the purine ring which in turn shields the neighbouring carbons in the ^{13}C NMR spectra, hence the deshielding of carbons indicates which neighbouring nitrogen atoms are involved in the ionic bond. In Table 2, the ^{13}C NMR chemical shifts for the imidazole ring carbons i.e. C4, C5 and C8, are deshielded relative to adenine, highlighting the 5 membered ring's involvement in the ionic bond. Moreover, the C4 and C8 are the most deshielded, suggesting the N9 as the site of coordination. The deshielding of the ^1H and ^{13}C NMR chemical shifts of K-Ade(18C6) suggests that the 18C6 ether does not remove the K^+ counter ion from K-Ade.

Table 2.2: ^1H and ^{13}C NMR chemical shifts (ppm) of adenine, Na-Ade, K-Ade and K-Ade(18C6) in DMSO-d_6 as solvent at saturated concentrations. The values in parentheses are the changes relative to free Adenine.

	^1H NMR chemical shifts				
	C2-H	C8-H	NH_2		
adenine[a]	8.11	8.09	7.08		
Na-Ade[b]	7.90(−0.21)	7.66(−0.43)	5.94(−1.14)		
K-Ade[c]	7.72(−0.39)	7.42(−0.67)	-		
K-Ade(18C6)[d]	7.81(−0.30)	7.50(−0.57)	-		
	^{13}C NMR chemical shifts				
	C2	C4	C5	C6	C8
adenine[a]	152.4	150.6	118.2	155.6	139.2
Na-Ade[b]	146.9(−5.5)	157.7(+7.1)	119.7(+1.5)	154.3(−1.3)	149.4(+10.4)
K-Ade[c]	147.9(−4.5)	160.7(+10.1)	121.7(+3.5)	155.0(−0.6)	150.5(+11.3
K-Ade(18C6)[d]	147.5(−4.9)	161.2(+10.6)	121.8(+3.6)	154.0(−1.6)	151.1(+11.9)

[a] Adenine at 73.2 mM [b] Na-Ade at 52.2 mM, [c] K-Ade at 84.8 mM [d] K-Ade(18C6) at 78.7 mM

© University of Pretoria

From ^{13}C NMR spectroscopy, the site of coordination of the counter ion with the adeninate anion cannot be determined with certainty. The crystal structures of Na-Ade and K-Ade provide insight into the potential coordination sites in solution, refer to SI 1 for experimental details. The crystals were obtained for Na-Ade, Figure 2.7, and K-Ade (SI, Figure S1.13) in anhydrous DMSO-d_6, (crystallographic information: Table S1.3 in the SI) under inert conditions (N_2 gas). The XRD crystal structure obtained for Na-Ade(15C5) resulted in the same geometric parameters as those obtained for Na-Ade and therefore the data is not given. Selected geometric parameters of the crystal structures of Na-Ade and K-Ade are given in Table S1.4.

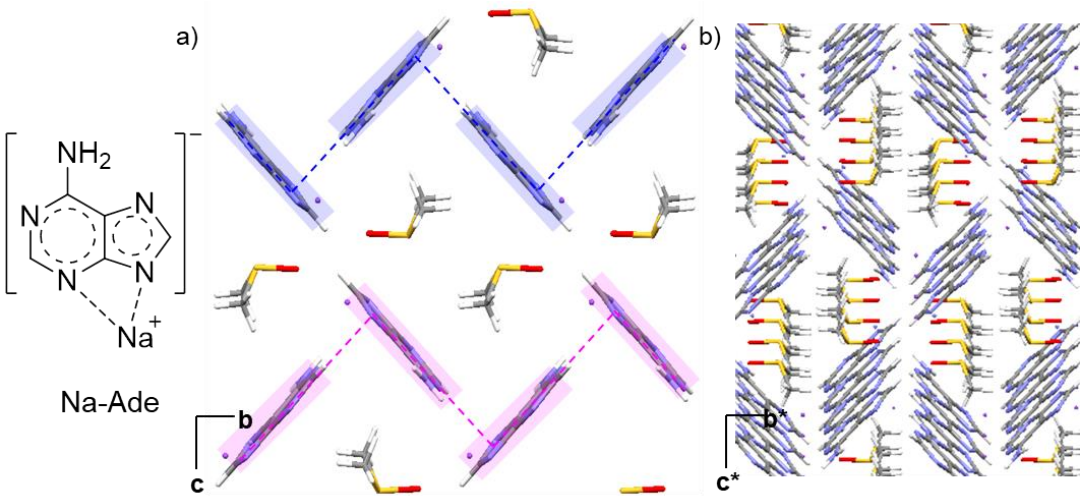

Figure 2.7: Molecular structure of Na-Ade and XRD structure of the zigzag packing morphology of crystals obtained from DMSO-d_6 solutions, viewed along the a axis. Refer to Figure S1.13 for K-Ade data.

The crystal system for both the Na-Ade and K-Ade display a zigzag packing morphology (Figure 2.7a) along the a axis in which there is a T-shape edge to face arrangement. Along the c axis, the next row of units is inverted along the b axis, cancelling the dipole moment of the units and lowering the energy. In both the Na- and K-Ade crystal structures, two DMSO-d_6 solvent molecules per Na-Ade/K-Ade are trapped within the channels formed by four Na-Ade (Figure 2.7b) and K-Ade units packed edge to face to form a rectangular cage. The DMSO-d_6 molecules occur in groups of two, oriented in the opposite direction to each other minimizing the steric hindrance between the methyl groups and increasing contact between the O atom and the cation. The crystal packing shows that each Na^+/K^+ counter ion is coordinated to three adeninate anion molecules via the N1, N7 and N9 atoms of three purine rings (Figure 2.8). Conversely, one adeninate anion is coordinated to three Na^+ or K^+ counter ions via the N1, N7 and N9 atoms. This is in agreement with previous research showing that the coordination sites of the adeninate anion are predominantly N1, N9 and N7.[122]

The crystal structure of K-Ade(18C6), Figure 2.9, provides information on the effect of the crown ether, showing the N3 and N9 atoms acting as a chelate in coordination with one K^+ counter ion almost equally positioned between the N3 and the N9 atom. The K^+ ion is simultaneously interacting with one 18C6 ether molecule and one adeninate anion. The K^+ and 18C6 coordination is slightly perched, with a *d* value of 0.924(8) Å (distance of K^+ from the centroid of the 18C6, Figure 2.9b).

© University of Pretoria

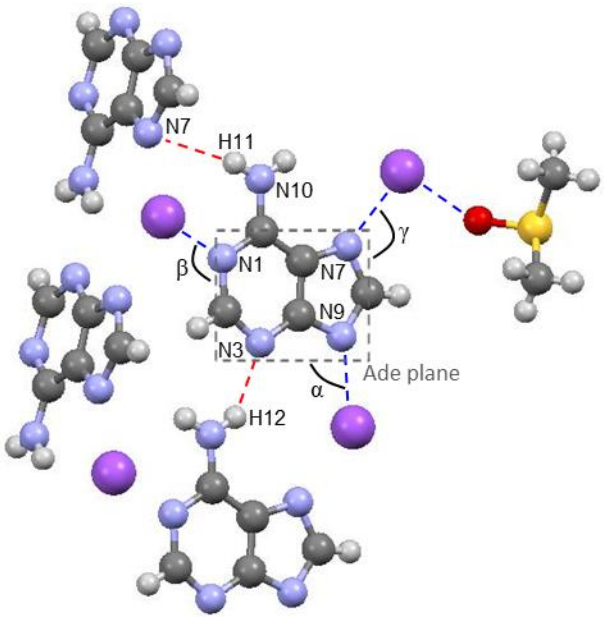

Figure 2.8: Coordination obtained from XRD of Na-Ade showing one counter ion complexed with three adenine molecules and one adenine complex with three counter ions. The numbering of specified atoms and dihedral angles relate to the geometric parameters are given in Table S1.4. Refer to Figure S1.14 for K-Ade data.

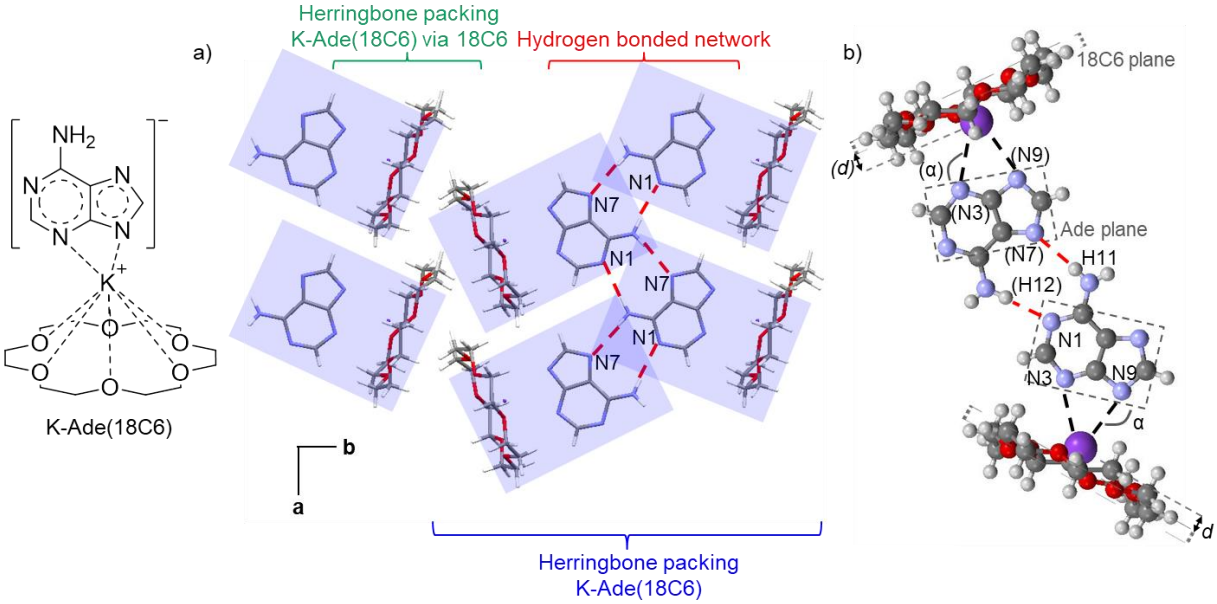

Figure 2.9: a): Herringbone (blue) XRD packing morphology of the K-Ade(18C6) crystal obtained from DMSO-d_6 solutions viewed along the indicated axis and b) the hydrogen bonding (red lines) and interaction with the K^+ ion at the N3 and N9 atoms (black lines). The numbering of specified atoms and dihedral angles relate to the geometric parameters are given in Table S1.4.

A herringbone packing morphology of the K-Ade(18C6) units along the a axis is observed (Figure 2.9a) wherein a hydrogen-bonded network exists in which the adeninate anion molecules are linked

© University of Pretoria

via mixed WC and HG type hydrogen bonding. From the same set of crystals, a second morphology is obtained, Figure S1.15, in which there is a positional disorder in the system. Note that no DMSO solvent is included in the crystals in the presence of crown ether.

From the above results, it can be inferred that the N3 and N9 atoms are the most likely preferred sites of coordination in solution as the positively charged counter ion will interact with two lone pairs, one on each nitrogen atom. The size dependency of the counter ion for the N3-N9 coordination will favour that of the K^+ ion as it is larger and more suitable for the bridging between the two atoms, K-Ade(N3N9) in Figure 2.10. The Na^+ ion can chelate, Na-Ade(N3N9), or coordinate via either the N9 or the N3 site (Na-Ade(N9) and N-Ade(N3)).

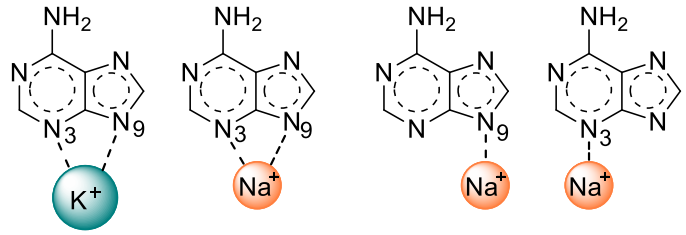

Figure 2.10: Proposed counter ion coordination between K^+ and Na^+ with the adeninate anion via the N3N9, N9 or N3 nitrogen atoms.

Co-ordination at the N3 and N9 sites avoids possible repulsion from the hydrogen atoms of the NH_2 group associated with coordination at the N1 and N7 atoms, Figure 2.11 M-Ade(N1) and M-Ade(N7). No direct evidence for cation-π interactions, Figure 2.11 M-Ade(π), has been observed and the effect of the presence of the different counter ions on the ^{13}C NMR chemical shifts is too large to be due to only electrostatic interactions between the π system and the counter ion. The difference between the ^{13}C chemical shifts of K-Ade and Na-Ade range from 0.9 – 3.0 ppm for the imidazole ring whereas the difference between K^+ and Na^+ in a cation-π interaction with benzene is predicted to be 0.13 ppm.[123] It has been shown that compounds containing heteroatoms, such as imidazole, pyridine and aniline have the cation interact with the heteroatom in preference to the aromatic system, with the cation-π interaction being significantly low for imidazole.[124]

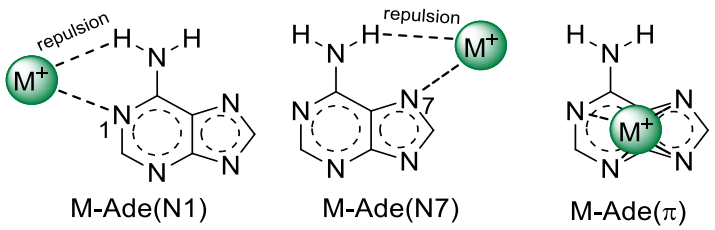

Figure 2.11: Unlikely ion-pair interactions. Repulsion of counter ion M^+ (where $M^+ = Na^+$ or K^+) with the hydrogen on the NH_2 disfavours coordination via the N1 (M-Ade(N1)) and N7 (M-Ade(N7)) atoms. The potential cation-π interaction (M-Ade(π)) is predicted to be weaker than the cation-heteroatom interactions.

© University of Pretoria

2.3.3 Concentration dependent ^{1}H NMR chemical shifts of Na-Ade, K-Ade, Na-Ade(15C5) and K-Ade(18C6)

Concentration dependent ^{1}H NMR studies were performed to investigate the ion-dependent self-aggregation of the ionic complexes. The concentration dependent ^{1}H NMR spectra of Na-Ad and K-Ade are shown in Figures S5a and b. To gain further understanding of the influence of the cation and the effect of the potential complexation of the K-Ade with 18C6, ^{1}H NMR studies in the presence of 2.4 equivalents of 15C5 ether for Na-Ade (Na-Ade(15C5)) and 18C6 ether for K-Ade (K-Ade(18C6)), (Figure S1.5c and d) were conducted. A graphical representation of the shifts on a common axis is given in Figure 2.12.

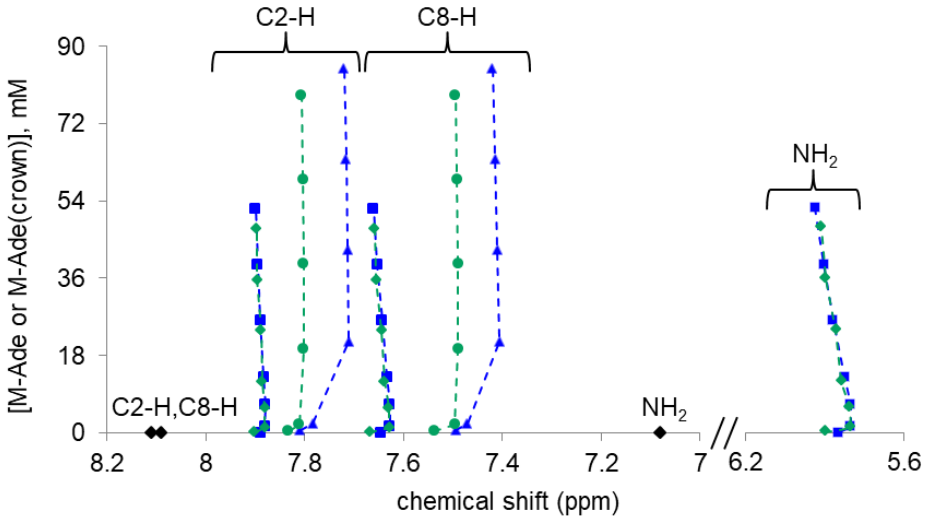

Figure 2.12: Graphical representation of the concentration dependent ^{1}H NMR chemical shift for the indicated protons of Na-Ade (blue squares), Na-Ade(15C5) (green diamonds), K-Ade (blue triangles) and K-Ade(18C6) (green circles) at the indicated concentrations (mM) in DMSO-d_6 at 320 K. Chemical shifts of Adenine purine protons are shown in black for comparison purpose.

The change in ^{1}H NMR chemical shifts with the change in concentration ($\Delta\delta = \delta_0-\delta_n$, where δ_0 is the chemical shift of the reference point at the lowest concentration and δ_n of higher concentration) of the ionic complexes are shown in Figure 2.13. Two concentration dependent regions with opposite changes in chemical shift are observed in Figure 2.13a, indicated as region 1 and region 2. Region 1 showed shielding of both purine protons. These changes in $\Delta\delta$ direction occur at a higher concentration for K-Ade (about double that of Na-Ade). Since changes in chemical shift imply a change in electron density around the nuclei, a change in the trend of $\Delta\delta$ with increasing concentration suggests a structural change with new non-covalent interactions such as the formation of aggregates.

The respective ^{13}C NMR spectra for region 2 of Na-Ade and K-Ade, Figure S1.6, show that the C2 becomes deshielded and the C8 shielded for Na-Ade with increasing concentration and vice versa for K-Ade indicating that there is an ion-dependent difference in the nature of the aggregates formed. The concentration dependent chemical shifts of the purine protons of Na-Ade(15C5) and K-Ade(18C6) still exhibit two regions, Figure 2.13b. The change in chemical shift with concentration is

© University of Pretoria

less prominent in K-Ade(18C6) than for K-Ade, having region 1 of the former affected to a smaller extent. Na-Ade(15C5) indicates a larger concentration dependent chemical shift change in region 1 compared to Na-Ade. With these observed differences in the chemical shifts of Na-Ade and K-Ade in the presence of the 15C5 and 18C6 ether, it is clear that complexation between the counter ion with the crown ether occurs to some extent, being larger for the K^+ complex than for the Na^+ complex.

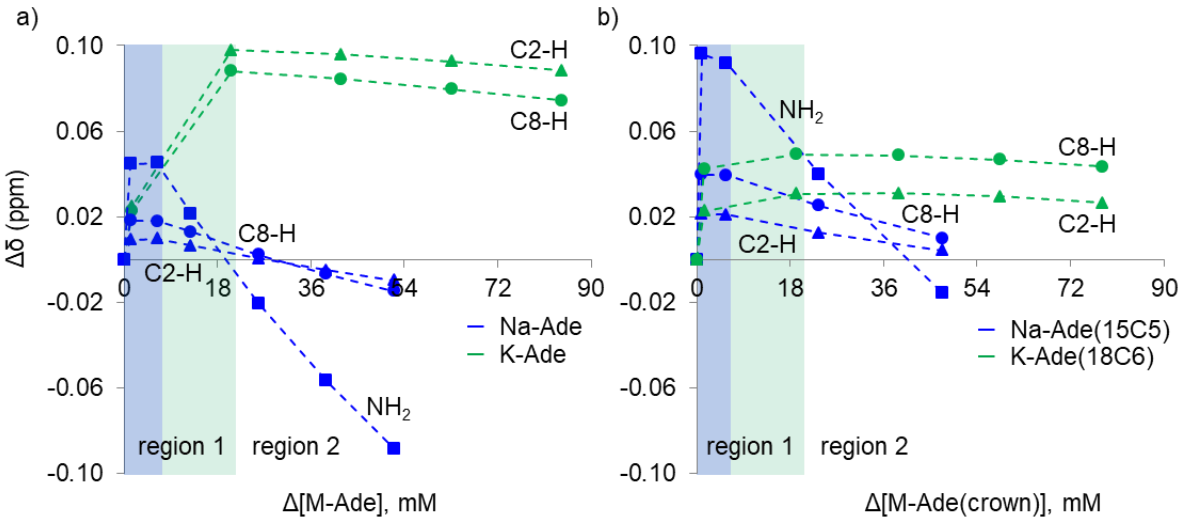

Figure 2.13: Change in chemical shift of purine protons with the change in concentration for a) Na-Ade (blue lines) and K-Ade (green lines) and b) Na-Ade(15C5) (blue lines) and K-Ade(18C6) (green lines) in DMSO-d_6 at 320 K. NH_2 – squares, C8-H – circles and C2-H – triangles. The added concentration of crown ether is 2.4 times that of Na-Ade (K-Ade). Region 1 (highlighted in blue and green for Na-Ade and K-Ade, respectively) and region 2 indicates concentration dependent change in chemical shift.

A plot of the change in chemical shift for the CH_2 of 15C5 ether of Na-Ade(15C5) and 18C6 ether of K-Ade(18C6) with change in concentration is shown in Figure 2.14.

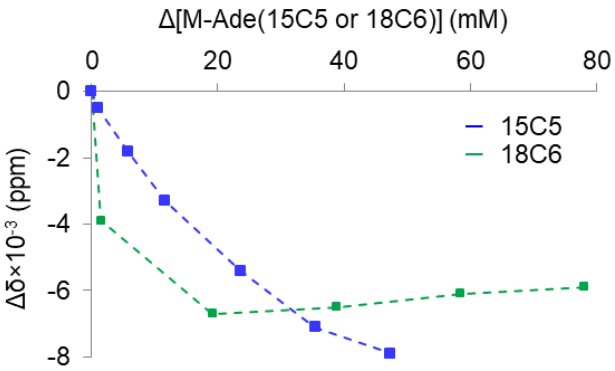

Figure 2.14: Change in chemical shift of the CH_2 protons of 15C5 and 18C6 ether with concentration in the presence of Ade^-Na^+ and Ade^-K^+, respectively, at a 2.4-fold excess concentration of crown ether and 320 K in DMSO.

© University of Pretoria

The complexation of a crown ether with a metal cation is driven by the electrostatic interaction of the metal cation with the ether backbone and results in a deshielding of the CH_2 protons as electron density is donated by the oxygen atoms to the counter ion.[125] The deshielding of the CH_2 protons upon increasing concentration of the Na-Ade(15C5) implies increased complexation with the Na^+. Similarly, the 18C6 initially experiences rapid deshielding from complexation with K^+ but this is followed by slight shielding, indicating partial release of the K^+ ion. Such an observation could indicate that the K^+ is complexing with another species such as the adeninate anion at higher concentrations.

2.3.4 ^{1}H NMR temperature coefficient of Na-Ade, K-Ade, Na-Ade(15C5) and K-Ade(18C6)

In ^{1}H NMR spectroscopy, the effect of aggregation on the proton chemical shift depends on whether the mode of interaction is hydrogen bonding or π-π stacking. For hydrogen-bonded aggregates, decreasing the concentration or increasing the temperature leads to the dissociation of the hydrogen bonded complex, increasing the shielding of the formerly hydrogen bonded protons. For π-π stacked complexes, decreasing the concentration or increasing the temperature leads to deshielding of the protons that were shielded by the ring current of the neighbouring molecule in the stacked complex. Temperature dependent studies are typically conducted over the range of concentrations to investigate how increasing the temperature of the solution affects the interactions between molecules as the distance between them is increased. The change in chemical shift of a proton with the change in temperature gives the temperature coefficient ($\Delta\delta/\Delta T$) which is used to monitor hydrogen bonding and π-π stacking between molecules.[72,98] $\Delta\delta_T = \delta_{T0} - \delta_{Tn}$, where δ_{T0} is the chemical shift of the reference point at the lowest temperature and δ_{Tn} of higher temperature. Dissociation of hydrogen bonds leads to shielding of the involved protons and therefore a negative $\Delta\delta/\Delta T$ value. Protons exposed to solvent molecules will experience a large negative temperature dependence of the chemical shift as the hydrogen bonds with the solvent are broken. The reduction in temperature coefficient with increasing concentration indicates hydrogen bonded adducts whereby shielding of the protons from hydrogen bonding with solvent molecules occurs, which in turn results in a decreased dependence of the proton chemical shift with temperature.[72] For molecules in solution, as the dissociation energy of hydrogen bonds increases, the dependence of the chemical shift on temperature decreases as a larger amount of energy is needed to distort the bond.[47] The effect of temperature on stacked dimers can also be studied using $\Delta\delta/\Delta T$.[98] Dissociation of dimers involved in π-π stacking results in the deshielding of purine protons and hence a positive temperature coefficient ($\Delta\delta/\Delta T > 0$).[98] Depending on the solvent used, hydrogen bonded (chloroform as a solvent) or stacked dimers (solvents such as water or DMSO) occur upon increasing concentrations of adenine, leading to the deshielding of the NH_2 protons[72] or shielding of the purine protons,[98] respectively. The competing H···O interaction between the amino group of adenine with water has a larger interaction energy than H···N, promoting the formation of stacked dimers over hydrogen bonded dimers.[16,30] DMSO should have a similar effect due to the partially negative oxygen available for hydrogen bonding.

To gain insight into the possible involvement of the Na- and K-Ade in hydrogen bonding and π-π stacking with increasing concentration, the change in the temperature coefficient for the purine protons of Na-Ade and K-Ade at various concentrations was investigated. The change in the temperature coefficient with concentration is shown for the purine protons of Na-Ade and K-Ade,

© University of Pretoria

Figure 2.15a, and for the CH_2 protons of the 15C5 and 18C6 ether, Figure 2.15b. Refer to Figure S1.8 for the temperature coefficient of Na-Ade(15C5) and K-Ade(18C6).

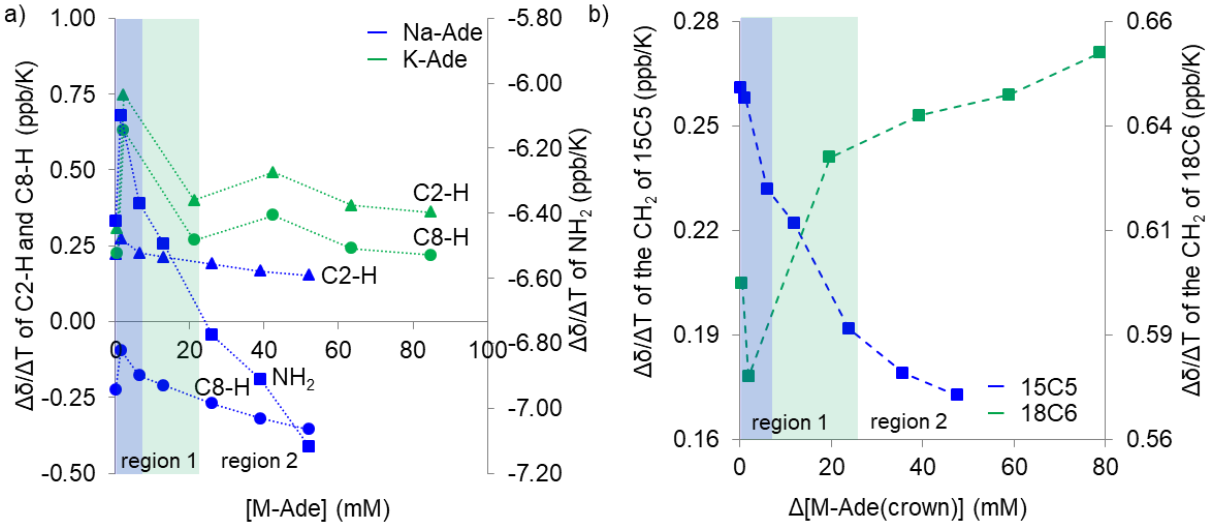

Figure 2.15: The change in temperature coefficients with concentration of ^{1}H chemical shifts of a) Na-Ade and K-Ade and b) CH_2 of 15-crown-5 ether and the 18-crown-6 ether in DMSO-d_6. NH_2 (squares), C8-H (circles) and C2-H (triangles). The shading relates to the regions defined in Figure 2.13. Refer to Figure S1.7 for the change in δ with temperature (300 K - 380 K).

The temperature coefficient of the NH_2 of Na-Ade (secondary axis in Figure 2.15a) is initially reduced (less negative) and then increased (more negative), showing a change between two forms of aggregates whereby the protons are involved in hydrogen bonding that is stronger in region 1 than in region 2. The increased shielding with increasing concentration in region 2 suggests that any aggregate formation involving these protons either (i) requires less energy to disrupt than the hydrogen bonding with solvent molecules or (ii) that the protons are directly exposed to the solvent. The concentration dependent chemical shift of Na-Ade; in Figure 2.13a, region 2; indicates that the molecules are involved in hydrogen bonding upon self-aggregation supporting the former conclusion. The absence of the NH_2 peak in the ^{1}H NMR spectra of K-Ade does not allow for this analysis.

The presence of 15C5 ether resulted in a reduced temperature coefficient of the NH_2 protons, Figure S1.8, in region 2 indicating either (i) shielding of these protons from the solvent or (ii) stronger hydrogen bonding involved in the aggregate formation as compared to that of the Na-Ade aggregates. This latter would suggest a difference in the arrangement between the aggregated molecules of Na-Ade(15C5) and Na-Ade. For K-Ade, the presence of the 18C6 ether eliminates the difference in temperature coefficient between regions 1 and 2 and there appears to be only a very slight concentration dependent change in the temperature coefficient.

The CH_2 of both the 15C5 and 18C6 ethers become deshielded with an increase in temperature, Figure 2.15b, suggesting increasing interaction of the counter ion with the relevant crown ether as the complex of the adeninate anion with Na^+ or K^+ is dissociated. Increasing concentrations of Na-

© University of Pretoria

Ade(15C5) resulted in a decrease in temperature-dependence, indicating that either (i) aggregation stabilizes complex formation between the Na-Ade with the 15C5 ether, preventing the dissociation of Na-Ade(15C5) into the free adeninate anion and Na(15C5) or (ii) aggregate formation in region 2 limits the amount of Na^+ ions available for complexation with the 15C5. The CH_2 of K-Ade(18C6) has increased temperature coefficients in region 2 where there is increased interaction between the K^+ ions and the 18C6 as the temperature is increased.

The above concentration and temperature dependent ^{1}H NMR chemical shifts have been used to propose two modes of aggregation that are discussed below.

2.3.5 Aggregation by π-π stacking and in-plane dimerization

Region 1 observed in the concentration dependent ^{1}H NMR spectra of Na- and K-Ade, Figure 2.13a, showed shielding of both purine protons, which indicates π-π stacking of the ionic complexes. The gain of electron density in the purine system (shielding of protons) with an increase in Na-/K-Ade concentration otherwise cannot be explained using general concepts. The shielding of the purine ring and NH_2 protons is attributed to the ring current effect experienced by the neighbouring molecule in π-π stacked dimers. The observed changes in region 1 are not explained by ion-pairing which would have caused deshielding of purine protons as electron density would be pulled from the ring system with the formation of an ionic bond/interaction. Hydrogen bonding is also ruled out since the NH_2 protons of Na-Ade become shielded which should not be observed with hydrogen bonding as hydrogen bonds would extend the N-H bond length resulting in deshielding of the proton.

Highlighting the gain and loss of electron density in the ^{13}C NMR chemical shifts of Na- and K-Ade relative to adenine, Figure 2.16a, it is clear that the purine ring is partially positive in the imidazole ring and negative in the pyrimidine ring. In the presence of competitive hydrogen bonding with DMSO solvent molecules, the dimerization between two M-Ade molecules would be driven by π-π stacking due to stabilizing electrostatic interactions between the oppositely charged sections of the purine ring, having the 5 membered ring of one molecule stack with the 6 membered ring of the neighbouring molecule. This can occur via either antiparallel face to face or antiparallel displaced stacking, Figure 2.16b. Anti-parallel stacking has been suggested for deprotonated purines.[126] These stacked dimers can be further enhanced by hydrogen bonding of the NH_2 group with the N3 and N9 atom on the neighbouring ring and additional stabilization can occur if the counter ion moves from in-plane to out-of-plane coordination (Figure 2.16c) allowing for a bridging interaction with both adeninate anion molecules, coordinating to the N3, N9 and N7 atoms. The larger sized K^+ counter ion could bridge between two neighbouring molecules more readily than the smaller, more tightly bound Na^+ counter ion. In aqueous media, the self-association of nucleotide bases is driven by π-π stacking in which the association constants for nucleic acids involved are in the order of purine-purine > purine-pyrimidine > pyrimidine-pyrimidine.[8] Therefore, at low concentrations, with competitive hydrogen bonding to DMSO solvent molecules, π-π stacking of the adenine salts is highly likely to be the dominant form of aggregation.

The ability of hydrogen bonding between Na-Ade and K-Ade molecules is considered, Figure 2.16d, in which Watson-Crick Hoogsteen (HB-N7N1), Hoogsteen-Hoogsteen (HB-N7N7) and Watson-Crick-Watson-Crick (HB-N1N1) bonding can occur. Analysis of the charge pairing indicates that the HB-

© University of Pretoria

N7N1 would be the most likely form and is the conformation observed in the hydrogen bonding of the K-Ade(18C6) crystal packing. However, in region 1, the possibility of these hydrogen bonded dimers is less likely to be the predominant species in solution as it would require the displacement of the hydrogen bonded DMSO solvent molecules whereas the π-π stacking has to displace the weaker solvent-purine ring dipole forces.

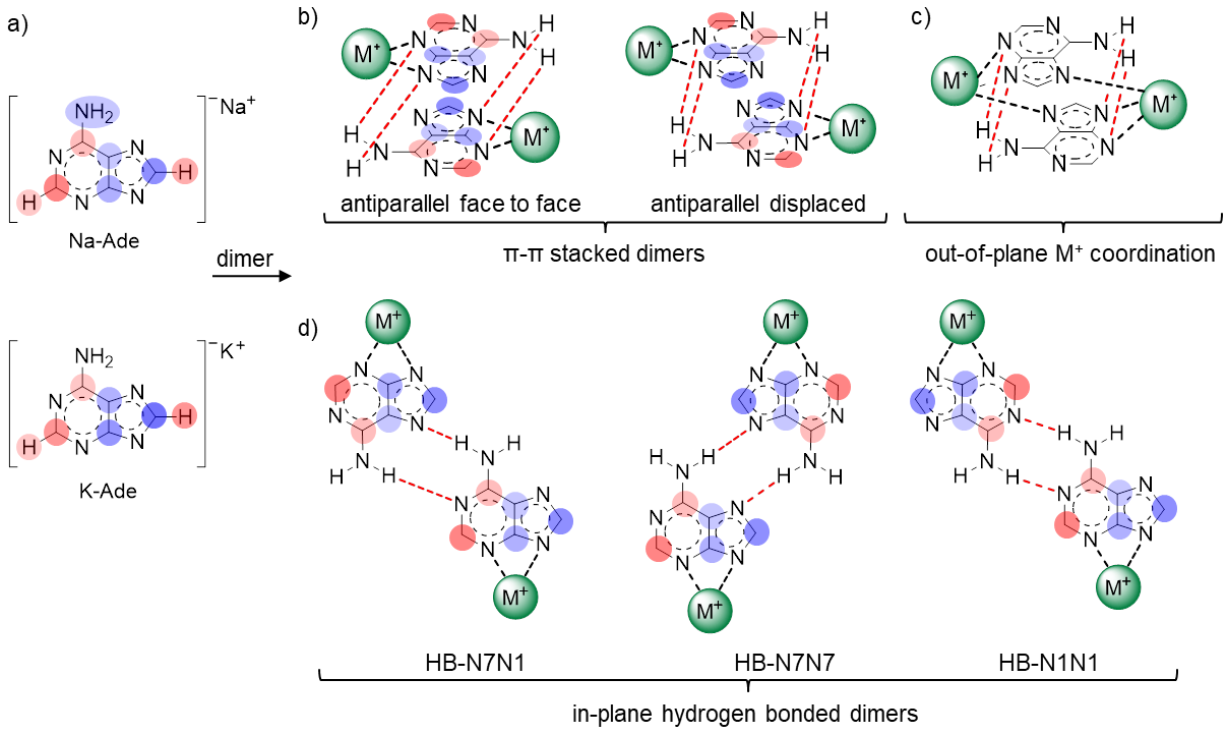

Figure 2.16: a) Cation induced change in atomic electron density in Na-Ade and K-Ade relative to Adenine, based on the NMR chemical shifts in Table 4. Two shades of blue indicate shifts towards more positive, red towards more negative charge. Suggested structures of π-π stacked dimers with the cation b) in-plane and c) shared between the two adeninate anions, and d) in-plane hydrogen bonded dimer structures. Hydrogen bonding is indicated by red lines.

The absence of the NH_2 peak at all concentrations in the ^1H NMR spectra of K-Ade indicates that the interaction of K^+ with the adeninate anion is different from that of Na^+. Thus, an alternative protonation state or proton exchange regime of the NH_2 group of K-Ade, either with the hydrogen bonded DMSO or neighbouring adeninate molecules, could explain why the protons are not observed in the ^1H NMR spectra. The nuclear electric quadrupole moment of K^+ is smaller than that of Na^+, so its coupling with the hydrogen atoms is an unlikely reason for additional relaxation. If the π-π stacked dimer does indeed occur, this phenomenon could be supported as the K^+ counter ion would be closer to the hydrogen atoms or shared or in a dynamic equilibrium between two adeninate anions.

The addition of 15C5 ether to Na-Ade did not result in a large difference in ^1H NMR chemical shifts concluding that it did not completely interact with the Na^+ from Na-Ade. The ability of the solvent to solvate the cation will influence the association constant for the M^+-crown formation.[127] Solvents with high solvating abilities (indicated by the Gutmann Donor number, DN) such as DMSO (DN =

© University of Pretoria

29.8), methanol (DN = 19) and water (DN = 18) compete with the crown ether for complexation of the metal cation and destabilize the complex.[127] The Na^+(15C5) complex is a perched complex allowing for the Na^+ to interact with solvent molecules.[125] Therefore, in the presence of DMSO solvent molecules and the highly competing adeninate anion, the complexation between Na^+ and 15C5 ether will be significantly reduced.

The addition of 18C6 to K-Ade resulted in reduced concentration dependence in region 1, Figure 2.13b, and at the very dilute concentrations of region 1, the ^{1}H NMR peak of the NH_2 protons became visible (Figure 2.6a insert). It is proposed that the 18C6 complexed with the K^+ formed a new complex whereby the K^+ ion is simultaneously interacting with the 18C6 and the adeninate anion. The crystal structure of K-Ade(18C6) reveals the feasibility of such an interaction and is supported by the lack of evidence for removal of the K^+ in the ^{1}H and ^{13}C NMR spectra. The K^+(18C6) complex is destabilized by the presence of the DMSO solvent molecules or any competitive complexing molecule, such as the adeninate anion, and hence the K^+ will not complex to the 18C6 ether alone. The formation of an adeninate-K^+-18C6 complex is likely to disfavour aggregation via π-π stacking. Thus, in region 1 of Figure 2.13b, monomers of K-Ade(18C6) complex are likely the predominant species. The increased shielding of the purine protons with concentration in region 1 can be linked to the gain of electron density in the purine ring as the 18C6 ether complexes with the K^+ of K-Ade, reducing the level of interaction between the adeninate anion and K^+. In-plane mixed WC-HG hydrogen bonded dimers such as those observed in the XRD crystal structure of K-Ade(18C6), Figure 2.9b, might occur in region 2. It is to be noted that the UV data in which the free adeninate anion was observed was obtained in high excess of the crown ether and at very low concentrations of the adeninate anion (below the limit of detection for NMR spectroscopy), which made it possible to remove the counter ion from the adeninate anion.

Evidence of abstraction of the K^+ from the 18C6 in Figure 2.14 region 2, in which the CH_2 protons become shielded as electron density is regained, suggests an influence of the aggregate formation on the interaction between K^+ and 18C6 ether, resulting in the partial release, Figure 2.17.

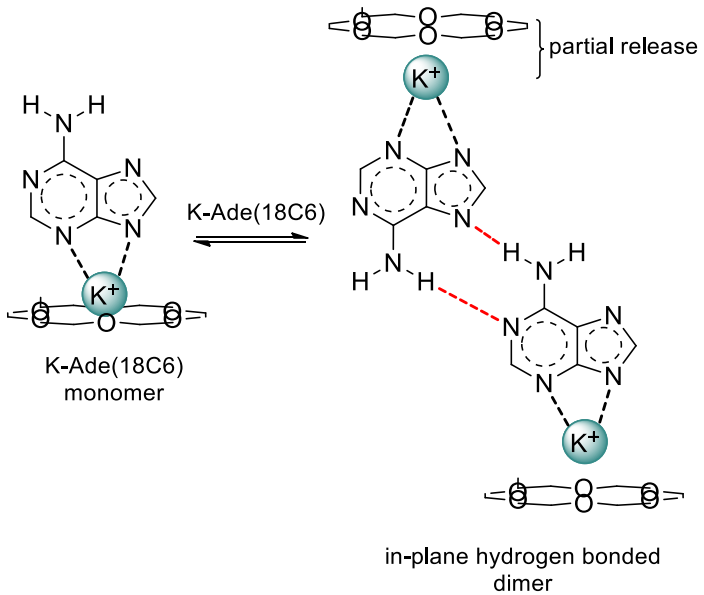

Figure 2.17: Hydrogen bonded aggregates of K-Ade(18C6). Hydrogen bonding is shown by red dashed line.

© University of Pretoria

Upon increasing the temperature and shifting the equilibrium towards the monomer form, the 18C6 would engage in tighter binding once again as suggested by the increased temperature coefficient in Figure 2.15b showing increased interaction between the K^+ ions and the 18C6. The absence of the NH_2 peak at higher concentrations could be a result of imine formation involving significant dynamics of chemical shifts. From the crystal structure of K-Ade(18C6), the hydrogen bond lengths between the NH···N7 and NH···N1 differ between the linked molecules, having the latter differ quite significantly, 2.262 vs 2.160 Å, which could arise from imine formation.

2.3.6 Higher order aggregates

Apart from providing insight into the site of coordination between the counter ion and the adeninate anion, the crystal structures provide an interesting comparison and perhaps even some guidance for the aggregate structures of Na- and K-Ade in solution. The Na- and K-Ade complexes in the crystal structures do not show in-plane adeninate-adeninate anion mixed WC-HG hydrogen bonded aggregates as observed in K-Ade(18C6), nor are π-π stacked aggregates evident. Instead, the Na- and K-Ade complexes are linked via the counter ions. Hydrogen bonds occur between the NH_2 of one molecule with an N3 and N7 of two neighbouring molecules. This could suggest that higher order aggregate formation in region 2 of Figure 2.13a is governed by the complexation of M-Ade molecules via the counter ions present, Figure 2.18, through the coordination of N1 or N7 to the counter ion of the neighbouring M-Ade molecule. Aggregation of this type could result in the migration of the counter ion between the N3 or N9 position allowing the N9 or N3, respectively, to be available for hydrogen bonding. Dissociation of these aggregates with increased temperature would result in shielding of the NH_2 protons involved in the hydrogen bond with the N3/N9 of the neighbouring molecule, and i.e. shielding of the C8–H and deshielding of the C2–H as the counter ion moves back from the N9 into the N3N9 coordination site, as observed with the temperature coefficient in Figure 2.15a. It has been suggested that the C8–H could be involved in hydrogen bonding with DMSO,[128] therefore, this effect has not been ruled out as an additional influence on the chemical shift.

The concentration dependent change in the temperature coefficient in Figure 2.15a for K-Ade showed that both purine protons undergo deshielding in region 2 that decreases with increasing concentration. This effect is ascribed to the temperature dependent solvent electric field effect as no explanation can be provided considering the disruption of hydrogen bonds. The cation has a peripheral solvation shell of DMSO solvent molecules which orient their dipoles towards the cation, Figure 2.18. The positive charge on the cation would be partially reduced as an inflow of electron density from the partially negative O atom of DMSO will occur, weakening the K^+ ionic bond with the adeninate anion. An increase in temperature disrupts this ordered arrangement of DMSO molecules,[67] strengthening the ionic bond between K^+ and the adeninate anion, leading to deshielding of both purine protons. If the higher order aggregates in region 2 shield the cations from the solvent, this effect would reduce with increased concentration, which is what is observed with the reduced temperature coefficient of K-Ade. The proposed aggregate formation is one whereby one K-Ade coordinates via the N7 to the K^+ of the neighbouring K-Ade molecule which then has another neighbouring molecule coordinate via the N1. This type of aggregation will begin to shield the counter ion from the solvent, reducing the solvent electric field effect.

© University of Pretoria

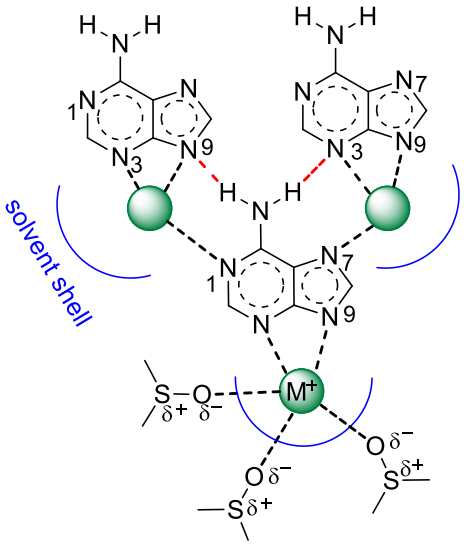

Figure 2.18: M-Ade aggregate formation via the N1 and/or the N7.

The above proposed aggregate formations do not rule out the π-π stacking believed to occur at the lower concentrations of region 1 as the complexation of the ionic complexes in higher order aggregates in region 2 can disrupt the aggregation in region 1. Adenine has been reported to form trimers and higher order aggregates upon self-association.[17] Dimer formation has been observed for adenine, adenosine and adenosine monophosphate at concentrations lower than 5 mM, followed by higher order aggregation at concentrations > 5 mM ascribed to the polymerization of dimers.[129] This provides confidence that dimer formation can occur at low concentrations (region 1), followed by the formation of higher order aggregates with increasing concentration (region 2).

2.3.7 Thermodynamics of the self-aggregation

Two processes are possible for a single adeninate anion, the first is the ion-pairing between the adeninate anion and the counter ion Na^+/K^+ and the second is the self-aggregation of the ion pairs. It is assumed here that i) the self-complexation between free adeninate anions is negligible and ii) a significant amount of ion-pairing already exists. The concentration dependence of the chemical shifts observed in Figure 2.13 for Na-/K-Ade, Na-Ade(15C5) and K-Ade(18C6), is ascribed to self-aggregation and can occur via monomeric metal-adeninate (M-Ade) addition, i.e. monomer→ dimer→ trimer etc. The isodesmic and trimer models were used to fit the normalized ^{1}H NMR data of region 2 (refer to Table S1.1 for the association constant values). In addition, the thermodynamic data for the 1:1 complexation between 15C5 ether with the Na^+ were obtained (Table S1.2). This was not possible for the complexation between 18C6 ether with K^+.

The van't Hoff plot for the self–aggregation of Na-Ade, Na-Ade(15C5) and K-Ade and for the 1:1 complexation between 15C5 ether and Na^+ is shown in Figure 2.19. The thermodynamic data are given in Table 2.3.

© University of Pretoria

Table 2.3: Aggregation constants and thermodynamic parameters for the self-aggregation of Na-Ade, Na-Ade(15C5) and K-Ade and the association constant for the 1:1 complexation between C15C and Na^+ in DMSO-d_6 as solvent at 305 K

Complex	K_{agg} (M^{-1})	ΔH (kJ mol^{-1})	ΔS (J $mol^{-1}K^{-1}$)	ΔG_{305K} (kJ mol^{-1})
Na-Ade[a]	2.4 ± 0.3	−4.7 ± 0.2	−8.0 ± 0.5	−2.2
Na-Ade(15C5)[a]	3.0 ± 0.5	−5.2 ± 0.5	−8.3 ± 1.6	−2.7
	K (M^{-2})			
K-Ade[b]	0.59 ± 0.03	−4.5 ± 0.3	−19 ± 1	+1.4
	K_1			
Na-Ade(15C5)[c]	28 ± 3	−23 ± 2	−50 ± 5	−8.4

[a] Isodesmic ^{1}H NMR model, [b] Trimer ^{1}H NMR model, [c] 1:1 Guest:host model

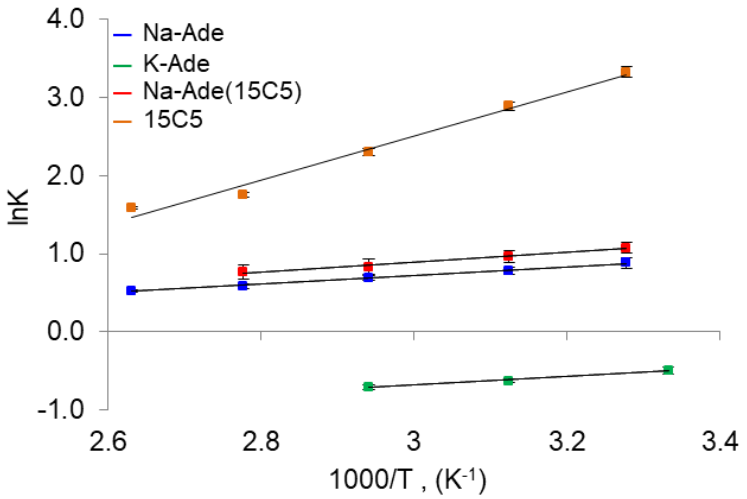

Figure 2.19: Van't Hoff plot of the association constant for the self-aggregation of Na-Ade (blue), Na-Ade(15C5) (red) and K-Ade (green) and the 1:1 complexation between 15C5 ether and Na^+ in DMSO-d_6 as the solvent.

The association constants of aggregation are small and dominated by enthalpic interactions in the order of −5 kJ mol^{-1}, which compares with a weak water-amide N···hydrogen bond and is smaller than that of the self-aggregation of 9-ethyladenine[25,130] which has an enthalpy of formation of −16.7 kJ mol^{-1} associated with more than one hydrogen bond. Cyclic dimer formation (two hydrogen bonds involved in the dimer) is largely preferred over linear dimers (one hydrogen bond).[14] Considering the above proposed ion-assisted aggregate formation, only one hydrogen bond is involved between two M-Ade molecules and it can therefore be expected that the enthalpy of formation will be about half. The gain in enthalpy is in part compensated by negative entropies of association of about −8 J $mol^{-1}K^{-1}$, which is much less than the value of −145 J $mol^{-1}K^{-1}$ that should typically be expected for the loss of translational entropy of a Na-Ade unit due to conformational order.[131] Much of it must be compensated by a large gain in entropy of liberated solvent molecules during aggregation of Na-Ade and the gain in vibrational entropy[132] from the formed weak hydrogen bond which would result in loose NH vibration. In addition, if the π-π stacked dimer, which would have more order, is dissociated upon larger aggregate formation, this would also increase the

© University of Pretoria

entropy. The equilibrium of the K-Ade aggregate is slightly disfavoured as seen by the slight positive ΔG.

The change in enthalpy (ΔH = −23 kJ mol^{-1}) for the 1:1 complexation between Na^+ and 15C5 ether is slightly larger than that previously reported in DMF[133] and DMSO[134] (ΔH = −20 and −15 kJ mol^{-1}, respectively) and is attributed to the use of anhydrous DMSO-d_6. The presence of water significantly reduces the binding of Na^+ to 15C5 ether.[134]

2.4 Conclusion

Disfavoured tautomeric and anionic forms of nucleic acids have gained attention recently with regards to their involvement in mutations, replication and translational errors as well as nucleic acid catalysis and RNA-ligand recognition. However, there is a lack of information surrounding the anionic forms of nucleobases such as the adeninate anion. In this chapter, the ion-pairing and self-aggregation ability of the adeninate anion in DMSO were investigated using NMR and UV spectroscopy and crystallographic methods. An understanding of the variability of chemical shifts is needed in the context of ongoing kinetic experiments by NMR.

The large ion-dependent difference in the UV absorbance λ_{max} from 272 nm for K-Ade to 269 nm for Na-Ade shows that ion-pairs exist between the adeninate anion and Na^+ and K^+ counter ions in DMSO at very dilute concentrations. The crystal structures obtained from the ionic complexes have the ion coordinate at the N1, N9 and N7 atoms of the purine ring. It is proposed that a chelating N3-N9 coordination is highly likely to exist in solution. The counter ions are not successfully removed by the addition of 15-crown-5 and 18-crown-6 ether from the Na- and K-Ade as no gain of electron density in the purine system was observed in the ^{1}H and ^{13}C NMR study. It is proposed that the addition of 18-crown-6 ether results in complex formation with the K-Ade, as indicated by the crystal structure of K-Ade(18C6).

In the concentration dependent ^{1}H NMR studies, two regions with an opposite chemical shift change are observed which indicate two aggregation steps. The first aggregation is ascribed to dimer formation via π-π stacking as suggested by the shielding of the purine protons by the ring current of the neighbouring stacked molecule. At higher concentrations, the dimer formation is followed by higher order aggregate formation of the Na- and K-Ade. The counter ion plays a role in the self-aggregation allowing for coordination to the counter ion of the neighbouring Na-/K-Ade ion pairs. The size of the counter ion influences how the aggregates are arranged or propagated through space, revealing a clear difference between the Na-Ade and K-Ade forms. The assembly of the Na- and K-Ade complexes in the crystal structures do not show WC or HG type arrangement of hydrogen bonded aggregates. The possibility of weak hydrogen bond formation involving the NH_2 is indicated by the small enthalpy of formation of about –5 kJ mol^{-1}. The small decrease in entropy of about –8 J mol^{-1}K^{-1} with aggregate formation indicates that there is a gain in entropy due to either the liberation of solvent molecules, rearrangement of dimer aggregates and/or there is a gain in vibrational entropy from the formation of weak hydrogen bonds.

Theoretical studies were conducted to investigate the proposed sites of coordination between the counter ions and the adeninate molecule and are presented in chapter 3. Current studies are underway to confirm the modes of aggregation, with this research providing a good starting point. Although these studies have been conducted in a non-aqueous environment, they provide insight

© University of Pretoria

into how the existence of the potential deprotonated adenine base can interact in the alkali metal ions present, having the dielectric constant of DMSO fall in between that within the DNA double helix and inside the cellular environment.[115]

The counter ion present plays an essential role in directing aggregate formation, adding new insight into how the adeninate anion interacts with neighbouring molecules, and hence provides information regarding the reactivity of the systems as well as insight for the association of adenine with alkali metal counter ions which can provide stability for these forms.

© University of Pretoria

2.5 References

[1] C. A. Hunter, *Chem. Soc. Rev.* **1994**, *23*, 101.

[2] F. Cozzi, J. S. Siegel, *Pure Appl. Chem.* **1995**, *67*, 683–689.

[3] M. O. Sinnokrot, C. D. Sherrill, *J. Am. Chem. Soc.* **2004**, *126*, 7690–7697.

[4] C. R. Martinez, B. L. Iverson, *Chem. Sci.* **2012**, *3*, 2191.

[5] H. DeVoe, I. Tinoco, *J. Mol. Biol.* **1962**, *4*, 500–517.

[6] S. Hanlon, *Biochem. Biophys. Res. Commun.* **1966**, *23*, 861–867.

[7] J. D. Watson, F. H. C. Crick, *Nature* **1953**, *171*, 737–738.

[8] P. O. P. TS'O, in *Basic Princ. Nucleic Acid Chem.*, Elsevier, **1974**, pp. 453–584.

[9] J. H. van de Sande, N. B. Ramsing, M. W. Germann, W. Elhorst, B. W. Kalisch, E. v. Kitzing, R. T. Pon, R. C. Clegg, T. M. Jovin, *Science (80-.).* **1988**, *241*, 551–557.

[10] K. Hoogsteen, *Acta Crystallogr.* **1959**, *12*, 822–823.

[11] Y. K. Cheng, B. M. Pettitt, *J. Am. Chem. Soc.* **1992**, *114*, 4465–4474.

[12] F. S. Mathews, A. Rich, *J. Mol. Biol.* **1964**, *8*, 89–95.

[13] T. D. Sakore, S. S. Tavale, H. M. Sobell, *J. Mol. Biol.* **1969**, *43*, 361–374.

[14] Y. Kyogoku, R. C. Lord, A. Rich, *Proc. Natl. Acad. Sci.* **1967**, *57*, 250–257.

[15] A. Dunger, H.-H. Limbach, K. Weisz, *J. Am. Chem. Soc.* **2000**, *122*, 10109–10114.

[16] C. Giessner-Prettre, B. Pullman, *J. Theor. Biol.* **1970**, *27*, 87–95.

[17] L. Katz, *J. Mol. Biol.* **1969**, *44*, 279–296.

[18] J. D. Engel, P. H. Von Hippel, *Biochemistry* **1974**, *13*, 4143–4158.

[19] E. M. Basílio Janke, K. Weisz, *J. Phys. Chem. B* **2013**, *117*, 4853–4859.

[20] G. Lancelot, *J. Am. Chem. Soc.* **1977**, *99*, 7037–7042.

[21] P. Rao, S. Ghosh, U. Maitra, *J. Phys. Chem. B* **1999**, *103*, 4528–4533.

[22] E. M. Basílio Janke, H.-H. Limbach, K. Weisz, *J. Am. Chem. Soc.* **2004**, *126*, 2135–2141.

[23] F. Aradi, *Magn. Reson. Chem.* **1990**, *28*, 246–249.

[24] F. Aradi, *Biophys. Chem.* **1992**, *44*, 143–150.

[25] Y. Kyogoku, R. C. Lord, A. Rich, *J. Am. Chem. Soc.* **1967**, *89*, 496–504.

[26] G. J. Thomas, Jr., Y. Kyogoku, *J. Am. Chem. Soc.* **1967**, *89*, 4170–4175.

[27] Y. Kyogoku, R. C. Lord, A. Rich, *Biochim. Biophys. Acta - Nucleic Acids Protein Synth.* **1969**, *179*, 10–17.

[28] N. G. Williams, L. D. Williams, B. R. Shaw, *J. Am. Chem. Soc.* **1989**, *111*, 7205–7209.

© University of Pretoria

[29] M. P. Schweizer, A. D. Broom, P. O. P. Ts'o, D. P. Hollis, *J. Am. Chem. Soc.* **1968**, *90*, 1042–1055.

[30] P. O. P. Ts'o, I. S. Melvin, A. C. Olson, *J. Am. Chem. Soc.* **1963**, *85*, 1289–1296.

[31] N. I. Nakano, S. J. Igarashi, *Biochemistry* **1970**, *9*, 577–583.

[32] T. N. Solie, J. A. Schellman, *J. Mol. Biol.* **1968**, *33*, 61–77.

[33] M. Dey, J. Grotemeyer, E. W. Schlag, *Zeitschrift für Naturforsch. A* **1994**, *49*, 776–784.

[34] E. Nir, C. Janzen, P. Imhof, K. Kleinermanns, M. S. de Vries, *Phys. Chem. Chem. Phys.* **2002**, *4*, 732–739.

[35] F. Aradi, A. Földesi, *Magn. Reson. Chem.* **1987**, *25*, 892–896.

[36] B. A. Cerda, C. Wesdemiotis, *J. Am. Chem. Soc.* **1996**, *118*, 11884–11892.

[37] N. Russo, M. Toscano, A. Grand, *J. Am. Chem. Soc.* **2001**, *123*, 10272–10279.

[38] M. T. Rodgers, P. B. Armentrout, *J. Am. Chem. Soc.* **2000**, *122*, 8548–8558.

[39] F. Greco, A. Liguori, G. Sindona, N. Uccella, *J. Am. Chem. Soc.* **1990**, *112*, 9092–9096.

[40] V. M. Marathias, P. H. Bolton, *Biochemistry* **1999**, *38*, 4355–4364.

[41] S. Naskar, R. Guha, J. Müller, *Angew. Chemie Int. Ed.* **2020**, *59*, 1397–1406.

[42] G. Beobide, O. Castillo, J. Cepeda, A. Luque, S. Pérez-Yáñez, P. Román, J. Thomas-Gipson, *Coord. Chem. Rev.* **2013**, *257*, 2716–2736.

[43] S. L. Anderson, K. C. Stylianou, *Coord. Chem. Rev.* **2017**, *349*, 102–128.

[44] J. An, S. J. Geib, N. L. Rosi, *J. Am. Chem. Soc.* **2009**, *131*, 8376–8377.

[45] H. Cai, M. Li, X.-R. Lin, W. Chen, G.-H. Chen, X.-C. Huang, D. Li, *Angew. Chemie Int. Ed.* **2015**, *54*, 10454–10459.

[46] A. Gładysiak, T. N. Nguyen, S. L. Anderson, P. G. Boyd, R. G. Palgrave, J. Bacsa, B. Smit, M. J. Rosseinsky, K. C. Stylianou, *Inorg. Chem.* **2018**, *57*, 1888–1900.

[47] G. C. Pimentel, A. L. McClellan, *Annu. Rev. Phys. Chem.* **1971**, *22*, 347–385.

[48] P. Thordarson, *Chem. Soc. Rev.* **2011**, *40*, 1305–1323.

[49] M. Saunders, J. B. Hyne, *J. Chem. Phys.* **1958**, *29*, 1319–1323.

[50] B. I. Sukhorukov, I. Y. Gukovsky, A. I. Petrov, A. S. Gukovskaya, A. A. Mayevsky, N. M. Gusenkova, *Int. J. Quantum Chem.* **1980**, *17*, 339–359.

[51] H. S. Gutowsky, A. Saika, *J. Chem. Phys.* **1953**, *21*, 1688–1694.

[52] F. Aradi, A. Földesi, *Magn. Reson. Chem.* **1989**, *27*, 592–598.

[53] A. J. Dale, T. Gramstad, *Spectrochim. Acta Part A Mol. Spectrosc.* **1972**, *28*, 639–650.

[54] A. J. Dingley, F. Cordier, S. Grzesiek, *Concepts Magn. Reson.* **2001**, *13*, 103–127.

© University of Pretoria

[55] P. A. Kollman, L. C. Allen, *Chem. Rev.* **1972**, *72*, 283–303.

[56] J.-S. Chen, C.-Y. Fang, J. K. Baird, *Zeitschrift für Phys. Chemie* **1997**, *199*, 49–60.

[57] J. Alsins, M. Björling, I. Furó, V. Egle, *J. Phys. Org. Chem.* **1999**, *12*, 171–175.

[58] T. Hupp, C. Sturm, E. M. Basílio Janke, M. P. Cabre, K. Weisz, B. Engels, *J. Phys. Chem. A* **2005**, *109*, 1703–1712.

[59] M. N. C. Zarycz, C. Fonseca Guerra, *J. Phys. Chem. Lett.* **2018**, *9*, 3720–3724.

[60] T. Steiner, *Angew. Chemie Int. Ed.* **2002**, *41*, 48–76.

[61] G. A. Jeffrey, W. Saenger, *Hydrogen Bonding in Biological Structures*, Springer Berlin Heidelberg, Berlin, Heidelberg, **1991**.

[62] K. S. Jeong, T. Tjivikua, A. Muehldorf, G. Deslongchamps, M. Famulok, J. Rebek, *J. Am. Chem. Soc.* **1991**, *113*, 201–209.

[63] S. Mecozzi, A. P. West, D. a Dougherty, *J. Am. Chem. Soc.* **1996**, *118*, 2307–2308.

[64] L. Moreira da Costa, S. R. Stoyanov, S. Gusarov, P. R. Seidl, J. Walkimar de M. Carneiro, A. Kovalenko, *J. Phys. Chem. A* **2014**, *118*, 896–908.

[65] R. Ferrazza, B. Rossi, G. Guella, *J. Phys. Chem. B* **2014**, *118*, 7147–7155.

[66] N. Muller, R. C. Reiter, *J. Chem. Phys.* **1965**, *42*, 3265–3269.

[67] N. S. Golubev, G. S. Denisov, S. N. Smirnov, D. N. Shchepkin, H.-H. Limbach, *Zeitschrift für Phys. Chemie* **1996**, *196*, 73–84.

[68] T. P. Pitner, D. W. Urry, *J. Am. Chem. Soc.* **1972**, *94*, 1399–1400.

[69] T. Higashijima, M. Tasumi, T. Miyazawa, *FEBS Lett.* **1975**, *57*, 175–178.

[70] M. Iqbal, P. Balaram, *Biopolymers* **1982**, *21*, 1427–1433.

[71] T. Cierpicki, I. Zhukov, R. A. Byrd, J. Otlewski, *J. Magn. Reson.* **2002**, *157*, 178–180.

[72] N. J. Baxter, M. P. Williamson, *J. Biomol. NMR* **1997**, *9*, 359–369.

[73] J. Černý, M. Kabeláč, P. Hobza, *J. Am. Chem. Soc.* **2008**, *130*, 16055–16059.

[74] J. Šponer, J. Leszczyński, P. Hobza, *J. Phys. Chem.* **1996**, *100*, 5590–5596.

[75] S. K. Burley, G. a Petsko, *Science (80-.).* **1985**, *229*, 23–28.

[76] C. A. Hunter, J. Singh, J. M. Thornton, *J. Mol. Biol.* **1991**, *218*, 837–846.

[77] I. Haq, J. Ladbury, *J. Mol. Recognit.* **2000**, *13*, 188–197.

[78] G. Barone, C. F. Guerra, N. Gambino, A. Silvestri, A. Lauria, A. M. Almerico, F. M. Bickelhaupt, *J. Biomol. Struct. Dyn.* **2008**, *26*, 115–129.

[79] D. Ranganathan, V. Haridas, R. Gilardi, I. L. Karle, *J. Am. Chem. Soc.* **1998**, *120*, 10793–10800.

[80] D. Philp, J. F. Stoddart, *Angew. Chemie Int. Ed. English* **1996**, *35*, 1154–1196.

© University of Pretoria

[81] C. A. Hunter, J. K. M. Sanders, *J. Am. Chem. Soc.* **1990**, *112*, 5525–5534.

[82] C. A. Hunter, *Angew. Chemie Int. Ed. English* **1993**, *32*, 1584–1586.

[83] T. C. Dinadayalane, J. Leszczynski, *Struct. Chem.* **2009**, *20*, 11–20.

[84] R. R. Choudhury, R. Chitra, *CrystEngComm* **2010**, *12*, 2113–2121.

[85] E. Arunan, H. S. Gutowsky, *J. Chem. Phys.* **1993**, *98*, 4294–4296.

[86] C. D. Sherrill, *Acc. Chem. Res.* **2013**, *46*, 1020–1028.

[87] T. F. Headen, P. L. Cullen, R. Patel, A. Taylor, N. T. Skipper, *Phys. Chem. Chem. Phys.* **2018**, *20*, 2704–2715.

[88] D. B. Ninković, G. V. Janjić, S. D. Zarić, *Cryst. Growth Des.* **2012**, *12*, 1060–1063.

[89] C. Janiak, *J. Chem. Soc. Dalt. Trans.* **2000**, 3885–3896.

[90] R. Goddard, M. W. Haenel, W. C. Herndon, C. Krueger, M. Zander, *J. Am. Chem. Soc.* **1995**, *117*, 30–41.

[91] J. H. Williams, *Acc. Chem. Res.* **1993**, *26*, 593–598.

[92] M. Baranac-Stojanović, *RSC Adv.* **2014**, *4*, 308–321.

[93] R. B. Martin, *Chem. Rev.* **1996**, *96*, 3043–3064.

[94] M. Majumder, N. Sathyamurthy, *Theor. Chem. Acc.* **2012**, *131*, 1092.

[95] A. S. Shetty, J. Zhang, J. S. Moore, *J. Am. Chem. Soc.* **1996**, *118*, 1019–1027.

[96] R. J. Carbajo, J. L. Neira, **2013**, pp. 31–52.

[97] M. P. Schweizer, S. I. Chan, G. K. Helmkamp, P. O. P. Ts'o, *J. Am. Chem. Soc.* **1964**, *86*, 696–700.

[98] G. K. Helmkamp, N. S. Kondo, *Biochim. Biophys. Acta - Nucleic Acids Protein Synth.* **1968**, *157*, 242–257.

[99] R. F. Stewart, N. Davidson, *J. Chem. Phys.* **1963**, *39*, 255–266.

[100] W. B. Gratzer, C. W. F. McClare, *J. Am. Chem. Soc.* **1967**, *89*, 4224–4225.

[101] K. Bebenek, L. C. Pedersen, T. A. Kunkel, *Proc. Natl. Acad. Sci. U. S. A.* **2011**, *108*, 1862–1867.

[102] I. J. Kimsey, K. Petzold, B. Sathyamoorthy, Z. W. Stein, H. M. Al-Hashimi, *Nature* **2015**, *519*, 315–320.

[103] W. Wang, H. W. Hellinga, L. S. Beese, *Proc. Natl. Acad. Sci.* **2011**, *108*, 17644–17648.

[104] C. Tamm, P. Strazewski, *Angew. Chemie Int. Ed. English* **1990**, *29*, 36–57.

[105] P. C. Bevilacqua, R. Yajima, *Curr. Opin. Chem. Biol.* **2006**, *10*, 455–464.

[106] V. Singh, C. S. Peng, D. Li, K. Mitra, K. J. Silvestre, A. Tokmakoff, J. M. Essigmann, *ACS Chem. Biol.* **2014**, *9*, 227–236.

© University of Pretoria

[107] S. Kim, M. C. Lind, H. F. Schaefer, *J. Phys. Chem. B* **2008**, *112*, 3545–3551.

[108] S. Perun, A. L. Sobolewski, W. Domcke, *Chem. Phys.* **2005**, *313*, 107–112.

[109] I. Hünig, C. Plützer, K. A. Seefeld, D. Löwenich, M. Nispel, K. Kleinermanns, *ChemPhysChem* **2004**, *5*, 1427–1431.

[110] T. J. Torphy, *Am. J. Respir. Crit. Care Med.* **1998**, *157*, 351–370.

[111] E. Boichot, J. L. Wallace, N. Germain, M. Corbel, C. Lugnier, V. Lagente, J. J. Bourguignon, *J. Pharmacol. Exp. Ther.* **2000**, *292*, 647–53.

[112] B. Bielekova, A. Lincoln, H. McFarland, R. Martin, *J. Immunol.* **2000**, *164*, 1117–1124.

[113] M. K. Mishra, S. P. Kelley, V. Smetana, D. A. Dixon, A. S. McNeill, A.-V. Mudring, R. D. Rogers, *Proc. Natl. Acad. Sci.* **2020**, *117*, 18224–18230.

[114] R. E. Hoffman, E. D. Becker, *J. Magn. Reson.* **2005**, *176*, 87–98.

[115] S. Nakano, N. Sugimoto, *Biophys. Rev.* **2016**, *8*, 11–23.

[116] H. Sapper, W. Lohmann, *Biophys. Struct. Mech.* **1978**, *4*, 327–335.

[117] H. W. Vos, H. H. Blom, N. H. Velthorst, C. MacLean, *J. Chem. Soc. Perkin Trans. 2* **1972**, *2*, 635–639.

[118] H. V. Carter, B. J. McClelland, E. Warhurst, *Trans. Faraday Soc.* **1960**, *56*, 455–458.

[119] H. H. Hammud, K. H. Bouhadir, M. S. Masoud, A. M. Ghannoum, S. A. Assi, *J. Solution Chem.* **2008**, *37*, 895–917.

[120] N. J. Leonard, K. Ito, *J. Am. Chem. Soc.* **1973**, *95*, 4010–4016.

[121] G. M. Roberts, H. J. B. Marroux, M. P. Grubb, M. N. R. Ashfold, A. J. Orr-Ewing, *J. Phys. Chem. A* **2014**, *118*, 11211–11225.

[122] J. P. García-Terán, O. Castillo, A. Luque, U. García-Couceiro, P. Román, L. Lezama, *Inorg. Chem.* **2004**, *43*, 4549–4551.

[123] F. B. Sayyed, C. H. Suresh, *Chem. Phys. Lett.* **2012**, *523*, 11–14.

[124] S. Mecozzi, A. P. West, D. A. Dougherty, *Proc. Natl. Acad. Sci.* **1996**, *93*, 10566–10571.

[125] M. Irandoust, H. Daraei, R. Rostamian, *Polyhedron* **2011**, *30*, 1207–1212.

[126] W. Schimmack, H. Sapper, W. Lohmann, *Biophys. Struct. Mech.* **1975**, *1*, 311–318.

[127] E. Karkhaneei, A. Afkhami, M. Shamsipur, *Polyhedron* **1996**, *15*, 1989–1994.

[128] L. Katz, S. Penman, *J. Mol. Biol.* **1966**, *15*, 220–231.

[129] J. Morcillo, E. Gallego, F. Peral, *J. Mol. Struct.* **1987**, *157*, 353–369.

[130] G. G. Hammes, A. C. Park, *J. Am. Chem. Soc.* **1969**, *91*, 956–961.

[131] S. W. Benson, *Thermochemical Kinetics*, John Wiley & Sons, New York, **1976**.

[132] J. D. Dunitz, *Chem. Biol.* **1995**, *2*, 709–712.

© University of Pretoria

[133] M. Jóźwiak, *J. Mol. Liq.* **2003**, *108*, 175–198.

[134] M. Jóźwiak, H. Piekarski, A. Jóźwiak, *J. Mol. Liq.* **2003**, *106*, 15–29.

© University of Pretoria

Chapter 3 Towards a molecular understanding of the preferential site of coordination of sodium and potassium ions to the adeninate anion in DMSO by quantum chemical studies

3.1 Introduction

The binding of metal ions to nucleobases influences the structural integrity of DNA and plays a role in synthesis, replication, recognition and cleavage of DNA and RNA.[1] Interactions of alkali and alkaline earth metal ions with nucleotides occur predominantly at the anionic oxygen atoms of the phosphate groups to neutralize the negative charge providing stabilization of the DNA and RNA structures.[2–4] However, they can also interact with the nucleobase moiety and neutralize the phosphate group charge via a zwitterion effect. At high concentration of metal ions, binding can interfere with hydrogen bonding and stacking interactions between base pairs and compromise the structural stability of DNA.[5] Transition metals interact more frequently with the nucleobase as compared to the phosphate groups,[6–8] as they are more likely to interact with nitrogen and sulphur atoms.[9,10] In the major groove of duplex DNA the N7 nitrogen atom of adenine and guanine is the most likely site for metal ion coordination whereas in the minor grove these sites are the N3 and O2 of adenine and thymine, respectively.[3,4,11] However, for free nucleobases, nucleotides and nucleosides, the unidentate or bidentate coordination of metal or multiple metal ions can occur anywhere.[3]

The metal ion in metal-nucleotide complexes perturbs the electronic environment of the nucleobase and in turn, influences the strength of hydrogen bonding and stacking interactions.[8] In addition, the coordination of metal ions to nucleotides can allow for rare tautomeric forms to occur[12] and potentially stabilize the formation of anionic forms. Rare tautomeric and anionic forms of nucleobases are involved in base mispairing which leads to mutations and other biological phenomena.[13–15]

The interaction between nucleotides and metal ions constitutes part of the role of the environment in tautomeric equilibria of nucleobases, which encompasses the effect of hydration and other non-covalent interactions with surrounding nucleotides. Theoretical studies of the complexation of metal ions with nucleobases have predominantly involved the neutral form of the free base with alkali, alkaline earth and transition metal ions according to eqn 3.1,

$$\mathrm{B} + \mathrm{M}^{n+} \rightleftarrows \mathrm{BM}^{n+}, \qquad (3.1)$$

where B = uracil, thymine, adenine, cytosine and guanine and M^{n+} = Li^+, Na^+, K^+, Ag^+, Au^+ and Cu^+ for n = 1 and Be^{2+}, Mg^{2+}, Ca^{2+}, Mn^{2+} and Zn^{2+} for n=2. Dominant and rare tautomeric forms of

© University of Pretoria

nucleobases in complexation with metal ions have been investigated and compared to experimental work.[5,16]

3.2 Metal ion coordination to dominant tautomeric forms of nucleobases

3.2.1 Alkali metal ions

Alkali metal ion affinities to nucleobases obtained experimentally in the gas-phase via mass spectrometry indicate that ions bind preferentially to guanine > cytosine > adenine > thymine > uracil.[1] The Li^+ ion has the highest affinity to nucleobases followed by Na^+ and then K^+ with coordination occurring at any heteroatom of the nucleobase.[1,5] The preference for the binding of Li^+ > Na^+ > K^+ is attributed to the increase in the strength of the ion-dipole and ion-induced dipole interactions with the decrease in size of the cation, whereby the smaller the ion, the greater the charge-to-radius ratio.[5,17] It is to be noted here that solution and gas phase binding energies may differ.[18]

Theoretical calculations in the gas phase of metal ion coordination to the dominant form (keto and amino forms)[19–22] of nucleobases show preference for bidentate chelation compared to unidentate coordination. Chelation of small metal ions with adenine or guanine results in the formation of an external ring between the nucleobase and the cation. This new ring formation has been used to explain the preference of metal ion site coordination of these compounds. The bridging of the metal ion between the N1 and NH_2 of adenine, **1** in Figure 3.1, and the N3 and NH_2 of guanine **2** results in a four-membered coordination ring. Bridging of the metal ion between the N7 and NH_2 of adenine **3** and the N7 and O6 of guanine **4** results in the formation of five-membered rings.[5,23]

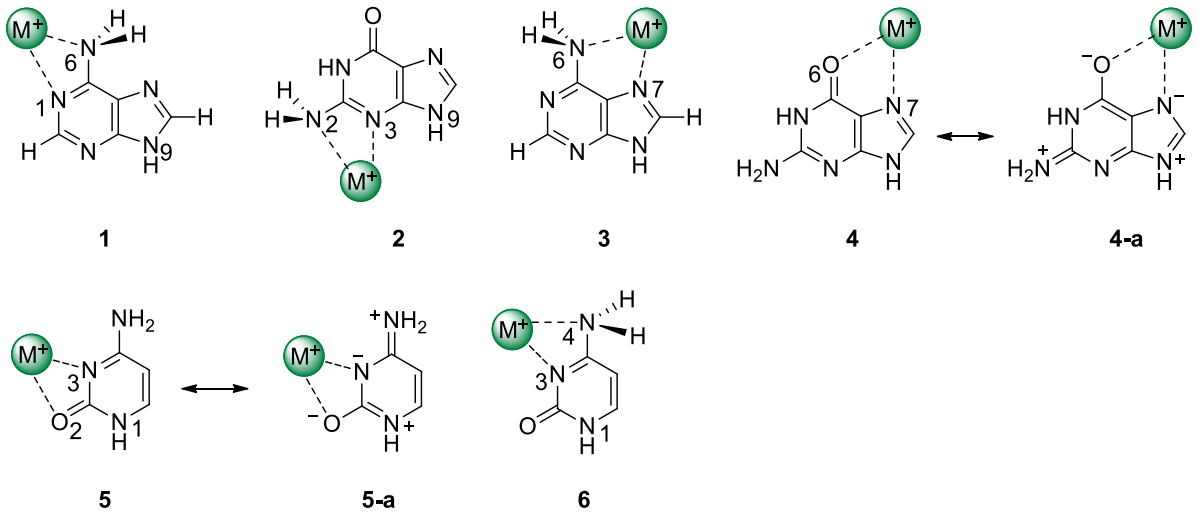

Figure 3.1: Chelation of metal ion with the dominant forms of adenine, guanine and cytosine nucleobases.

© University of Pretoria

Chelation of metal ions to these nucleobases in which the five-membered coordination ring is formed are more favourable than the four-membered ring formation and is attributed to the former possessing less steric strain, i.e. chelation of Li^+, Na^+ and K^+ ions at the N1 nitrogen atom of adenine is less favourable by 1.9, 1.0 and 0.1 kcal mol^{-1}, respectively, than chelation at the N7 atom (at MP2 level). [5] This trend is reproducible at the B3LYP level.[16,20] Chelation of the metal ion series at the N3 atom of guanine is > 30 kcal mol^{-1} higher in energy than chelation at the N7 for all alkali metals.[16] The energy differences between the sites of coordination are smallest for K^+ and largest for Li^+. The chelation of metal ions at the N1 (**1**) and N7 (**3**) nitrogen atoms of adenine results in the change in hybridization of the amino group as it is twisted out of plane going from sp^2 in the uncomplexed neutral adenine to sp^3 in the metal complexed state.[5,12] In turn, this reduces the stabilization from π-resonance delocalization of the NH_2 group throughout the purine ring. However, this is compensated for by reduced repulsion between the metal ion and the protons on the amino group as well as allowing for chelation to occur which results in stronger binding of the metal ion. The chelation of K^+ at the N7 and NH_2 of adenine restricts rotation of the amino group through direct interaction with the NH_2 nitrogen atom, leading to large, experimentally observed, entropy effects.[1] The restriction of rotation of the NH_2 group leads to the two protons no longer being equivalent. This has been observed in the case of N1 and N7 coordinated Pt(II)-dien-adenosine complexes via ^1H NMR spectroscopy in DMF whereby splitting of the NH_2 peak occurs, however, this is only observed at temperatures lower than 248 K.[24]

Large entropy effects due to restricted NH_2 rotation are observed for the chelation of the M^+ ion in guanine **4** and cytosine **5** complexes.[1] The formation of an immonium ion which results in resonance effects is proposed to block the rotation of the NH_2 group which is not directly involved in the coordination of the metal ion (**4-a** and **5-a**).[1] Chelation of Li^+ and alkaline earth metals (Mg^{2+} and Ca^{2+}) with the N3 and $N4H_2$ group of cytosine **6** has been reported,[16,23] whereas no optimized structures have been reported for Na^+ and K^+. Bidentate chelation with the N3 and O2 atom of cytosine occurs for all alkali and alkaline earth metals and is the most stable form compared to chelation with the N3 and $N4H_2$, i.e. –21.4 kcal mol^{-1} more favourable for the Li^+ ion.[16]

The N3 nitrogen atom of neutral adenine **7** (Figure 3.2) is the least preferred site for unidentate in-plane coordination of the M^+ ion i.e. 6.8, 3.5 and 0.2 kcal mol^{-1} less stable than the chelated N7 isomer for Li^+, Na^+ and K^+ ions, respectively.[5] The N7 > N1 > N3 metal ion affinity trend of adenine is not replicated in the proton affinity trend of N1 > N3 > N7 of neutral adenine and is ascribed to the lack of the chelating ability of the proton.[5]

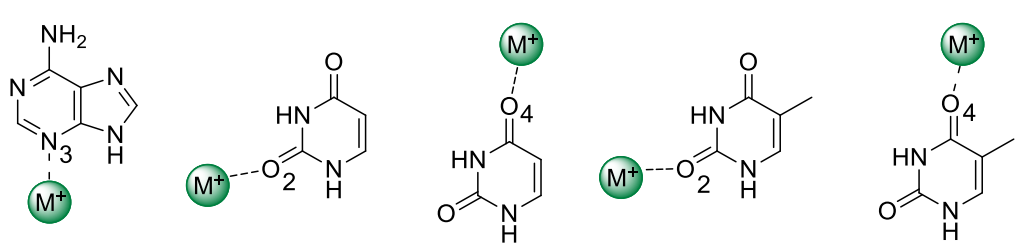

7 **8** **9** **10** **11**

Figure 3.2: Unidentate metal ion coordination of dominant tautomeric form of adenine, uracil and thymine.

© University of Pretoria

Neutral uracil and thymine form unidentate coordinated metal complexes. No chelated metal complexes of the neutral forms occur. This results in these nucleobases having the lowest metal ion affinity. Metal ions can coordinate at the O2 or O4 atoms of uracil (**8** and **9**) and thymine (**10** and **11**), whereby the O4 coordination is the most favoured. Gas phase calculations at MP2 level of theory show that coordination of Li^+ and Na^+/K^+ at the O4 atom of uracil is –3.4 and –2.8 kcal mol^{-1} more stable than coordination at the O2 atom.[5] The complexation of Li^+, Na^+ and K^+ at the O4 atom of thymine is –1.5, –1.2 and –1.1 kcal mol^{-1} more stable than coordination at the O2 atom. Similar results are obtained at DFT level of theory.[16,23] It is to be noted that these complexes do not have the ion in a linear arrangement as depicted in Figure 3.2, but rather the ion is slightly shifted out of the linear arrangement, bent by 4 – 6°.

3.2.2 Alkaline earth metals

Theoretical studies involving coordination of alkaline earth metals to the dominant tautomer forms of neutral nucleobases revealed the same preference for chelation over unidentate coordination as well as the same trends for the preferred site of coordination to nucleobases as discussed for alkali metals.[12,16] This suggests that the preferential site of metal ion coordination to the dominant forms of nucleobases is independent of the size and charge of the ion. The interaction between alkaline earth metal with nucleobases is stronger than that of alkali metals i.e. the binding enthalpy of Be^{2+} is more than –150 kcal mol^{-1} more favourable than the Li^+ complexation with nucleobases, having the interaction distance around 0.4 Å shorter than the corresponding Li^+ complexes.[16] This is due to the larger charge-to-radius ratio, and decreases in the order $Be^{2+} > Mg^{2+} > Ca^{2+}$ for the alkaline earth metals, having the binding enthalpy of Be^{2+} more than –100 and –125 kcal mol^{-1} more favourable than the corresponding Mg^{2+} and Ca^{2+} nucleobase complexes, respectively. Analysis of the Mulliken charges located on the counter ion and the nucleobase in the metal-nucleobase complex, indicated that the alkaline earth metals experience the largest gain of electron density from the nucleobase compared to the alkali metal ions in the order $Be^{2+} > Mg^{2+} > Ca^{2+} > Na^+ > K^+$.[16]

The electrostatic and polarization contribution to the binding energy are stabilizing, having the latter play an important role in cation-π complexes.[16] Stabilization from charge transfer is largest for $Ca^{2+} > Mg^{2+} > Be^{2+}$ and is attributed to the deformation of the purine rings upon cation-π complex formation. The more planar ring structure in Ca^{2+} complexation maintains the π-electron system (aromaticity) which can donate electron density more readily.[16]

3.2.3 Tautomeric forms of alkali and alkaline earth metal ion complexes

In addition to the theoretical studies involving the complexation of metal ions to the dominant tautomeric form of nucleobases, coordination of metal ions to rare tautomers has also been investigated. Two main types of adenine tautomers were investigated. The first involves the N7(H) and N1(H) tautomers of adenine, having the former known to exists experimentally in minor amounts in the uncomplexed form.[25,26] Thus, the complexation with metal ions is rendered likely to occur. Compared to the N9(H) tautomer **3**, the N7(H) and N1(H) tautomers of adenine with the metal ion chelated at the N3 and N9 atoms (**12** and **13**) of the purine ring (Figure 3.3) are more stable i.e. –17.1 and –14.9 kcal mol^{-1} for the Na^+ metal complex.[12] Experimental evidence (Ultraviolet photodissociation spectroscopy) of a single isolated K^+ adenine complex is ascribed to the bidentate N3,N9 coordination to the N7(H) adenine tautomer.[27]

© University of Pretoria

The second type of adenine tautomer involves the imine tautomeric forms. The imine tautomeric metal complexes are more stable than the former mentioned isomers, i.e. the Na^+ imine tautomers **15** - **17** are more than –20 kcal mol^{-1} more stable than the N9(H) **3** tautomer. However, theoretically, the most stable isomer is a zwitterionic structure of adenine **14**, which is –31.1 kcal mol^{-1} more stable that the **3** isomer for the Na^+ ion. A large tautomeric penalization energy is paid in order to form the uncomplexed tautomer and hence complexation of these tautomers to metal ions is deemed less likely to exist if tautomerization is to occur first.[12] These trends are observed for Li^+, Na^+, K^+, Mg^{2+} and Ca^{2+}.[2,12,23,28,29]

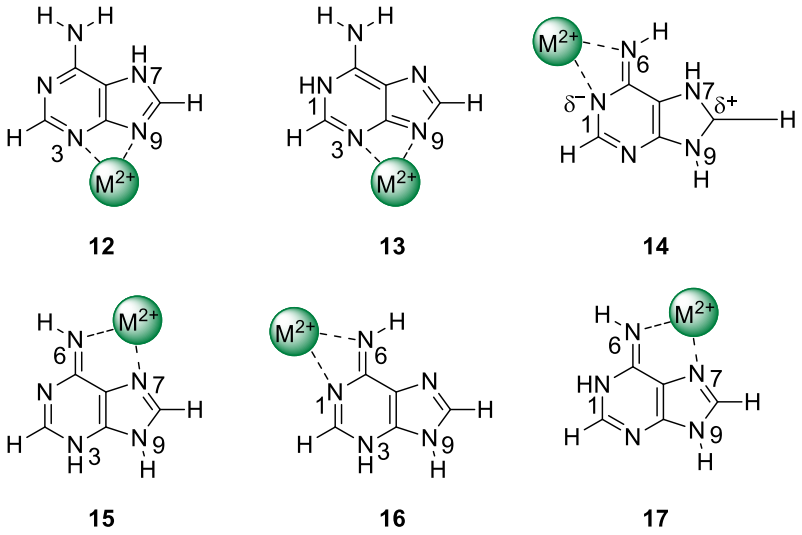

Figure 3.3: Metal ion complexes with tautomeric forms of adenine.

3.2.4 Transition metals

A few theoretical studies have involved the coordination of transition metals with nucleobases, most pertaining to the stabilization of rare tautomeric forms.[12,30,31] The complexation of neutral and cationic Au with neutral adenine is dominated by energetically equivalent isomers with tridentate coordination to the purine ring.[31] Neutral Au coordinates most favourably at the N1, N3 and N7 atoms of the N9(H) dominant tautomer of adenine (**18** – **20** in Figure 3.4), in which the energy differences between these three isomers are minimal at DFT/B3LYP level of theory. The interaction bonds of neutral Au are longer than those of the cationic Au^+ forms, i.e. 2.34 - 2.36 vs 2.04-2.06 Å, showing that the cationic Au form interacts more strongly with adenine. However, the most stable isomers of these complexes involve the rare N7(H) and imine tautomeric forms of adenine (**21** and **22**). The N7(H) tautomeric form is −2.6 kcal mol^{-1} more favourable than the imine form.

Cu^+ adenine complexes result in a different trend, having coordination at the N7 of the N9(H) imine form **25** the most dominant.[30] This is followed by a unidentate coordination at the N3 atom of N7(H) adenine tautomer **24** and a bidentate N7 coordinated N9(H) tautomeric adenine form **23**, being 5.4 and 9.8 kcal mol^{-1} less favourable than the N7 coordinated imine isomer, respectively. The bond distances for Cu^+ range from 1.916 to 2.077. Two of the most stable Zn^{2+} adenine complexes

© University of Pretoria

include the imine tautomer of adenine whereby a bidentate coordination occurs between Zn^{2+} with the N7 and NH_2, having the position of the ring protons at the i) N3 and N9 (**26**), and ii) the N1 and N9 (**27**) position.[12] The isomer **26** is –9.6 kcal mol^{-1} more stable than isomer **27**. Complexation of Zn^{2+} with a zwitterionic structure of adenine **28** is –5.1 kcal mol^{-1} more stable than isomer **26**, however, formation of the zwitterion exhibits a large tautomeric penalization energy of around 50 kcal mol^{-1}, and therefore is less likely to exist.

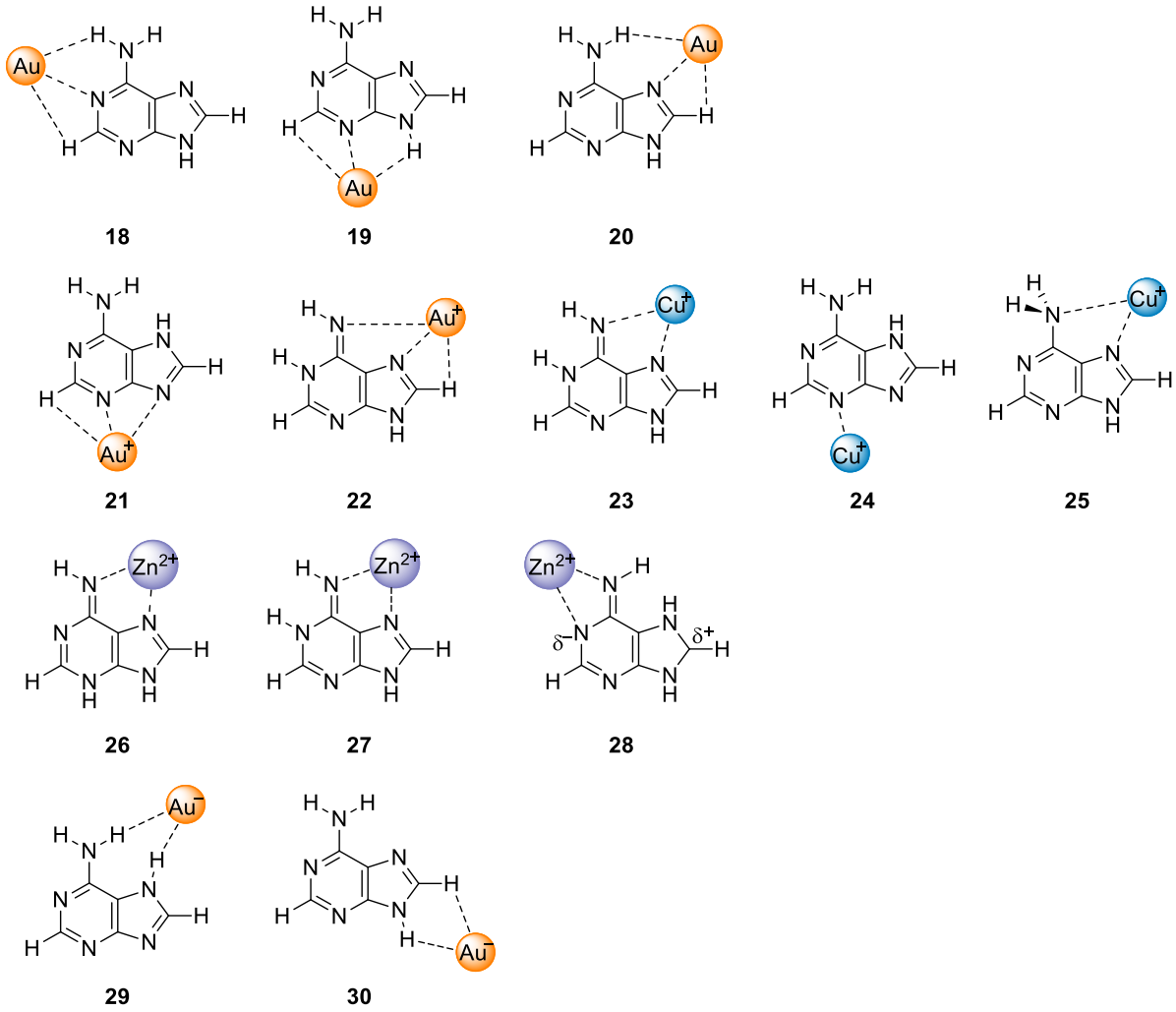

Figure 3.4: Coordination of neutral, cationic and anionic Au, Au^+, Zn^{2+} and Cu^+ to adenine.

The anionic Au forms a unidentate or bidentate coordination to the protons of the purine ring and not the electron rich nitrogen atoms, **29** and **30** in Figure 3.4. Only two isomers are energetically accessible whereby the Au anion interacts in a Watson-Crick like fashion with a rare N7(H) tautomeric form and the other via the protons of the N9 and the C8-H of the dominant N9(H) adenine tautomer (which is around 5.6 kcal mol^{-1} less favourable than the former). The protons of adenine act as hydrogen donors and the anionic Au metal behaves as the proton acceptor in which the extra electron is located on the Au ion leading to the formation of nonconventional hydrogen bonds which stabilize the complex. For both the cationic and anionic Au adenine complexes, in

© University of Pretoria

which the interactions are mainly electrostatic, the interaction between the metal ion and adenine is stronger than for neutral Au adenine complexes.

3.2.5 The role of the NH_2 group in metal ion binding

In the above discussions it is clear that bidentate or tridentate coordination involving the lone pair of electrons on the NH_2 is a common feature upon metal ion coordination to adenine. However, no single crystal X-ray structure of metal complexed adenine in its neutral form has provided evidence for the coordination of the NH_2 group via a change in hybridization from sp^2 to sp^3 by twisting out of plane to metal ions[32], as suggested by theoretical studies. Comparisons between Pt^{II} and Pd^{II} complexed N9-methyalted adenine crystal structures with theoretical calculations have demonstrated good agreement regarding the double bond nature of C6-N6 bond, thus showing sp^2 hybridization upon metal ion complexation.[33] Evidence of direct participation of the N6 in chelation of metal ions has only been observed when either the rare imine tautomeric[15] form of adenine is present or when the NH_2 group undergoes deprotonation, $^-$N6H.[35–38] Coordination of a transition metal ion at the N6 position requires deprotonation of the NH_2 group.[3]

A range of Cu^{II} coordinated adenine complexes (neutral and anionic) have been isolated (crystal structures) whereby the NH_2 was observed to act as a hydrogen donor to provide additional stabilization to the complexes formed and retains the planar structure most of the time.[39] Cp_2Mo^{II} coordinates in a bidentate fashion to N9-methyladenine via the N1 and the $^-$N6H, **31** in Figure 3.5, having the C6-N6 bond distance as 1.314 Å, and is the kinetic product which can be converted to the thermodynamic product (**32**) which involves bidentate coordination via the N7 and $^-$N6H.[38]

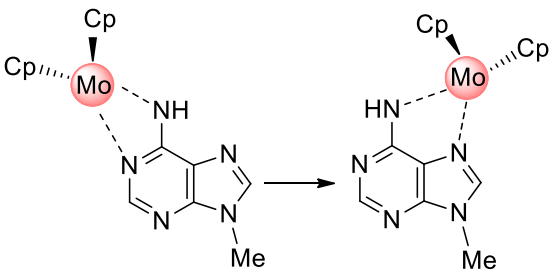

31 **32**

Figure 3.5: Isomerization of $[Cp_2Mo(II)(9\text{-methyladenyl})][PF_6]$ from the bidentate coordination via the N1 and N6 (31) to the N7 and N6 (32) of adenine.

Cp-Rh(II)-N9-methyladenine,[37,40] Cp-Ir(III)-N9-ethyladenine,[41] Cp-Ir(III)-adenine[41] and (p-cymene)Ru(II)[35] complexes form cyclic trimer complexes (cyclic tetramer for Cp-Ir(III)-adenine). In each complex the rhodium, iridium or ruthenium is coordinated via the N7 and $^-$N6H, and the adenine moiety acts as a bridging ligand through the N1 for the N9 substituted adenines (**33** in Figure 3.6), and the N9 for the adenine Ir and Ru complexes (**34**).

Although no out-of-plane twisting of the NH_2 group has ever been reported experimentally, it is to be noted that the complexes of the crystal structures used to investigate the probability of the hybridization change contain metals with additional ligands attached.[33,35] Hence, these structures cannot be compared directly to the free metal ion-adenine complexes studied theoretically. This is

© University of Pretoria

due to the participation of the $NH_2/^{-}N6H$ group in additional stabilizing interactions with the ligands on the metal ion. In gas phase studies of adenine with a metal, experimental or theoretical, the system differs from those discussed above. However, the above complexes demonstrate the versatility of the NH_2 group upon complex formation with metal ions, i.e. its mode of coordination and changes in the hybridization upon complex formation with metal ions

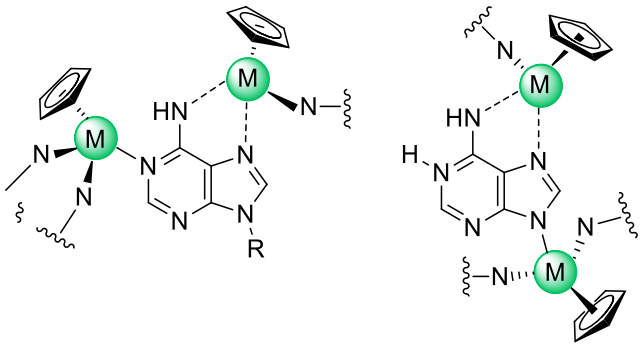

33 **34**

Figure 3.6: Bidentate metal ion complexation at the N7 and N6 atoms of adenine, where M = Rh(II), Ir(III), or Ru(II).

3.2.6 Cation-π complexes

In addition to the in-plane metal ion complexed nucleobases, cation-π complexation between metal ions with the five and six membered ring system of adenine (and other nucleobases) have been studied theoretically with Li^{+}, Be^{2+}, Mg^{2+} and Ca^{2+} metal ions.[5] Be^{2+} can form cation-π interactions with all nucleobases except guanine, in which only the Li^{+} ion has shown to form a cation-π interaction with guanine. No Na^{+} and K^{+} cation-π interactions with nucleobases have been isolated.[16] Distortion of the planar ring structures of nucleobases occurs upon cation-π complexation and the degree of distortion is dependent on the cation present, decreasing as the size of ion increases for alkaline earth metals. Adenine and guanine retain their planarity relatively well in cation-π complexation, having the planar torsion angle ranging from 154-175° from the planar 180°. The calculated distortion energy for the 6 membered ring of adenine with Be^{2+}, Mg^{2+} and Ca^{2+} is 18.07, 9.21 and 4.65 kcal mol^{-1}, respectively. However, the cytosine, thymine and uracil complexes are largely distorted upon complexation, having the planar torsion angle (C2-N3-N1-C5 for cytosine, N3-C4-C2-C6 for thymine and C2-N3-N1-C5 for uracil) < 150°, resulting in the distortion energy > 40 kcal mol^{-1} for the Be^{2+} complexes. This deformation of the ring structure is attributed to the presence of the carbonyl group. Distortion of imidazole and pyrimidine structures from cation-π complexation is minimal, whereas for benzene the ring structure remains planar. The metal ions are positioned closer to the heteroatoms of the nucleobases in the cation-π complexes potentially due to the larger electron density on the heteroatoms.[5,16] The cation-π binding interaction is large compared to hydrogen bonding, having Be^{2+} interact the strongest. It has been proposed that Be^{2+} and Mg^{2+} cation-π complexes with nucleobases have more covalent bond-like character than an ionic interaction.

© University of Pretoria

The above discussion has shown that metal ions can in principle coordinate at any site of nucleobases, whether it be at the in-plane nitrogen atoms or cation-π interactions. Various tautomers have been predicted to exist due to the coordination of metal ions and may result in more stable metal-ion complexes than dominant tautomeric forms. The presence of rare tautomeric and anionic forms of nucleic acids can form Watson-Crick mispairs that are involved in mutations and replication and translational errors,[13–15,42] as well as playing a role in nucleic acid catalysis[43] and RNA-ligand recognition.[44] As the understanding of the stabilization of rare tautomeric forms grows via computational studies, research into deprotonated nucleobases is limited. Hence, in this research we provide novel insight into the coordination of biologically important metal ions, Na^+ and K^+, with deprotonated adenine using Interacting Quantum Atoms (IQA) analysis and a Reaction Energy Profile Fragment Attributed Molecular System Energy Change (REP-FAMSEC) protocol. A comparison of the performance of Coupled cluster (CCSD) and Density functional theory (DFT) level of theory for the analysis of metal complexed adeninate isomers is carried out in this study.

3.3 Computational Methods

All electronic structure calculations were performed in Gaussian 09 rev. E.01[45] (DFT), and Gaussian 16 rev. E.01[46] (CCSD studies). Energy optimization of the free adeninate anion and all monomeric structural isomers for the Na- and K-Ade complexes was performed at the DFT/B3LYP/6-311++g(d,p)/GD3, DFT/M06-2X/6-311++g(d,p)/GD3, CCSD/6-311++g(d,p) and CCSD/aug-cc-pvdz levels of theory (GD3 stands for Grimm's empirical dispersion correction as incorporated in Gaussian). The computations were performed in solvent (DMSO) using the Polarizable Continuum Model (PCM). To verify that the structures obtained at the DFT/B3LYP level of theory are at an energy minimum, frequency calculations were performed to ensure no imaginary/negative frequency was present. The optimized monomeric isomers for the Na- and K-Ade complexes were used as an input for the study involving explicit DMSO solvent molecules. Four fully optimized DMSO solvent molecules at the DFT/B3LYP/6-311++g(d,p)/GD3/PCM(DMSO) were pre-organized around the optimized isomers of the Na- and K-Ade complexes. Full optimization of explicitly solvated complexes was performed without constraints at the DFT/B3LYP/6-311++g(d,p)/GD3/PCM(DMSO) level. IQA[47] calculations were done using AIMAll (Version 19.10.12).[48] Software developed in-house was used to run the REP-FAMSEC[49] calculations. All log and wave function files for the DFT and CCSD structures are available at 10.25403/UPresearchdata.19188800.

3.4 Results and Discussion

Experimental ^1H and ^{13}C NMR spectroscopy studies on the ion-pairing between Na^+ and K^+ ions with the free adeninate anion (Ade^-) in anhydrous DMSO suggested that the counter ion coordinates in-plane at the bottom portion of the purine ring. The coordination is proposed to occur via a unidentate or bidentate fashion at the N9 and N3 donor atoms. Furthermore, the crystal structure obtained for the Na- and K-Ade complexes from anhydrous DMSO as the crystalizing solvent, showed that one Ade^- has three counter ions coordinated via the N1, N7 and N9 atoms of the purine ring. In addition, the unexplained absence of the NH_2 peak in the ^1H NMR of K-Ade raised suspicion that the K^+ counter ion interacted at a different site compared to the Na^+. It is to be noted that both the Na-Ade and K-Ade crystal structures did not display a change in the hybridization of the NH_2 group or deprotonation of the NH_2 group upon coordination of the metal ions at the N1, N7 and N9 nitrogen atoms.

© University of Pretoria

It is of interest to use computational chemistry to understand the factors governing the most likely coordination site of the counter ion with the adeninate anion and to validate the suggested coordination sites from experimental work, moving from crystal structures to free monomers in solution. To our knowledge, this is the first computational investigation into metal ion coordination to the adeninate anion. Furthermore, previous studies were conducted in the gas phase and using DFT and MP2 level of theory.[5,12,16,23] Here, we investigate the systems at the superior CCSD level and compare with results obtained at the DFT/B3LYP level of theory.

3.4.1 Relative stability of Na- and K-Ade ionic complexes

A set of structural isomers for the Na-Ade and K-Ade complexes was modelled by varying the position of the counter ion (i) in the plane of the purine ring of Ade^- whereby the cation is placed next to the endo purine ring N-atoms i.e. N1, N3, N7, N9 and chelated between the N3N9 nitrogen atoms and (ii) out of plane positions i.e. the cation is placed above the NH_2 functional group or between the two rings making up the π system. The structures of all successfully optimized complexes are shown in Figure 3.7. Optimization at CCSD/aug-cc-pvdz was not achieved for the K^+ complexes. The difference in electronic energies (Δ*E*) of the Na- and K-Ade structural isomers relative to the lowest energy complex (LEC), i.e. the (N9) and (N3N9) for the Na^+ and K^+ complexes, respectively, is given in Table 3.1.

Table 3.1: Relative to the LEC, the difference in electronic energy (Δ*E* in kcal mol^{-1}) of Na- and K-Ade complexes

Na-Ade	Δ*E*				K-Ade	Δ*E*		
isomer	B3LYP[a]	*CCSD*[b]	*CCSD-aug*[c]	M06-2X[d]	isomer	B3LYP[a]	*CCSD*[b]	M06-2X[c]
(N9)	0.0	0.0	0.0	0.0	(N3N9)	0.0	0.0	0.0
(N3N9)	0.0	0.1	0.2	–0.7	(N7)	2.2	2.5	3.4
(N3)	0.8	1.0	0.9	–0.6	(N1)	3.3	3.6	4.6
(N7)	1.2	1.1	0.9	1.3	(N10)	4.4	4.4	6.0
(N1)	3.2	2.5	2.3	2.9	(π)	-	-	4.9
(N10)	5.0	3.8	3.8	5.2				
(π)	2.2	5.4	5.0	-				

[a] B3LYP/6-311G++(d,p)/PCM(DMSO) [b] CCSD/6-311++g(d,p)/PCM(DMSO) [c] CCSD/aug-cc-pvdz/PCM (DMSO) [d] DFT/M06-2X /6-311++g(d,p)/PCM(DMSO)

The Δ*E* trend for nitrogen-coordinated Na^+ and K^+ adeninate complexes of N9 = N3N9 < N3 < N7 < N1 < N10 (replicated in the Δ*G* values obtained at DFT/B3LYP, see Supporting Information 2 Table S2.1) is recovered by CCSD and DFT/B3LYP calculations, thus showing good agreement between the two levels of theory. Refer to Tables S2-5 for the bond lengths of each complex optimized at DFT/B3LYP and CCSD level of theory. The Δ*E* trend for isomers calculated at the DFT/M06-2X level of theory does not recover that of the superior CCSD and therefore is disregarded as an appropriate level of theory for this type of work and will no longer be considered. All isomers discovered at CCDS level of theory are reproduced at the DFT/B3LYP level of theory. The smaller Na^+ ion occupies the in-plane N3, N9 and N3N9 positions as unique isomers whereas the larger K^+ ion occupies only the N3N9 position, leading to a smaller number of isomers for the K-Ade complex. No isomer resulted in a NH_2 hybridization change from sp^2 to sp^3 due to bidentate coordination at the N1/N7 atom with the -NH_2

© University of Pretoria

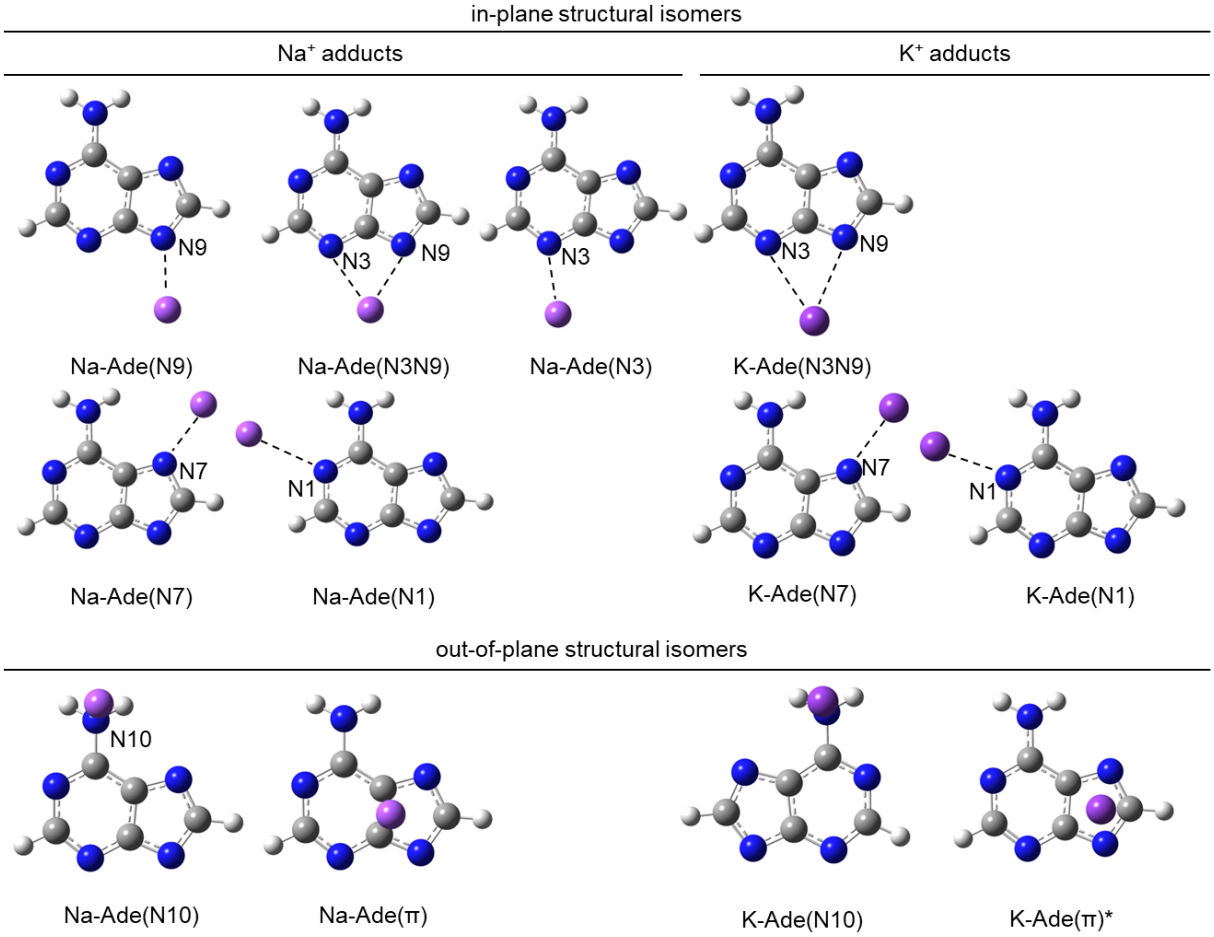

Figure 3.7: Optimized structures of Na- and K-Ade complexes at CCSD/6-311++g(d,p)/PCM(DMSO), * structure of K-Ade(π) obtained at DFT/M06-2X /6-311++g(d,p)/PCM(DMSO).

functional group, as previously reported for neutral adenine.[5,12] The CCSD and DFT/B3LYP calculations discovered a Na-Ade(π) isomer and not a K-Ade(π) isomer, Figure 3.7. This is the first theoretical report of the Na^+ ion being involved in a cation-π interaction with the purine ring of adenine, and is potentially driven by the electrostatic attraction of the negatively charged adeninate anion. Previous theoretical work showed no involvement of the Na^+ in a cation-π interactions with the purine ring of neutral adenine.[16] There is only one 'major' discrepancy between the CCSD and B3LYP stability of the cation-π interaction of Na-Ade(π). The isomer is more stable than the Na-Ade(N10) by –2.8 kcal mol^{-1} at the DFT/B3LYP level and less stable by more than 1.2-1.6 kcal mol^{-1} at CCSD, Table 3.1.

The DFT/B3LYP level of theory overestimates the cation-π interaction (see bond lengths in Table S2.2 and S2.3), in line with previous reports.[50] The complexation between Ade^- and the Na^+/K^+ counter ion is spontaneous for all isomers having the energy of formation ($E_f = E_{M\text{-}Ade} - (E_{Ade}+E_M)$) twice as large for the in plane (N3)/(N3N9)/(N9) isomers compared to the (N10) isomer for both the Na^+/K^+ complexes, Table 3.2. The large negative E_f for the formation of ion pairs provides insight as to why no free Ade^- was observed in the experimental research described in Chapter 2. The Gibbs free energy of formation, G_f, obtained for the DFT/B3LYP structures, Table S2.1, indicates that formation of M-Ade(N10) is nonspontaneous.

© University of Pretoria

Table 3.2: The Energy of Formation (E_f) of Na- and K-Ade complexes (kcal mol^{-1})

Na-Ade			E_f		K-Ade		E_f	
isomer	B3LYP[a]	*CCSD*[b]	*CCSD-aug*[c]	M06-2X[d]	isomer	B3LYP[a]	*CCSD*[b]	M06-2X[c]
(N9)	–10.6	–7.4	–6.8	–9.2	(N3N9)	–10.1	–8.9	–10.3
(N3N9)	–10.6	–7.3	–6.6	–9.9	(N7)	–7.9	–6.4	–6.9
(N3)	–9.8	–6.3	–5.8	–9.8	(N1)	–6.8	–5.3	–5.7
(N7)	–9.4	–6.3	–5.8	–7.9	(N10)	–5.7	–4.5	–4.3
(N1)	–7.5	–4.9	–4.5	–6.4	(π)	-	-	–5.4
(N10)	–5.6	–3.5	–3.0	–4.0				
(π)	–8.5	–1.9	–1.8					

[a] DFT/B3LYP/6-311G++(d,p)/PCM(DMSO) [b] CCSD/6-311++g(d,p)/PCM(DMSO) [c] CCSD/aug-cc-pvdz/PCM(DMSO) [d] DFT/M06-2X /6-311++g(d,p)/PCM(DMSO)

3.4.2 Preferential coordination sites between Na^+ and K^+ and the adeninate anion from IQA and REP-FAMSEC methods

REP-FAMSEC[49] is a recent protocol developed in our research group based on the parent FAMSEC method.[51] REP-FAMSEC allows for the study of the change in intra- and inter-molecular interactions of a molecular system (diatomic for whole fragments) relative to a reference state due to the change in the immediate or distant molecular environment.

The observed trends of the Δ*E* for the optimized Na- and K-Ade structural isomers in Table 3.1 indicates that the counter ion is likely to coordinate in the in-plane fashion at either endo purine nitrogen atom. The stability of the site of coordination at these nitrogen atoms decreases in the order N9 = N3N9 > N3 > N7 > N1 for the Na^+ complexes and N3N9 > N7 > N1 for the K^+ complexes. Coordination at the exo-purine ring N10 nitrogen atom and the formation of the cation-π interaction are the least favourable isomers to occur.

This finding reveals that the chemistry between the Na^+ and K^+ counter ions with the adeninate anion is significantly different when compared with the neutral adenine tautomers in which the proton occupies the N9 > N7 > N3 > N1 sites for the various tautomeric forms.[19,25] The preferential site of coordination of alkali metals with Ade^- differs from that of the metal ion affinity trend of N7 > N1 > N3 for the neutral dominant tautomeric form of adenine, N9(H).[5] As the proton occupies the N9 position for neutral adenine, this is not surprising. However, chelation at the N3 and N9 position of the N7(H) and N1(H) tautomers of neutral adenine is highly favourable over any chelation of the N9(H) adenine.[12] Favourable coordination of metal ions at the N3 and N9 of neutral adenine tautomeric forms, together with the experimental evidence that suggests chelation or unidentate coordination at the N3 and N9 atoms of Ade^- and theoretical support thereof, highlights these atoms involvement in ion pairing. It is interesting to note that the M-Ade trend is in line with the site of alkylation of the adeninate anion whereby experimental research has shown that the N9 (major product) and N3 (minor product) atom are the sites of alkylation.[52–54]

The Δ*E* of the M-Ade structural isomers is informative regarding the potential sites of coordination of the Na^+ and K^+ counter ion with the adeninate purine ring, however it does not give any insight into i) how the electron density of the adeninate molecule changes, ii) how the adeninate anion is stabilized upon coordination of the Na^+ and K^+ metal ions, and iii) which atoms and molecular

© University of Pretoria

fragments are involved in the most stabilizing interactions between the counter ion and the adeninate anion. A detailed investigation of the above molecular systems using IQA/REP-FAMSEC defined energy terms is carried out to identify the key factors that play a role in the stability of the structural isomers. The structures obtained at CCSD and DFT/B3LYP level of theory are used for the analysis as the structural isomers and similar Δ*E* trends were achieved within these two levels of theory. The superior CCSD level of theory is used as the leading investigating tool and DFT/B3LYP is used to evaluating the suitability of using this lower level of theory.

3.4.3 Understanding Na^+ and K^+ complexation trends with the adeninate anion

The numbering of the atoms for the adeninate anion shown in Figure 3.8 is used throughout the chapter.

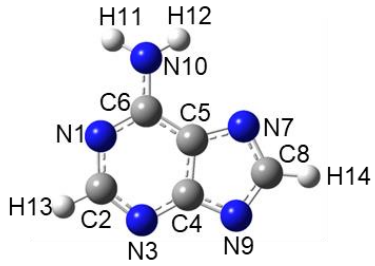

Figure 3.8: The numbering of the atoms of the adeninate anion.

It is of interest to explore whether the charge on the nitrogen atoms of the purine ring can account for the observed trend in isomer stability, having the counter ion coordinated at the most negatively charged nitrogen atom. In addition, the change in the net atomic charges (from QTAIM calculations using Bader's net atomic charges[55]) of the nitrogen atoms upon complexation can provide insight into ion-induced polarization of the adeninate molecule and how the system reacts to the coordination of metal ions. The net atomic charge for each nitrogen atom, Q(N), of Ade^- and the relative changes, $\Delta Q(N) = Q(N)_{M\text{-}Ade} - Q(N)_{Ade^-}$, upon formation of Na-Ade and K-Ade complexes at CCSD and DFT/B3LYP are given in Table 3.3 and Table 3.4, respectively. For the complete list of Q(A) calculated for all atoms at CCSD and DFT/B3LYP, refer to Table S2.6 and S2.7 in the SI. The net charge of adeninate anion, $Q(Ade^-)$ is obtained by the summation of the net atomic charges of Ade^- and before coordination of M^+, $Q(Ade^-) = -1$. The change, $\Delta Q(Ade^-) = Q(M^+\text{-}Ade^-) - \Delta Q(\text{free-}Ade^-)$, indicates the outflow (positive) or inflow (negative) of electron density upon complexation of the metal ion.

Firstly, the negative charge −1 on Ade^- is mainly and almost equally distributed among all the endo-purine ring nitrogen atoms, having the N3 atom carrying the most electron density (–1.276 *e*), followed by the N1 atom (–1.266 *e*), then the N9 and N7 atoms. The exo-purine nitrogen atom, N10, carries significantly less charge (–1.147 *e*), and could be a contributing factor as to why the M-Ade(N10) isomer is the least likely to exist. These trends in charge distribution are replicated in the DFT/B3LYP data. The possibility of the metal ion coordinating to potentially any endo-purine ring nitrogen atom is in line with the electron density being distributed throughout the ring system.

© University of Pretoria

The change in the net atomic charge of nitrogen atom, Δ*Q*(N) term in Table 3.3, shows that the complexation of the counter ion Na^+ and K^+ with Ade^- results in a change of electron density throughout the purine ring and is not only linked to the involved nitrogen donor atom(s) with which the counter ion coordinates. The most significant change occurs at the nitrogen donor atom in each of the structural isomers. These atoms gain the most electron density, polarizing the molecule in return. The N3- (–0.026 *e*), N3N9- (–0.021 and –0.026 *e* for the N3 and N9, respectively) and N9- atoms (–0.022 *e*) of the corresponding isomers gain the most electron density compared to the N7, N1 and N10 isomers (similar values are obtained at the DFT/B3LYP level of theory).

Table 3.3: Net atomic charge of N-atoms of free Ade^- *Q*(N), and the changes in charge of the N-atoms of M-Ade relative to free Ade^-, Δ*Q*(N), the net molecular charge of Ade^- *Q*(Ade^-) and the change Δ*Q*(Ade^-), the net atomic charge of free Na^+, (*Q*(Na^+)) and K^+ (*Q*(K^+)) and the change in charge relative to free Na^+, (Δ*Q*(Na^+)) and K^+ (Δ*Q*(K^+)), upon formation of Na- and K-Ade structural isomers, at CCSD level of theory (all values in *e*)

	Q		Δ*Q*						
			Na-Ade complexes						
Atom N	Ade^-		(N1)	(N3)	(N3N9)	(N9)	(N7)	(N10)	(π)
N3	–1.276		0.005	–0.026	–0.021	0.001	0.004	0.005	0.001
N1	–1.266		–0.017	0.006	0.010	0.004	0.003	0.001	0.001
N9	–1.248		0.005	–0.002	–0.026	–0.022	0.006	0.005	0.001
N7	–1.234		0.004	0.008	0.016	0.008	–0.020	0.004	0.001
N10	–1.147		0.000	–0.004	–0.005	–0.002	0.005	0.017	0.000
Q(Ade^-)	–1.000	Δ*Q*(Ade^-)	0.028	0.031	0.039	0.034	0.031	0.021	0.003
Q(Na^+)	1.000	Δ*Q*(Na^+)	–0.028	–0.031	–0.040	–0.034	–0.031	–0.021	–0.003
			K-Ade complexes						
Atom N			(N1)		(N3N9)		(N7)	(N10)	
N3			0.005	-	–0.010	-	0.003	0.005	-
N1			–0.006	-	0.007	-	0.002	0.002	-
N9			0.004	-	–0.009	-	0.004	0.005	-
N7			0.003	-	0.011	-	–0.005	0.004	-
N10			0.001	-	–0.006	-	0.005	0.013	-
Q(Ade^-)		Δ*Q*(Ade^-)	0.025	-	0.041	-	0.028	0.021	-
Q(K^+)	1.000	Δ*Q*(K^+)	–0.025	–	-0.041	-	–0.029	–0.021	-

Formation of the (N3N9) isomer did not result in a reduced electron gain at the two nitrogen donor atoms, the N3 and N9, but rather a similar gain of electrons at each N-atom is observed and it is comparable to gains computed for the unidentate coordinated N3 and N9 isomers. Comparing the magnitude of Δ*Q*(N) of the Na^+ and K^+ complexes shows a 2–3 times greater change in the N-donor atom(s) of the Na^+ structural isomers compared to the equivalent K^+ isomers. This is attributed to the Na^+ ion interacting stronger with the anion due to its larger charge-to-radius ratio and hence a greater electrostatic interaction with the adeninate anion. This is in line with the experimental observation (Chapter 2) that the Na^+ ion interacts more strongly with Ade^- than K^+. The gain in

© University of Pretoria

electron density at the nitrogen donor atom(s) is accompanied by a loss of electron density throughout the purine ring system and not only the atoms adjacent to the N-donor atoms.

Table 3.4: Net atomic charge of N-atoms of free Ade^- Q(N), and the changes in charge of the N-atoms of M-Ade relative to free Ade^-, ΔQ(N), the net molecular charge of Ade^- $Q(Ade^-)$ and the change $\Delta Q(Ade^-)$, the net atomic charge of free Na^+, ($Q(Na^+)$) and K^+ ($Q(K^+)$) and the change in charge relative to free Na^+, ($\Delta Q(Na^+)$) and K^+ ($\Delta Q(K^+)$), upon formation of Na- and K-Ade structural isomers, at the DFT/B3LYP level of theory (all values in *e*)

	Q		ΔQ						
			Na-Ade complexes						
Atom N	Ade^-		(N1)	(N3)	(N3N9)	(N9)	(N7)	(N10)	(π)
N3	–1.193		0.003	–0.025	–0.024	0.001	0.004	0.006	0.002
N1	–1.177		–0.014	0.006	0.010	0.005	0.004	0.002	0.002
N9	–1.166		0.003	–0.002	–0.025	–0.023	0.006	0.007	0.003
N7	–1.159		0.002	0.008	0.017	0.008	–0.019	0.006	0.003
N10	–1.105		0.001	–0.006	–0.007	–0.004	0.008	0.019	–0.004
$Q(Ade^-)$	–1.000	$\Delta Q(Ade^-)$	0.017	0.041	0.051	0.043	0.040	0.026	0.006
$Q(Na^+)$	1.00	$\Delta Q(Na^+)$	–0.017	–0.041	–0.052	–0.043	–0.040	–0.026	–0.006
			K–Ade complexes						
Atom N			(N1)		(N3N9)		(N7)	(N10)	
N3			0.004	-	–0.009	-	0.004	0.006	-
N1			–0.004	-	0.007	-	0.003	0.002	-
N9			0.005	-	–0.008	-	0.005	0.007	-
N7			0.004	-	0.011	-	–0.004	0.006	-
N10			0.004	-	–0.005	-	0.008	0.012	-
$Q(Ade^-)$		$\Delta Q(Ade^-)$	0.030	-	0.050	-	0.036	0.025	-
$Q(K^+)$	1.00	$\Delta Q(K^+)$	–0.030	-	–0.050	-	–0.036	–0.024	-

The overall positive change in the net molecular charge of the adeninate anion upon metal ion complexation, i.e. $\Delta Q(Ade^-) > 0$, shows an outflow of *e* to M^+, Table 3.3. The outflow of electron density, which shows charge transfer from Ade^- to M^+, is similar between Na^+ and K^+ complexes even though the charge polarization is much smaller for K-Ade complexes. The results from DFT/B3LYP show that for the (N1) isomer, the K^+ decreases in charge by almost twice (–0.030 *e*) as much as the Na^+ (–0.017 *e*). The redistribution of electron density in the adeninate anion compensates for the overall loss of electron density from the purine ring system for the formation of the ionic bond. For both the Na^+ and K^+ complexes, the N3N9 isomer loses the most electron density i.e. $\Delta Q(Ade^-)$ = 0.039 and 0.041 *e*, respectively. The loss of electron density is gained by the coordinated counter ion, $\Delta Q(Na^+)$ and $\Delta Q(K^+)$ values in Table 3.3. Although there is some discrepancy for the N1 data between the CCSD and DFT/B3LYP level of theory, the order of increasing charge of Na^+ and K^+ ions for both the Na- and K-Ade isomers highlights the N3N9 isomer transferring the most electron density from Ade^- as contribution from both the N3 and N9 atoms occurs.

It is reasonable to assume that the changes in Q(A) of the adeninate purine ring upon cation complexation should in turn result in changes in the intramolecular covalent bond (C-B) and long-distance (L-D) interactions. These changes are investigated in the following section.

© University of Pretoria

3.4.4 Influence of complexation on covalent and long-distance intramolecular interactions of adeninate anion

The total intramolecular interaction energy[49] of the free adeninate anion, ${}_{\text{intra}}E_{\text{int}}^{\text{Ade}^-}$, consists of all diatomic interactions between covalently bonded (${}^{\text{C-B}}E_{\text{int}}^{\text{Ade}^-}$) atoms and long distance interactions between non-bonded atoms (${}^{\text{L-D}}E_{\text{int}}^{\text{Ade}^-}$), eqn 3.2:

$$ {}_{\text{intra}}E_{\text{int}}^{\text{Ade}^-} = {}^{\text{C-B}}E_{\text{int}}^{\text{Ade}^-} + {}^{\text{L-D}}E_{\text{int}}^{\text{Ade}^-} \tag{3.2} $$

The change in the total intramolecular interaction energy of Ade^- upon complexation with the metal ion (eqn 3.3) for each isomer of the Na-Ade and K-Ade complexes at CCSD and DFT/B3LYP is shown in Table 3.5 and Table 3.6, respectively. Note that the ${}^{\text{M-Ade}}_{\text{intra}}E_{\text{int}}^{\text{Ade}^-}$ term in eqn 3.3 does not include interactions between Ade^- and M^+.

$$ \Delta_{\text{intra}}E_{\text{int}}^{\text{Ade}^-} = {}^{\text{M-Ade}}_{\text{intra}}E_{\text{int}}^{\text{Ade}^-} - {}_{\text{intra}}E_{\text{int}}^{\text{Ade}^-} \tag{3.3} $$

Table 3.5: Changes in the total intramolecular interaction energy of Ade^-, the covalent bond (C-B) strength including the exchange correlation and classical term components, and long-distance (L-D) interactions computed on the formation of the Na-Ade and K-Ade structural isomers at the CCSD level of theory. All values in kcal mol^{-1}

conformer	(N9)	(N3N9)	(N3)	(N7)	(N1)	(N10)	(π)
				Na-Ade complexes			
$\Delta_{\text{intra}}E_{\text{int}}^{\text{Ade}^-}$	–21.3	–29.4	–23.0	–15.6	–10.8	17.8	2.8
$\Delta^{\text{C-B}}E_{\text{int}}^{\text{Ade}^-}$	–27.8	–38.8	–29.4	–17.9	–11.3	27.7	3.7
$\Delta^{\text{C-B}}V_{\text{XC}}^{\text{Ade}^-}$	2.8	3.7	2.7	2.7	2.3	2.5	0.2
$\Delta^{\text{C-B}}V_{\text{Cl}}^{\text{Ade}^-}$	–30.6	–42.5	–32.1	–20.5	–13.6	25.2	3.5
$\Delta^{\text{L-D}}E_{\text{int}}^{\text{Ade}^-}$	6.5	9.5	6.4	2.3	0.5	–9.9	–0.9
				K-Ade complexes			
$\Delta_{\text{intra}}E_{\text{int}}^{\text{Ade}^-}$	-	–19.9	-	–7.0	–4.6	13.5	-
$\Delta^{\text{C-B}}E_{\text{int}}^{\text{Ade}^-}$	-	–25.2	-	–7.5	–3.6	21.5	-
$\Delta^{\text{C-B}}V_{\text{XC}}^{\text{Ade}^-}$	-	3.1	-	1.8	1.5	1.9	-
$\Delta^{\text{C-B}}V_{\text{Cl}}^{\text{Ade}^-}$	-	–28.3	-	–9.3	–5.1	19.6	-
$\Delta^{\text{L-D}}E_{\text{int}}^{\text{Ade}^-}$	-	5.3	-	0.5	–0.9	–8.0	-

The coordination of the counter ion at the in plane positions of the purine stabilizes the adeninate anion the most, having $\Delta_{\text{intra}}E_{\text{int}}^{\text{Ade}^-}$ in favour of the (N3N9) isomer by more than –6 kcal mol^{-1} (> –10 kcal mol^{-1} for the DFT/B3LYP structures) in both the Na^+ and K^+ complexes. An overall trend for the preference in site coordination of (N3N9) > (N3) ≥ (N9) > (N7) > (N1) is observed for both the Na^+ and K^+ complexes. The coordination of the Na^+ and K^+ counter ion with the amino group (N10) largely destabilizes the adeninate anion by +17.8 and +13.5 kcal mol^{-1}, respectively, suggesting that this isomer does not form. The coordination of Na^+ with the π system of the adeninate anion results in

© University of Pretoria

relatively small and unfavourable change (2.8 kcal mol^{-1}) indicating that the cation-π interaction is weaker than the in-plane ionic interactions. Thus, the cation-π and N10 complexes are rejected as possible isomers of Na- and K-Ade complexes. This is in support of our experimental work which did not suggest complexation at the N10 or the presence of cation-π interaction with the adeninate anion.

Partitioning the $\Delta_{\text{intra}}E_{\text{int}}^{\text{Ade}^-}$ into the contributions from the covalent, ($\Delta^{\text{C-B}}E_{\text{int}}^{\text{Ade}^-}$) and long-distance, ($\Delta^{\text{L-D}}E_{\text{int}}^{\text{Ade}^-}$) interactions, shows that the above stabilizing change in the adeninate anion is entirely due to strengthened covalent bonds. Notably, there is an opposite trend between C-B and L-D interactions with the latter becoming weaker and the former much stronger when Ade^- is complexed by either Na^+ or K^+. Analysis of the two components of the covalent bond interaction, i.e. the electrostatic/coulombic ($^{\text{C-B}}V_{\text{Cl}}^{\text{Ade}^-}$) and exchange-correlation/covalent ($\Delta^{\text{C-B}}V_{\text{XC}}^{\text{Ade}^-}$) terms, in Table 3.5, indicates an overall outflow of electron density from interatomic regions (bonds) to atomic basins (atoms) as the $\Delta^{\text{C-B}}V_{\text{XC}}^{\text{Ade}^-}$ term slightly weakens. Due to the redistribution of electron density experienced by the adeninate anion upon complexation of the cation (as shown in Table 3.3) and the resulting charge polarization, the C-B interactions strengthen due to the more favourable coulombic term,[47,56] Table 3.5. The C-B interactions are strengthened twice as much for the Na^+ complexes than the K^+ complexes, as is reflected in the $\Delta_{\text{intra}}E_{\text{int}}^{\text{Ade}^-}$. This is due to the Na^+ ion perturbing the electronic environment to a larger extent than K^+ as a result of the larger charge-to-radius ratio of Na^+.

Table 3.6: Changes in the total intramolecular interaction energy of Ade^-, the covalent bond (C-B) strength including the exchange correlation and classical term components, and long-distance (L-D) interactions computed on the formation of the Na-Ade and K-Ade structural isomers at the DFT/B3LYP level of theory. All values in kcal mol^{-1}

isomer	(N9)	(N3N9)	(N3)	(N7)	(N1)	(N10)	(π)
				Na-Ade complexes			
$\Delta_{\text{intra}}E_{\text{int}}^{\text{Ade}^-}$	–22.2	–32.5	–23.3	–12.3	–8.1	20.2	1.0
$\Delta^{\text{C-B}}E_{\text{int}}^{\text{Ade}^-}$	–29.1	–43.1	–30	–14.2	–9.3	31.6	1.8
$\Delta^{\text{C-B}}V_{\text{XC}}^{\text{Ade}^-}$	4.2	6	4.6	3.5	2	2.3	0.5
$\Delta^{\text{C-B}}V_{\text{Cl}}^{\text{Ade}^-}$	–33.3	–49.1	–34.6	–17.8	–11.3	29.3	1.3
$\Delta^{\text{L-D}}E_{\text{int}}^{\text{Ade}^-}$	7.0	10.6	6.7	1.9	1.2	–11.4	–0.8
				K-Ade complexes			
$\Delta_{\text{intra}}E_{\text{int}}^{\text{Ade}^-}$	-	–19.1	-	–3.3	–0.7	14.9	-
$\Delta^{\text{C-B}}E_{\text{int}}^{\text{Ade}^-}$	-	–24.5	-	–2.5	2	24	-
$\Delta^{\text{C-B}}V_{\text{XC}}^{\text{Ade}^-}$	-	4.4	-	2.2	1.9	1.6	-
$\Delta^{\text{C-B}}V_{\text{Cl}}^{\text{Ade}^-}$	-	–28.9	-	–4.7	0	22.3	-
$\Delta^{\text{L-D}}E_{\text{int}}^{\text{Ade}^-}$	-	5.4	-	–0.8	–2.7	–9.1	-

To better understand which diatomic interactions changed the most upon metal ion coordination and weather this trend is in line with the degree of change in ΔQ(N) of the N-donor atoms, a graphical representation of the most stabilized/strengthened (blue) and destabilized/weakened (red) covalently bonded diatomic interactions, $\Delta^{\text{C-B}}E_{\text{int}}^{\text{A,B}}$, are shown for the Na- and K-Ade isomers in Figure 3.9 and Figure 3.10, respectively, for the CCSD level of theory (refer to Figure S2.1 and S2.2

© University of Pretoria

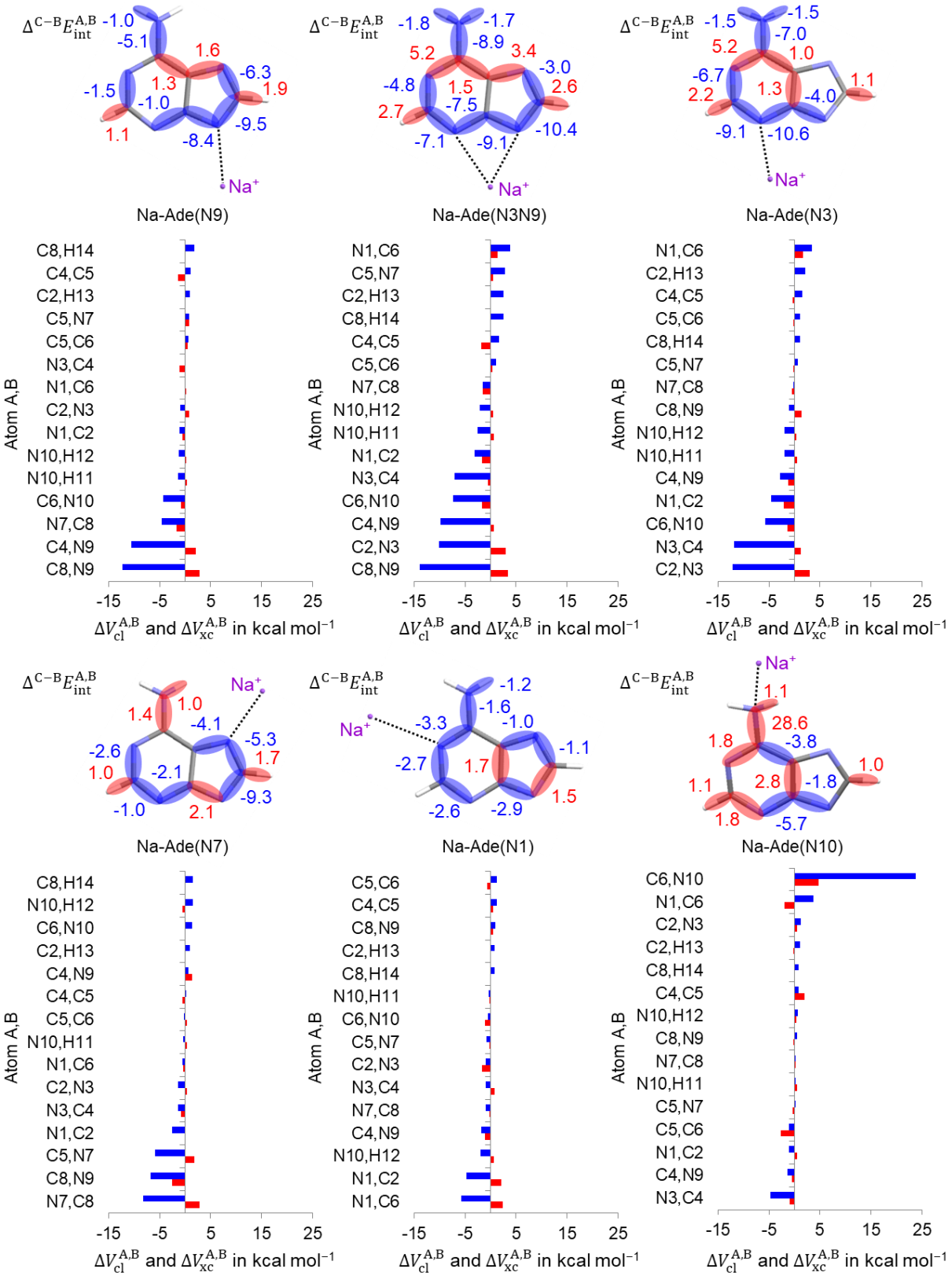

Figure 3.9: Changes in the diatomic covalent bond intramolecular interactions, $\Delta^{C-B}E_{int}^{A,B}$, and its $\Delta V_{cl}^{A,B}$ and $\Delta V_{xc}^{A,B}$ components. Blue and red sites indicate stabilizing and destabilizing energy terms of the adeninate anion upon coordination of Na^+ for the Na-Ade isomers, at CCSD level of theory.

© University of Pretoria

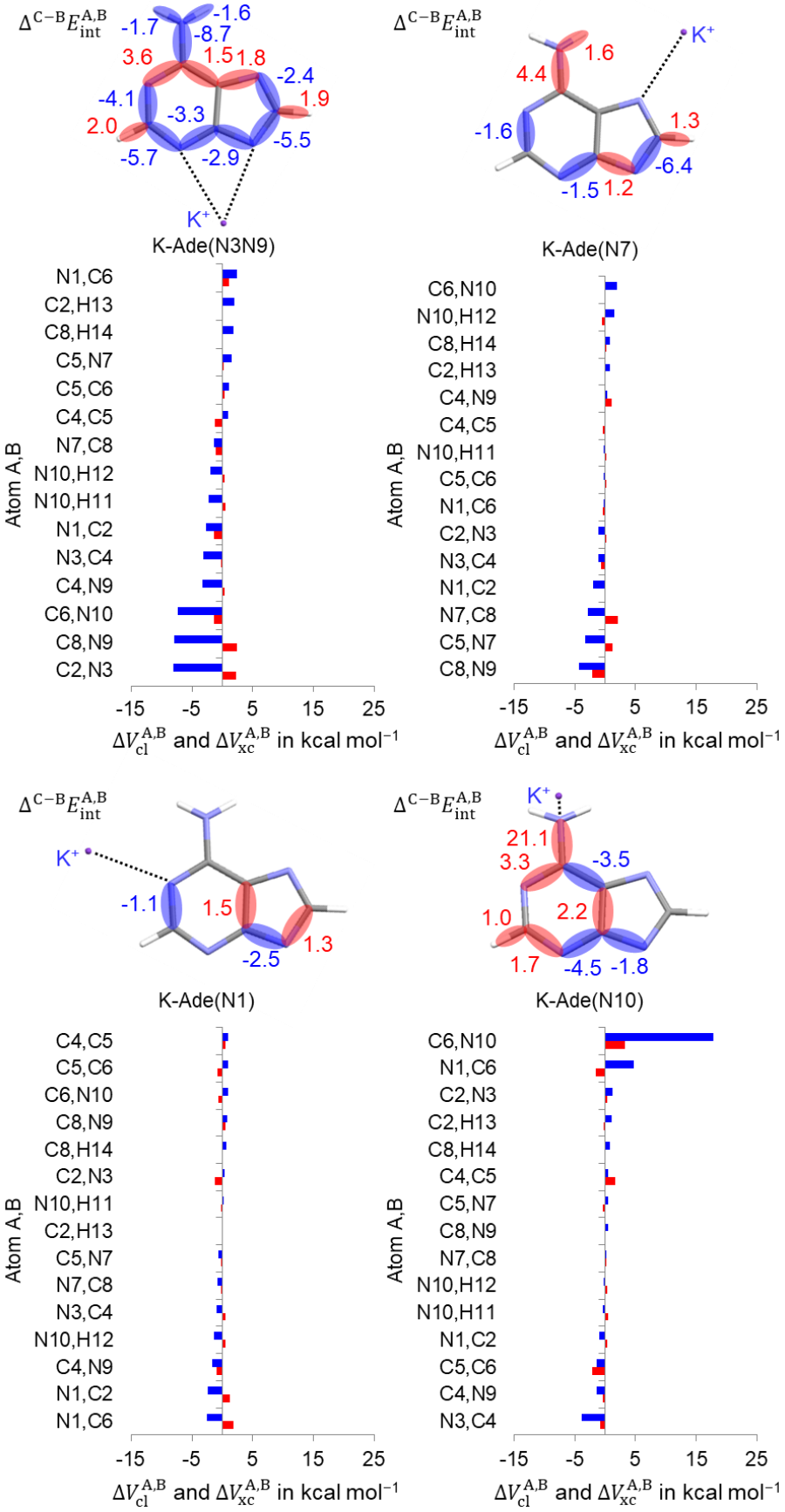

Figure 3.10: Changes in the diatomic covalent bond intramolecular interactions, $\Delta^{C-B}E_{int}^{A,B}$, and its $\Delta V_{cl}^{A,B}$ and $\Delta V_{xc}^{A,B}$ components. Blue and red sites indicate stabilizing and destabilizing energy terms of the adeninate anion upon coordination of K^+ for the Na-Ade isomers, at CCSD level of theory.

© University of Pretoria

for DFT/B3LYP values). Only $\Delta^{C-B}E_{int}^{A,B}$ interactions that changed by more than +1 or −1 kcal mol^{-1} are shown, thus Na-Ade(π) is not included (see Figure S2.3 and S2.4 for Na-Ade(π) data at CCSD and DFT/B3LYP levels of theory, respectively). In addition, the individual change in the coulombic ($\Delta V_{cl}^{A,B}$) and exchange-correlation ($\Delta V_{xc}^{A,B}$) terms of the covalently bonded atoms A and B of the purine ring are shown by the bar graphs for each M-Ade structure.

From Figure 3.9 and Figure 3.10, it can be seen that the Na-and K-Ade(N3N9) isomer has a large portion of the purine ring stabilized. The two bonds on either side of the N3 and N9 donor atoms are stabilized the most and to a larger extent for the Na-Ade(N3N9) isomer in comparison to K-Ade(N3N9), in agreement with the degree of change in ΔQ(Ade$^-$) from Table 3.3. The gain in electron count of the N3 and N9 donor atoms, ΔQ(N) < 0, and the loss of electrons at the adjacent carbon atoms leads to an increase in charge polarization of the purine ring. This is reflected in the weakening of the $\Delta V_{xc}^{A,B}$ term and the strengthening of the $\Delta V_{cl}^{A,B}$ term, Figure 3.9 and Figure 3.10. There is movement of electrons from the interatomic regions between these covalently linked atoms to their atomic basins as the metal ion complexes with Ade$^-$ are formed. This enhanced polar covalent bond character is more dominant for the Na^+ ion complexation than the K^+ ion, which is in line with the smaller Na^+ ion resulting in a larger ion-induced dipole moment.[5] The interaction between atom C6 and N10 is strengthened to a significant extent for the in-plane N3, N3N9 and N9 isomers upon coordination of the counter ion as measured by the $\Delta^{C-B}E_{int}^{C6,N10}$ of –7.0, –8.9 and –5.1 kcal mol^{-1}, respectively for the Na^+ complexes and –8.7 kcal mol^{-1} for the K-Ade(N3N9) isomer. The C6–N10 interaction is destabilized for the (N7) and (N10) structural isomers, having the interaction of the M-Ade(N10) isomer destabilized the most i.e. $\Delta^{C-B}E_{int}^{A,B}$ = 28.6 and 21.1 kcal mol^{-1} for the Na^+ and K^+ complex, respectively. Both the $\Delta V_{xc}^{A,B}$ and $\Delta V_{cl}^{A,B}$ terms are positive, having the coulombic term significantly weakened.

The strengthening and weakening of the C6–N10 interaction for the isomers is of particular interest. Previous research has shown the versatility of the NH_2 group of adenine in its mode of coordination and changes in the hybridization upon coordination of metal ions. However, much research has focused on the direct interactions of the amino group with the metal ions. In this research, it is clear that the nature of the NH_2 group and its interaction with the purine ring is affected by the coordination of the metal ion on the opposite side of the ring, i.e. the N3 and N9 nitrogen atoms. To gain insight into the origin of the stabilization/destabilization of the C6–N10 bond, the electron density (ρ) at the bond critical point of the C6–N10 bond, BCP(C6,N10), for all isomers and for Ade$^-$ is plotted against the C6–N10 bond length, d(C6,N10), Figure 3.11 (see Figure S2.5 for DFT/B3LYP data). The BCP is defined as the point along the bond path between two atoms where the shared electron density is at a minimum.[57]

The C6–N10 bond length is shortened for the (N1), (N3), (N3N9) and (N9) structural isomers relative to Ade$^-$ (1.385 Å) and is accompanied by an increase in ρ. The bond length is increased for the (N7) and (N10) isomers of both Na- and K-Ade complexes with a corresponding decrease in the ρ at BCP(C6,N10). Relating this gain/loss in electron density between the C6 and N10 atom to the electron pairs delocalization index (DI(C6,N10)), which indicates the average number of electron pairs delocalized between the two atoms, Figure 3.12, shows that there is a decrease in shared electrons for the (N10) and (N7) Na- and K-Ade isomers relative to Ade$^-$ (see Figure S2.6 for DFT/B3LYP data). More electrons are delocalized between atoms of the C6–N10 bond of the (N1),

© University of Pretoria

(N3), (N3N9) and (N9) structural isomers, having this effect largest for the Na- and K-Ade(N3N9) isomer.

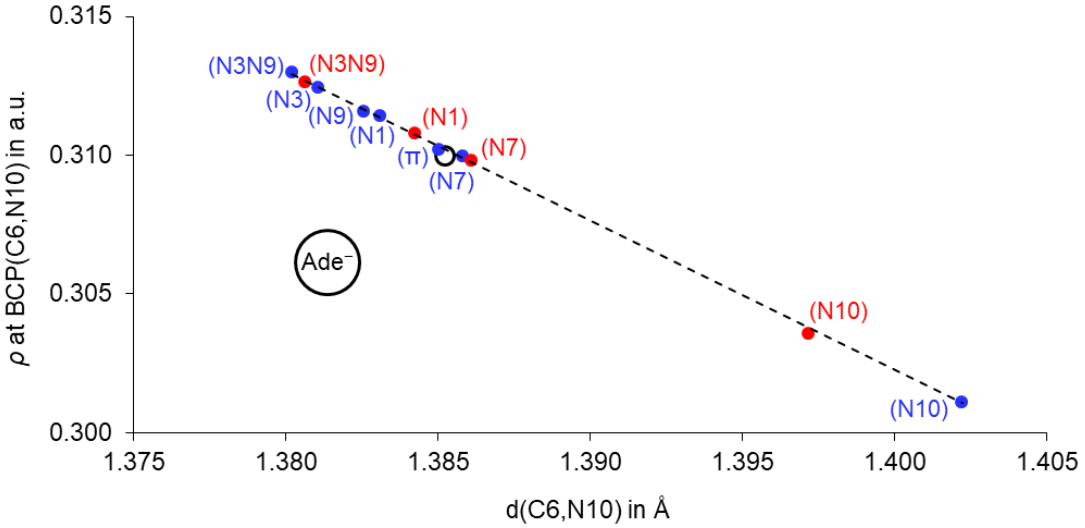

Figure 3.11: Relationship between rho (ρ) at BCP(C6,N10) and the C6–N10 bond length of the Na^+ (blue circles), K^+ (red circles) structural isomers and Ade^- (black outlined circle) at CCSD level of theory.

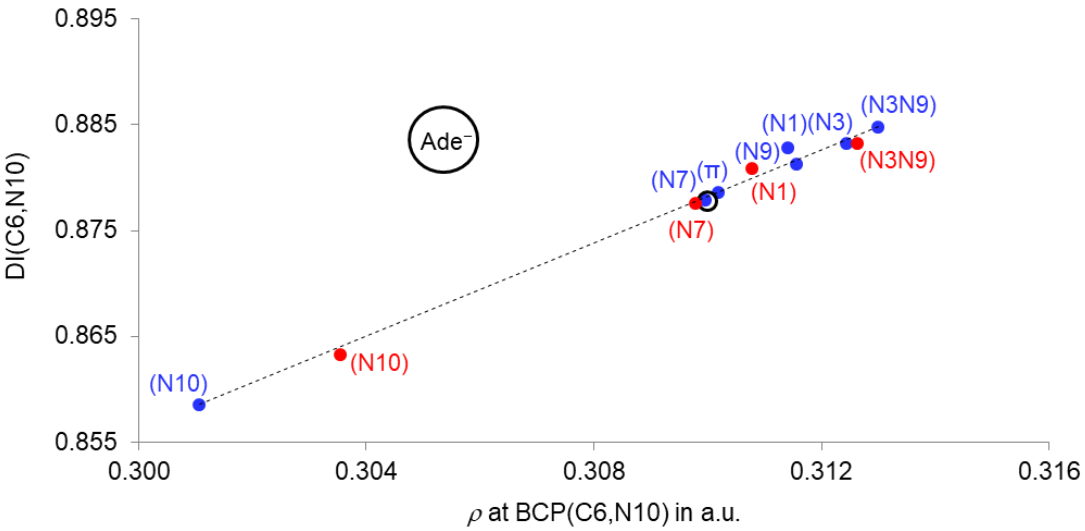

Figure 3.12: Relationship between rho (ρ) at BCP(C6,N10) and the DI(C6,N10) bond length of the Na^+ (blue circles), K^+ (red circles) structural isomers and Ade^- (black outlined circle) at CCSD level of theory.

The change in the DI of the C6–N10 bond and the change in the net atomic charge, hence also charge density, of the two atoms influence the interaction energy between atoms C6 and N10, $\Delta^{\mathrm{C-B}}E_{\mathrm{int}}^{\mathrm{C6,N10}}$, as seen in Figure 3.9 and Figure 3.10. The classical term, $V_{\mathrm{cl}}^{\mathrm{C6,N10}}$, consists of all electrostatic contributions, eqn 3.4,

© University of Pretoria

$$V_{\mathrm{cl}}^{\mathrm{C6,N10}} = V_{\mathrm{nn}}^{\mathrm{C6,N10}} + V_{\mathrm{ne}}^{\mathrm{C6,N10}} + V_{\mathrm{en}}^{\mathrm{C6,N10}} + V_{\mathrm{C}}^{\mathrm{C6,N10}} \quad (3.4)$$

where $V_{\mathrm{nn}}^{\mathrm{C6,N10}}$ is the inter-nuclear repulsion energy between the nuclei of atoms C6 and N10, $V_{\mathrm{ne}}^{\mathrm{C6,N10}}$ is the interatomic electron-nuclear attraction energy between the nucleus of atom C6 and the electrons of atom N10 and vice versa in $V_{\mathrm{en}}^{\mathrm{C6,N10}}$. $V_{\mathrm{C}}^{\mathrm{C6,N10}}$ is the coulombic contribution to the $V_{\mathrm{ee}}^{\mathrm{C6,N10}}$ term, eqn 3.5,

$$V_{\mathrm{ee}}^{\mathrm{C6,N10}} = V_{\mathrm{C}}^{\mathrm{C6,N10}} + V_{\mathrm{xc}}^{\mathrm{C6,N10}} \quad (3.5)$$

where $V_{\mathrm{ee}}^{\mathrm{C6,N10}}$ is the interatomic electron-electron repulsion energy between the electrons of atoms C6 and N10. In general, the interaction energy between atoms A and B, $E_{\mathrm{int}}^{\mathrm{A,B}}$, is not a measure of covalent bond strength, but is an intrinsic measure of the physical interaction strength between atom A and B.[58] It is suggested that $V_{\mathrm{xc}}^{\mathrm{A,B}}$ is better used for the strength of a covalent bond.[56] A plot of the $\Delta V_{\mathrm{ne}}^{\mathrm{C6,N10}}$ and $\Delta V_{\mathrm{nn}}^{\mathrm{C6,N10}}$ terms versus the C6–N10 bond length, Figure 3.13, shows a linear relationship between the two terms and the bond length (see Figure S2.7 for DFT/B3LYP data).

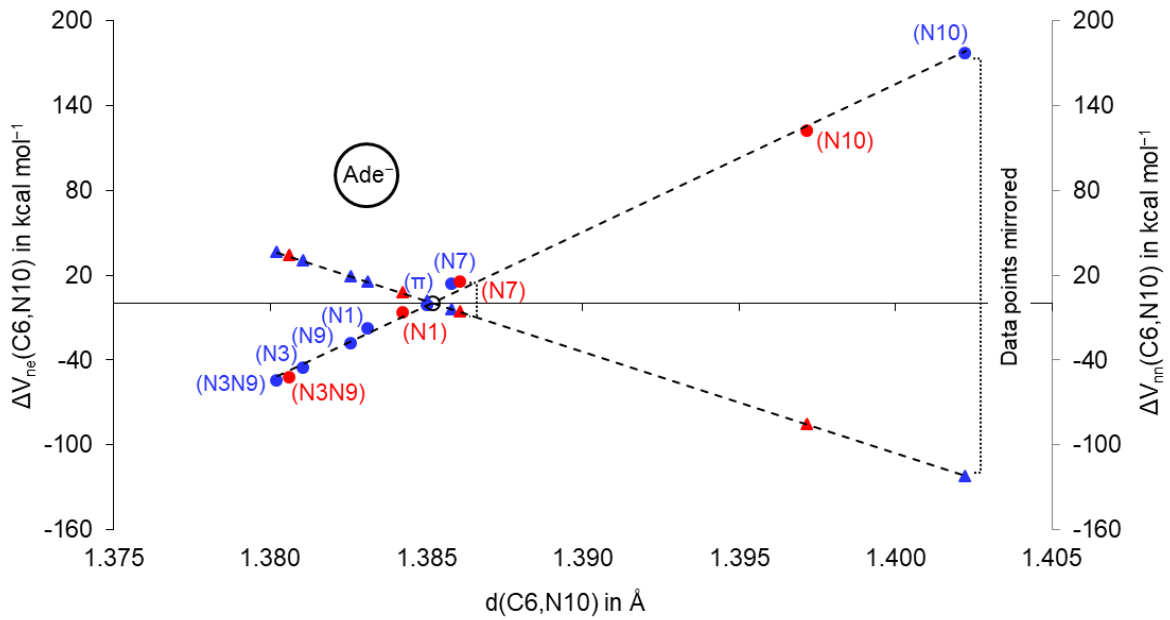

Figure 3.13: Relationship between $\Delta V_{\mathrm{ne}}^{\mathrm{C6,N10}}$ (primary axis, circles) and $\Delta V_{\mathrm{nn}}^{\mathrm{C6,N10}}$ (secondary axis, triangles) with the C6–N10 bond length of the Na^+ (blue data points) and K^+ (red data points) structural isomers and Ade^- (black outlined circle) at CCSD level of theory.

There is an inverse relationship between the bond distance of C6–N10 and the $\Delta V_{\mathrm{nn}}^{\mathrm{C6,N10}}$ term which is a result from the decrease in nuclei-nuclei repulsion as the distance increases between the atoms

© University of Pretoria

involved. More important is the dominating $\Delta V_{\mathrm{ne}}^{\mathrm{C6,N10}}$ term. An increase in the bond length upon coordination of the counter ion, such as for the (N10) and (N7) isomers, result in a large decrease in attraction between the nuclei of C6 and the electrons of N10. The N10 isomer experiences the largest unfavourable change, i.e. $\Delta V_{\mathrm{ne}}^{\mathrm{C6,N10}}$ = 176.6 and 121.9 kcal mol^{-1} for the Na^+ and K^+ complex. Here, the electron density at the BCP(C6,N10) decreases, leading to an increase in bond length by 0.0170 and 0.0119 Å, respectively, relative to Ade^-. The destabilizing change in $V_{\mathrm{ne}}^{\mathrm{C6,N10}}$ overrides the stabilizing change in $\Delta V_{\mathrm{nn}}^{\mathrm{C6,N10}}$ by 54.4 and 36.0 kcal mol^{-1} for Na- and K-Ade(N10), respectively.

The shortening of the bond upon coordination and a gain in electron pairs delocalized between C6 and N10, such as for the (N3), (N3N9) and (N9) isomers, results in a favourable increase in attraction of the $V_{\mathrm{ne}}^{\mathrm{C6,N10}}$ term. The term is more favourable by -18.0 and -19.0 kcal mol^{-1} for the Na- and K-Ade(N3N9) isomer than the destabilizing $\Delta V_{\mathrm{nn}}^{\mathrm{C6,N10}}$ term which arises as the nuclei-nuclei repulsion increases with a decrease in distance between the C6 and N10 atoms.

The formation of the ionic bond between Ade^- and the Na^+ and K^+ metal ion can be studied in terms of the total intermolecular interaction energy, ${}_{\mathrm{inter}}E_{\mathrm{int}}^{\mathrm{M^+,Ade^-}}$, between the two ions, Table 3.7. It is immediately clear from Table 3.7 that the intermolecular interactions are i) the leading interactions in whole molecular system, being much larger than the changes observed for intramolecular interactions of the adeninate anion, ii) are highly favourable for all structural isomers of the Na^+ and K^+ complexes and iii) are dominated by the electrostatic term. The most favourable coordination site in terms of the most stabilizing intermolecular interactions for the in-plane isomers is (N3N9) > (N9) ≥ (N3) > (N7) > (N1), having the (N3N9) isomer –10 kcal mol^{-1} more favourable than the other isomers for both the Na^+ and K^+ complexes. These trends are recovered at the DFT/B3LYP level of theory (Table 3.8). The preference of the bidentate chelation over the unidentate coordination is in line with the theoretical studies conducted for metal ion pairing with neutral adenine.[5,12]

Table 3.7: Intermolecular interaction energy and its exchange correlation and classical components for the ionic bond between Ade^- and M^+, where M^+ = Na^+ and K^+, of the Na- and K-Ade structural isomers, CCSD level of theory. All values in kcal mol^{-1}

conformer	(N9)	(N3N9)	(N3)	(N7)	(N1)	(N10)	(π)
				Na-Ade complexes			
${}_{\mathrm{inter}}E_{\mathrm{int}}^{\mathrm{Na^+,Ade^-}}$	–112.5	–122.6	–109.8	–92.5	–80.3	–78.2	–75.1
$V_{\mathrm{xc}}^{\mathrm{Na^+,Ade^-}}$	–12.1	–14.3	–11.1	–11.2	–9.8	–7.5	–0.8
$V_{\mathrm{cl}}^{\mathrm{Na^+,Ade^-}}$	–100.3	–108.3	–98.7	–81.2	–70.4	–70.7	–74.4
				K-Ade complexes			
${}_{\mathrm{inter}}E_{\mathrm{int}}^{\mathrm{K^+,Ade^-}}$	-	–116.2	-	–86.0	–75.3	–77.2	-
$V_{\mathrm{xc}}^{\mathrm{K^+,Ade^-}}$	-	–20.6	-	–13.9	–12.3	–10.5	-
$V_{\mathrm{cl}}^{\mathrm{K^+,Ade^-}}$	-	–95.6	-	–72.1	–63.0	–66.6	-

© University of Pretoria

Table 3.8: Intermolecular interaction energy and its exchange correlation and classical components for the ionic bond between Ade^- and M^+, where M^+ = Na^+ and K^+, of the Na- and K-Ade structural isomers, DFT/B3LYP level of theory. All values in kcal mol^{-1}

isomer	(N9)	(N3N9)	(N3)	(N7)	(N1)	(N10)	(π)
				Na-Ade complexes			
${}_{\text{inter}}E_{\text{int}}^{\text{Na}^+,\text{Ade}^-}$	–116.7	–128.3	–114.1	–94.7	–66.8	–78.4	–76.9
$V_{\text{xc}}^{\text{Na}^+,\text{Ade}^-}$	–15.3	–18.6	–14.2	–14.2	–4.5	–8.8	–1.8
$V_{\text{cl}}^{\text{Na}^+,\text{Ade}^-}$	–101.5	–109.7	–99.8	–80.6	–62.2	–69.6	–75.1
				K-Ade complexes			
${}_{\text{inter}}E_{\text{int}}^{\text{K}^+,\text{Ade}^-}$	-	–116.8	-	–86.1	–74.8	–78.4	-
$V_{\text{xc}}^{\text{K}^+,\text{Ade}^-}$	-	–21.7	-	–15	–12.6	–10.3	-
$V_{\text{cl}}^{\text{K}^+,\text{Ade}^-}$	-	–95.1	-	–71.1	–62.2	–68.1	-

Electrons are shared between the adeninate anion and the Na^+ and K^+ ion, resulting in the large stabilizing $V_{\text{xc}}^{\text{M}^+,\text{Ade}^-}$ term. The interaction between adeninate anion and the Na^+ ion of the (π) isomer are strictly electrostatic; having minimal contribution from the exchange-correlation term. The intermolecular interaction energy between the adeninate anion with the Na^+ and K^+ ion is partitioned into individual coulombic, $V_{\text{cl}}^{\text{A,M}^+}$, and exchange-correlation, $V_{\text{XC}}^{\text{A,M}^+}$ contributions from atom A of the purine ring with M^+. Figure 3.14 and Figure 3.15 show the $V_{\text{cl}}^{\text{A,M}^+}$ and $V_{\text{XC}}^{\text{A,M}^+}$ contributions for Na- and K-Ade isomers, respectively.

Figure 3.14 and Figure 3.15 shows that the formation of the ionic bond is governed by the electrostatic interaction with the N-donor atom(s), boxed in purple. The (N3N9) isomer has two dominant interactions arising from the donor N3 and the N9 atoms with the counter ion in both Na- (–157.9 and –149.7 kcal mol^{-1}) and K-Ade (–137.3 and –136.1 kcal mol^{-1}) complexes. The summation of the overall interaction between atoms N3 and N9 with M^+, ${}_{\text{inter}}E_{\text{int}}^{\text{N3,M}^+} + {}_{\text{inter}}E_{\text{int}}^{\text{N9,M}^+}$, results in a significantly favourable interaction of –321.3 and –293.1 kcal mol^{-1} for the Na^+ and K^+ complex, respectively. Thus, the chelated (N3N9) isomer is the most stabilized compared to the unidentate coordinated isomers due to the stabilizing interaction from the two nitrogen atoms. In addition, the larger charge-to-radius ratio of Na^+ results in a larger surface charge density. This in turn leads to the electrostatic interaction between the nitrogen donor atom(s), N*X*, and the Na^+ ion, $V_{\text{cl}}^{\text{N}X,\text{Na}^+}$, being more favourable by −20 kcal mol^{-1} than the interaction with the K^+ ion, $V_{\text{cl}}^{\text{N}X,\text{K}^+}$, for all Na-Ade isomers. The preference for the binding of Na^+ > K^+ follows that previously reported for neutral adenine.[1,5]

The summation of all changes experienced by the adeninate anion upon coordination of the counter ion ($\Delta_{\text{intra}}E_{\text{int}}^{\text{Ade}}$) and the formation of the new ionic bond between the two ions (${}_{\text{inter}}E_{\text{int}}^{\text{M}^+,\text{Ade}^-}$), eqn 3.6, leads to the total interaction energy of the molecular system, $E_{\text{int}}^{\text{MS}}$:

$$E_{\text{int}}^{\text{MS}} = \Delta_{\text{intra}}E_{\text{int}}^{\text{Ade}} + {}_{\text{inter}}E_{\text{int}}^{\text{M}^+,\text{Ade}^-} \qquad (3.6)$$

© University of Pretoria

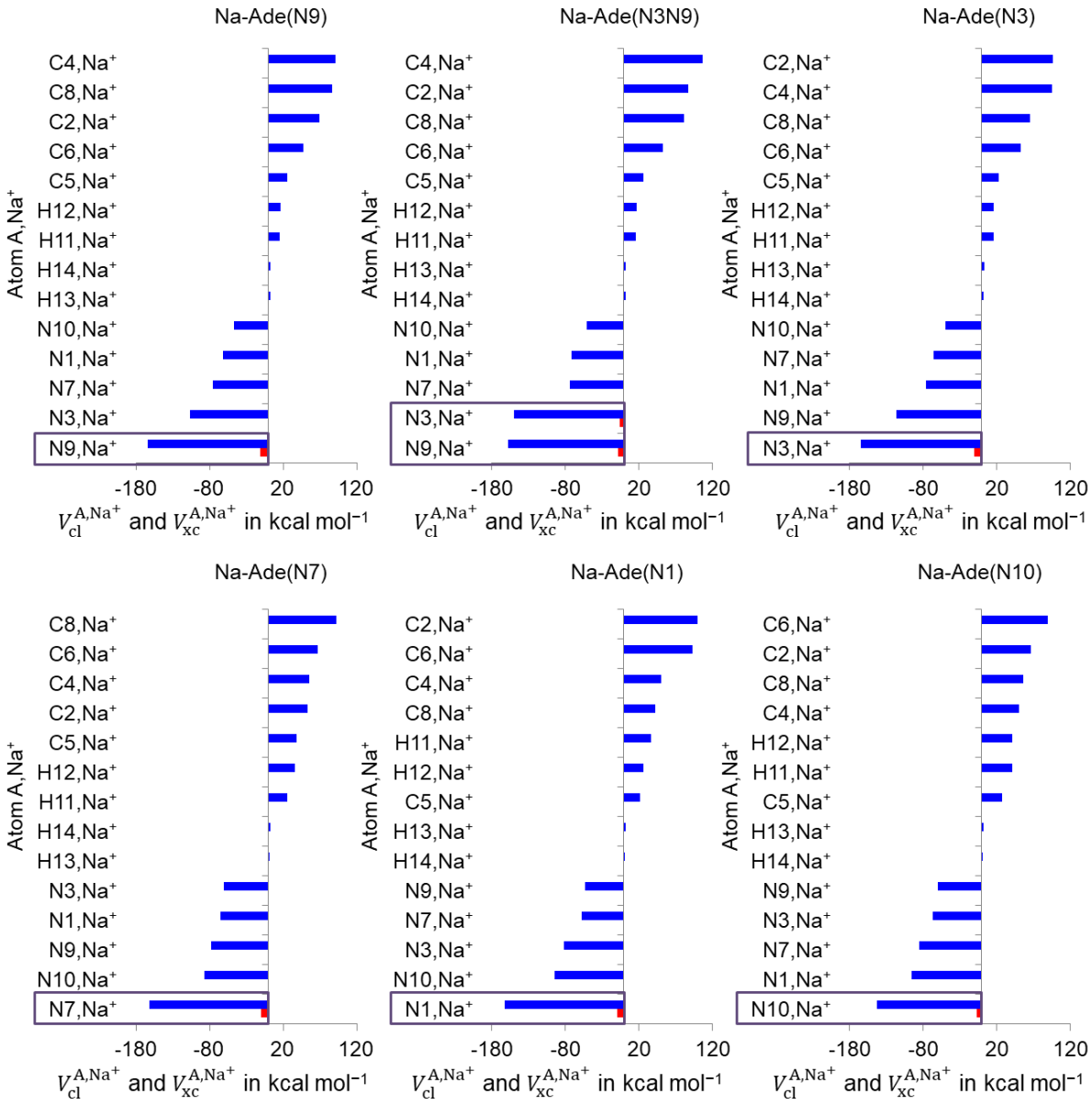

Figure 3.14: All individual coulombic, $V_{\mathrm{cl}}^{\mathrm{A,Na^+}}$ - blue bars, and exchange-correlation, $V_{\mathrm{XC}}^{\mathrm{A,Na^+}}$ - red bars, contributions to ${}_{\mathrm{inter}}E_{\mathrm{int}}^{\mathrm{Na^+,Ade^-}}$ from atom A with Na^+, where atom A is all atoms of the adeninate anion, for the Na-Ade isomers, at CCSD level of theory.

Table 3.9 and Table 3.10 show the $E_{\mathrm{int}}^{\mathrm{MS}}$ for the Na- and K-Ade isomers obtained at the CCSD and DFT/B3LYP level of theory, respectively. It is without question that the formation of ion-pairs is largely stabilizing to the molecular system and thus the existence of free Ade^- in DMSO is unlikely to occur under the experimental conditions in Chapter 2.

The theoretical results reported in this chapter support the proposed hypothesis derived from the experimental work in Chapter 2 whereby the unidentate N3 and N9 coordination and the bidentate N3N9 chelation of Na^+ ion to Ade^- is proposed to exist in DMSO solution, while the K^+ is too large in size to occupy the N3 and N9 sites as unique isomers. The (N3N9), (N3) and (N9) isomers experience

© University of Pretoria

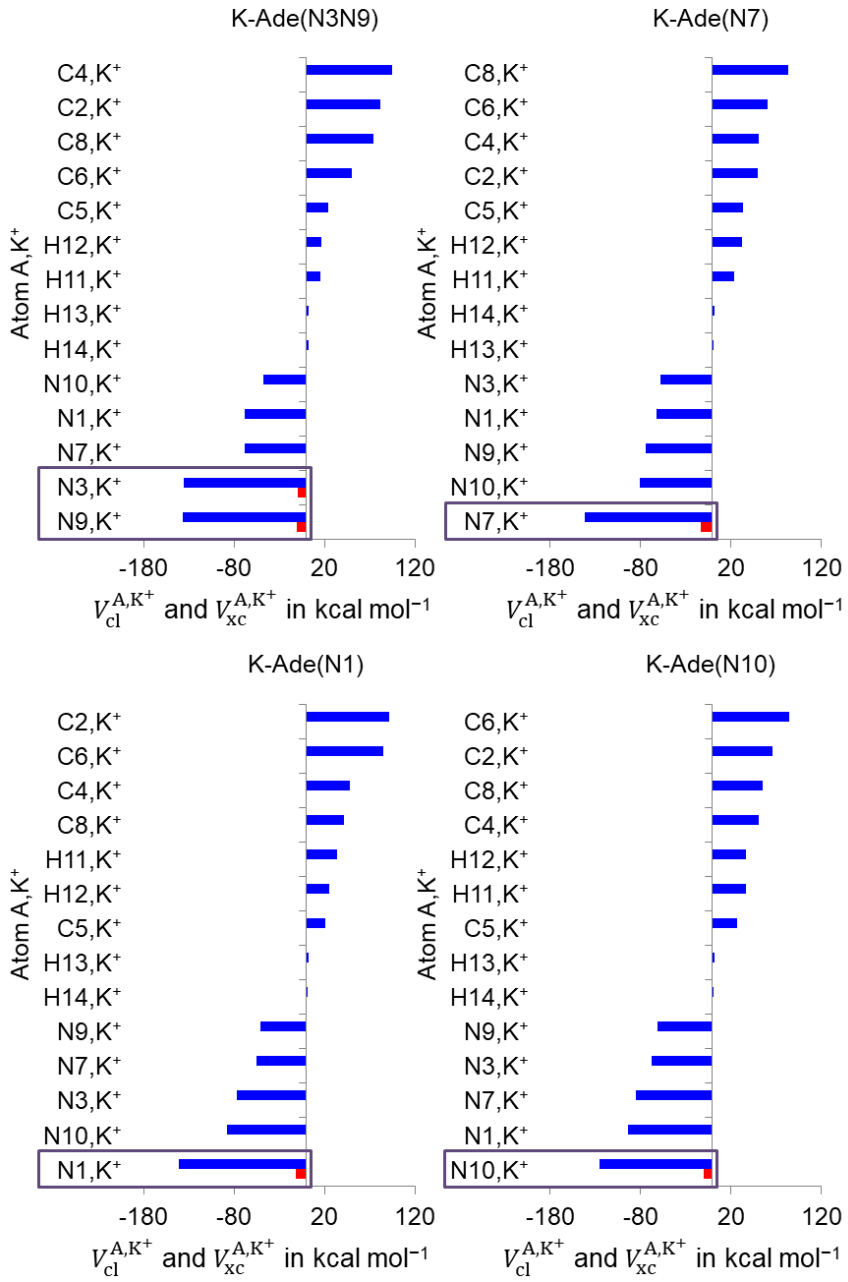

Figure 3.15: All individual coulombic, $V_{\mathrm{cl}}^{\mathrm{A,K^+}}$ - blue bars, and exchange-correlation, $V_{\mathrm{XC}}^{\mathrm{A,K^+}}$ - red bars, contributions to ${}_{\mathrm{inter}}E_{\mathrm{int}}^{\mathrm{K^+,Ade^-}}$ from atom A with K^+, where atom A is all atoms of the adeninate anion, for the K-Ade isomers, at CCSD level of theory.

the most favourable overall interaction energy relative to the (N1), (N7) and (N10) isomer i.e. $E_{\mathrm{int}}^{\mathrm{MS}}$ is more than −30 kcal mol^{-1} in favour for both the Na- and K-Ade complexes, Table 3.9. Chelation at the N3N9 leads to the most stabilizing change in energy compared to unidentate coordination sites for the Na^+ ion.

From the experimental results reported in chapter 2, it is predicted that DMSO solvent molecules are interacting via hydrogen bonding with the NH_2 group of the adeninate molecule. As a result, this could further discourage the formation of the (N1) and (N7) isomers as competing DMSO solvent

© University of Pretoria

molecules could weaken the interactions between the counter ion and the adeninate anion. Hence, it was important to model the above structural isomers in the presence of explicit DMSO solvent molecules.

Table 3.9: Summation of the intramolecular and intermolecular interaction energy (in kcal mol^{-1}) of the Na- and K-Ade structural isomers at CCSD level of theory

isomer		(N9)	(N3N9)	(N3)	(N7)	(N1)	(N10)	(π)
$E_{\text{int}}^{\text{MS}}$	Na-Ade	–133.8	–152.0	–132.8	–108.0	–91.1	–60.4	–72.4
	K-Ade		–136.1		–93.0	–79.9	–63.7	

Table 3.10: Summation of the intramolecular and intermolecular interaction energy (in kcal mol^{-1}) of the Na- and K-Ade structural isomers at DFT/B3LYP level of theory

isomer		(N9)	(N3N9)	(N3)	(N7)	(N1)	(N10)	(π)
$E_{\text{int}}^{\text{MS}}$	Na-Ade	–138.9	–160.8	–137.4	–107.1	–74.9	–58.2	–75.9
	K-Ade	-	–136	-	–89.4	–75.5	–63.5	

3.4.5 Effect of the solvent environment on the Na^+ and K^+ coordination site of the adeninate anion

The ^{1}H NMR experiments carried out in Chapter 2 indicated the presence of hydrogen bonding between DMSO solvent molecules and the NH_2 group of the adeninate anion. Modelling the above structural isomers in the presence of explicit DMSO solvent molecules could better mimic the effect of the molecular environment. It is of interest to evaluate in the presence of explicit DMSO solvent molecules i) whether the same or new isomers are obtained theoretically, ii) how the presence of DMSO solvent molecules influences the intermolecular interactions between the counter ion and the adeninate anion and iii) and how DMSO solvent molecules interact with the adeninate anion.

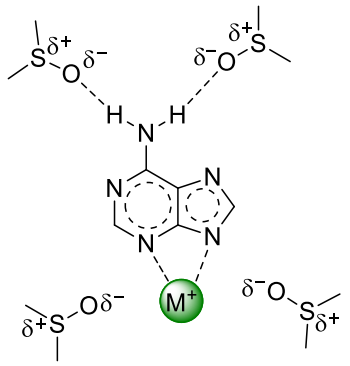

Figure 3.16: Orientation of the four DMSO solvent molecules for M-Ade(N3N9).

© University of Pretoria

The inclusion of 4 explicit DMSO solvent molecules was chosen to investigate the effect of solvating DMSO. The DMSO molecules were pre-organized around the optimized in-plane and out-of-plane M-Ade structural isomers as follows: two of the explicit DMSO solvent molecules are orientated to interact with the protons of the NH_2 group of the metal coordinated adeninate anion to allow for hydrogen bonding interactions between the amino protons with the oxygen atoms of the two DMSO molecules, Figure 3.16. The other two DMSO molecules are positioned close to the N3 and N9 nitrogen atoms. Such prepared solvated structures of complexes were optimized without restrictions.

3.4.6 Na- and K-Ade isomers in the presence of explicit DMSO solvent molecules

In the presence of four explicit solvent molecules, the optimized in-plane isomers (Figure 3.17) of the Na^+ and K^+ complexes still exist. However, the in-plane isomers are far from having the counter ion coordinated "in-plane". The counter ion is simultaneously coordinated to the adeninate anion and neighbouring explicit DMSO solvent molecule(s) and thus is shifted out of plane. Therefore, these isomers are better referred to as heteroatom coordinated isomers.

The out-of-plane (N10) isomer is obtained for the Na^+ complex, Figure 3.18 Na-Ade(N10)-4DMSO, whereby the counter ion coordinates with the N10 atom, having the protons of the amino group positioned away from the Na^+ ion. A new isomer was theoretically predicted, Na- and K-Ade(N10-rev)-4DMSO in Figure 3.18, which is not possible to isolate with the implicit DMSO calculations. The counter ion is simultaneously coordinated to three DMSO solvent molecules and in which two of the DMSO molecules form hydrogen bonds with NH_2 of the adeninate anion. This structural arrangement allows the protons of the amino group to orient towards the M^+ ion. Such an arrangement in implicit DMSO is unable to exist as the NH_2 orientates its protons away from the M^+ ion.

No out-of-plane cation-π isomer is theoretically predicted in the presence of the 4 explicit DMSO molecules for the Na- and K-Ade complexes. This is expected as the interaction of the cation with the π system of the adeninate molecule is weak and thus easily dissociated in the presence of competing coordination to the oxygen atom of the DMSO solvent molecules. Two explicit DMSO molecules are involved in hydrogen bonding with the protons of the NH_2 group irrespective of the site of metal ion coordination i.e. this occurs for all Na- and K-Ade heteroatom coordinated isomers (Figure 3.17) and the (N10) isomer (Figure 3.18). The two DMSO molecules positioned at the bottom of the adeninate molecule interact through the O atom with the counter ion coordinated at the N3, N9 or N3N9 position for the (N3), (N9) and (N3N9) structural isomers of both the Na- and K-Ade complexes. In the case of the (N1), (N7) and (N10) isomers, the two DMSO molecules disperse away and shift to form hydrogen bonds with the NH_2 group or coordinate with the counter ion at the N1, N7 and N10, respectively. This suggests that the counter ion plays a role in how DMSO solvates the adeninate purine ring.

The use of explicit solvent molecules has provided valuable insight into the mutual hydrogen bonding of the NH_2 group with the DMSO solvent and the persistence of the coordination of metal ions at the purine ring nitrogen atoms. IQA data is required to investigate whether the trend from the REP-FAMSEC based analysis of the implicit solvent model system of the structural isomers for the most favourable site of coordination is recovered. In addition IQA is used to investigate how the

© University of Pretoria

strength of the interaction between the counter ion and Ade^- changes in the presence of the explicit DMSO solvent molecules.

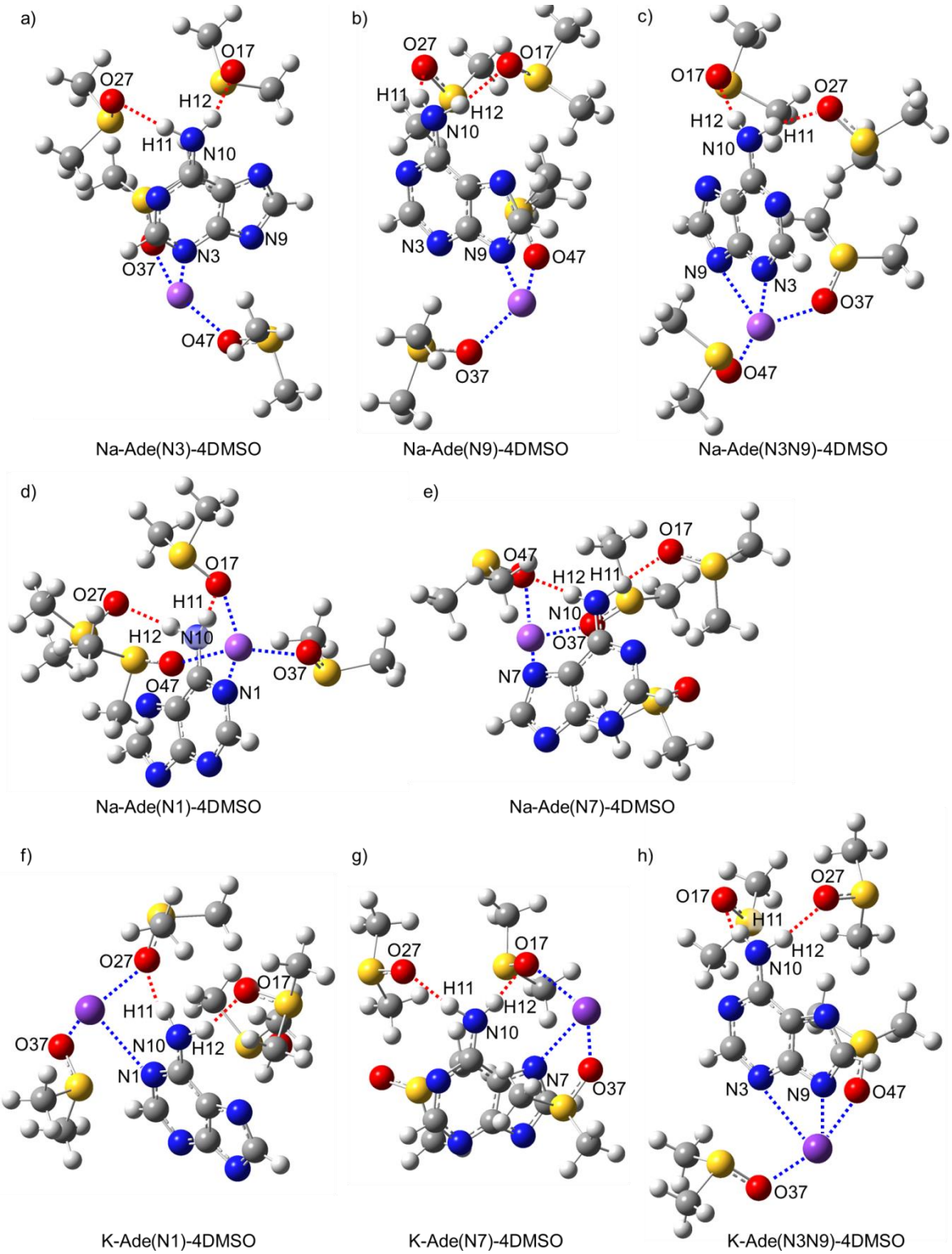

Figure 3.17: Optimized structures of heteroatom coordinated isomers of Na-Ade (a-e) and K-Ade (f-g) complexes with 4 explicit DMSO solvent molecules at DFT/B3LYP/6-311G++(d,p)/PCM(DMSO).

© University of Pretoria

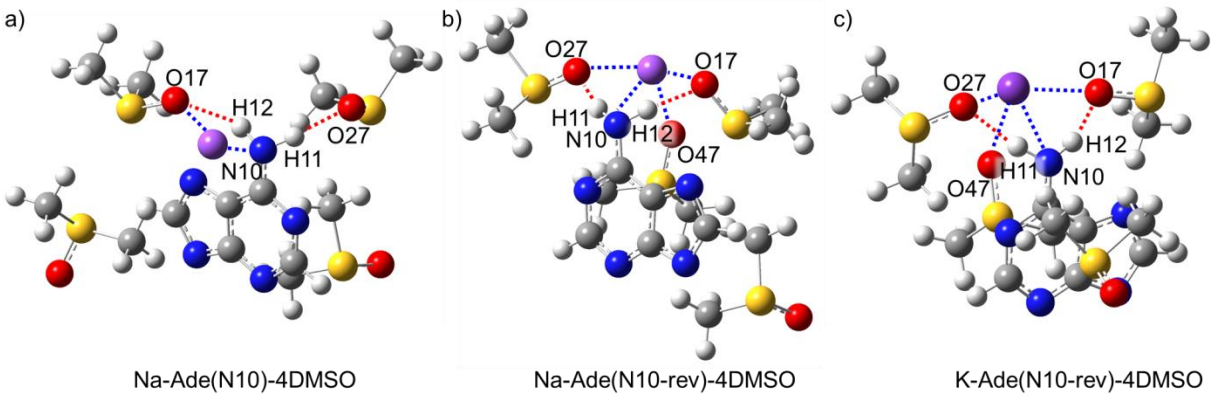

Figure 3.18: Optimized structures of (N10) isomers of Na-Ade (a and b) and K-Ade (c) complexes with 4 explicit DMSO solvent molecules at DFT/B3LYP/6-311G++(d,p)/PCM(DMSO).

3.4.7 Influence on the interaction between counter ion and the adeninate anion in the presence of explicit DMSO solvent molecules

The analysis of the intermolecular interaction between the Ade^- with the Na^+ and K^+ counter ion for the various sites of coordination in the presence of the four explicit DMSO solvent molecules is of most interest in this large molecular system. The overall intermolecular interaction between the adeninate anion and the M^+ counter ion, ${}_{\text{inter}}E_{\text{int}}^{\text{Ade}^-,\text{M}^+}$, and the contribution from the nitrogen donor atom N*X* with the Na^+ and K^+ ion, ${}_{\text{inter}}E_{\text{int}}^{\text{N}X,\text{M}^+}$, with the individual exchange-correlation, $V_{\text{xc}}^{\text{N}X,\text{M}^+}$, and coulombic, $V_{\text{cl}}^{\text{N}X,\text{M}^+}$, contributions from atom N*X* with M^+, are shown in Table 3.11. The inclusion of explicit DMSO solvent molecules results in slightly weaker interaction energies between the metal ion and the nitrogen atoms than those obtained in the implicit DMSO solvent model.

Table 3.11: Diatomic intermolecular interactions between the coordinating nitrogen atom(s) of Ade– and the counter ion, Na^+/K^+, in Na- And K-Ade-4DMSO complexes

Isomer-4DMSO	(N9)	(N3N9)		(N3)	(N7)	(N1)	(N10-rev)
	Na-Ade-4DMSO complexes						
${}_{\text{inter}}E_{\text{int}}^{\text{Ade}^-,\text{Na}^+}$	−113.9	−124.5		−110.1	−89.6	−75.8	−37.4
Donor atom(s)	N9	N9	N3	N3	N7	N1	N10
${}_{\text{inter}}E_{\text{int}}^{\text{N}X,\text{Na}^+}$	−164.0	−148.5	−154.9	−164.0	−162.2	−154.0	−106.2
$V_{\text{xc}}^{\text{N}X,\text{Na}^+}$	−11.0	−5.6	−8.1	−10.0	−10.8	−7.7	−0.4
$V_{\text{cl}}^{\text{N}X,\text{Na}^+}$	−152.9	−142.9	−146.8	−154.0	−151.4	−146.3	−105.8
	K-Ade-4DMSO complexes						
${}_{\text{inter}}E_{\text{int}}^{\text{Ade}^-,\text{K}^+}$	-	−113.8		-	−83.0	−72.7	−41.4
Donor atom(s)		N9	N3	-	N7	N1	N10
${}_{\text{inter}}E_{\text{int}}^{\text{N}X,\text{K}^+}$	-	−132.1	−138.6	-	−140.8	−140.5	−107.5
$V_{\text{xc}}^{\text{N}X,\text{K}^+}$	-	−6.8	−9.9	-	−10.8	−9.9	−1.4
$V_{\text{cl}}^{\text{N}X,\text{K}^+}$	-	−125.3	−128.7	-	−130.0	−130.5	−106.1

© University of Pretoria

Coordination of the M^+ ion with the adeninate anion leads to an overall favourable interaction between the two ions for all coordination sites. Chelation at the N3 and N9 nitrogen atoms is the most preferred site for coordination of the Na^+ and K^+ counter ion with the adeninate anion, being > –10 kcal mol^{-1} more favourable than the unidentate coordination at the N3 and N9 atom and > –30 kcal mol^{-1} more favourable than the N7, N1 and N10 atoms for the Na^+ and K^+ complexes. The most dominant diatomic contribution to the stabilizing interaction energy of ${}_{\text{inter}}E_{\text{int}}^{\text{Ade}^-,\text{M}^+}$ arises from the nitrogen atom to which the metal ion is coordinated, having the interaction dominated by the electrostatic interaction between the atom and the counter ion, $V_{\text{cl}}^{NX,\text{M}^+}$ in Table 3.11.

The observed trends in preferential coordination sites are highly comparable between the explicit and implicit models and provide further support that in DMSO solvent the Na^+ and K^+ counter ion is most likely to be chelated at the N3 and N9 atom of the adeninate anion. This finding is in agreement with previous studies which showed preference for bidentate coordination to the N3N9 of the Ade-N7(H) over unidentate coordination of neutral adenine.[12,27] The recovery of the trend of the metal ion coordination site with the adeninate anion in the presence of explicit DMSO molecules is indeed a favourable result and eliminates any suspicion that the metal ion will coordinate at a different site when explicit solvent models are used.

3.5 Conclusion

Previous research conducted for the ion pairing between metal ions and nucleobases has investigated the neutral and tautomeric forms. The importance of research into the rare tautomeric and anionic forms of nucleobases has gained attention due to their involvement in base mispairing which in turn leads to mutations and other biological phenomena. In this research the ion pairing between Ade^- with Na^+ and K^+ ions in DMSO is investigated theoretically for the first time. The theoretical studies conducted here are performed in DMSO as solvent to match the experimental environment; however, it provides a guide for further investigations in water or other solvents as well as ion-pairing with other alkaline earth and transition metals.

Various Na- and K-Ade structural isomers, namely the (N1), (N7), (N3), (N3N9) and (N9) and the out-of-plane (N10) and (π) isomers, were optimized and evaluated using IQA data at CCSD and DFT/B3LYP level of theory. The results from the relative change in electronic energy were insufficient to resolve which Na- and K-Ade isomer species are most likely to be present in solution. The analysis of the interaction energies and REP-FAMSEC methods employed here in this research made it possible to eliminate the least likely isomers to occur and investigate the governing factors which drive the ion-pair formation, having both the superior CCSD and the DFT/B3LYP level of theory in good agreement for the in-plane metal coordinated isomers. The DFT/B3LYP level of theory over estimates the cation-π interaction between the purine ring and the Na^+ ion.

The most favourable site of coordination in descending order is (N3N9) > (N9) > (N3) > (N7) > (N1) > (N10) > (π) for the Na^+ complexes and (N3N9) > (N7) > (N1) > (N10) for the K^+ ion at the CCSD level of theory. The formation of these ionic complexes is driven largely by electrostatic interactions whereby the in-plane coordination results in significant energy contribution due to shared electron density between the two ions. There is a strong preference for the binding of Na^+ over K^+, as reported for neutral adenine. The larger charge-to-radius ratio of the Na^+ ion perturbs the electronic environment to a larger extent, resulting in highly favourable charge polarization of the adeninate

© University of Pretoria

anion. The charge transfer is similar between Na^+ and K^+ complexes even though the charge polarization is much smaller for K-Ade complexes.

The in-plane isomers experience a large favourable intermolecular interaction between the adeninate molecule and the counter ion. Chelation at the N3N9 is stabilized the most compared to unidentate coordination sites as both the N3 and N9 atoms contribute towards highly favourable interactions with the counter ion and result in the most favourable increase in polarization of the adeninate molecule. In addition, the (N3), (N3N9) and (N9) isomers result in the stabilization of the C6–N10 bond demonstrated by a shortened bond length upon coordination of the counter ion. The change in the C6–N10 bond character provides large stabilization to the adeninate anion. Coordination of the counter ion at the N10 atom results in large destabilization of the intramolecular interaction energy within the adeninate anion. This destabilization is dominated by the lengthening of the C6-N10 bond, resulting in the highly unfavourable diatomic interaction energy between the two atoms. The formation of the M-Ade-(π) isomer via a cation-π interaction is driven strictly by electrostatic interactions which are much weaker than those reported for the in-plane isomers.

The preservation of the in-plane isomers by the inclusion of explicit DMSO solvent molecules at the DFT/B3LYP level of theory provides further support for these isomers to be the most likely to occur. The prediction of chelation at the N3 and N9 atoms of the purine ring being the most likely sites of ion coordination is still valid using explicit DMSO solvent molecules. The M-Ade-(π) isomer is easily disrupted by the presence of explicit DMSO solvent molecules. This finding supports the experimental prediction that the isomer does not exist in DMSO.

Based on our experimental study in chapter 2 we proposed that in DMSO solution ion-pairs exist between Na^+ and K^+ ions with the adeninate anion in which the counter ion is coordinated via unidentate or chelation at the N3 and/or N9 atoms of the purine ring. The theoretical studies reported in this chapter fully support the proposal. The results rule out the possibility of the M-Ade(N10) and (π) isomer occurring in DMSO.

This study has provided insight into the stabilization of the adeninate anion, which can exist biologically, by the surrounding Na^+ and K^+ ions. Thus, the coordination of Ca^{2+} and Mg^{2+} to the adeninate anion could potentially follow the same preferred chelation at the N3 and N9 atoms. The coordination of Na^+ and K^+ ions influence the electronic environment to a large extent throughout the adeninate anion. The formation of metal complexed adeninate ion-pairs will therefore influence the aggregation mode of the species. Aggregate formation governed by hydrogen bonding and π-π stacking may be weakened or enhanced or an alternative mode of aggregation could occur, such as ion-coordinated aggregate formation, as proposed in Chapter 2. Furthermore, the adeninate anion is an intermediate in the synthesis of biologically important N9-substituted adenines, and thus the presence of the counter ion could influence the reactivity and regio-selectivity of the adeninate anion.

© University of Pretoria

3.6 References

[1] B. A. Cerda, C. Wesdemiotis, *J. Am. Chem. Soc.* **1996**, *118*, 11884–11892.

[2] N. Russo, M. Toscano, A. Grand, *J. Am. Chem. Soc.* **2001**, *123*, 10272–10279.

[3] B. Lippert, *Coord. Chem. Rev.* **2000**, *200–202*, 487–516.

[4] M. P. Long, S. Alland, M. E. Martin, C. M. Isborn, *Phys. Chem. Chem. Phys.* **2020**, *22*, 5584–5596.

[5] M. T. Rodgers, P. B. Armentrout, *J. Am. Chem. Soc.* **2000**, *122*, 8548–8558.

[6] F. Leonarski, L. D'Ascenzo, P. Auffinger, *Inorganica Chim. Acta* **2016**, *452*, 82–89.

[7] R. B. Martin, *Acc. Chem. Res.* **1985**, *18*, 32–38.

[8] H. Sigel, *Chem. Soc. Rev.* **1993**, *22*, 255.

[9] H. Zheng, M. Chruszcz, P. Lasota, L. Lebioda, W. Minor, *J. Inorg. Biochem.* **2008**, *102*, 1765–1776.

[10] M. M. Harding, M. W. Nowicki, M. D. Walkinshaw, *Crystallogr. Rev.* **2010**, *16*, 247–302.

[11] N. V. Hud, M. Polak, *Curr. Opin. Struct. Biol.* **2001**, *11*, 293–301.

[12] M. Kabeláč, P. Hobza, *J. Phys. Chem. B* **2006**, *110*, 14515–14523.

[13] K. Bebenek, L. C. Pedersen, T. A. Kunkel, *Proc. Natl. Acad. Sci. U. S. A.* **2011**, *108*, 1862–1867.

[14] I. J. Kimsey, K. Petzold, B. Sathyamoorthy, Z. W. Stein, H. M. Al-Hashimi, *Nature* **2015**, *519*, 315–320.

[15] C. Tamm, P. Strazewski, *Angew. Chemie Int. Ed. English* **1990**, *29*, 36–57.

[16] W. Zhu, X. Luo, C. M. Puah, X. Tan, J. Shen, J. Gu, K. Chen, H. Jiang, *J. Phys. Chem. A* **2004**, *108*, 4008–4018.

[17] R. H. Cox, *J. Phys. Chem.* **1969**, *73*, 2649–2651.

[18] J. M. Daniel, S. D. Friess, S. Rajagopalan, S. Wendt, R. Zenobi, *Int. J. Mass Spectrom.* **2002**, *216*, 1–27.

[19] M. Hanus, M. Kabeláč, J. Rejnek, F. Ryjáček, P. Hobza, *J. Phys. Chem. B* **2004**, *108*, 2087–2097.

[20] C. Colominas, F. J. Luque, M. Orozco, *J. Am. Chem. Soc.* **1996**, *118*, 6811–6821.

[21] A. O. Alyoubi, R. H. Hilal, *Biophys. Chem.* **1995**, *55*, 231–237.

[22] M. J. Scanlan, I. H. Hillier, *J. Am. Chem. Soc.* **1984**, *106*, 3737–3745.

[23] N. Russo, M. Toscano, A. Grand, *J. Phys. Chem. B* **2001**, *105*, 4735–4741.

[24] J. Arpalahti, K. D. Klika, R. Sillanpää, R. Kivekäs, *J. Chem. Soc. Dalt. Trans.* **1998**, 1397–1402.

[25] A. Laxer, D. T. Major, H. E. Gottlieb, B. Fischer, *J. Org. Chem.* **2001**, *66*, 5463–5481.

[26] K. Aidas, K. V. Mikkelsen, J. Kongsted, *Phys. Chem. Chem. Phys.* **2010**, *12*, 761–768.

© University of Pretoria

[27] J. Y. Baek, C. M. Choi, H. J. Eun, K. S. Park, M. C. Choi, J. Heo, N. J. Kim, *Chem. Phys. Lett.* **2015**, *635*, 163–167.

[28] N. Russo, M. Toscano, A. Grand, *J. Phys. Chem. A* **2003**, *107*, 11533–11538.

[29] O. A. Stasyuk, H. Szatyłowicz, T. M. Krygowski, *Org. Biomol. Chem.* **2014**, *12*, 456–466.

[30] N. Russo, M. Toscano, A. Grand, *J. Mass Spectrom.* **2003**, *38*, 265–270.

[31] J. Valdespino-Saenz, A. Martínez, *J. Mol. Struct. THEOCHEM* **2010**, *939*, 34–43.

[32] C. Fonseca Guerra, P. J. Sanz Miguel, A. Cebollada, F. M. Bickelhaupt, B. Lippert, *Chem. - A Eur. J.* **2014**, *20*, 9494–9499.

[33] R. Silaghi-Dumitrescu, B. Mihály, T. Mihály, A. A. A. Attia, P. J. Sanz Miguel, B. Lippert, *JBIC J. Biol. Inorg. Chem.* **2017**, *22*, 567–579.

[34] H. T. Chifotides, K. R. Dunbar, *Acc. Chem. Res.* **2005**, *38*, 146–156.

[35] S. Korn, W. S. Sheldrick, *Inorganica Chim. Acta* **1997**, *254*, 85–91.

[36] B. Longato, L. Pasquato, A. Mucci, L. Schenetti, E. Zangrando, *Inorg. Chem.* **2003**, *42*, 7861–7871.

[37] R. H. Fish, G. Jaouen, *Organometallics* **2003**, *22*, 2166–2177.

[38] L. Y. Kuo, M. G. Kanatzidis, M. Sabat, A. L. Tipton, T. J. Marks, *J. Am. Chem. Soc.* **1991**, *113*, 9027–9045.

[39] D. Choquesillo-Lazarte, M. del P. Brandi-Blanco, I. García-Santos, J. M. González-Pérez, A. Castiñeiras, J. Niclós-Gutiérrez, *Coord. Chem. Rev.* **2008**, *252*, 1241–1256.

[40] D. P. Smith, E. Baralt, B. Morales, M. M. Olmstead, M. F. Maestre, R. H. Fish, *J. Am. Chem. Soc.* **1992**, *114*, 10647–10649.

[41] P. Annen, S. Schildberg, W. S. Sheldrick, *Inorganica Chim. Acta* **2000**, *307*, 115–124.

[42] W. Wang, H. W. Hellinga, L. S. Beese, *Proc. Natl. Acad. Sci.* **2011**, *108*, 17644–17648.

[43] P. C. Bevilacqua, R. Yajima, *Curr. Opin. Chem. Biol.* **2006**, *10*, 455–464.

[44] V. Singh, C. S. Peng, D. Li, K. Mitra, K. J. Silvestre, A. Tokmakoff, J. M. Essigmann, *ACS Chem. Biol.* **2014**, *9*, 227–236.

[45] M. J. Frisch, G. W. Trucks, H. B. Schlegel, G. E. Scuseria, M. A. Robb, J. R. Cheeseman, G. Scalmani, V. Barone, G. A. Petersson, H. Nakatsuji, X. Li, M. Caricato, A. V. Marenich, J. Bloino, B. G. Janesko, R. Gomperts, B. Mennucci, H. P. Hratchian, J. V. Ortiz, a. F. Izmaylov, J. L. Sonnenberg, Williams, F. Ding, F. Lipparini, F. Egidi, J. Goings, B. Peng, A. Petrone, T. Henderson, D. Ranasinghe, V. G. Zakrzewski, J. Gao, N. Rega, G. Zheng, W. Liang, M. Hada, M. Ehara, K. Toyota, R. Fukuda, J. Hasegawa, M. Ishida, T. Nakajima, Y. Honda, O. Kitao, H. Nakai, T. Vreven, K. Throssell, J. A. Montgomery Jr., J. E. Peralta, F. Ogliaro, M. J. Bearpark, J. J. Heyd, E. N. Brothers, K. N. Kudin, V. N. Staroverov, T. A. Keith, R. Kobayashi, J. Normand, K. Raghavachari, A. P. Rendell, J. C. Burant, S. S. Iyengar, J. Tomasi, M. Cossi, J. M. Millam, M. Klene, C. Adamo, R. Cammi, J. W. Ochterski, R. L. Martin, K. Morokuma, O. Farkas, J. B. Foresman, D. J. Fox, **2016**, Gaussian 09, Revision E.01, Gaussian, Inc., Wallin.

© University of Pretoria

[46] M. J. Frisch, G. W. Trucks, H. B. Schlegel, G. E. Scuseria, M. A. Robb, J. R. Cheeseman, G. Scalmani, V. Barone, G. A. Petersson, H. Nakatsuji, X. Li, M. Caricato, A. V. Marenich, J. Bloino, B. G. Janesko, R. Gomperts, B. Mennucci, H. P. Hratchian, J. V. Ortiz, a. F. Izmaylov, J. L. Sonnenberg, Williams, F. Ding, F. Lipparini, F. Egidi, J. Goings, B. Peng, A. Petrone, T. Henderson, D. Ranasinghe, V. G. Zakrzewski, J. Gao, N. Rega, G. Zheng, W. Liang, M. Hada, M. Ehara, K. Toyota, R. Fukuda, J. Hasegawa, M. Ishida, T. Nakajima, Y. Honda, O. Kitao, H. Nakai, T. Vreven, K. Throssell, J. A. Montgomery Jr., J. E. Peralta, F. Ogliaro, M. J. Bearpark, J. J. Heyd, E. N. Brothers, K. N. Kudin, V. N. Staroverov, T. A. Keith, R. Kobayashi, J. Normand, K. Raghavachari, A. P. Rendell, J. C. Burant, S. S. Iyengar, J. Tomasi, M. Cossi, J. M. Millam, M. Klene, C. Adamo, R. Cammi, J. W. Ochterski, R. L. Martin, K. Morokuma, O. Farkas, J. B. Foresman, D. J. Fox, **2016**, Gaussian 16, Revision C.01, Gaussian, Inc., Wallin.

[47] M. A. Blanco, E. Francisco, A. M. Pendás, *J. Chem. Theory Comput.* **2005**, *1*, 1096–1109.

[48] T. A. Keith, **2019**, AIMAll (Version 19.10.12), TK Gristmill Software,.

[49] I. Cukrowski, G. Dhimba, D. L. Riley, *Phys. Chem. Chem. Phys.* **2019**, *21*, 16694–16705.

[50] A. R. Neves, P. A. Fernandes, M. J. Ramos, *J. Chem. Theory Comput.* **2011**, *7*, 2059–2067.

[51] I. Cukrowski, *Comput. Theor. Chem.* **2015**, *1066*, 62–75.

[52] D. M. S. Buyens, P. Mangondo, I. Cukrowski, L. A. Pilcher, *J. Heterocycl. Chem.* **2017**, *54*, 2946–2950.

[53] N. Platzer, H. Galons, Y. Bensaïd, M. Miocque, G. Bram, *Tetrahedron* **1987**, *43*, 2101–2108.

[54] H.-S. M. Siah, L.-L. Gundersen, *Synth. Commun.* **2013**, *43*, 1469–1476.

[55] R. F. W. Bader, *Atoms in Molecules A QuantumTheory*, OxfordUniversity Press Inc., New York, **1990**.

[56] A. M. Pendás, J. L. Casals-Sainz, E. Francisco, *Chem. - A Eur. J.* **2019**, *25*, 309–314.

[57] R. F. W. Bader, T. S. Slee, D. Cremer, E. Kraka, *J. Am. Chem. Soc.* **1983**, *105*, 5061–5068.

[58] D. Menéndez-Crespo, A. Costales, E. Francisco, Á. Martín Pendás, *Chem. - A Eur. J.* **2018**, *24*, 9101–9112.

© University of Pretoria

Chapter 4 Experimental and theoretical investigation into the reaction kinetics of the benzylation of sodium complexed adeninate anion in anhydrous DMSO

4.1 Introduction

4.1.1 Alkylation sites of nucleic acids in DNA and RNA, free nucleobases and their anions

The factors governing the alkylation of nucleic acids and nucleobases have been of interest for many years due to the tremendous biological importance of their derivatives. The oxygen and nitrogen atoms of nucleic acids in DNA and RNA are available for alkylation by carcinogens and chemotherapy drugs, resulting in several competing reaction centres. This excludes the nitrogen atoms involved in the glycosyl bond with the deoxyribose. A great amount of research has been dedicated to understanding the site preference of alkylation of the nucleophilic atoms of nucleic acids in DNA and RNA.[1–5]

The adeninate anion, which is of interest in this research, is an intermediate in the synthesis of N9-substituted adenines which have important biological roles. N9-alkyladenine derivatives have highly potent cyclic nucleotide phosphodiesterase (PDE) inhibition,[6,7] with high selectivity for PDE-4 conferring anti-asthmatic activity,[8] anti-inflammatory activity[9] and activity against diseases such as multiple sclerosis and autoimmune disease.[10] A number of N9-substituted adenine derivatives have antiviral activity for viruses (such as HIV),[11] are cytotoxic to tumour cell lines[12] and are antagonists for the adenosine receptors[13] which show promise as potential therapeutic agents for cardiovascular and neurodegenerative diseases.

The site preference for the alkylation of heterocyclic anions has been proposed to be a result of the interplay between product stability (thermodynamic control), steric control and charge control driven by electrostatics.[14–23] Simple alkylating reagents which react via an S_N2 mechanism, such as methyl and ethyl alkylating agents, react predominantly at the purine ring nitrogen atoms of nucleic acids in DNA. The most common site for modification is at the N7 atom of guanine (**1** in Figure 1) in the major groove,[2,24] which is the most electronegative position in DNA.[25] The N3 of adenine (**2**) in the minor groove is the next site of alkylation, followed by N1 of adenine and then the N1 of cytosine (**3**).[4,5,24] The N1, N3 atoms and the NH_2 group of guanine and adenine, the O6 of guanine,[26] O4 of thymine[27] (**4**) and the N3 and O2 of cytosine have also been identified as alkylation sites by carcinogenic compounds such as alkanediazonium ions, epoxides and quinone methides.[1,28–30]

The major sites of alkylation of nucleic acids in RNA in decreasing order are the N7 of guanine > N1 of adenine > N1 of cytosine > N3 of adenine.[5,31] In double stranded DNA the N1 of adenine and N3 of cytosine are involved in hydrogen bonding which potentially reduces the alkylation at these atoms compared to RNA. Other environmental factors such as the possible stabilizing electrostatic environment[1] for adenine and guanine or steric repulsion[32] for cytosine and thymine from the sugar-phosphate backbone of DNA can further promote alkylation at certain atoms. Free nucleosides

© University of Pretoria

and nucleotides have the major sites of alkylation at the N7 of guanine, N1 of adenine and N3 of cytosine.[31] The site of protonation is reported to be the same.[3,31] The major site preference for alkylation and protonation of the free nucleobases are the N7 of guanine,[3] N3 of adenine[16,33] (N1 for protonation[34]) and N3 of cytosine.[3] Thymine and uracil do not react under the same alkylating conditions as the other nucleobases, but can be alkylated under alkali conditions at the N3 position.[31,33,35]

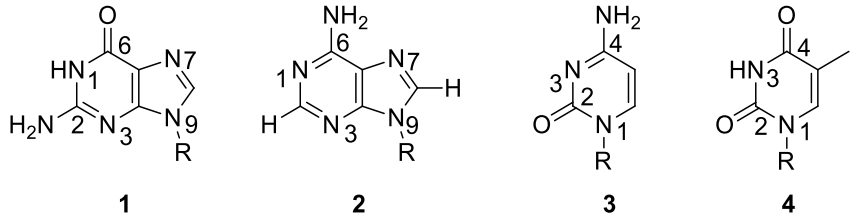

Figure 4.1: Chemical structures and numbering of guanine, adenine, cytosine and thymine.

Direct alkylation of the anions of nucleobases has long presented the problem of yielding complicated mixtures of regio-isomers. It has been shown experimentally that deprotonated adenine, which has four available nucleophilic nitrogen atoms, reacts predominantly at the N9 atom followed by the N3 and N7 via an S_N2 mechanism, (Figure 4.2).[36,37] This differs from the product stability of alkylated adenine which increases in the order of N9R- > N7R- > N3R- > N1R-Ade,[36] which follows the order of proton tautomeric stability of neutral adenine.[38,39]

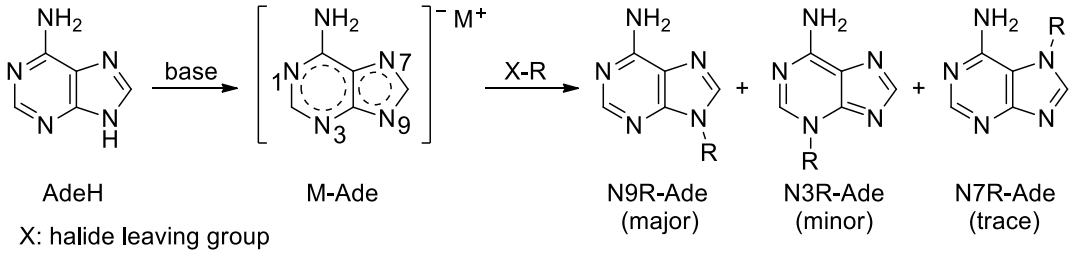

Figure 4.2: S_N2 substitution reaction for the synthesis of N9-alkylated adenine.

Deprotonated guanine yields a mixture of N7 and N9 regio-isomers as the major products along with alkylation at the N1, N3, O6 and NH_2 group in minor amounts.[40,41] Multi synthetic routes have been investigated to gain control over the regio-selectivity of nucleobase alkylation, however, this will not be discussed here.

The site preference for the alkylation of nucleic acids and their bases at the various endo-nitrogen and exo-cyclic heteroatoms depends on the nucleophilicity of the heteroatoms, structure of the electrophile, the nature of the leaving group and the solvent used during alkylation.[14,15,17,21] The influence of these factors on the alkylation of nucleic acids and nucleobases will be discussed.

© University of Pretoria

4.1.2 Factors governing the site of alkylation of nucleic acids, nucleobases and the adeninate anion

4.1.2.1 S_N1 versus S_N2 alkylating reagents

The site preference of alkylation of DNA nucleic acids, nucleobases, nitrogen-containing aromatic heterocycles and the anions thereof is governed by steric and electrostatic control and the mechanism of alkylation, S_N1 and S_N2.[1,3,42] Alkylating agents that favour the S_N2 mechanism, such as dimethyl-[43] and diethyl-sulfates,[44] azaserine[45], melphalan[24] and nitrogen mustards,[2] react predominantly at the N7 atom of guanine (major) and N3 of adenine (minor) of nucleic acids. Agents which promote the S_N1 mechanism, such as dimethyl-[46] and diethyl-nitrosamines[47] and higher alkyl agents, result in higher O6 to N7 guanine alkylated ratios. Reagents such as pyrrolizidines[48,49] and *N*-nitroso-*N*-benzylurea,[50] which react via an S_N1 mechanism alkylate at the amino group of guanine and adenine. The ability of the alkylating reagent to dissociate into an ion-pair plays a significant role in the alkylation preference in DNA as it dictates the extent of the mechanism involved as "S_N1-like" or "S_N2-like".[1] The Swain and Scott parameter[51] and Pearson's "hard and soft acids and bases" principle[52] have been used to predict and explain the dependence of the regio-selectivity of alkylating reagents in general.

Electrophiles which are more "S_N2-like" with a larger Swain-Scott substrate constant react primarily at the nitrogen atoms of nucleic acids, and agents which are more "S_N1-like" react at the oxygen atoms, thus shifting the alkylation of nucleic acids from predominantly N to O.[1] However reactions which involve significant charge development at the reaction site deviate from the Swain-Scott equation. Pearson's principle better explains the regio-selectivity of these electrophiles in which "hard" or non-polarizable electrophiles with higher charge density react with the "harder" O atom and "soft" or polarizable reagents react at the softer N atom.[1]

4.1.2.2 Nucleophilicity of the atoms of nucleic acids

The most nucleophilic sites on nucleic acids have been identified by the use of electrostatic potential energy maps where areas of negative potential are attractive and usually the minima indicates the sites of nucleophilic reactivity i.e. the nitrogen and oxygen atoms.[3,25,53,54] Areas that contain positive potential/maxima indicate an electron deficiency, such as hydrogen atoms which are generally involved in hydrogen bonding.

The nucleophilic atoms of the nucleic acid adenine base are the N3 ≈ N1 > N7 >> NH_2.[3,25,54] While the nitrogen of the NH_2 has a small negative electrostatic potential, the regions of the hydrogen atoms in the plane of the purine ring are electron deficient. The O2 and O4 of thymine are electron rich, in which the former has a more negative electrostatic potential.[54,55] The negative potentials of thymine are much less than those of adenine, guanine and cytosine and thus explain why thymine is not as reactive towards alkylation as other nucleobases.[3] The same is observed for uracil. Cytosine displays two highly attractive regions, the O2 and N3, and an area of very low electrostatic potential at the NH_2. There has been a discrepancy for the order of highest negative electrostatic potential energy between the O2 and N3 atoms whereby either the O2[53] or the N3[3,56] have the most negative electrostatic potential. This issue arises from the level of theory used to calculate the electrostatic potential.[53] However, recent research indicates that the O2 atom has the overall highest negative electrostatic potential.[54] The O6 and N7 atoms of guanine are the most nucleophilic, having the N7 the most electron rich.[57] The N7 minimum is deeper than that of all

© University of Pretoria

adenine nitrogen atoms[25] and therefore renders the site the most nucleophilic in DNA and contributes towards the N7 being the most common site for nucleic acid modification.

In double stranded helices and hydrogen bonded base-pairs it has been shown that the electrostatic potentials around the heteroatoms differ from that obtained for isolated nucleobases.[25] The N7 of guanine retains the deepest minimum in the double helix in the major groove, having the major groove hold the largest negative potential.[58] Furthermore, all minima are extensively deeper than the free nucleobases, nucleosides and nucleotides. The order of nucleophilicity for hydrogen bonded base-pair of the i) adenine-thymine is the N3 of adenine > N7 of adenine > O2 of thymine > O4 of thymine and ii) for the guanine-cytosine base pair is N7 of guanine > N3 of guanine > O6 of guanine > O2 of cytosine.[59] The N7 of guanine is the most nucleophilic out of all positions in both base-pairs. For a deeper understanding of the effect of the double helix sugar-phosphate backbone see reference 25. A shielding effect on the electrostatic potential of DNA arises from the coordination of Na^+ and Mg^{2+} ion to the phosphate groups in which the N7 and N3 of guanine and the N3 of adenine express the deepest minima.[60]

In chapter 3 it was shown by analysis of the net atomic charge of the purine atoms of the free adeninate that the endo-cyclic nitrogen atoms possess equal charge distribution. The coordination of a counter ion, Na^+ and K^+, at the most stable N3N9 position leads to polarization of the anion molecules. The Na^+ and K^+ complexed adeninate anion has a large accumulation of charge density at the N3 and N9 atoms, rendering these more nucleophilic. Previous research showed minimal effect on the site of alkylation due to the change in the counter ion, Li^+, Na^+ and K^+, Table 4.1, for benzyl chloride and chloromethyl pivalate. It has been proposed that the observed negligible change in product ratio with change in counter ion is evidence for the presence of solvent separated ion pairs, in which the free adeninate anion is the active molecule in solution.[17]

Table 4.1: N9:N3:N7 product ratio (%) from the alkylation of the adeninate anion using different bases.[17]

Alkylation site	N9	N3	N7
Base		Benzyl chloride	
LiH	69	25	5
NaH	71	23	7
KH	69	25	6
		Chloromethyl pivalate	
LiH	11	0	89
NaH	7	0	93
KH	8	0	92
		t-Butyl chloroacetate	
LiH	69	31	0
NaH	81	12	7
KH	81	7	12

30 °C in DMSO, 0.02 M M-Ade, 1 eq. alkylating reagent for 16 hours

© University of Pretoria

The presence of ion pairs, having the ion association largest for $Li^+ > Na^+ > K^+$, has shown to result in a decrease of reaction rates with a decrease in cationic radius for enolate anions[61,62] with Li^+ decreasing the rate significantly. The alkylation of the adeninate anion with t-butyl chloroacetate results in a significant effect on the site preference in the presence of Li^+. This observation has been ascribed to ion-pair formation between the Li^+ and the adeninate anion in which the Li^+ is coordinated at the N9 atom.

4.1.2.3 Effect of reactant structure on bimolecular S_N2 transition state geometry

Factors, such as the change in the leaving group or substituents of the alkylating reagent which lead to promoted dissociation of the leaving group, reduce the sensitivity of the agent to the nucleophilicity of the nucleic acid base, and will be discussed below.[50]

Two shifts in the transition state (TS) position on the potential energy surface can occur upon changing the chemical structure of the alkylating reagent, i.e. the change in leaving group (LG) or substituent R attached to the electrophilic carbon (C_α), Figure 4.3, influences the bond cleavage of the TS.[63] The first is the change in the position of the TS parallel to the reaction coordinate, Hammond's postulate.[64] This involves an inverse relationship between the length of the Nu—C_α and C_α—LG bond. The decrease in the Nu—C_α bond and an increase in the C—LG bond results in a later transition state which resembles more of the product, and vice versa results in an earlier TS which resembles the reactant.[65] The change in the TS to later (product like) or earlier (reactant like) along the reaction coordinate is due to thermodynamic changes, i.e. generally endothermic reactions have a late TS while exothermic reactions have an earlier TS.[64,65]

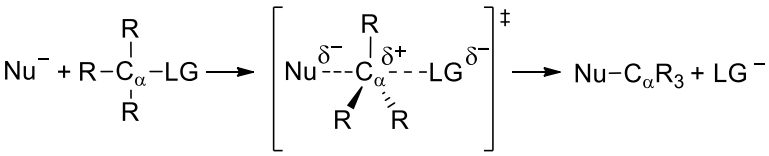

Figure 4.3: S_N2 reaction mechanism. Nu− is the nucleophile and LG is the leaving group.

The second movement of the TS position which arises from reagent variation involves a perpendicular shift to the reaction coordinate whereby both the Nu—C_α and C_α—LG bond lengths increase or decrease.[66,67] The "tightness" or "looseness" of the TS arises from the shortening or lengthening of both the Nu—C_α and C_α—LG bonds, respectively, in which the former has a gain in localization of charge at the C_α and the LG. The tightness of the TS is influenced by the energetics of the unimolecular dissociation of the electrophile. Hence the change in the TS structure with the variation in the electrophile can be described as being later or earlier and looser or tighter.

The prediction of the change in TS structure with variation in the electrophile is well understood using the More O'Ferrall plot,[68] Figure 4.4, although factors such as steric and solvent effects complicate the application of the predictions to actual experimental work. A brief description of the use of More O'Ferrall plot will be given here. The plot is a simplified expression of the potential energy surface connecting reagents (bottom left) and products (top right) through a TS.[63,67] Two

© University of Pretoria

extreme intermediates are also represented whereby i) there is only an increase in C_α—LG dissociation (along the *y* axis) leading to the separate ion $C_\alpha R_2^+$ and LG^- (top left) such as in the case for S_N1 reactions and ii) an increase in Nu—C_α formation (along the *x* axis) leading to Nu—$C_\alpha R_2$—LG (bottom right). Curve A represents that of a S_N2 reaction whereas curve B is that for an S_N1 reaction. The plot works with two rules a) the stabilization of the reagents or products results in the movement of the TS in the opposite direction along the reaction coordinate and b) the stabilization of the intermediates results in the movement of the TS towards the stabilized intermediate.[67] As an example for an S_N2 mechanism: variation in an electrophile which results in more stabilized unimolecular dissociation, i.e. stabilizing $C_\alpha R_2^+$ and LG^-, will result in movement of the TS towards the top left, point 1, perpendicular to the reaction coordinate. This results in a reduction of the Nu—C_α bond formation and an increase in the dissociation of C_α—LG. As both bonds are lengthened, the TS is therefore "looser". If the products are stabilized, the TS will move towards the reagents, point 2, along the reaction coordinate and result in a reduction of the Nu—C_α bond formation and less C_α—LG dissociation, and thus a more "reagent-like" or earlier TS. However, a combination of parallel and perpendicular movement can occur together in which the TS shift is the resultant of the vectors for the individual movements: If we take the combination of the two examples above the TS will shift towards point 3, and result in a TS with a longer Nu—C_α bond and a relatively unchanged $C_\alpha R_2$—LG bond.

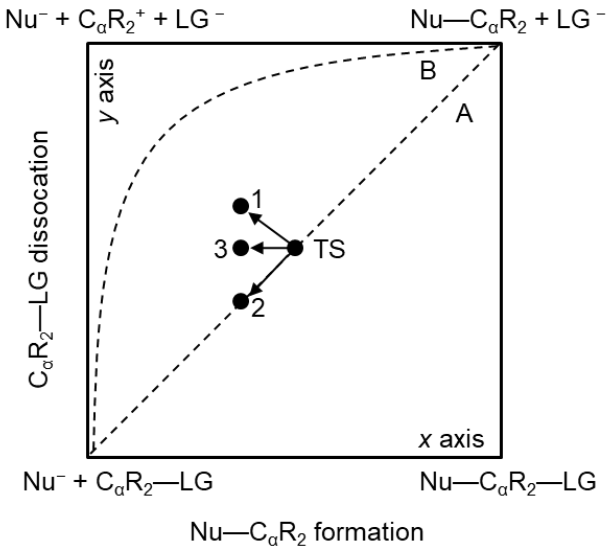

Figure 4.4: A More O'Ferrall plot for an S_N2 reaction (A) and an S_N1 reaction (B).

The above influence of the change in electrophile on the TS structure has been used to explain the shift of N7 to O6 alkylation of guanine when changing the alkylating reagent from methane- to ethane- diazonium[1] and sulfonate[69] and methyl and methyl-N-nitrosourea.[69] The shift has been ascribed to the more "S_N1-like" nature of the latter ions relative to the methanediazonium ion.[70] These reactions occur via an S_N2 mechanism, however the extent of the unimolecular dissociation of ethane and propanediazonium are larger than that of the methane agent. The ethylation of guanine was calculated to be more endothermic than that of methylation, resulting in a later TS.[1] The

© University of Pretoria

favourable dissociation of the ethanediazonium ion[70] (−32 kcal mol^{-1} more favourable than that of methanediazonium) leads to the lengthening of both the Nu—C_α and C_α—LG bonds and thus yields a looser TS. Therefore, a later and looser TS occurs for the "S_N1-like" reagents in which the TS geometry has the forming Nu—C_α bond longer than those for more "S_N2-like" agents. This entails that the perturbation of the overlapping orbitals and the degree of charge transfer will be less for the former reagents than those of tighter TS structures with a shorter Nu—C_α bond. Hence, "S_N1-like" reagents are less sensitive to the nucleophilic nature of the atom being alkylated as at further distances of the N7 and O6 atom the electrostatic control becomes less as a coalescence to a single broad area on the potential energy map is observed.[57]

The effect of the leaving group on the preference in alkylation site was investigated for adenosine and guanosine using benzyl bromide, benzyl chloride and benzyl tosylate.[71] Decreasing stability of the departing anion in the order of Br > Cl > OTs, leads to less benzylation at the less nucleophilic NH_2 group of adenosine and guanosine.[50,71] The greater the positive charge density at the C_α position ("harder" centre) with decreasing polarizability of the LG leads to greater reaction at the "harder" O6 atom of guanine. The effect on the TS can be predicted by using the More O'Ferrall plot whereby greater polarizability of the LG stabilizes the ion formation $C_\alpha R_2^+$ and LG^- (top left) and the product formation (top right), i.e. movement of TS to point 3. The new TS will be a resultant of these two vectors in which the Nu—C_α bond is lengthened with less positive charge dispersion from C_α to the Nu and there is minimal change of the C_α—LG bonds, leading to a looser and earlier TS.[63] The effect of the change in the leaving group (Cl, Br and I) on the site of alkylation of the adeninate anion is minimal, as seen in the case of the benzyl halides in Table 4.2. This has also been observed in the case of adenine and other heterocycles.[14–16,18,21]

The site preference for alkylation of the adeninate anion is mildly sensitive to changes in the alkylating reagent structure, Table 4.2. Alkylation at the N7 occurs in trace amounts in most cases except for when chloromethyl pivalate is used as the alkylating reagent.[15,17]

Table 4.2: Dependence of the adeninate anion N9:N3:N7 product ratio on the alkylating reagent[15]

	N9R-Ade	N3R-Ade	N7R-Ade
Alkylating reagent			
Methyl Iodide	77	17	6
Ethyl Iodide	80	15	5
Benzyl chloride	76	21	3
Benzyl bromide	68	27	4
Benzyl iodide	68	23	6
4-methoxybenzyl chloride	69	25	6
Phenacyl chloride	86	7	7
t-butyl chloroacetate	78	7	14
Chloromethyl pivalate	15	0	85

30 °C in DMF, 0.02 M Na-Ade, 10 eq. alkylating reagent for 16 hours

© University of Pretoria

Increasing the dissociation of $C_\alpha R_2^+$ and LG^- i.e. moving from methyl iodide through to benzyl iodide, causes slightly larger amounts of the N3-Me product to form. The effect of the methoxy electron donating group of 4-methoxybenzyl chloride stabilizes the unimolecular dissociation of the electrophile, which in turn leads to an earlier and looser TS. In both cases the "SN1-like" nature of the electrophile increases which promotes the formation of the N3 alkylated derivative. However, from Table 4.2 the increase observed experimentally is not so pronounced. The opposite would occur with electron withdrawing groups. This is a consequence of coulombic forces which arise from the negative charge of the adeninate anion. The negative charge is equally distributed on the N1, N3, N7 and N9 nitrogen atoms of the purine ring, thus rendering each nitrogen atom to be equally alkylated under electrostatic control. The tighter TS leads to a larger dependence on steric and product stability control.[14,15,72] Steric hindrance is presumed to largely discourage the formation of N7-alkylated adenine.[15,17] In the case of chloromethyl pivalate hydrogen bonding between the electrophile and the NH_2 group of the adeninate anion shifts the product ratio to favour that of the N7R-Ade, Figure 4.5.[15,73]

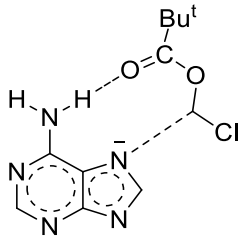

Figure 4.5: Hydrogen bond formation between chloromethyl pivalate and NH_2 of the adeninate anion.

4.1.2.4 Effect of solvent on the site of alkylation of nucleic acids

The influence of solvent on the site of alkylation of nucleic acids has been addressed in several studies.[50,71,74] With increasing electrophilic nature of the solvent (such as going from DMF to H_2O) the dissociation of the C_α—LG bond is stabilized (promoted) due to the increased solvation of the halide[75] and thus leads to looser and earlier TS structures due to the more "S_N1-like" character. This in turn has been shown to lead to less selectivity and leads to complicated mixtures of nucleic acid derivatives. The benzylation of adenosine and guanosine in protic solvents shifts the major product from the N1 of adenine and the N7 of guanine to the NH_2 position, having benzylation at the O6 of guanosine also increase but to a lesser extent.[71] Similar findings have been reported for the alkylation of nucleic acids in which 7-bromo-methylbenz[*a*]anthracene in aqueous solution lead to high yields of the NH_2 derivatives of guanine, adenine and cytosine instead of alkylation at the endo-cyclic nitrogen atoms, i.e. the N7 of guanine, N1 of adenine and the N3 of cytosine.[74] However, this is not observed for dimethyl sulfate[74] and *N*-nitroso-*N*-benzylurea[50] in which the aqueous solvent has little effect on the reagent structures and therefore retained their "S_N2-like" nature. Shifting from polar aprotic solvents to polar protic solvents in the alkylation of the adeninate anion causes in significant amounts of N3 alkylated adenine to form due to the loosening of the TS in polar protic solvents.[17,72] This in turn leads to enhanced electrostatic control.

© University of Pretoria

It is to be noted that the yield of alkylated derivatives in aqueous solution is lower than in organic or binary solvent mixtures with higher % organic solvent.[50] This is due to the decrease in nucleophilicity of the bases of nucleic acids from the solvation and hydrogen bond formation with protic solvents which leads to lower reactivity. Similar results are observed for the reactivity of the anions of nucleobases[42]

4.1.2.5 Steric effects on entropy

Lastly, the influence of steric effects on the TS entropy is discussed. The effect of the size and nature of the substituents (degrees of freedom) of the electrophile at or near the reactive site results in steric hindrance to rotation (resulting from overcrowding at the reaction centre and interaction of substituents with solvent molecules) and strain (repulsion between electrons of nearby atoms) in the TS. This affects the entropy, $\Delta S^{\ddagger}$, and enthalpy, $\Delta H^{\ddagger}$, of activation.[76] The change in $\Delta S^{\ddagger}$ indicates the degree of structural changes in solvent and in reactants upon formation of the TS. The liberation of solvent for example in the TS results in an increase in $\Delta S^{\ddagger}$. The larger and more complex the substituents are close to the reactive site of a reactant, i.e. the larger the entropy of the molecule, the greater the loss in translational and vibrational degrees of freedom in the TS. This in turn leads to a larger decrease in $\Delta S^{\ddagger}$ (more negative).[76] The effect of steric strain in the TS on entropy of activation is well explained by the strain-entropy principle.[77,78] The principle states that if a substituent is replaced by a group with more internal degrees of freedom and the TS results in greater repulsion between the reaction centre and the larger substituent, there will be an increase in the loss in internal motion and therefore a decrease in $T\Delta S^{\ddagger}$ which is accompanied by an increase in $\Delta H^{\ddagger}$ and free energy of activation, $\Delta G^{\ddagger}$. This differs from the enthalpy-entropy compensation effect (EEC). The EEC refers to the linear relationship between $\Delta H^{\ddagger}$ and $\Delta S^{\ddagger}$, ΔH and ΔS, or between the Arrhenius pre-exponential factor and E_a, of closely related reactions.[79,80] Both parameters change in the same direction, i.e. an increase in $\Delta H^{\ddagger}$ is compensated for by an increase in $\Delta S^{\ddagger}$. This generally refers to either i) the same reaction performed in different solvents or ii) when one of the reagents differs slightly i.e. by a single substituent.[80]

The effect of steric hindrance and steric strain on the preferred site for the alkylation of the adeninate anion has been used to explain the minimal amount of alkylation at the N7 and N1, if any, due to the presence of the NH_2 group at the C6 position of the purine ring.[15] The N9- and N3-alkylated products are therefore believed to form more readily than the N1 and N7.

4.1.3 The benzylation of the adeninate anion

It has been shown previously by ^{1}H NMR spectroscopy of the final reaction mixture after a period of time that N9- (major) and N3-benzyladenine (minor) are the major products from the benzylation of the adeninate anion using benzyl bromide in DMSO and DMF.[15,17,37] The variation of the leaving group of the benzyl halide was shown to have a minimal effect on the product ratio[15].

Benzyl halides have been proposed to form a carbocation at the C_α position which is resonance stabilized, Figure 4.6, and can undergo an S_N1 reaction, having the alkylation occur predominantly at the C_α position and not the ring positions.[81] However, benzyl halides are known to react predominantly via and accelerate S_N2 reactions. This is known as the S_N2 benzylic effect and results in a decrease in the activation barrier by around 4-5 kcal mol^{-1} compared to saturated alkyl halides.[82,83] The effect is ascribed to the conjugative stabilization of the incoming negative charge

© University of Pretoria

on the nucleophile in the transition state by the π system of the benzylic ring.[83,84] In addition, secondary and tertiary benzyl halides can react via E2 bimolecular elimination reactions, leading to the formation of alkenes.[82] The effect of the presence of electron donating and electron withdrawing groups on the benzylic ring of the benzyl halide results in the loosening and tightening of the transition state structure, respectively, as discussed in section 4.1.2.3.[63,85] It has been shown that looser TS structures lead to larger amounts of the N3 alkylated adenine derivative while still retaining the N9 isomer as the major product.

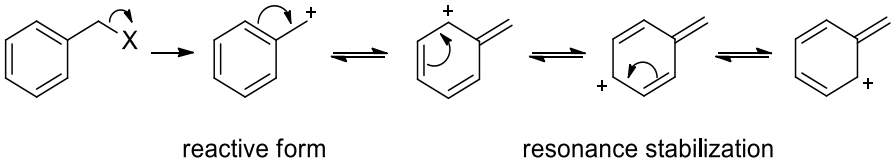

Figure 4.6: Carbocation formation of benzyl halides and delocalization of the positive charge.

The exploration into the regio-selectivity of the adeninate anion highlights a combination of contributing factors governing the site of alkylation: product stability, steric hindrance, electrostatic control, nature of the alkylating group and solvent and possibly the presence of ion pairs and dimers.[15,17] These factors are known to influence S_N2 reactions.[86,87] Although there have been extensive investigations into the role of these factors in governing the regio-selectivity of the alkylation of the adeninate anion, no real-time ^{1}H NMR analysis, rate constants and thermodynamic data have been obtained experimentally. From chapters 2 and 3 it has been strongly suggested that the adeninate anion doesn't exist in its free form in anhydrous DMSO but is ion-paired with the counter ion, Na^+ or K^+, which is most likely chelated at the N3 and N9 atoms of the purine ring. The evidence for the ion-pairing adds new insight into the reacting complex indicating that it is not the free adeninate anion but rather the metal complexed adeninate salt that is undergoing alkylation. This contradicts the previously reported hypothesis that solvent separated ion pairs exist between Na^+ and K^+ with Ade^- in DMSO.[17]

In this research the alkylation of the adeninate anion in anhydrous DMSO is investigated by dynamic ^{1}H NMR spectroscopy for the first time. Benzyl bromide (**1** in Figure 4.7), (1-bromoethyl)benzene (**2**) and pentafluorobenzyl bromide (**3**) were used to benzylate the adeninate anion under the same conditions and the reactions were monitored in real time. The bulkier substituent at the alpha carbon of **2** should lead to a looser TS structure with the lengthening of both the Nu—C_α and C_α—LG bonds, promoting N3 alkylation. The presence of the electron withdrawing atoms of **3** would destabilize the unimolecular dissociation of the reagent and lead to a tighter TS with a decrease in both the C_α—LG and Nu—C_α bond lengths with less positive charge development on C_α. This should in turn yield larger N9 alkylation due to enhancing product stability control. The influence of structure of three benzyl halides on the N9:N3 product ratio of benzylated adenine is reported.

This is followed by the reaction kinetics and reporting of the thermodynamic parameters for the benzylation of the adeninate anion using benzyl chloride. In addition, the S_N2 mechanism is

© University of Pretoria

theoretically modelled for each pathway leading to N1-, N3-, N7- and N9-benzylated adenine in the presence and absence of the sodium counter ion.

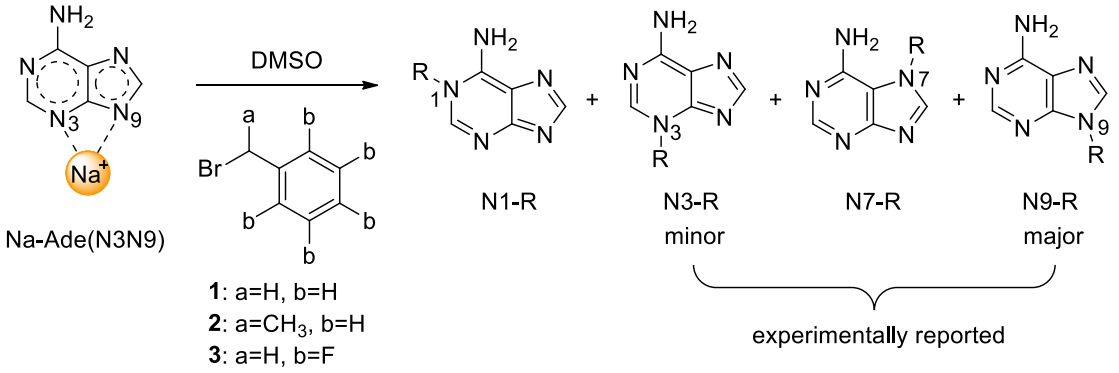

Figure 4.7: Alkylation of Na-Ade in anhydrous DMSO using benzyl bromide (**1**), (1-bromoethyl)benzene (**2**) or pentafluorobenzyl bromide (**3**) as the alkylating reagent. Products formed are N1-, N3-, N7- and N9-R adenine derivatives.

4.2 Experimental details

General: The ^{1}H NMR spectra were recorded at 300 MHz with a Bruker 300 AVANCE Ultrashield Plus. Heteronuclear Multiple Bond Correlation (HMBC) spectra were recorded at 400.13 MHz with a Bruker 400 AVANCE Ultrashield Plus. The ^{13}C NMR spectra were recorded at 101 MHz using the Bruker 400 AVANCE Ultrashield Plus. The ^{13}C NMR spectra were calibrated using the DMSO-d_6 solvent peak at 39.5 ppm. All reagents were purchased from Sigma-Aldrich. Stock solutions and dilutions of Na-Ade and K-Ade were prepared and sealed within the glovebox using the anhydrous DMSO-d_6. Sodium and potassium hydride are used as bases to avoid introduction of water into the reactions.

Materials and Methods

The anhydrous DMSO-d_6 was prepared as follows: Powdered 4 Å molecular sieves were heated at 200 °C under vacuum for 4 days and placed inside a glovebox. The sieves were added to DMSO-d_6 and left for 24 hours. The solvent was analysed via ^{1}H NMR to confirm the absence of water. The molecular sieves were removed by passing the solvent through a 25 mm hydrophilic polyamide syringe filter.

Preparation of Na-Ade stock for Na-Ade and benzyl chloride concentration dependent studies: A stock solution of Na-Ade was prepared within the glovebox: NaH (0.383 mmol, 1.20 eq.) was added to a heterogeneous mixture of adenine (0.319 mmol, 1 eq.) and anhydrous DMSO-d_6 (5000 µl). Solution was stirred until bubbles of H_2 gas generated from the deprotonation of adenine by NaH ceased. From this, 4 concentrations were prepared for the Na-Ade concentration dependent study, A (5.85), B (12.2), C (25.0) and D (48.5 mM). Each reaction contained TEA (12.9 mM) and was initiated by the addition of BnCl (12.9 mM). The ^{1}H NMR spectra were immediately recorded at 295 K. For the BnCl concentration dependent study, from the Na-Ade and anisole stock solution, 10 dilutions were prepared to contain Na-Ade (13.5 mM) in a final total volume of 400 µl. Five of the dilutions were used for the study in the presence of TEA and the other five for the study in the

© University of Pretoria

presence of DBU. The reactions were initiated by the addition of BnCl with the ratio of BnCl:base as 1:1. The concentrations of BnCl used in the BnCl concentration profile are: (A) 13.8, (B) 27.6, (C) 55.2, (D) 82.8 and (E) 110 mM. All reactions were run at 295 K. The method of initial rates is used to obtain the observed rate of reaction.

Temperature dependent chemical kinetics for the benzylation of the Na-Ade: From the stock solution of Na-Ade prepared above, 3500 µl, anisole (0.137 mmol, 1.0 eq.) and DBU (0.151, 1.1 eq.) were added. The stock is diluted to a final concentration of Na-Ade (6.65 mM), anisole (6.69 mM) and DBU (7.14 mM) for each ^{1}H NMR kinetic run of a total volume of 400 µl. For each ^{1}H NMR kinetic run, BnCl (14.01 mM, 2.1 eq.) is added to the NMR tube, mixed and the ^{1}H NMR data is immediately recorded. Three replicates were run for each temperature selected: 300, 305, 310, 315 and 320 K. The method of initial rates was used to obtain the observed rate of reaction using Graphpad Prism 5. In all kinetic experiments, anisole is used as the internal standard. The mixture of Na-Ade and anisole in anhydrous DMSO-d_6 resulted in no observed concentration dependent ^{1}H NMR chemical shifts or formation of additional peaks with increasing concentration of anisole, Figure S3.1 in Supporting Information 3, making it an appropriate internal standard to use for this study as there is no reactivity between the two compounds. Integration of the methyl peak of anisole and the CH_2 peak of N9- and N3-Bn was used to calculate the concentration of N9- and N3-Bn from a known concentration of anisole using eqn 4.1,

$$\mathrm{C} = \mathrm{CCF} \times \frac{\mathrm{AI}}{\mathrm{NN}} \qquad (4.1)$$

where C is the concentration, CCF is the concentration conversion factor, AI is the absolute integral and NN is the number of protons. CCF is calculated when C is the known concentration of anisole, AI is the methyl group integral and NN is 3.

Computational details

All electronic structure calculations were performed in Gaussian 09 rev. E.01[88] (DFT). All structures were optimized at the DFT/B3LYP/6-311++g(d,p) level of theory with empirical dispersion GD3 correction.[89] The computations were performed in solvent (DMSO) using the Polarizable Continuum Model (PCM). To verify that the structures obtained at the DFT level of theory are at a minimum, frequency calculations were performed to ensure no imaginary/negative frequency was present except for the transition state structures. The optimized Na-Ade(N3N9) complex was used as an input for the study involving explicit DMSO solvent molecules. Four fully optimized DMSO solvent molecules were pre-organized around the optimized Na-Ade(N3N9) and the solvated complex was optimized without constraints. The pre-reactive complexes of Ade^- or Na-Ade(N3N9) with benzyl chloride was achieved by optimizing the two structures separated at a distance of 4 Å between the $\underline{C}H_2$ of BnCl and the reactive nitrogen, N*X*, of the adeninate anion, either N1, N3, N7 or N9 leading to N1-, N3-, N7- or N9-Bn, respectively. See Figure S3.11 and S3.12 for the scan of Ade^-or Na-Ade(N3N9) with BnCl, respectively. The two molecules in the adduct were scanned along the reaction coordinate (decreasing the distance between the electrophilic $\underline{C}H_2$ carbon on the BnCl and the reactive nitrogen by 0.1 Å steps), through a TS to the final product of each pathway. The transition state was obtained using the Berny algorithm. Frequency calculations were performed on

© University of Pretoria

all TS structures. Intrinsic reaction coordinate[90,91] (IRC) calculations were performed to ensure that the transition states connected the reactants and products. In the log file from the frequency calculation in Gaussian, the low vibrational frequencies which may contribute to error in the partition function are listed along with their contribution to the internal thermal energy, entropy and heat capacity of the system and can be removed in order to correct for them. Reagent, TS, and product log files are available at 10.25403/UPresearchdata.19188800.

4.3 Results and discussion

4.3.1 The effect of the structure of benzyl halide derivatives on the N9 and N7 product ratio

The dynamic ^{1}H NMR spectra for the alkylation of Na-Ade using benzyl bromide, (1-bromoethyl)benzene, and pentafluorobenzyl bromide are shown in Figure 4.8a, b and c, respectively. The ^{1}H NMR peaks corresponding to the N9 and N3 alkylated adenine derivatives are indicated in Figure 4.8 and the ^{1}H NMR chemical shifts of isolated products are shown in Table 4.3. The N9 alkylated adenine isomer is the major product in all three reactions, followed by the N3 derivative.

The dynamic ^{1}H NMR spectra in Figure 4.8 show that multiple reactions are occurring or products are being formed in the presence of the Na-Ade and the alkylating reagent. The complexity of the dynamic ^{1}H NMR spectra reduces when moving from alkylating reagent **1** to **3**, having benzyl bromide, Figure 4.8a, resulting in a large number of unaccounted for proton peaks in addition to that of the N9- and N3-benzyladenine. The N7-benzyladenine isomer is identified with the proton peaks occurring at 8.44 (C8-H), 8.18 (C2-H) and 5.70 (CH_2) ppm, in line with previous reports,[16,17,92] however the product could not be isolated from the reaction mixture as its yield was too low. The remaining ^{1}H NMR peaks do not correlate with reported N1- and N6-benzyladenine or with dibenzylated adenine derivatives, 3,7-dibenzyladenine and 1,9-dibenzyladenine.[16,17,93,94] Evidence for the formation of N7-pentafluorobenzyladenine is also observed having the CH_2 peak occurring around 6.0 ppm.

Table 4.3: ^{1}H NMR chemical shifts for N9- and N3-R adenine derivatives in anhydrous DMSO-d_6

	C8-H	C2-H	C6H5	CH2	CH	CH_3
benzyl bromide						
N9-benzyladenine	8.26	8.16	7.23–7.33	5.36	-	-
N3-benzyladenine	7.76	8.57	7.27–7.47	5.51	-	-
(1-bromoethyl)benzene						
N9-(1-phenylethyl)-adenine	8.40	8.11	7.39–7.25	-	5.82	1.94
N3-(1-phenylethyl)-adenine	7.75	8.57	7.49–7.27	-	6.10	2.02
pentafluorobenzyl bromide						
N9-pentafluorobenzyladenine	8.20	8.11	-	5.51	-	-
N3-pentafluorobenzyladenine	7.70	8.53	-	5.67	-	-

The ratio of N9:N3:N7 alkylated products is 1:0.4:0.08 and 1:0.3:0.12 for reactions using **1** and **3**, respectively. There is no evidence for the formation of N7-alkylated adenine with reagent **2** and the ratio for N9:N3 is 1:0.5. The absence of the benzylation at the N7 atom is attributed to steric

© University of Pretoria

hindrance due to the presence of the methyl group at the α-carbon and the NH_2 group of the purine ring near the reactive site.

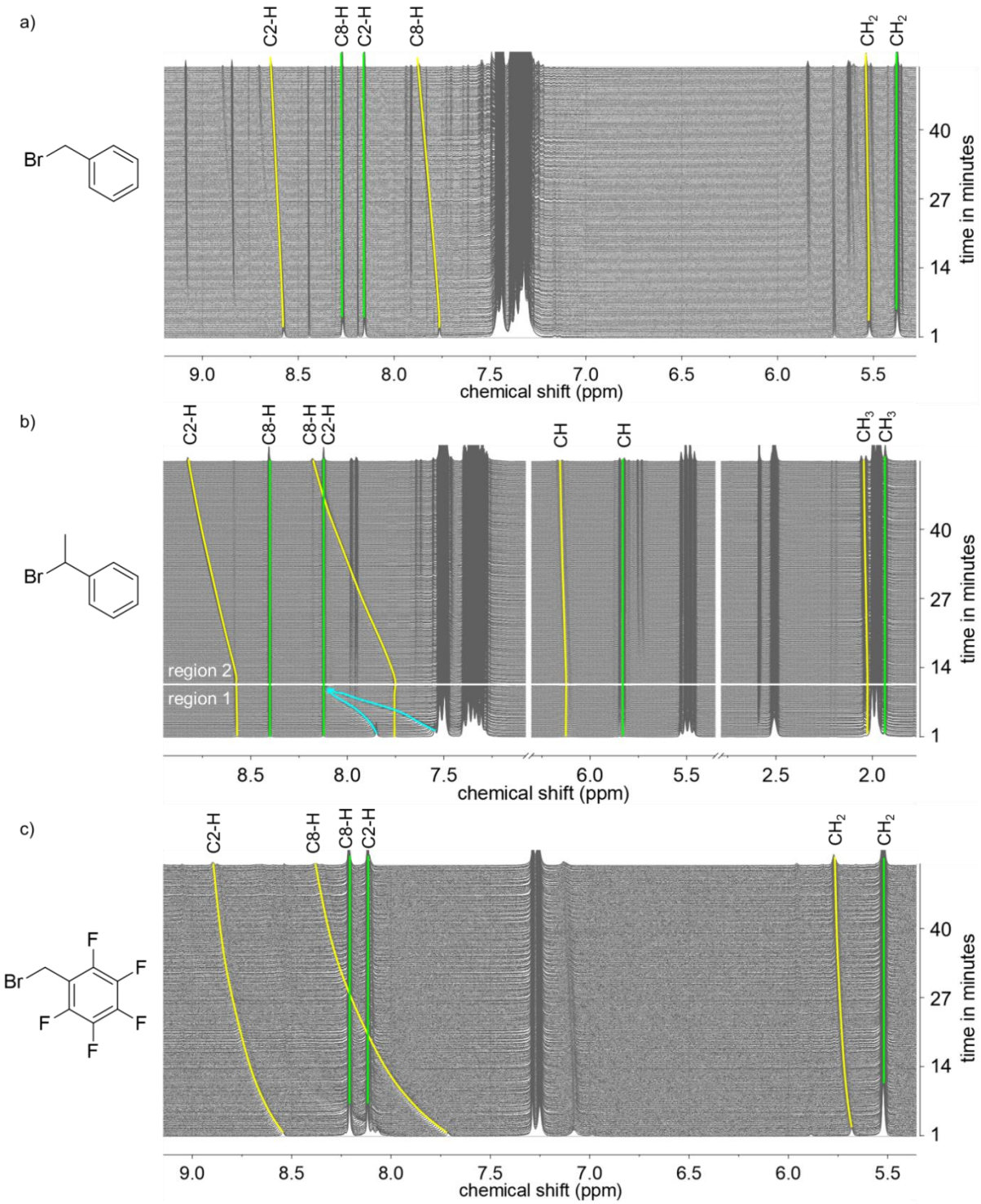

Figure 4.8: Dynamic ^{1}H NMR spectra for the alkylation of adeninate anion (40 mM) with a) benzyl bromide, b) (1-bromoethyl)benzene and c) pentafluorobenzyl bromide at 5 eq. in anhydrous DMSO-d_6. N9- and N3-R adenine alkylated derivatives are shown by the green and yellow lines, respectively.

© University of Pretoria

The slight increase and decrease in the N3-benzylated product in the presence of reagents **2** and **3**, respectively, compared to **1** is attributed to the slight loosening and tightening of the TS associated with these two compounds. However, these differences are not significant enough to conclude that these structural changes influence the site preference of alkylation to any appreciable extent. It is possible that there is an entropy-enthalpy compensation effect that enables the N9 and N3 regio-isomer to retain similar Gibbs free energy of activation despite the change in alkylating reagent.

4.3.2 Identification of the side reaction occurring during the benzylation of the adeninate anion

The alkylation using the reagent (1-bromoethyl)benzene resulted in an overall slower reaction due to the additional methyl group at the site of nucleophilic attack, resulting in steric hindrance and therefore a larger activation barrier for the reactants to cross. The slow reaction rate allows for the identification of an additional side reaction occurring in solution. The dynamic ^{1}H NMR spectra in Figure 4.8b are divided into regions 1 and 2 separated by a white line. Region 1 indicates that alkylation of the adeninate anion is taking place alongside an additional reaction marked by the migration (blue arrows) of the Na-Ade purine protons from 7.80 and 7.50 ppm to under the C2-H of N9-(1-phenylethyl)-adenine at 8.11 ppm. This side reaction is the protonation of Na-Ade to form neutral adenine. In region 2, a subsequent protonation of N3-(1-phenylethyl)-adenine occurs only after the Na-Ade is depleted by protonation and alkylation. The C2-H and C8-H proton peaks become deshielded, shifting from 8.57 and 7.75 to 8.82 and 8.17, respectively, with a deshielding effect of the CH peak from 6.10 to 6.15 ppm. The peak migration of N3-benzyl adenine due to protonation is slightly visible in the ^{1}H NMR spectra of benzyl bromide where the C2-H and C8-H proton peaks become deshielded, shifting from 8.57 and 7.76 to 8.63 and 7.86 ppm, respectively. The effect is more pronounced with pentafluorobenzyl bromide, having the C2-H and C8-H migrate from 8.53 and 7.70 to 8.89 and 8.37, respectively. It is to be noted that the N3-isomer is protonated before N9-alkylated adenine in all three reactions studied above.

Due to the difference in the above protonation behaviour between the three different alkylating groups, the source of the proton is proposed to be a side reaction involving the alkylating reagent. Furthermore, from Chapter 2, a solution of only Na-Ade and anhydrous DMSO does not result in protonation of Na-Ade. To explain how the proton originates from the alkylating reagent, it is proposed that the Kornblum oxidation reaction occurs as a side reaction during the alkylation of Na-Ade in anhydrous DMSO. The Kornblum oxidation reaction is the oxidation of primary and secondary alkyl halides by DMSO to yield aldehydes or ketones, respectively.[95,96] The alkyl halides **1**, **2** and **3** undergo S_N2 nucleophilic substitution by a DMSO solvent molecule displacing the halide and forming an alkoxy sulfonium ion intermediate, Figure 4.9. In the presence of a base (B^-), a proton at the site of the nucleophilic attack is abstracted, resulting in an aldehyde for reagents **1** and **3** and a ketone for reagent **2,** and dimethyl sulphide. In the alkylation reactions performed in this research, the Na-Ade acts as the base to remove the proton of the alkoxy sulfonium ion, thus yielding neutral adenine. The aldehydes resulting from the alkylating reagents **1** and **3** are evident by the presence of an aldehyde peak at 10.02 and 10.14 ppm, respectively, in the ^{1}H NMR spectra (Figure S3.2a and b, respectively). The formation of methylphenyl ketone from the alkylating reagent **2** is observed in the ^{1}H NMR spectra of that reaction. The proton peak present at 2.58 (CH_3) and benzylic protons at 7.97 and 7.95 (Figure S3.2c) correspond to those reported for methylphenyl ketone in DMSO-d_6.[97]

© University of Pretoria

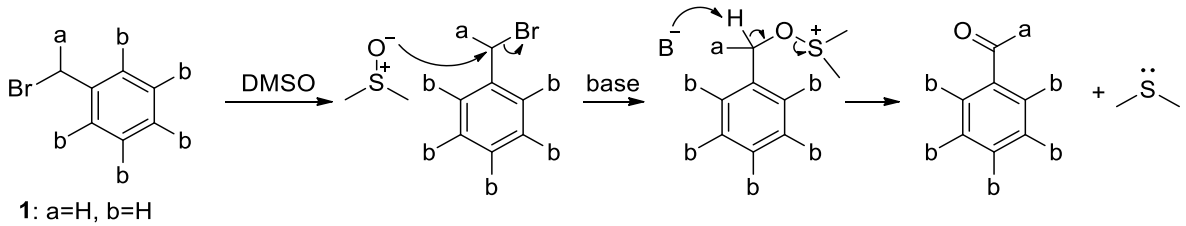

1: a=H, b=H
2: a=CH_3, b=H
3: a=H, b=F

Figure 4.9: Kornblum oxidation reaction involving DMSO and alkyl halides **1**, **2** and **3** in the presence of a base.

The Kornblum oxidation reaction is much slower for benzyl bromide, and hence, in Figure 4.8a, the protonation of the N3-benzyladenine is not as significant as with alkylating reagent **2**. It is unclear if the presence of the Na^+ counter ion facilitates the reaction. The observed migration of the peak(s) in Figure 4.8 from the original Na-Ade position to the final position of neutral adenine as compared to a depletion and appearance of the corresponding peaks indicates that there is an equilibrium between the adeninate anion and neutral adenine. The same effect is observed for the protonation of the N3-alkylated adenine. This indicates that there is movement of the proton between the protonated species in solution with Na-Ade and/or *N*-alkylated adenine derivatives.

4.3.3 The effect of the counter ion present on the N9 and N7 product ratio

In addition to the investigation of the effective product ratio with the change in the benzylic alkylating reagent, the N9:N3 product ratios for the alkylation of the adeninate anion with reagent **2** were assessed in the presence of KH and KH with 18-crown-6 ether (18C6), Figure 4.10a and b, respectively. It is of interest to investigate whether the K^+ counter ion influences the product ratio to any notable extent as compared to the Na^+ counter ion.

It has been shown in Chapters 2 and 3 that an ion-pair exists between K^+ and the adeninate anion, K-Ade, and the introduction of the 18-crown-6-ether did not show evidence for the abstraction of the K^+ from the K-Ade complex. From Figure 4.10a and b, it is clear that no obvious change in the reaction progression occurs when KH is used as a base and when 18C6 is present. The N9- and N3-benzylated adenine products are the only observed alkylated products with the protonation of the K-Ade and N3 product still occurring. The N9:N3 product ratio is 1:0.5 for both sets of reactions and is no different to that reported for Na-Ade. This is in agreement with previous research whereby the presence of Na^+, K^+ and Li^+ did not alter the N9:N3 product ratio for benzyl halide.[17] However there are some important differences in the shape of the proton peaks in the spectra in Figure 4.10a and b. The C8-H and C2-H of the N9- and N3-benzylated products appear to be replicated in the presence of KH, having the replicated peaks appear downfield from the main peaks.

The new duplicate peaks of the C8-H and C2-H in the N9-benzylated product occur downfield by 0.02 and 0.03 ppm, respectively, and 0.05 and 0.02 for the C2-H and C8-H of the N3-benzylated product. It is unclear as to why the peaks are duplicated; however, it is likely linked to the presence of the K^+ ion. This doubling of peaks no longer occurs in the presence of the 18C6, but rather a broadening of the protonated K-Ade and N3-benzylated product peaks is observed. The broadening of these

© University of Pretoria

proton peaks in the dynamic ^{1}H NMR could be due to proton exchange or partial complexation with the 18C6.[98]

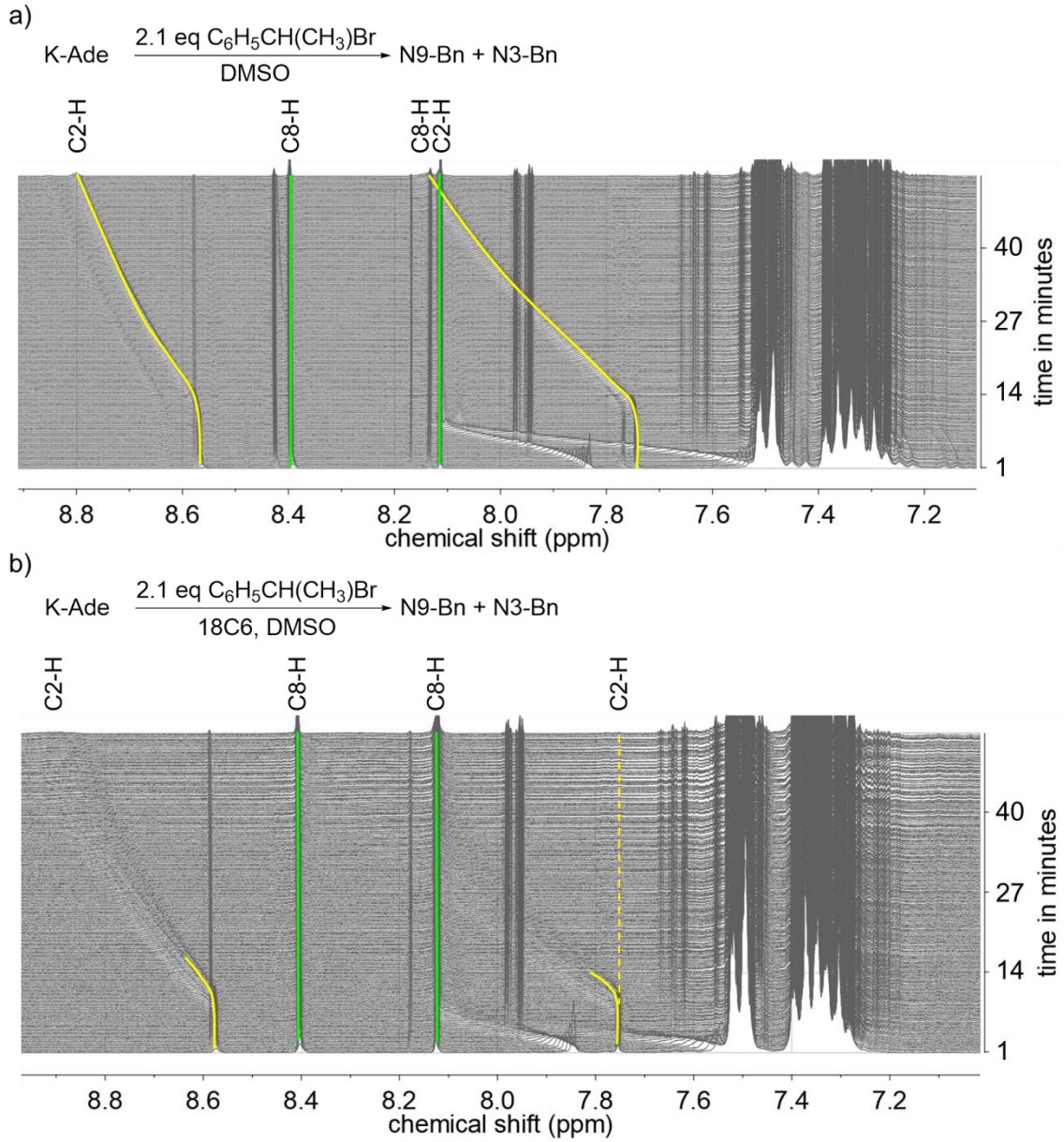

Figure 4.10: Dynamic ^{1}H NMR spectra for the alkylation of K-Ade with a) (1-bromoethyl)benzene and b) (1-bromoethyl)benzene in the presence of 18-crown-6 ether in DMSO-d_6 at 295K.

The depletion of the starting material, Na-Ade and K-Ade in reactions described above, by the proposed Kornblum oxidation reaction prevents accurate reaction rates from being obtained. In addition, it explains the low yields reported for the isolation of pure *N*-alkylated adenine derivatives. In order to resolve this issue, a non-nucleophilic base was added to compete for the available proton on the alkoxy sulfonium ion intermediate. Two bases were investigated, namely triethylamine (TEA) and 1,8-Diazabicyclo(5.4.0)undec-7-ene (DBU).

© University of Pretoria

Furthermore, it is clear from the dynamic ^{1}H NMR in Figure 4.8a and c that the reactions occur at an extremely high rate and are near completion by the time the ^{1}H NMR spectra are recorded (within a minute). In order to address this without reducing the Na-Ade concentration to a point where it will be too low to monitor correctly by ^{1}H NMR spectroscopy, benzyl chloride was used instead of benzyl bromide in order to reduce the reaction rate in all subsequent kinetic studies.

4.3.4 Reaction order of the benzylation of Na-Ade in anhydrous DMSO

The formation of each of the products from the benzylation of Na-Ade by benzyl chloride is described by eqn 4.2 to 4.4, where k_1, k_2 and k_3 are the rate constants for the formation of N9-, N3- and N7-Bn, respectively. The reactions occur parallel to each other where each pathway competes for Na-Ade.

$$\mathrm{Na{-}Ade + BnCl} \xrightarrow{k_1} \mathrm{N9{-}Bn + NaCl} \tag{4.2}$$

$$\mathrm{Na{-}Ade + BnCl} \xrightarrow{k_2} \mathrm{N3{-}Bn + NaCl} \tag{4.3}$$

$$\mathrm{Na{-}Ade + BnCl} \xrightarrow{k_3} \mathrm{N7{-}Bn + NaCl} \tag{4.4}$$

The overall rate equation for the depletion of the starting material, Na-Ade, is described by eqn 4.5 and the formation of the N9-, N3- and N7-Bn products is shown by eqn 4.6, where N*X* refers to the regioisomers N9-, N3-, and N7-Bn and k_n is k_1, k_2 or k_3 .

$$r_{\mathrm{Na{-}Ade}} = -\frac{d[\mathrm{Na{-}Ade}]}{dt} = (k_1 + k_2 + k_3)[\mathrm{Na-Ade}][\mathrm{BnCl}] \tag{4.5}$$

$$r_{\mathrm{N}X\mathrm{{-}Bn}} = \frac{d[\mathrm{N}X\mathrm{{-}R}]}{dt} = k_{\mathrm{n}}[\mathrm{Na{-}Ade}][\mathrm{BnCl}] \tag{4.6}$$

Firstly, it is important to confirm that both the N9- and N3-benzyladenine isomers form via an S_N2 mechanism. The dependency of the rates of formation of the products on the concentration of BnCl and Na-Ade was investigated. The variation of the BnCl concentration was performed in the presence of both DBU and TEA to explore if both bases act as a good mop up base for the available proton on the alkoxy sulfonium ion intermediate. The formation of N7-benzyladenine (N7-Bn) was not investigated due to the extremely low concentration of the product introducing experimental error in measuring the accurate rates of formation.

At early times in the reaction, the concentration of Na-Ade and BnCl changes by a negligible amount and thus the rate of reaction is the slope of concentration vs time plot, referred to as the initial rates. All rates measured in this chapter are determined by the initial rates methods whereby less

© University of Pretoria

than 10 to 12 % of Na-Ade is depleted. The CH_2 protons of N9- and N3-Bn were chosen to calculate the concentration as they exhibited the shortest relaxation time out of all the product protons, Table 4.4. All kinetic experiments were run at five times the longest CH_2 T_1 value (N9-benzyladenine 695 ms)

Table 4.4: Proton T_1 relaxation times of Na-Ade, N9- and N3-benzyladenine in DMSO-d_6 at 295 K.

	NH_2	C2-H	C8-H	CH_2
Na-Ade	642 ms	7.989 s	4.657s	-
N9-benzyladenine	-	8.731 s	4.089s	695 ms
N3-benzyladenine	1.121 s	1.897 s	698 ms	509 ms

The dynamic ^{1}H NMR spectra for the BnCl concentration study at 1 and 8 equivalents of BnCl in the presence of equal equivalents of TEA and DBU are shown in Figure 4.11. No protonation of Na-Ade and N3-Bn is observed in the presence of TEA and DBU as both bases compete for the labile proton on the alkoxy sulfonium ion intermediate. In addition, only the ^{1}H NMR chemical shifts corresponding to N9-, N3- and N7-Bn are observed. It is interesting to note that in the dynamic ^{1}H NMR spectra the N9-Bn and N3-Bn proton peaks are shielded at the very early stages in the reaction having the CH_2 peak of both N9- and N3-Bn originate from 5.13 ppm. The peaks become deshielded resulting in the final chemical shifts reported for the isolated products, i.e. the CH_2 peak migrates to 5.36 and 5.51 ppm for the N9- and N3-Bn, respectively. The migration of the proton peaks at the beginning of the reaction is not due to protonation, yet it is unclear as to why this is observed.

The dependence of the rate of reaction of N9- and N3-Bn on the concentration of BnCl and Na-Ade and the corresponding reaction order plots are given in Figure 4.12. Refer to Figures S3 – S5 for the regions used for the initial rates. Initial rates were calculated using eqn 4.7.

$$r_{\mathrm{N}X\text{–Bn}} = \frac{\Delta[\mathrm{N}X\text{–R}]}{\Delta t} \qquad (4.7)$$

The slopes of the log(rate) vs log[BnCl] and log[Na-Ade], Table 4.5, show that the reaction is first order in respect to BnCl for N9- and N3-Bn.

Table 4.5: Slope derived from the log(rate) vs log(BnCl) and log(Na-Ade) for N9-Bn and N3-Bn in anhydrous DMSO at 295 K.

concentration varied	BnCl[a]		Na-Ade[b]
	base present		
Isomer	DBU	TEA	TEA
N9-Bn	1.01 ± 0.03	1.02 ± 0.03	0.89 ± 0.02
N3-Bn	1.10 ± 0.04	1.10 ± 0.04	0.86 ± 0.02

[a] [Na-Ade] = 13.5 mM [b] [BnCl] = 12.9 mM

© University of Pretoria

The rate dependence deviates from 1st order at very high concentrations of Na-Ade (48.5 mM) and is attributed to interference from dimer formation as well as solubility problems at high concentrations of the Na-Ade salt. Thus, the data support the assignment of an S_N2 mechanism for the formation of both products.

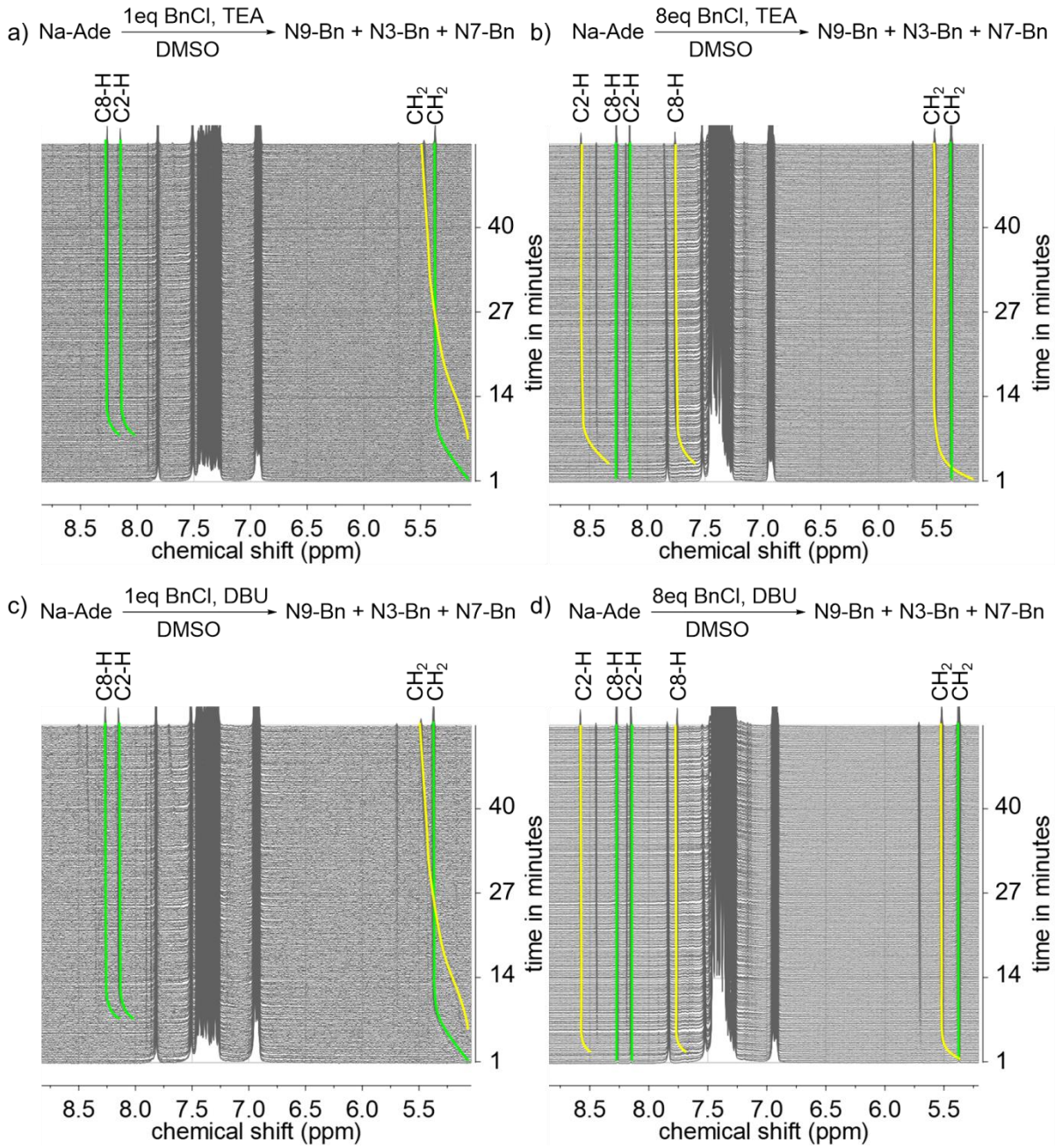

Figure 4.11: Dynamic ^{1}H NMR spectra for the alkylation of adenine with benzyl chloride in the presence of a) 1 eq. BnCl and TEA, b) 8 eq. BnCl and TEA, c) 1 eq. BnCl and DBU and d) 8 eq. BnCl and DBU in anhydrous DMSO at 295 K. N9- and N3-Bn adenine alkylated derivatives are shown by the green and yellow lines, respectively.

© University of Pretoria

There is no significant difference in the rate and order of reaction in the presence of DBU and TEA, thus showing that both these bases can be used to mop up the available proton on the alkoxy sulfonium ion intermediate. The N9/N3 product ratio is independent of the mop up base present. The dependence of the N9/N3 ratio on the increase of the individual concentration of Na-Ade and BnCl reagent does not differ significantly, being 2.8 with increasing Na-Ade concentration and between 2.5–2.9 with increasing BnCl concentration. This is similar to the observed N9/N3 ratio of 2.5 for the reaction with benzyl bromide in section 4.3.1 which supports previous research showing the product ratio was insensitive to the variation in LG.

At high concentrations of DBU, it is reasonable to suspect that DBU itself can act as a nucleophilic base. The chemical features of DBU, being sterically hindered, render it a good non-nucleophilic base, however, its nucleophilic nature has been revealed in the presence of halogenated compounds.[99,100] Briefly shown here DBU does indeed act as a nucleophile in the presence of BnCl in anhydrous DMSO-d_6, Figure 4.13. The resulting product of nucleophilic attack from DBU with BnCl has the CH_2 peak occur at 4.86 ppm. This peak is absent when TEA is used as a base. However, the reaction between DBU and BnCl is much slower in comparison to that of the benzylation of Na-Ade. There is only a 5% decrease in BnCl within 30 minutes for a 1:1 eq. of BnCl:DBU in DMSO. The indifference between the rate of formation of N9- and N3-Bn in the presence of TEA and DBU indicates that the minor depletion of BnCl by DBU is not of concern regarding measuring initial rates for N9- and N3-Bn.

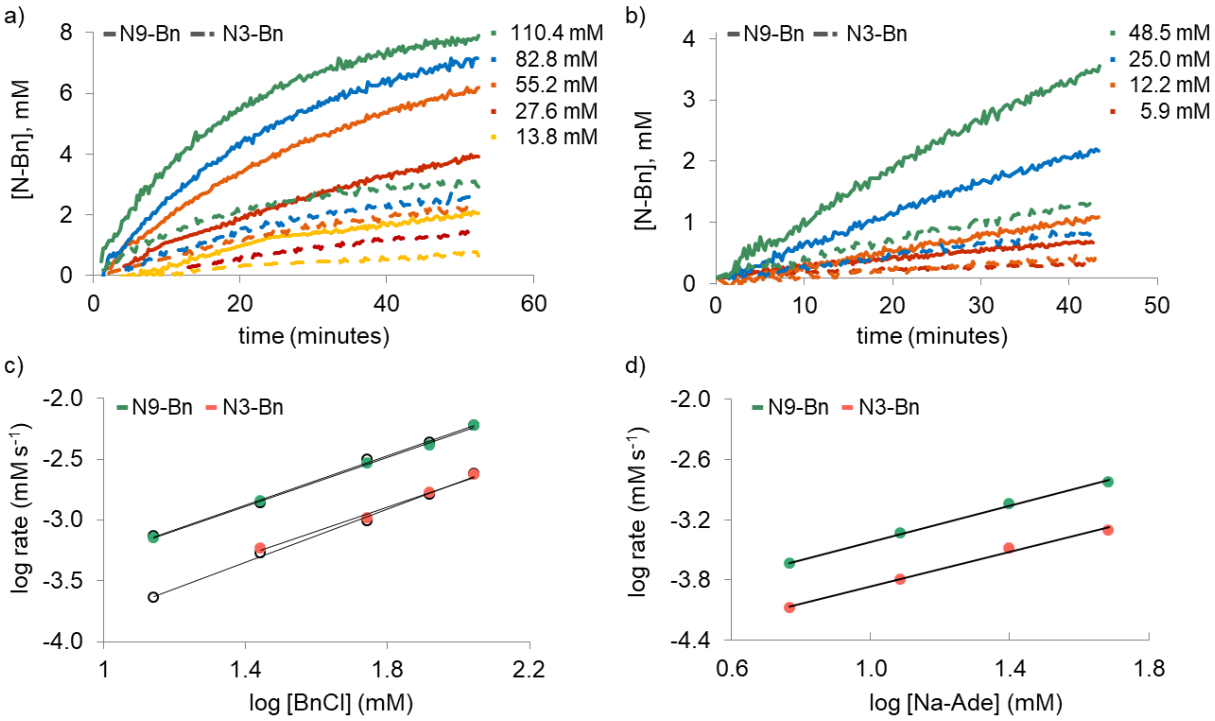

Figure 4.12: The reaction profile dependency of N9-Bn and N3-Bn on the concentration of a) BnCl in the presence of BnCl:DBU 1:1 at concentrations 13.8 - yellow, 27.6 - red, 55.2 - orange, 82.8 - blue and 110 mM – green, and b) Na-Ade at concentrations 5.85 - red, 12.2 - orange, 25.0 - blue and 48.5 mM - green in DMSO-d_6 at 295 K. The corresponding log(rate) vs c) log[BnCl] in the presence of DBU (solid circles) and TEA (black outlined circles) and d) log[Na-Ade] for N9-Bn and N3-Bn in anhydrous DMSO.

© University of Pretoria

The lack of protonation of DBU in the presence of only benzyl chloride in Figure 4.13 would suggest that the Kornblum oxidation reaction proposed in section 4.3.3 is promoted either by the counter ion or by the entire Na-Ade complex.

The above experimental studies have demonstrated that the benzylation of Na-Ade using a benzyl halide occurs via an S_N2 mechanism in which a side reaction occurs that deplete the Na-Ade starting material. The N9:N3 product ratio is insensitive to the structural differences of the benzyl halide derivatives, variation in LG and the counter ion present. In the presence of a mop up base, DBU or TEA, there is no change in the mechanism of alkylation or N9:N3 product ratio and the protonation of Na-Ade is reduced.

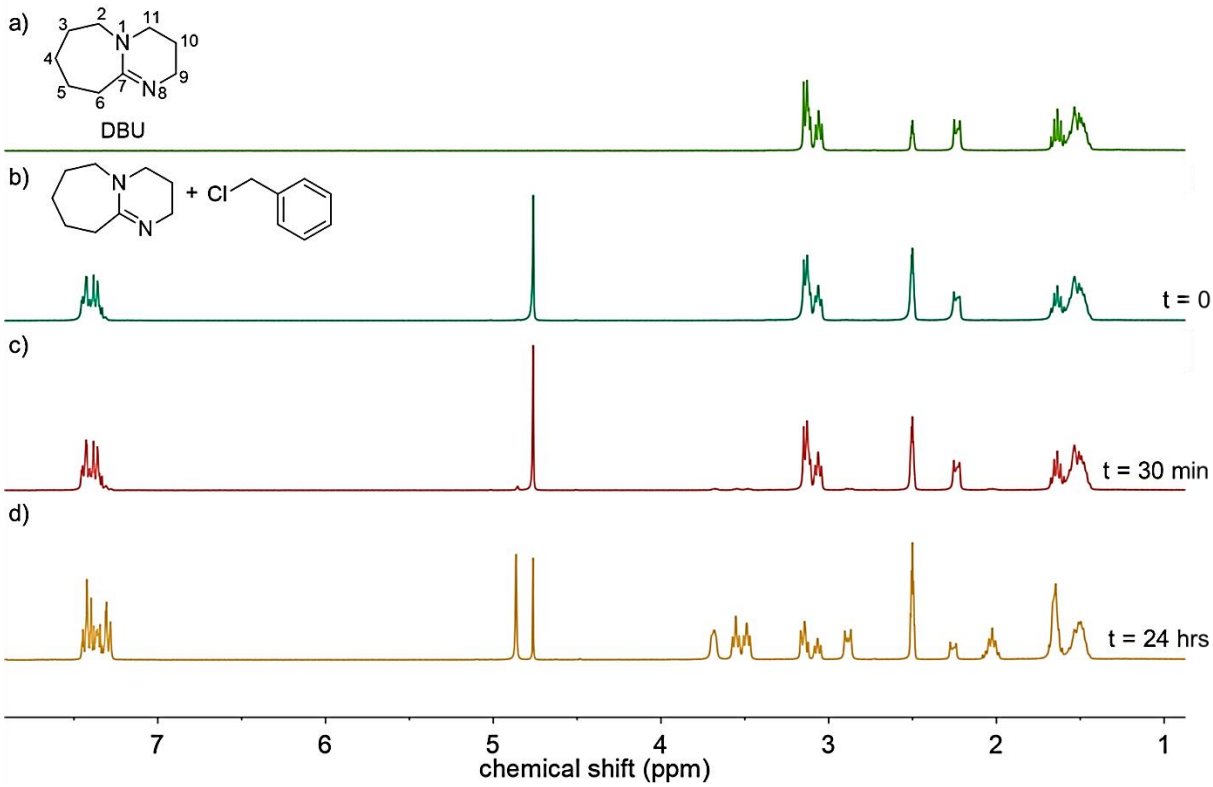

Figure 4.13: ^{1}H NMR of a solution of a) DBU (63.9 mM), and DBU and BnCl (65.17 mM) at b) t=0, c) t=30 minutes and d) t=24 hours.

4.3.5 Thermodynamic data for the formation N9- and N3-benzyladenine in anhydrous DMSO

The thermodynamic parameters were obtained for the benzylation of Na-Ade using benzyl chloride in anhydrous DMSO and in the absence and the presence of a 15-crown-5 ether (15C5). In chapter 2 it was suggested that the 15C5 doesn't remove the Na^+ from the Na-Ade complex nor does it complex with the Na-Ade to a large extent. However, it could assist in the removal of the Na^+ coordinated at the N3N9 position of the purine ring by interacting with the counter ion as it departs. Alternatively, it could result in a larger energy barrier due to steric hindrance in case the 15C5 ether

© University of Pretoria

interacts with the Na^+ to any extent. Any change in the kinetic parameters will provide evidence for the presence of ion pairs in anhydrous DMSO.

A set of reactions for the benzylation of Na-Ade with BnCl were performed for the temperature range 300 K to 320 K, increasing by 5 K intervals. The reactions were performed in the presence of 1.2 eq. of DBU to limit the protonation of Na-Ade. The formation of N9- and N3-Bn was monitored via dynamic ^{1}H NMR spectroscopy, Figure 4.14. The rates of formation for the products were obtained via initial rates (Figure S3.6 and S3.8 and Table S3.3 and S3.4) using the integral of the CH_2 peak of both products with anisole as the internal standard.

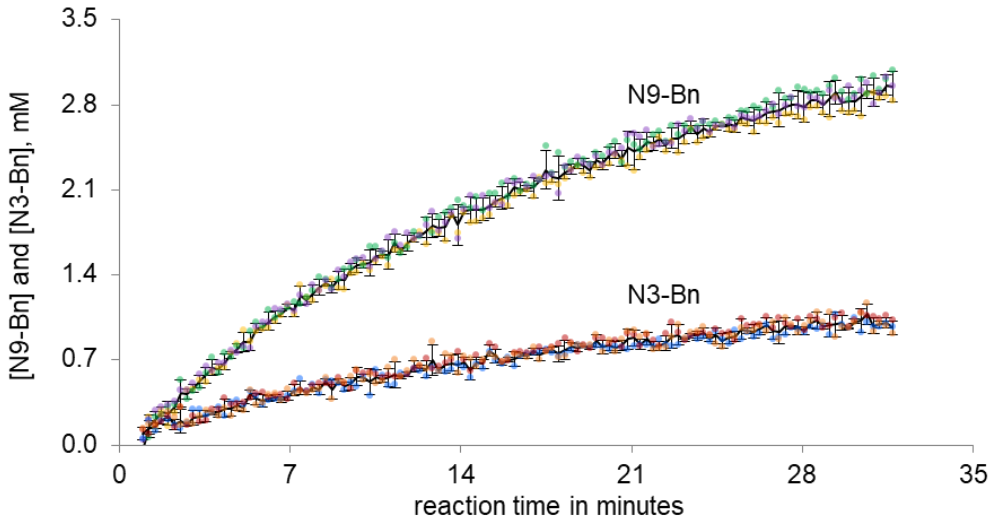

Figure 4.14: Plot of N9- and N3-Bn concentration over time during the benzylation of Na-Ade (6.65 mM) with BnCl (14.1 mM) and DBU (7.14 mM) in anhydrous DMSO-d_6 at 320 K. The average over three replicates is shown by the solid black line with error bars.

The observed rate of formation of N9- and N3-Bn over the temperature range in the absence and presence of 15C5 is shown in Figure 4.15a and the thermodynamic parameters are given in Table 4.6. The Gibbs free energy of activation, $\Delta G^{\ddagger}_{300}$, is calculated directly from the rate constants using eqn 4.8,

$$k_{obs} = \frac{k_B T}{h c_0} \exp\left(-\frac{\Delta G^{\ddagger}_{300}}{RT}\right) \qquad (4.8)$$

$\Delta H^{\ddagger}$ of N9- and N3-Bn in the absence and presence of 15C5 is calculated from the Eyring plots, Figure 4.15b. The linearized Eyring equation for a second order reaction is given in eqn 4.9,

© University of Pretoria

$$ln\frac{k_{obs}}{T} = \frac{-\Delta H^{\ddagger}}{RT} + ln\left(\frac{k_B}{h}\right)\frac{1}{c_0} + \frac{\Delta S^{\ddagger}}{R} \quad (4.9)$$

where k_B is the Boltzmann's constant = 1.381610223 J K^{-1}, T is the absolute temperature in degrees Kelvin [K], h is Planck's constant (6.63 × 10^{-34} J s), R is the gas constant (8.3145 J $mol^{-1}K^{-1}$), c_0 is taken as 1M, and $\Delta H^{\ddagger}$ and $\Delta S^{\ddagger}$ are the enthalpy and entropy of activation.

The $\Delta S^{\ddagger}$ of N9- and N3-Bn is calculated from eqn 4.10 using the values of $\Delta H^{\ddagger}$ and $\Delta G^{\ddagger}_{300}$ calculated above.

$$\Delta G^{\ddagger}_{300} = \Delta H^{\ddagger} - T\Delta S^{\ddagger} \quad (4.10)$$

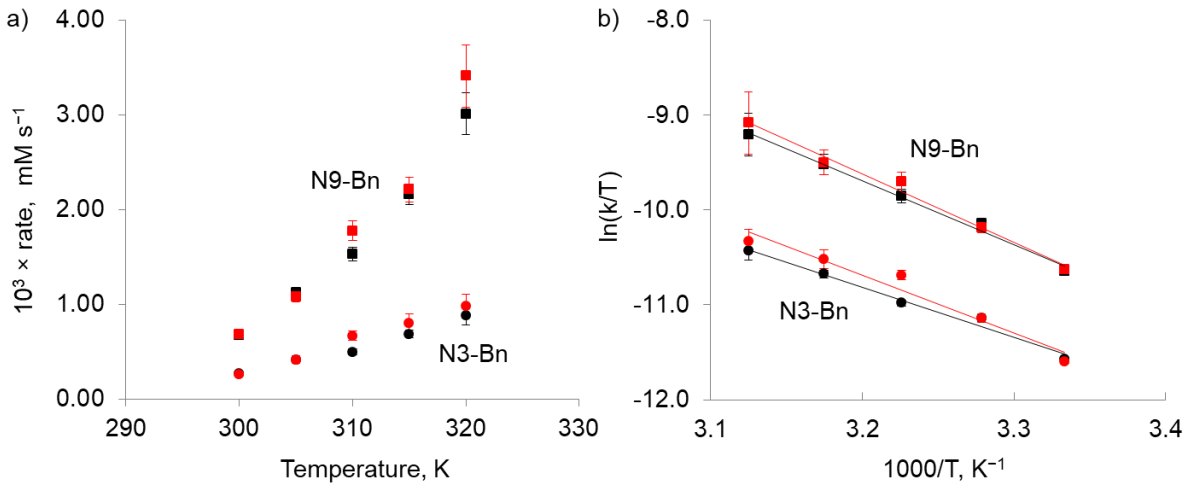

Figure 4.15: a) Observed rate of formation for N9- and N3-Bn in the absence (black data points) and presence (red data points) of 15C5 and b) the Eyring plots thereof in anhydrous DMSO-d_6 for the temperature range indicated, increasing in 5 K intervals.

The thermodynamic results in Table 6 will be discussed under three main points based on i) the relationship between N9- and N3-Bn, ii) the effect of the presence of the 15C5 and iii) the entropy-enthalpy compensation effect.

The relationship between the thermodynamic parameters of N9-Bn and N3-Bn: Of most interest in Table 4.6 is the resultant $\Delta G^{\ddagger}_{300}$ value of 86 kJ mol^{-1} for N9-Bn which is 2 kJ mol^{-1} lower in energy than for N3-Bn. An increase in $\Delta G^{\ddagger}$ of 2 kJ mol^{-1} leads to an increase in rate constant ratio of 2.5, which is the ratio obtained for N9-Bn/N3-Bn rates. However, the energy barrier ($\Delta H^{\ddagger}$) for the N9-Bn pathway is larger than that of the N3-Bn by around 12 and 9.5 kJ mol^{-1} in the presence and absence of the 15C5, respectively.

The increase in the $\Delta H^{\ddagger}$ of N9-Bn in both reaction mixtures is largely compensated for by the increase in the entropy term which results in a more favourable $\Delta G^{\ddagger}_{300}$ value for the formation of N9-

© University of Pretoria

Bn. The loss of entropy for N3-Bn is significantly larger than that of N9-Bn by almost −50 J mol^{-1} K^{-1} (−40 J mol^{-1} K^{-1} for the 15C5 reaction). This result implies that the system becomes highly ordered for the N3-Bn TS.

Table 4.6: Experimental thermodynamic parameters for the formation of N9- and N3-Bn in anhydrous DMSO in the absence and presence of 15C5

	N9-Bn			N3-Bn		
Reaction mixture	$\Delta H^{\ddagger}$ kJ mol^{-1}	$\Delta S^{\ddagger}$ J mol^{-1} K^{-1}	$\Delta G^{\ddagger}_{300}$ kJ mol^{-1}	$\Delta H^{\ddagger}$ kJ mol^{-1}	$\Delta S^{\ddagger}$ J mol^{-1} K^{-1}	$\Delta G^{\ddagger}_{300}$ kJ mol^{-1}
15C5 absent	56 ± 3	−100 ± 3	86	44 ± 3	−148 ± 3	88
15C5 present	60 ± 4	−85 ± 4	86	51 ± 6	−125± 6	88

The $\Delta S^{\ddagger}$ for bimolecular nucleophilic S_N2 reactions is always negative as the TS is well organized and results in a loss of 3 translational[101] (estimated around −145 J mol^{-1}K^{-1}) and 2 to 3 rotational degrees of freedom.[102] The TS of the N9-Bn is "looser" than that of N3-Bn and is accompanied by a larger pre-exponential factor, A in Table 4.7, derived from the Arrhenius plot (Figure S3.7 and S3.9) using eqn 4.11,

$$k = Ae^{E_a/RT} \qquad (4.11)$$

where A is the pre-exponential factor and E_a is the activation energy.

Contributions to the looseness of the TS originate from the geometric distortion relative to the reactants, the depletion of bonding electrons between the atoms involved in the transfer of the molecular group as well as antibonding interactions between electron pairs.[103] Additionally, the change in charge distribution of the molecules in the TS conformation can lead to changes in the solvent shell from i) reorganization of the solvent molecules around the TS and ii) changes in the strength of interaction between the TS molecules with the solvent and therefore contribute to an increase or decrease in the entropy of activation.[103–105] The increase in the $\Delta\Delta S^{\ddagger}$ of N9-Bn can result from a combination of the above factors.

Table 4.7: Arrhenius parameters for N9-Bn and N3-Bn

	N9-Bn		N3-Bn	
Reaction mixture	E_a, kJ mol^{-1}	A, M s^{-1}	E_a, kJ mol^{-1}	A, M s^{-1}
15C5 absent	58.5	1.18×10^8	46.3	3.45×10^5
15C5 present	62.8	6.42×10^8	53.3	5.78×10^6

© University of Pretoria

The effect of the presence of 15C5 on the thermodynamic parameters: The 15C5 is proposed to complex to a minor extent to the Na-Ade complex without fully removing the counter ion. In the presence of the 15C5, the $\Delta H^{\ddagger}$ is increased for the formation of N9- and N3-Bn by 4.2 and 7.0 kJ mol^{-1}, respectively, indicating the simultaneous complexation of the Na^+ to the Ade and 15C5 results in steric hindrance for the incoming benzyl chloride. However, there is a resultant increase (less negative) in the $\Delta S^{\ddagger}$ term of 14.2 and 22.9 J mol^{-1} K^{-1} for the N9- and N3-Bn, respectively. The effect of the 15C5 of the thermodynamic parameters indeed provides further evidence that the Na-Ade ion pair is present and is the reactive species in solution.

The entropy-enthalpy compensation effect: Comparing the two reaction mixtures the increase in the $\Delta H^{\ddagger}$ of both the N9- and N3-Bn in the presence of 15C5 is compensated for by the increase in $\Delta S^{\ddagger}$ resulting in no change in the $\Delta G^{\ddagger}_{300}$ term. A plot of the $\Delta H^{\ddagger}$ vs $T\Delta S^{\ddagger}$ for both the N9- and N3-Bn, Figure 4.16, shows the slopes are close to unity indicating almost full compensation between $\Delta H^{\ddagger}$ and $T\Delta S^{\ddagger}$. Although there are only two points for each plot, we recognize that the compensation effect can be present. Furthermore, a linear relationship exists between all four points in Figure 4.16 with a slope of 0.85 (see Figure S3.10 for the fit of all four points) indicating that the unfavourable change in entropy when moving from the N9 to the N3 nucleophilic position is not fully compensated by the change in enthalpy. The pathways leading to the different benzylation products of Na-Ade can be considered as closely related reactions whereby the different reactive N atom sites of the purine ring acts as a variation in the reactant.

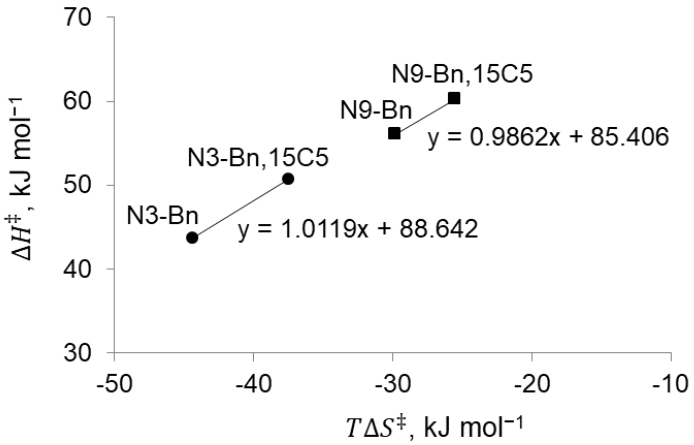

Figure 4.16: $\Delta H^{\ddagger}$ vs. T$\Delta S^{\ddagger}$ enthalpy-entropy compensation plot for the formation of N9-Bn and N3-Bn in the absence and presence of 15C5 in anhydrous DMSO at 300 K.

The influence of temperature on the measured rate ratio of N9-Bn/N3-Bn ($rate_{N9\text{-}Bn}/rate_{N3\text{-}Bn}$) in the absence and presence of 15C5 is shown in Figure 4.17. At high temperatures, the increase in temperature facilitates the equilibrium of reaction and thus promotes the formation of the thermodynamic product, which is N9-Bn in this reaction. This effect is reduced in the presence of 15C5 such that the change in rate ratio over the temperature range 300 to 310 K is hardly altered.

The results discussed above show that the selectivity for the site of alkylation is determined by the $\Delta S^{\ddagger}$ term and is highly favourable for the N9-Bn pathway despite the larger enthalpy of activation.

© University of Pretoria

The effect on the thermodynamic parameters due to the presence of the 15C5 provides further evidence for the presence of ion-pairing between the adeninate anion and the Na^+ ion.

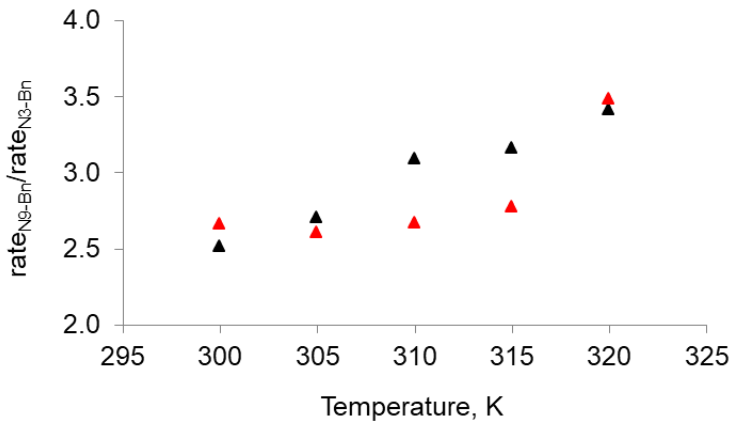

Figure 4.17: The change in measured the ratio of the rate of N9-Bn/N3-Bn with temperature in the absence (black data points) and presence (red data points) of 15C5 in anhydrous DMSO.

A theoretical investigation was carried out to gain a deeper understanding of the alkylation reaction pathway leading to the regio-selectivity of the adeninate anion. From the above data, it is proposed that the governing factor for predominant alkylation at the N9 site is an entropic bottleneck. Theoretical studies could provide support for this suggestion.

4.3.6 Theoretical studies on the benzylation of the adeninate anion

4.3.6.1 Background in Transition State Theory

The higher enthalpy of activation accompanied by the increase in entropy for the formation of the looser TS structure of the N9-Bn brings to mind the picture of two potential energy surfaces shown in Figure 4.18. Two reaction pathways followed by the same set of reactants, pathways 1 and 2, lead to different transition states, TS_1 and TS_2, of equal activation energy (E_a). The region of TS_1 has a more gradual curvature of the potential energy surface (PES) perpendicular to the reaction coordinate than that of TS_2. This results in more molecules having sufficient energy to pass through the TS_1 region at any given finite temperature as compared to TS_2 which experiences an entropic bottleneck.[106] In terms of energy states the shape of the PES at the TS region is indicative of the population of different energy levels resulting from the number of paths leading to the TS. The occupation of the TS energy levels will obey the Boltzmann distribution law having the majority of molecules in the lower energy levels.[107]

The information about the surface shape of the TS region is obtained by the vibrational frequencies of the activated complex. For an activated complex with *N* atoms there will be 3*N*−7 vibrational modes, where each mode of vibration has a characteristic frequency (reactants and products will have 3*N*−6 vibrational modes). One of these vibrational modes corresponds to the motion of the reaction coordinate and is represented as an unstable vibrational degree of freedom (negative frequency). The remaining vibrational modes of the activation complex are known as normal modes which do not contribute towards the reaction coordinate, but contribute towards the energy of the

© University of Pretoria

species. These frequencies sample the surface area perpendicular to the reaction path. The lower the gradient of the curvature of the PES at the TS (gradual surface increase), the smaller the corresponding values of the frequencies and therefore the lower the zero-point vibrational energy correction (ZPVE) of the TS energy which results from the vibrational motions of a molecule at 0 K. This in turn will affect the rate of reaction, whereby pathway 1 will occur at a higher rate than pathway 2 even though the electronic activation energy E_a of both pathways is equal.

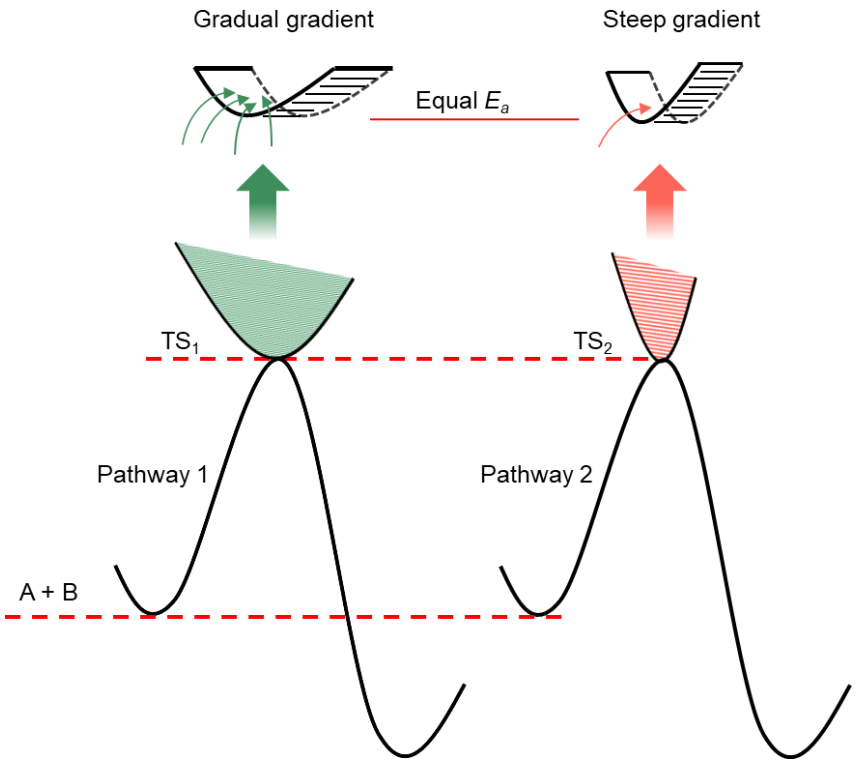

Figure 4.18: Comparison of the curvature of the PES of two transition states reached via pathways 1 and 2.[106]

The incorporation of the TS vibrational frequencies is carried in the vibrational partition function[107] term, Q_{vib}:

$$Q_{vib} = \prod_{i=1}^{3N-6} \frac{1}{1-e^{\left(-\frac{h\nu_i}{k_B T}\right)}} \qquad (4.12)$$

where h is Planck's constant, ν_i is the oscillating frequency, k_B is the Boltzmann constant and T is temperature. The total partition function of a molecule, Q, gives information about how the energy levels of a molecule are populated and is the product of the contribution from electronic, translational, rotational and vibrational energy to the total energy of a molecule:

© University of Pretoria

$$Q = Q_{elec} \times Q_{trans} \times Q_{rot} \times Q_{vib} \quad (4.13)$$

Where Q_{elec}, Q_{trans}, Q_{rot} and Q_{vib} are the partition function contributions from the electronic, translational, rotational and vibrational energy levels.[107] The larger the value of Q, the more states are occupied at a given temperature. Hence, including the total Q for the TS and reactants in the rate constant, k, equation (eqn 4.14) allows for other regions of the PES to be explored,

$$k = \frac{k_B T}{h} \frac{Q^{\ddagger}}{Q_A Q_B} EXP^{\frac{-E_a}{k_B T}} \quad (4.14)$$

where k is the calculated rate constant and $Q^{\ddagger}$, Q_A and Q_B are the partition function of the TS and reagent A and B, respectively, and E_a is the activation energy including the ZPVE correction.

However, large errors are introduced into the partition function due to the failure of the harmonic oscillator approximation for low vibrational frequencies (LVF),[108,109] typically less than 100 cm^{-1}. This is a common deficiency to all software packages. Hence, computed ΔG values must be taken with caution, particularly when differences in activation energies for competing pathways are small. Internal rotations about a single bond in a molecule and vibrational motions of weak bonds between molecules, such as in hydrogen-bonded systems, are sources of LVF.[108,110] Considering a bimolecular TS, the molecules can have LVF also resulting from motions of the two molecules relative to each other. In a flexible molecule or TS, the LVF resulting from skeletal, torsional and bending vibrations, contribute a large amount to the Q, making it extremely large and unreliable. Truhlar's quasiharmonic approximation[109] is used to account for the failure of the harmonic oscillator model for low-frequency vibrational modes and their contribution to thermodynamic parameters. This is done by setting all LVFs less than 100 cm^{-1} to 100 cm^{-1}.

4.3.6.2 Theoretical modelling of the benzylation of the adeninate anion

In chapter 3 it was shown that the N1, N3, N7 and N9 nitrogen atoms of the purine ring of the free adeninate anion carry an almost equal negative charge. From this perspective, there is an equal opportunity for alkylation to occur at each atom under electrostatic control. In the ion-paired Na-Ade complex, the counter ion is shown to be coordinated to the bottom nitrogen atoms on the purine ring, either in a unidentate or bidentate fashion. The complexation of the Na^+ ion at the N3, N3N9 and N9 positions results in large polarization of the adeninate ion in which the N3 and N9 atoms gain negative charge. Thus, if the reaction is dominated by electrostatics, the alkylation site is likely to be at the N9 and N3 atoms. However, the experimental results of the benzylation of K-Ade resulted in the same alkylation pattern as for Na-Ade even though the polarization is largely reduced in the case of the K^+ counter ion due to decreased perturbation of the electronic environment of the purine ring. This should theoretically render the endo-purine ring nitrogen atoms all likely sites for alkylation in the K-Ade complex.

In both the free ion and ion-paired complexes, the formation of the N1- and N7-Bn may experience steric hindrance originating from the NH_2 group near the reaction site, discouraging alkylation at these two sites. Hence, it is not difficult to rationalize the major N9- and N3-Bn products based on steric hindrance whether the counter ion is coordinated to the purine ring or not.

© University of Pretoria

In this study, in order to explore and, hopefully, confirm the experimental thermodynamic parameters and TS structure information, the four pathways leading to N1-, N3-, N7- and N9-Bn in the presence and absence of the Na^+ counter ion were modelled leading to a total of 8 pathways investigated. The reaction pathways were initially modelled in the absence of the Na^+ ion before recognizing that adeninate and the counter ion occur as ion-pairs. The data is reported here as it provides a means of comparison between reactivity of the free adeninate anion and the Na-Ade complex.

Transition state structures

All 8 reaction pathways studied led to the formation of a typical S_N2 TS and transfer of the benzylic group to one of the reactive nitrogen atoms of the purine ring. The reaction coordinate is defined here as the decrease in the distance between the specified N*X* atom of the purine ring and the carbon of the $\underline{C}H_2$ group of BnCl, d(N*X*,$\underline{C}H_2$). The structures of the optimized TS in the absence and presence of the Na^+ ion are shown in Figure 4.19 and Figure 4.20, respectively. The TS of all 8 pathways are described as "tight" as the bond distance between the bonding centres of the N*X*, $\underline{C}H_2$ and Cl in the TS are extended by around 1.5 to 1.7 times the equilibrium bond distance in the product and reagent. A "loose" TS has the bond distance extended by 2.9 ± 0.2 times the length of the stable bond distance in the reactant and product i.e. for N, O and C atoms this extend in bond length is around 4–4.5 Å.[101]

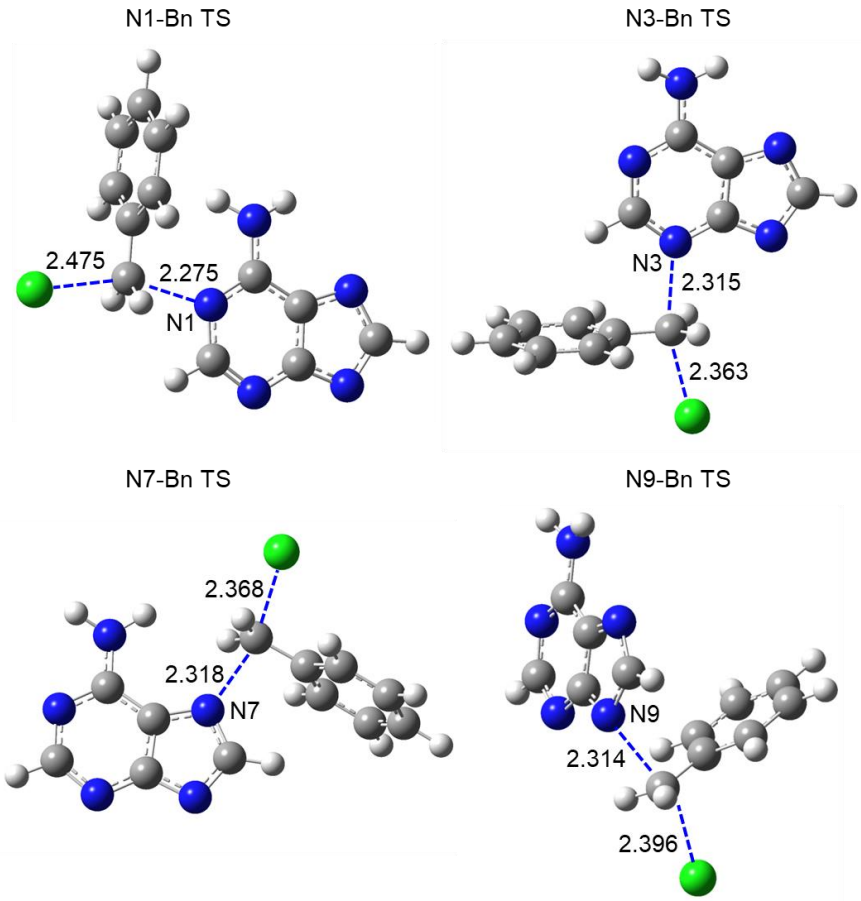

Figure 4.19: Optimized transition state structures in the absence of the Na^+ ion (N1-Bn, N3-Bn, N7-Bn and N9-Bn). N*X*—$\underline{C}H_2$ and $\underline{C}H_2$—Cl bond lengths are shown in Å.

© University of Pretoria

The Na^+ complexes have a later TSs than those without the cation. The bond distance of the benzyl chloride $\underline{C}H_2$—Cl bond extends from 1.860 Å in the free BnCl reagent to between 2.314 Å and 2.475 Å for the pathways without the Na^+ ion and between 2.436 and 2.514 Å for the Na^+ complexed pathways. This is accompanied by a decrease in the N*X*—$\underline{C}H_2$ bond distance, being short for the Na^+ complexed TSs. This decrease in the N*X*—$\underline{C}H_2$ bond distance is the smallest for the Na-N9-TS indicating that its TS is looser and earlier than the N1, N3 and N7 TSs. This is consistent with Hammond's postulate[64] as experimentally the N9-Bn pathway had the lowest free energy barrier ($\Delta G^{\ddagger}$) and therefore it is predicted that it has an earlier TS. There is similarity between the Na^+ TS structures of N1 and N7 and those of N3 and N9. The N1 and N7 TS structures both have the Na^+ ion coordinated at the N3 and N9 nitrogen atoms. The N3 and N9 TS appear to show a cation-π interaction between the Na^+ and the benzene ring of BnCl.

The N1 pathway has the latest TS, having the N*X*—$\underline{C}H_2$ bond distance 0.04 and 0.06 Å shorter than that of the N3, N7 and N9 TS in the absence and presence of the Na^+ ion, respectively. In turn, this TS should have a higher energy barrier and lower exothermicity. However, the N*X*—$\underline{C}H_2$ bond distances do not differ significantly between the different pathways, suggesting that steric hindrance at the N1 and N7 might not play a role in the regio-selectivity of alkylation.

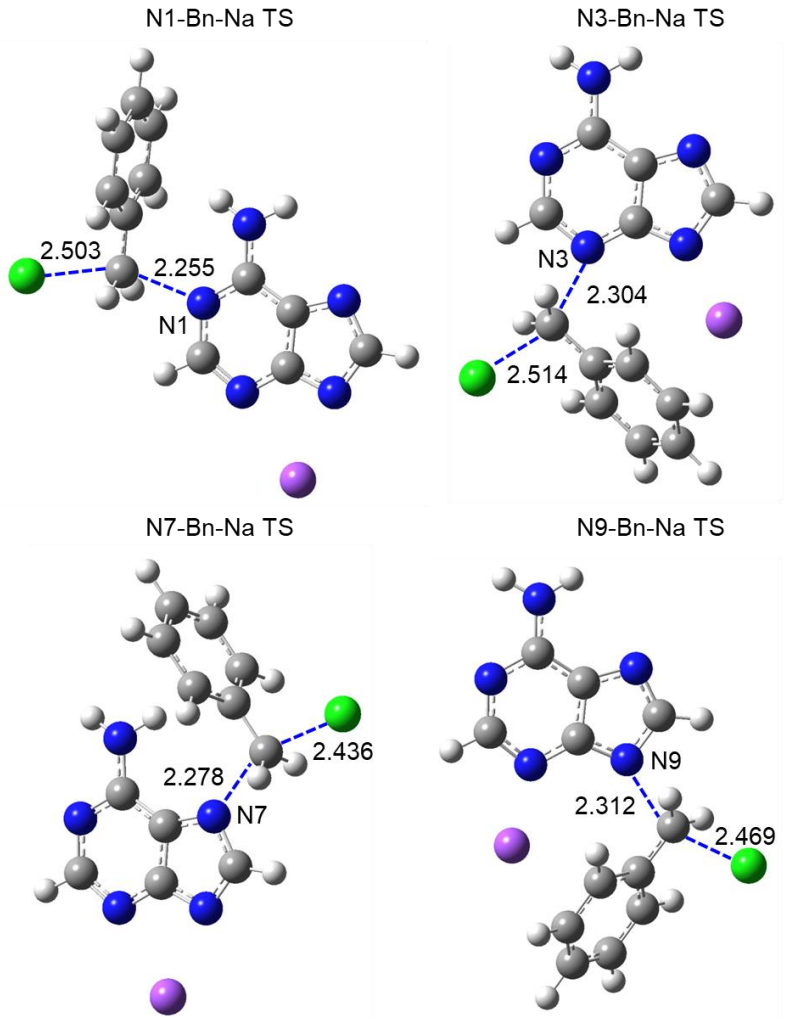

Figure 4.20: Optimized transition state structures in the presence of Na^+ (N1-Bn-Na, N3-Bn-Na, N7-Bn-Na and N9-Bn-Na). N*X*—$\underline{C}H_2$ and $\underline{C}H_2$—Cl bond lengths are shown in Å.

© University of Pretoria

4.3.6.2.1 Energetics of the reaction pathway in the absence and presence of the Na^+ counter ion

The reaction energies for all 8 reaction paths were calculated. This included the reactants, pre-reactive complexes, transition states, and products. The change in the ΔE_{ZPVE} for the N1, N3, N7 and N9 reaction profiles in the absence and presence of the Na^+ ion are shown in Figure 4.21a and b, respectively. The corresponding Gibbs free energy (ΔG) plots are shown in Figure 4.22a and b. The ΔE_{ZPVE} and ΔG along the reaction coordinate are taken relative to the sum of the ΔE_{ZPVE} and ΔG of the free reactants, respectively.

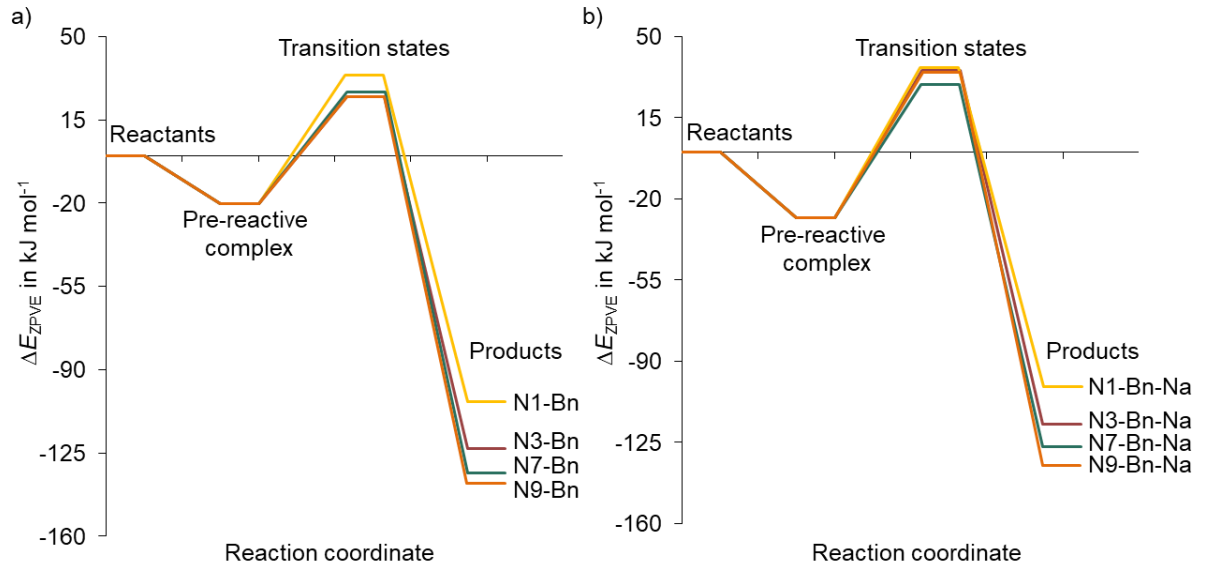

Figure 4.21: The ΔE_{ZPVE} along the reaction path for the formation of N1-, N3-, N7- and N9-Bn in a) the absence and b) in the presence of the Na^+ ion.

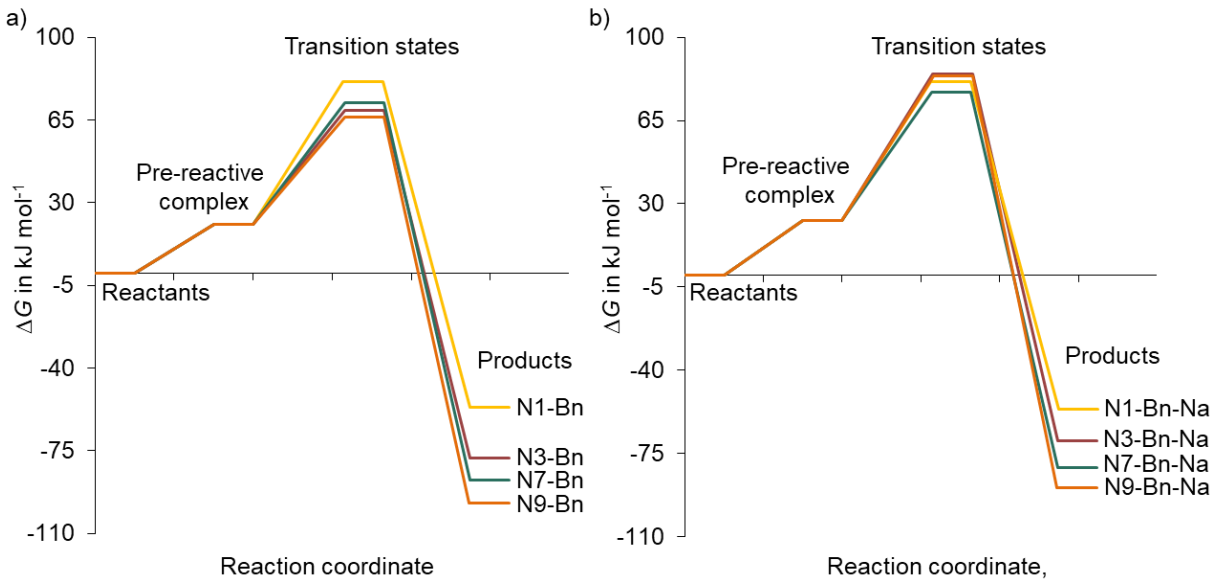

Figure 4.22: The ΔG along the reaction path for the formation of N1-, N3-, N7- and N9-Bn in a) the absence and b) in the presence of the Na^+ ion.

© University of Pretoria

An energetically favourable pre-reactive complex is formed between Ade^- or Na-Ade with BnCl, Figure 4.21. The two molecules interact with each other through long range interactions, lowering the energy relative to the separated reactants by −20 kJ mol^{-1} (−28 kJ mol^{-1} for the system with Na^+). However, ΔG of the pre-reactive complex is > 20 kJ mol^{-1} higher in energy than the separated reactants, Figure 4.22. This is attributed to the loss of entropy due to the reorganization of the molecules.

From the pre-reactive complex, the molecules pass through the TS. In the absence of the Na^+ ion, the N1-Bn TS has the largest energy barrier having the $\Delta G^{\ddagger}$ 15 kJ mol^{-1} larger than N9-TS. The lowest energy barrier is for the N9-Bn TS, being 3 and 6 kJ mol^{-1} lower in energy than the N3 and N7 TS, respectively. However, for the Na^+ complexed TSs, the barrier height for the N9-Bn-Na and N3-Bn-Na are 17 kJ mol^{-1} ($\Delta G^{\ddagger}$) larger in energy than in the absence of the Na^+, leaving the N7-Bn-Na pathway with the lowest energy barrier. This is a result of the Na^+ ion in the immediate reactive site and will be discussed further on.

The most exothermic reaction is the formation of N9-Bn, in agreement with Hammonds postulate which predicts that a reaction with an earlier TS will be more exothermic.[64] In the presence and absence of the Na^+ ion, the N9-Bn product is the energetically most stable product, followed by the N7-, N3- and then the N1-Bn. N9-alkylated adenine derivatives are known to be the thermodynamic product, which is recovered here. The N9-Bn is favoured by −10 kJ mol^{-1} (−8.3 kJ mol^{-1} for the Na-Ade system) over N7-Bn. However, it is interesting that although the N7-Bn product is more favourable than N3-Bn by −10 kJ mol^{-1} it doesn't form in any appreciable amount in the reaction if the product ratio is governed by thermodynamic control. The N1-Bn is the least exothermic pathway with the highest energy barrier, as is expected from the later TS structure. Note that the relative difference in energies of the products does not play a role as the products cannot overcome large energy barrier for the reverse reaction.

4.3.6.2.2 Computed thermodynamic parameters for the benzylation of the adeninate anion

The thermodynamic parameters and rate constants were calculated i) including all LVFs and ii) setting all the LVFs less than 100 cm^{-1} to 100 cm^{-1}. The new contribution to the partition function (Q_{vib}), entropy (S_{vib}), internal thermal energy (E_{vib}) and heat capacity (C_{vib}) from the vibrational motions after setting the LVF to 100 cm^{-1} were calculated using equations 4.15 to 4.18, having $3N-6$ for reactants and $3N-7$ for the TS in which the negative frequency is not included,

$$Q_{vib} = \prod_{i=1}^{3N-6} \frac{1}{1-e^{\left(-\frac{h\nu_i}{k_B T}\right)}} \tag{4.15}$$

$$S_{vib} = R\sum_{i=1}^{3N-6}\left(\frac{h\nu_i/k_B T}{e^{h\nu_i/k_B T}-1} - ln\left(1-e^{-h\nu_i/k_B T}\right)\right) \tag{4.16}$$

$$E_{vib} = R\sum_{i=1}^{3N-6}\frac{h\nu_i}{k_B}\left(\frac{1}{2}+\frac{1}{e^{h\nu_i/k_B T}-1}\right) \tag{4.17}$$

© University of Pretoria

$$C_{vib} = R\sum_{i=1}^{3N-6} e^{hv_i/k_BT}\left(\frac{{}^{hv_i}/_{k_BT}}{e^{-hv_i/k_BT}-1}\right)^2 \quad (4.18)$$

where h is Planck's constant, v_i is the oscillating frequency, k_B is the Boltzmann constant and T is temperature. The rate constant, k, for each pathway was calculated using TS theory, eqn 4.19, where c_0 is 24.48 L mol^{-1} to account for the Gaussian calculation being at a standard pressure of 1 atm while the rate constant is in concentration units of mol L^{-1}.[111] The activation energies for all the possible reaction paths were calculated as the difference between the Gibbs free energy of the transition state complexes and the sum of the Gibbs free energy of the reactants.

$$k = \frac{k_BT}{hc_0}e^{\left({}^{\Delta G^{\ddagger}}/_{RT}\right)} \quad (4.19)$$

The change in energy (ΔE_{ZPVE}) and the Gibbs free energy of activation ($\Delta G^{\ddagger}$) for the calculated N1-, N3-, N7- and N9-Bn pathways in the absence and presence of the Na^+ ion is given in Table 4.8. The experimental $\Delta G^{\ddagger}$ value of 86 and 88 kJ mol^{-1} for the N9- and N3-Bn, respectively, is well recovered by the modelling of the reaction pathways in the presence of the Na^+ ion i.e. 83.9 and 84.9 kJ mol^{-1} for N9- and N3-Bn-Na, respectively. In the absence of the Na^+, the $\Delta G^{\ddagger}$ is better recovered using Truhlar's quasiharmonic approximation i.e. the calculated value of 81.5 (N9-Bn) and 80.8 (N3-Bn).

Table 4.8: Calculated thermodynamic parameters and rate constant for the formation of N1-, N3-, N7- and N9-Bn including all LVFs and using Truhlar's quasiharmonic approximation – values in brackets, in the absence and presence of the Na^+ ion

	ΔE_{ZPVE} (kJ mol^{-1})	$\Delta G^{\ddagger}$ (kJ mol^{-1})	k, M^{-1} s^{-1}	$k_{N9\text{-}Bn}/k_{NX\text{-}Bn}$
			Ade^- + BnCl	
N1-Bn	33.6 (34.9)	81.1 (89.9)	2.0×10^{-3} (4.53×10^{-5})	391 (29)
N3-Bn	24.6 (26.0)	68.9 (80.8)	2.14×10^{-1} (1.78×10^{-3})	2.8 (0.70)
N7-Bn	26.7 (28.1)	72.5 (83.0)	5.08×10^{-2} (7.25×10^{-4})	12 (1.8)
N9-Bn	24.8 (26.4)	66.3 (81.5)	6.08×10^{-1} (1.32×10^{-3})	-
			Na-Ade + BnCl	
N1-Bn	36.6 (38.3)	81.5 (94.2)	1.34×10^{-3} (7.86×10^{-6})	0.34 (1.9)
N3-Bn	35.2 (36.3)	84.6 (93.3)	3.78×10^{-4} (1.16×10^{-5})	1.3 (1.3)
N7-Bn	29.4 (30.7)	76.9 (86.7)	8.66×10^{-3} (1.64×10^{-4})	0.06 (0.1)
N9-Bn	34.6 (35.6)	83.9 (92.7)	5.07×10^{-4} (1.47×10^{-5})	-

The predicted N9/N3 and N9/N7 product ratios will be discussed in terms of modelling the reaction pathways in the presence and absence of the Na^+ ion.

In the absence of the Na^+ ion: The experimental rate ratio N9-Bn/N3-Bn of 2.5 and the N9/N7 of 12.5 is very well recovered. The inclusion of LVFs in the $Q^{\ddagger}$, Q_A and Q_B terms for the $Ade^-$and BnCl reaction results in the rate constant of the N9-Bn pathway being 2.8 times larger than that of N3-Bn and 12 times larger than that of N7-Bn. The lack of N1-Bn product formation from experimental work is supported by the extremely large calculated N9/N1 ratio of 391. These trends are not

© University of Pretoria

replicated using Truhlar's quasiharmonic approximation. The calculated N9-Bn/N3-Bn and N9-Bn/N7-Bn rate constant ratios are 0.7 and 1.8. Thus, although LVF can pose an issue when calculating thermodynamic properties, the inclusion of LVFs has allowed the trend from experimental work to be reproduced very well in the theoretical calculations.

In the presence of Na^+ ion: The increase in barrier height for the N9-Bn-Na and N3-Bn-Na pathway due to the presence of the Na^+ ion results in the rate constants for these two paths being much smaller than the experimental values. However, since explicit solvent molecules were not included in the study, this is not an accurate representation of the reaction. There are strong interactions between the Na^+ counter ion and DMSO solvent molecules which results in an out of plane displacement, as shown in Chapter 3. Therefore, the increase in the barrier height of the N3- and N9-pathway theoretically represents the barrier to the dissociation of the ion pair by the incoming electrophile without the assistance of the solvent. In addition, the repulsion between the positive charge on the Na^+ ion and the developing positive charge of the incoming electrophile will contribute to the increase in activation energy.

To demonstrate this point, two scans have been performed in which the Na^+ is moved away from the adeninate anion. The first scan involves the complex with the sodium ion chelated at the N3N9 position (Na-Ade(N3N9)) in which the implicit solvent system is used to incorporate the DMSO solvent. The ΔE along the reaction coordinate d(N9,Na^+) is shown in Figure 4.23. The second scan incorporates 4 explicit DMSO solvent molecules, Na-Ade(N3N9)-4DMSO, Figure 4.24.

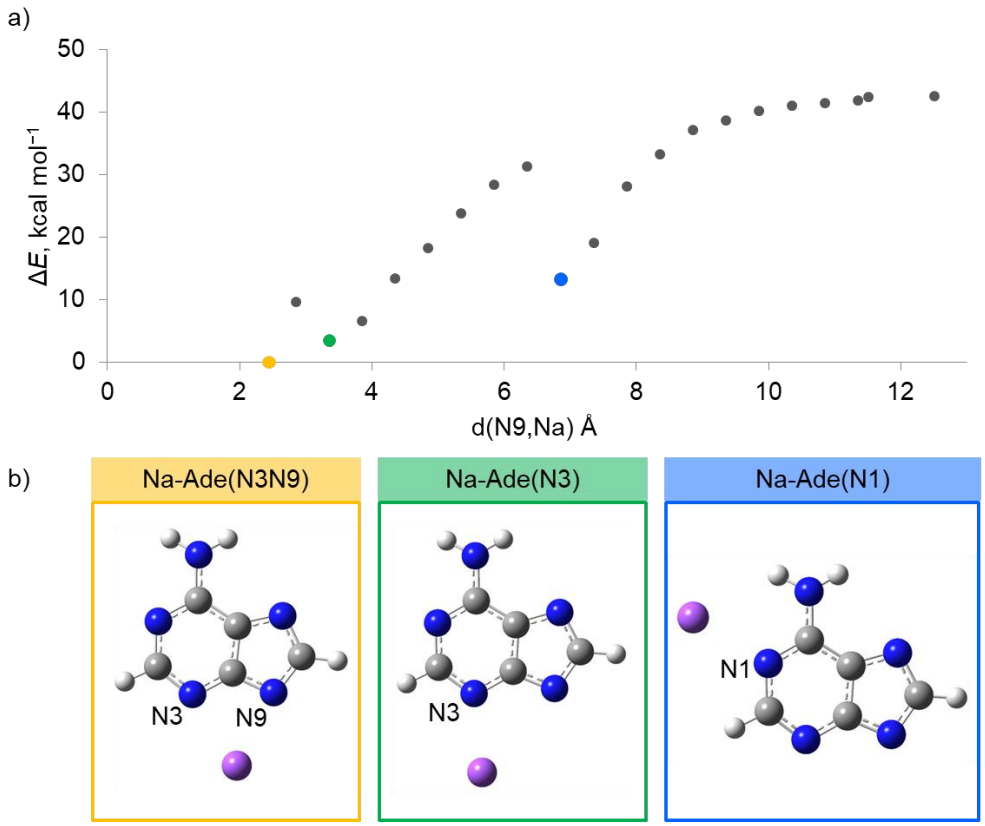

Figure 4.23: a) ΔE (kJ mol^{-1}) along the reaction coordinate d(N9, Na) in Å, resulting from scanning the Na^+ ion away from the adeninate anion of the Na-Ade(N3N9) complex, and b) optimized structures for the yellow, green and blue points shown in (a).

© University of Pretoria

In Figure 4.23, to fully remove the Na^+ counter ion, the molecular system experiences an energy penalty of 43 kJ mol^{-1}. As the Na^+ ion is moved further away from the N3N9 site of the adeninate anion it is attracted to the N3 and then the N1 nitrogen atom. From the N3N9 position (yellow point) the system is stabilized along the reaction coordinate which corresponds to complexation at the N3 and N1 atom (green and blue point, respectively).

To fully remove the Na^+ counter ion from the adeninate anion in the presence of the four DMSO solvent molecules, the molecular system pays a penalty of 15 kJ mol^{-1}, Figure 4.24. Thus, the presence of explicit solvent molecules lowers the energy required to dissociate the sodium chelated adeninate complex by −28 kJ mol^{-1} relative to the system studied using implicit DMSO solvent. This is due to the favourable interactions between the DMSO molecules and the Na^+ counter ion. In Figure 4.24, the three highly stabilized energy structures are shown. The molecular system is largely stabilized relative to the starting structure (yellow dot) by −40 kJ mol^{-1} as the counter ion complexes simultaneously at the N1 atom and with three DMSO solvent molecules (green point). As the Na^+ is scanned away from the N1 atom, three DMSO solvent molecules migrate with the ion, stabilizing the system again by −10 kcal mol (blue point) relative to the starting structure.

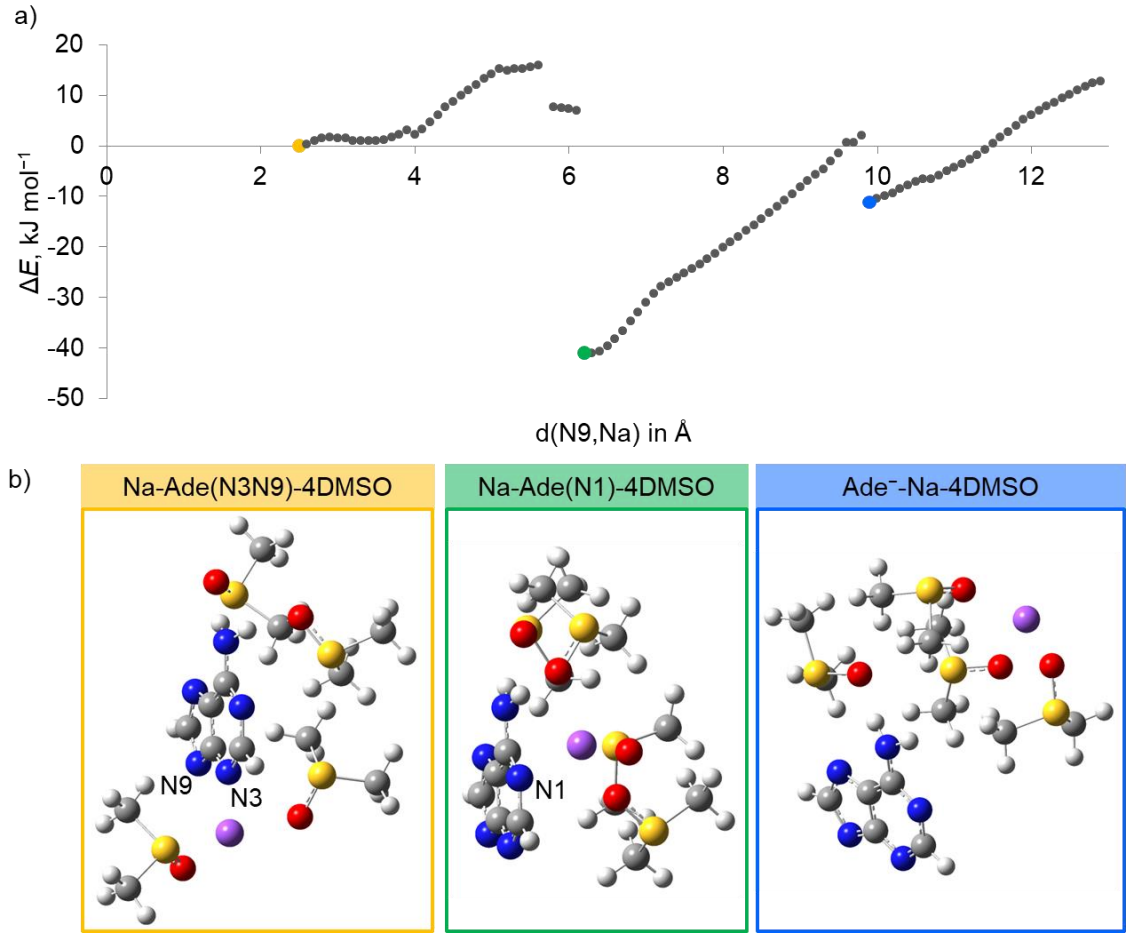

Figure 4.24: a) Δ*E* (kJ mol^{-1}) along the reaction coordinate d(N9, Na) in Å, resulting from scanning the Na^+ ion away from the adeninate anion of the Na-Ade(N3N9)-4DMSO complex, and b) optimized structures for the yellow, green and blue points shown in (a).

© University of Pretoria

Hence, if the benzylation of the adeninate anion is to be studied in the presence of the Na^+ counter ion, the DMSO molecules will need to be included as they will greatly reduce the amount of energy required to shift the Na^+ ion out of place as the electrophile is approached by N3 and N9 atoms of the purine ring. In Chapter 3 it was shown that the interaction between the DMSO molecules and the Na^+ ion shifts the complexed metal counter ion out-of-plane and should result in less interference from the Na^+ counter ion as the electrophile is approached by the nucleophile, even though it is still complexed to the adeninate anion. This could explain why, in this and previous research, the N9:N3:N7 product ratio is unaffected by the change in counter ion (K^+, Na^+ and Li^+) in polar aprotic solvents.[17] The polar protic solvents can potentially play a critical role in facilitating the removal of the counter ion, reducing its influence on the alkylation pattern. Furthermore, the DMSO solvent molecules form highly favourable hydrogen bonds with the NH_2 group of the adeninate anion, increasing the energy barrier for benzylation at the N1 and N7 atoms. To study this system further, IQA and REP-FAMSEC will be key methods to gain insight into the interaction energies governing benzylation at the four endo-purine ring nitrogen atoms.

4.4 Conclusion

Adenine and its anion have multiple sites of reactivity. Factors such as steric hindrance, product stability, nucleophilicity, nature of the electrophile and solvent influence the site of alkylation. In the 1960s to 1990s significant effort was made to understand the factors governing the regio-selectively of the alkylation of the adeninate anion. However, no experimentally determined kinetic data has ever been reported. In this chapter, real time dynamic ^1H NMR spectroscopy of the benzylation of the adeninate anion in anhydrous DMSO has been presented for the first time.

The site preference of benzylation of the adeninate anion is insensitive to the alkylating reagents used in this study, i.e. benzyl bromide, benzyl chloride, (1-bromoethyl)benzene, and pentafluorobenzyl bromide, or the counter ion present, Na^+ and K^+. The N9 and N3 alkylated adenine derivatives are the dominant species in solution, having the former the major isomer with the N9/N3 product ratio of 2.5. The identified side reaction which depletes the Na-Ade starting material is ascribed to the Kornblum oxidation reaction involving the DMSO and alkyl halides. The resulting protonation of the adeninate anion to adenine is greatly reduced in the presence of a mop-up base.

The benzylation of Na-Ade occurs via an S_N2 mechanism in which the enthalpy of formation for N3-Bn is −12 kJ mol^{-1} lower in energy than N9-Bn. The increase in the barrier height of N9-Bn is largely compensated for by the increase in the entropy term, being significantly smaller by +50 J mol^{-1} K^{-1} than that of N3-Bn. This leads to the overall Gibbs free energy of N9-Bn being −2.3 kJ mol^{-1} lower in energy than for N3-Bn which experiences an entropic bottleneck. This is supported by computational studies where the N9:N3:N7-Bn product ratio is governed by barrier width. The narrow well shape of the PES at the TS region of the N3-Bn pathway leads to a drastic decrease in the rate in comparison to the N9-Bn pathway. The incorporation of the Na^+ ion in the computational modelling of the pathways leads to high energy barriers for the formation of N9- and N3-Bn resulting from the dissociation of the Na^+ ion as the electrophile approaches the N3 and N9 reactive sites. The inclusion of explicit DMSO solvent molecules reduces the energy required for the dissociation of the Na^+ ion.

© University of Pretoria

4.5 References

[1] G. P. Ford, J. D. Scribner, *Chem. Res. Toxicol.* **1990**, *3*, 219–230.

[2] K. W. Kohn, J. A. Hartley, W. B. Mattes, *Nucleic Acids Res.* **1987**, *15*, 10531–10549.

[3] R. Bonaccorsi, A. Pullman, E. Scrocco, J. Tomasi, *Theor. Chim. Acta* **1972**, *24*, 51–60.

[4] W. A. Denny, *Expert Opin. Ther. Pat.* **2000**, *10*, 459–474.

[5] P. Lawley, P. Brookes, *Biochem. J.* **1963**, *89*, 127–138.

[6] P. Raboisson, C. Lugnier, C. Muller, J.-M. Reimund, D. Schultz, G. Pinna, A. Le Bec, H. Basaran, L. Desaubry, F. Gaudiot, M. Seloum, J.-J. Bourguignon, *Eur. J. Med. Chem.* **2003**, *38*, 199–214.

[7] J.-J. Bourguignon, L. Désaubry, P. Raboisson, C.-G. Wermuth, C. Lugnier, *J. Med. Chem.* **1997**, *40*, 1768–1770.

[8] T. J. Torphy, *Am. J. Respir. Crit. Care Med.* **1998**, *157*, 351–370.

[9] E. Boichot, J. L. Wallace, N. Germain, M. Corbel, C. Lugnier, V. Lagente, J. J. Bourguignon, *J. Pharmacol. Exp. Ther.* **2000**, *292*, 647–53.

[10] B. Bielekova, A. Lincoln, H. McFarland, R. Martin, *J. Immunol.* **2000**, *164*, 1117–1124.

[11] G. H. Hakimelahi, T. W. Ly, A. A. Moosavi-Movahedi, M. L. Jain, M. Zakerinia, H. Davari, H.-C. Mei, T. Sambaiah, A. A. Moshfegh, S. Hakimelahi, *J. Med. Chem.* **2001**, *44*, 3710–3720.

[12] S. Phadtare, D. Kessel, T. H. Corbett, H. E. Renis, B. E. Court, J. Zemlicka, *J. Med. Chem.* **1991**, *34*, 421–429.

[13] C. Lambertucci, I. Antonini, M. Buccioni, D. D. Ben, D. D. Kachare, R. Volpini, K.-N. Klotz, G. Cristalli, *Bioorg. Med. Chem.* **2009**, *17*, 2812–2822.

[14] I. Mahadevan, M. Rasmussen, *Tetrahedron* **1993**, *49*, 7337–7352.

[15] M. Rasmussen, J. Hope, *Aust. J. Chem.* **1982**, *35*, 525.

[16] A. Beasley, M. Rasmussen, *Aust. J. Chem.* **1981**, *34*, 1107.

[17] M. Rasmussen, J. Hope, *Aust. J. Chem.* **1982**, *35*, 535.

[18] N. M. Chung, H. Tieckelmann, *J. Org. Chem.* **1970**, *35*, 2517–2520.

[19] G. Hopkins, J. Jonak, H. Minnemeyer, H. Tieckelmann, *J. Org. Chem.* **1967**, *32*, 4040–4044.

[20] N. P. Ramzaeva, I. N. Goncharova, M. Y. Lidak, Y. S. Gol'dberg, M. V. Shimanskaya, *Chem. Heterocycl. Compd.* **1987**, *23*, 93–98.

[21] M. Rasmussen, J. Chan, *Aust. J. Chem.* **1975**, *28*, 1031.

[22] J. Kjellberg, N. G. Johansson, *Nucleosides and Nucleotides* **1989**, *8*, 225–256.

[23] M. R. Haque, M. Rasmussen, *Tetrahedron* **1994**, *50*, 5535–5554.

[24] M. R. Osborne, P. D. Lawley, *Chem. Biol. Interact.* **1993**, *89*, 49–60.

[25] A. Pullman, B. Pullman, *Q. Rev. Biophys.* **1981**, *14*, 289–380.

© University of Pretoria

[26] T. Lindahl, B. Sedgwick, M. Sekiguchi, Y. Nakabeppu, *Annu. Rev. Biochem.* **1988**, *57*, 133–157.

[27] B. Singer, S. J. Spengler, H. Fraenkel-Conrat, J. T. Kusmierek, *Proc. Natl. Acad. Sci.* **1986**, *83*, 28–32.

[28] M. Koskinen, P. Vodička, K. Hemminki, *Chem. Biol. Interact.* **2000**, *124*, 13–27.

[29] W. F. Veldhuyzen, Y. Lam, S. E. Rokita, *Chem. Res. Toxicol.* **2001**, *14*, 1345–1351.

[30] P. D. Lawley, M. Jarman, *Biochem. J.* **1972**, *126*, 893–900.

[31] P. D. Lawley, in *Prog. Nucleic Acid Res. Mol. Biol.*, **1966**, pp. 89–131.

[32] N. NAKAYAMA, S. TANAKA, O. KIKUCHI, *J. Theor. Biol.* **2002**, *215*, 13–22.

[33] B. C. Pal, *Biochemistry* **1962**, *1*, 558–563.

[34] C. Marian, D. Nolting, R. Weinkauf, *Phys. Chem. Chem. Phys.* **2005**, *7*, 3306.

[35] M. Koskinen, E. K. H. Schweda, K. Hemminki, *J. Chem. Soc. Perkin Trans. 2* **1999**, 2441–2445.

[36] D. M.-J. S. Buyens, Alkylation of Adenine: A Synthetic and Computational Study of the Reaction Mechanism, **2015**.

[37] D. M. S. Buyens, P. Mangondo, I. Cukrowski, L. A. Pilcher, *J. Heterocycl. Chem.* **2017**, *54*, 2946–2950.

[38] M. Hanus, M. Kabeláč, J. Rejnek, F. Ryjáček, P. Hobza, *J. Phys. Chem. B* **2004**, *108*, 2087–2097.

[39] D. M. Close, C. E. Crespo-Hernández, L. Gorb, J. Leszczynski, *J. Phys. Chem. A* **2008**, *112*, 12702–12706.

[40] F. P. Clausen, J. Juhl-Christensen, *Org. Prep. Proced. Int.* **1993**, *25*, 373–401.

[41] G. Ferenc, P. Padar, J. Szolomajer, L. Kovacs, *Curr. Org. Chem.* **2009**, *13*, 1085–1135.

[42] M. Breugst, F. Corral Bautista, H. Mayr, *Chem. - A Eur. J.* **2012**, *18*, 127–137.

[43] P. D. Lawley, W. Warren, *Chem. Biol. Interact.* **1976**, *12*, 211–220.

[44] L. Sun, B. Singer, *Biochemistry* **1975**, *14*, 1795–1802.

[45] J. Zurlo, T. J. Curphey, R. Hiley, D. S. Longnecker, *Cancer Res.* **1982**, *42*, 1286 LP – 1288.

[46] P. J. O'Connor, M. J. Capps, A. W. Craig, *Br. J. Cancer* **1973**, *27*, 153–166.

[47] A. E. Pegg, B. Balog, *Cancer Res.* **1979**, *39*, 5003 LP – 5009.

[48] J. Woo, S. T. Sigurdsson, P. B. Hopkins, *J. Am. Chem. Soc.* **1993**, *115*, 3407–3415.

[49] G. J. Atwell, J. Fan, K. Tan, W. A. Denny, *J. Med. Chem.* **1998**, *41*, 4744–4754.

[50] R. C. Moschel, W. R. Hudgins, A. Dipple, *J. Org. Chem.* **1980**, *45*, 533–535.

[51] C. G. Swain, C. B. Scott, *J. Am. Chem. Soc.* **1953**, *75*, 141–147.

[52] R. G. Pearson, *J. Am. Chem. Soc.* **1963**, *85*, 3533–3539.

© University of Pretoria

[53] G. P. Ford, B. Wang, *Carcinogenesis* **1993**, *14*, 1465–1467.

[54] J. S. Murray, Z. Peralta-Inga, P. Politzer, K. Ekanayake, P. LeBreton, *Int. J. Quantum Chem.* **2001**, *83*, 245–254.

[55] N. Russo, M. Toscano, A. Grand, F. Jolibois, *J. Comput. Chem.* **1998**, *19*, 989–1000.

[56] A. Pullman, A. M. Armbruster, *Theor. Chim. Acta* **1977**, *45*, 249–256.

[57] R. Bonnaccorsi, E. Scrocco, J. Tomasi, A. Pullman, *Theor. Chim. Acta* **1975**, *36*, 339–344.

[58] D. Perahia, A. Pullman, B. Pullman, *Int. J. Quantum Chem.* **2009**, *16*, 353–363.

[59] D. Perahia, A. Pullman, *Theor. Chim. Acta* **1978**, *48*, 263–266.

[60] D. Cauchy, R. Lavery, B. Pullman, *Theor. Chim. Acta* **1980**, *57*, 323–327.

[61] E. M. Arnett, S. G. Maroldo, G. W. Schriver, S. L. Schilling, E. B. Troughton, *J. Am. Chem. Soc.* **1985**, *107*, 2091–2099.

[62] A. L. Kurts, A. Macias, I. P. Beletskaya, O. A. Reutov, *Tetrahedron* **1971**, *27*, 4759–4767.

[63] J. M. Harris, S. G. Shafer, J. R. Moffatt, A. R. Becker, *J. Am. Chem. Soc.* **1979**, *101*, 3295–3300.

[64] G. S. Hammond, *J. Am. Chem. Soc.* **1955**, *77*, 334–338.

[65] J. E. Leffler, *Science (80-.).* **1953**, *117*, 340–341.

[66] E. R. Thornton, *J. Am. Chem. Soc.* **1967**, *89*, 2915–2927.

[67] J. M. Harris, J. L. Paul, *Isr. J. Chem.* **1985**, *26*, 325–330.

[68] R. A. M. O'Ferrall, *J. Chem. Soc. B* **1970**, 274–277.

[69] D. T. Beranek, C. C. Weis, D. H. Swenson, *Carcinogenesis* **1980**, *1*, 595–606.

[70] G. P. Ford, J. D. Scribner, *J. Am. Chem. Soc.* **1983**, *105*, 349–354.

[71] R. C. Moschel, W. R. Hudgins, A. Dipple, *J. Org. Chem.* **1979**, *44*, 3324–3328.

[72] A. J. Parker, *Chem. Rev.* **1969**, *69*, 1–32.

[73] M. Rasmussen, N. J. Leonard, *J. Am. Chem. Soc.* **1967**, *89*, 5439–5445.

[74] A. Dipple, P. Brookes, D. S. Mackintosh, M. P. Rayman, *Biochemistry* **1971**, *10*, 4323–4330.

[75] U. Mayer, V. Gutmann, W. Gerger, *Monatshefte f*[illegible]*r Chemie* **1975**, *106*, 1235–1257.

[76] L. L. Schaleger, F. A. Long, **1963**, pp. 1–33.

[77] R. W. Taft, *J. Am. Chem. Soc.* **1953**, *75*, 4534–4537.

[78] R. W. Taft, *J. Am. Chem. Soc.* **1952**, *74*, 5372–5376.

[79] A. Pan, T. Biswas, A. K. Rakshit, S. P. Moulik, *J. Phys. Chem. B* **2015**, *119*, 15876–15884.

[80] L. Liu, Q. Guo, *Chem. Rev.* **2001**, *101*, 673–696.

© University of Pretoria

[81] J. Clayden, N. Greeves, S. Warren, P. Wothers, *Organic Chemistry*, OxfordUniversity Press Inc., New York, **2000**.

[82] P. R. Rablen, B. D. McLarney, B. J. Karlow, J. E. Schneider, *J. Org. Chem.* **2014**, *79*, 867–879.

[83] R. E. Rawlings, A. K. McKerlie, D. J. Bates, Y. Mo, J. M. Karty, *European J. Org. Chem.* **2012**, *2012*, 5991–6004.

[84] J. F. King, G. T. Y. Tsang, *J. Chem. Soc. Chem. Commun.* **1979**, *47*, 1131.

[85] F. Ruff, Ö. Farkas, Á. Kucsman, *European J. Org. Chem.* **2006**, *2006*, 5570–5580.

[86] T. A. Hamlin, M. Swart, F. M. Bickelhaupt, *ChemPhysChem* **2018**, *19*, 1315–1330.

[87] Z. Wu, C. Rong, T. Lu, P. W. Ayers, S. Liu, *Phys. Chem. Chem. Phys.* **2015**, *17*, 27052–27061.

[88] M. J. Frisch, G. W. Trucks, H. B. Schlegel, G. E. Scuseria, M. A. Robb, J. R. Cheeseman, G. Scalmani, V. Barone, G. A. Petersson, H. Nakatsuji, X. Li, M. Caricato, A. V. Marenich, J. Bloino, B. G. Janesko, R. Gomperts, B. Mennucci, H. P. Hratchian, J. V. Ortiz, a. F. Izmaylov, J. L. Sonnenberg, Williams, F. Ding, F. Lipparini, F. Egidi, J. Goings, B. Peng, A. Petrone, T. Henderson, D. Ranasinghe, V. G. Zakrzewski, J. Gao, N. Rega, G. Zheng, W. Liang, M. Hada, M. Ehara, K. Toyota, R. Fukuda, J. Hasegawa, M. Ishida, T. Nakajima, Y. Honda, O. Kitao, H. Nakai, T. Vreven, K. Throssell, J. A. Montgomery Jr., J. E. Peralta, F. Ogliaro, M. J. Bearpark, J. J. Heyd, E. N. Brothers, K. N. Kudin, V. N. Staroverov, T. A. Keith, R. Kobayashi, J. Normand, K. Raghavachari, A. P. Rendell, J. C. Burant, S. S. Iyengar, J. Tomasi, M. Cossi, J. M. Millam, M. Klene, C. Adamo, R. Cammi, J. W. Ochterski, R. L. Martin, K. Morokuma, O. Farkas, J. B. Foresman, D. J. Fox, **2016**, Gaussian 09, Revision E.01, Gaussian, Inc., Wallin.

[89] S. Grimme, J. Antony, S. Ehrlich, H. Krieg, *J. Chem. Phys.* **2010**, *132*, 154104.

[90] L. Deng, T. Ziegler, *Int. J. Quantum Chem.* **1994**, *52*, 731–765.

[91] L. Deng, T. Ziegler, L. Fan, *J. Chem. Phys.* **1993**, *99*, 3823–3835.

[92] R. Marek, A. Křístková, K. Maliňáková, J. Toušek, J. Marek, M. Hocek, O. L. Malkina, V. G. Malkin, *J. Phys. Chem. A* **2010**, *114*, 6689–6700.

[93] N. J. Leonard, T. R. Henderson, *J. Am. Chem. Soc.* **1975**, *97*, 4990–4999.

[94] J. R. Fox, Proton Magnetic Resonance Spectral Assignments and Deuterium Exchange Reactions in Substituted Purines, University of illinois, Urbana, IL, **1965**.

[95] N. Kornblum, J. W. Powers, G. J. Anderson, W. J. Jones, H. O. Larson, O. Levand, W. M. Weaver, *J. Am. Chem. Soc.* **1957**, *79*, 6562–6562.

[96] N. Kornblum, W. J. Jones, G. J. Anderson, *J. Am. Chem. Soc.* **1959**, *81*, 4113–4114.

[97] Y.-P. Zhu, M. Lian, F.-C. Jia, M.-C. Liu, J.-J. Yuan, Q.-H. Gao, A.-X. Wu, *Chem. Commun.* **2012**, *48*, 9086.

[98] H.-J. Buschmann, *Polyhedron* **1992**, *11*, 559–561.

[99] M. Baidya, H. Mayr, *Chem. Commun.* **2008**, 1792.

[100] N. Ghosh, *Synlett* **2004**, *2*, 574–575.

© University of Pretoria

[101] S. W. Benson, *Thermochemical Kinetics*, John Wiley & Sons, New York, **1976**.

[102] D. Lexa, J. M. Saveant, . Su Khac Binh, D. L. Wang, *J. Am. Chem. Soc.* **1988**, *110*, 7617–7625.

[103] S. S. Shaik, *J. Am. Chem. Soc.* **1988**, *110*, 1127–1131.

[104] J. Chandrasekhar, S. F. Smith, W. L. Jorgensen, *J. Am. Chem. Soc.* **1985**, *107*, 154–163.

[105] E. Buncel, H. Wilson, *Acc. Chem. Res.* **1979**, *12*, 42–48.

[106] E. G. Lewars, *Computational Chemistry*, Springer Netherlands, Dordrecht, **2011**.

[107] Santosh K. Upadhyay, *Chemical Kinetics and Reaction Dynamics*, Springer Netherlands, Dordrecht, **2006**.

[108] P. Y. Ayala, H. B. Schlegel, *J. Chem. Phys.* **1998**, *108*, 2314–2325.

[109] R. F. Ribeiro, A. V. Marenich, C. J. Cramer, D. G. Truhlar, *J. Phys. Chem. B* **2011**, *115*, 14556–14562.

[110] G. Reinisch, J.-M. Leyssale, G. L. Vignoles, *J. Chem. Phys.* **2010**, *133*, 154112.

[111] E. Roduner, *Chem. Soc. Rev.* **2014**, *43*, 8226–8239.

© University of Pretoria

Chapter 5 The study of the kinetic isotope effect of ATP-C8D on shikimate kinase through high resolution mass spectrometry

5.1 Introduction

5.1.1 The shikimate pathway and shikimate kinase

The shikimate pathway, also known as the common aromatic biosynthetic pathway,[1] converts erythrose-4-phosphate and phosphoenolpyruvate to chorismate.[2] Chorismate is an essential intermediate required for branching pathways involved in the synthesis of aromatic amino acids, i.e. tyrosine, tryptophan and phenylalanine, and secondary metabolites such as p-amino-benzoic acid, folate and ubiquinone.[2–4] The shikimate pathway is present only in plants and microorganisms and not in animals, thus making the pathway a target to develop herbicides, antibacterial, antiparasitic and antifungal agents that are non-toxic to mammals.[4,5] Some examples of parasites in which the pathway is present and can aid in drug design are *Plasmodium falciparum* (malaria), *Toxplasma gondii* (toxoplasmosis) and *Cryptosporidium parvum* (cryptosporidiosis).[6,7] The pathway has also gained popularity for therapeutic agents against *Mycobacterium tuberculosis* and its drug-resistant strains, the causative agents of tuberculosis which is one of the leading diseases resulting in death each year.[5,8] One such target enzyme is *Mycobacterium tuberculosis* shikimate kinase[9,10] (*Mt*-SK) which catalyses the fifth reaction in the shikimate pathway. The enzyme is responsible for the phosphorylation of shikimate to shikimate-3-phosphate (S3P) using adenosine 5′-triphosphate (ATP) as a co-substrate, Figure 5.1.[3,11] Shikimate kinase is a promising target as inactivation of its encoding *aroK* gene induces partial or complete blockage of the conversion of shikimate to shikimate-3-phosphate, resulting in the loss of viability of *M. tuberculosis*.[12,13]

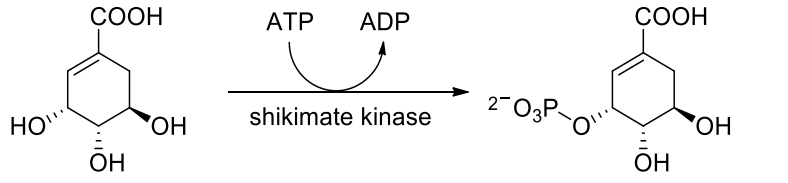

shikimate shikimate-3-phosphate

Figure 5.1: Phosphorylation of shikimate to shikimate-3-phosphate by shikimate kinase.

Shikimate kinase displays a random order binding of shikimate and ATP and an ordered release of the products where ADP is released before S3P. The binding of the first substrate, shikimate or ATP, increases the affinity for the second substrate.[14–16] The phosphoryl transfer is commonly proposed to occur via an in-line associative mechanism[16] (S_N2) like that reported for other kinases.[17–19] The Mg^{2+} ion is proposed to render the γ-phosphate group more electrophilic by withdrawing electron density.[16]

© University of Pretoria

5.1.2 The role of the adenyl moiety in molecular recognition

The three moieties of ATP, namely the adenyl,[20] ribose[21] and phosphate groups, and their associated metal ions,[15,22] all play a critical role in the recognition of ATP in the protein active site.[23–26] Molecular recognition is governed by molecular determinates which consist of various non-bonded intermolecular interactions between the substrate and the residues in the active site of the protein. Hydrogen-bonding is the most commonly referred to non-bonded intermolecular interaction of the adenyl moiety which occurs via the three hydrogen bond acceptors (N1, N3 and N7) and the two hydrogen bond donors (the two protons on the NH_2).[20] The adenyl moiety in the *Mt*-SK active site is involved in hydrogen bonding via the NH_2 group and the N1 atom.[14,16,27] In addition to the well-known hydrogen bonding interaction, the adenyl moiety can also exhibit equally important non-bonded π-π stacking and cation-π interactions between the conjugated π rings of the adenine base with surrounding aromatic amino acids and positively charged amino acids, respectively.

It is generally assumed that the adenine base of ATP facilitates molecular recognition and holding the ATP in the enzyme active site. However, it has been suggested that the C8–H proton of adenyl moiety plays a significant role in the regulation of kinase activity.[28,29] Two mechanisms have been proposed, namely the "push" mechanism for group 2 kinases i.e. the shikimate and adenylate kinase, and the "pull" mechanism for group 4 kinases.[28] The two mechanisms, which will be briefly discussed here, provide a means by which the C8 proton becomes labile to initiate a proton transfer cascade leading to the phosphoryl transfer. The "push" mechanism occurs via the deprotonation of the NH_2 exo-amino group of the adenyl moiety by a nearby carbonyl group of the protein backbone, Figure 5.2. The deprotonation triggers an electron cascade resulting in protonation of the adenyl C8 resulting in a change in the hybridization of the C8 from sp^2 to sp^3. A set of subsequent proton transfers occur between the surrounding amino acid residues and the phosphate groups along with deprotonation of the O1 hydroxyl group of shikimate, leading to the breakage of the O—P bond between the β-PO_4 and γ-PO_4 group during the phosphoryl transfer.[28]

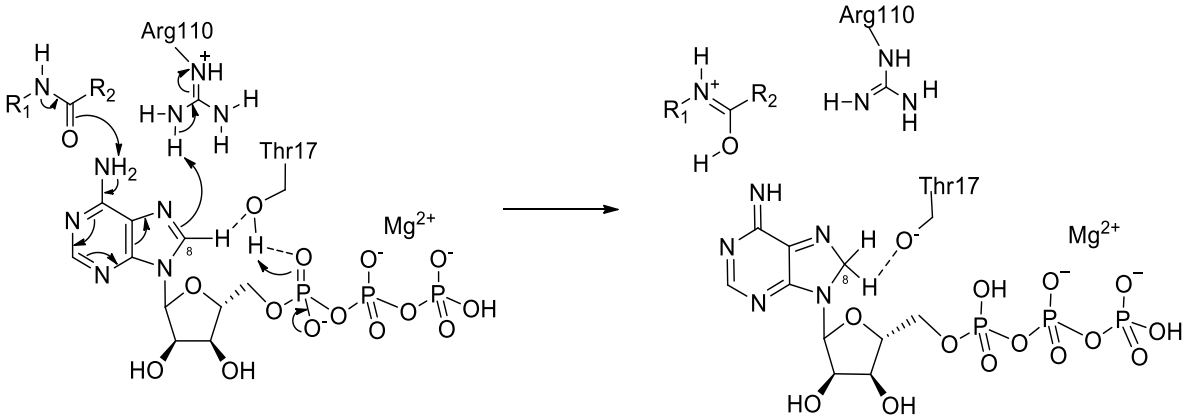

Figure 5.2: The "push" mechanism demonstrated for shikimate kinase, adjusted from reference [28].

The "pull" mechanism, Figure 5.3, occurs via the formation of a carbene at the C8 position through protonation of the adenyl N7 by an Arg residue which triggers deprotonation of the C8 position by a

© University of Pretoria

Ser/Thr residue. This in turn leads also to a set of subsequent proton transfer reactions and deprotonation of the O1 hydroxyl group of shikimate, allowing the phosphoryl transfer to take place.[28]

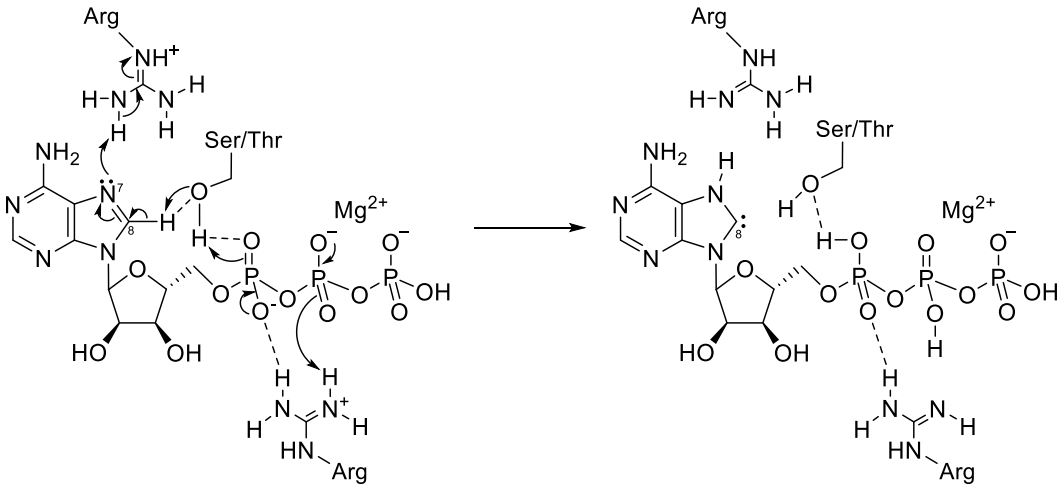

Figure 5.3: The "pull" mechanism demonstrated for shikimate kinase, adjusted from reference [28].

The formation of a nucleophilic carbene for conversion and deuteration of imidazole derivatives is not unknown. Previous studies on the deuteration of N9- and N3-benzyladenine as well as dichloropurine derivatives support a possible carbene mechanism for deuterium exchange at the C8-H position for N9 substituted adenines.[30,31] For N3-adenine derivatives, an sp^3 mediated mechanism is highly likely.

5.1.3 Kinetic isotope effects in enzymatic reactions

For many years kinetic isotope effects have been used to derive mechanisms and transition state structures for enzymatic reactions. KIEs arise from a change in rate constants and equilibrium isotope effects arise from the change in equilibrium constants, both due to an atom being replaced by its heavier isotope.[32] Primary KIEs occur when the bond to the isotope is directly involved in the reaction mechanism, i.e. bond to the isotope is broken or formed, and are of a magnitude larger than 2 for deuterium.[33,34] Secondary KIEs occur when the isotope is remote from the reactive site, i.e. one or more bonds away, and are smaller than primary isotope effects, typically in the range of 1.1 to 1.2 for deuterium.[35]

The main contribution to the KIE stems from the difference in the zero-point energy between the light atom and its isotopes, in which the heavier atom has lower ground energy.[36] The isotope effect is indicated by the superscript preceding the parameter investigated in which the superscript specifies the heavy atom used i.e. ^{D}k for the KIE of the rate constant using deuterium.[37] At 25 °C the maximum predicted primary KIE on the rate constant of a hydride transfer reaction resulting from bond breakage between a C–D versus a C–H bond is about 7 if it is the rate-determining step. This value is obtained from eqn 5.1,

© University of Pretoria

$$\mathrm{KIE} = \frac{k_{\mathrm{H}}}{k_{\mathrm{D}}} = \frac{e^{-\Delta H^{\ddagger}/RT}}{e^{-(\Delta H^{\ddagger}+4.8\mathrm{kJ\cdot mol^{-1}})/RT}} = e^{4.8kJ\cdot mol^{-1}/RT} \qquad (5.1)$$

where k_{H} and k_{D} are the rate constants for the hydride and deuteride transfer reactions, $\Delta H^{\ddagger}$ is the enthalpy of activation, R is the gas constant, and T is the temperature. The estimated value of the difference of the ground state between a C-D and a C-H bond is −4.8 kJ·mol^{-1}. The lower energy for the deuterium implies that 4.8 kJ·mol^{-1} more enthalpy of activation is required for bond cleavage.

KIEs can be larger (normal) or smaller (inverse) than unity, having the latter occur if the labelled substrate reacts faster than the unlabelled substrate.[36] The size of the primary KIE indicates the nature of the TS, having KIEs that approach the maximum theoretically determined value indicate a TS that resembles both the reactant and the product. Factors such as substrate binding, conformational changes, isomerization, and product release interfere with measuring the true intrinsic KIE of the rate constant of the isotopically sensitive step. This in turn results in masking of the intrinsic KIE.[36]

The intrinsic KIE is on the rate constant, ^{D}k ,of the bond cleavage step, Figure 5.4.[38] However, obtaining ^{D}k is not straightforward for many complex enzyme reactions as resolving individual rate constants and their isotope effects requires complex, stringent and difficult experiments.[39] More achievable is measuring the "observed" KIE on i) the overall rate, ^{D}v, ii) the maximal velocity V_{max} at saturating substrate concentrations, ^{D}V, and iii) on the specificity constant V_{max}/K_M (also indicated as k_{cat}/K_M) at low substrate concentration, $^{D}V/K$. [34,40] The meaning of V_{max}/K_M can be taken as the rate at which the enzyme and substrate come together to form a complex which will result in a catalytic event to produce the product.[41] V_{max} and V_{max}/K_M are complex functions consisting of several rate constants in which an isotope effect on one or more rate constants will be reflected to a greater or lesser extent on either V_{max} and V_{max}/K_M.[34] The larger KIE of either parameter will indicate the minimum value for ^{D}k.

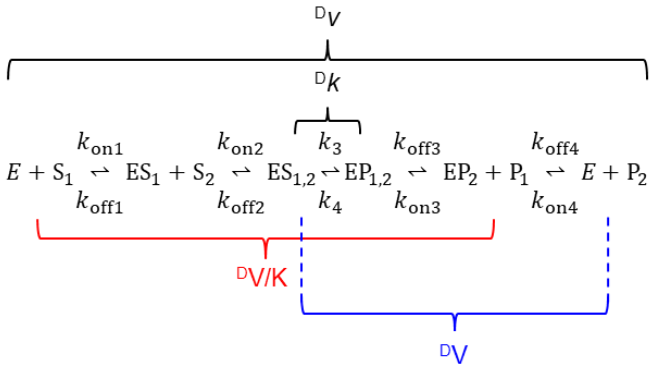

Figure 5.4: Range of measurable deuterium isotope effects for an ordered mechanism.

The KIE on V/K involves all steps from the free enzyme, E in Figure 5.4, up to and including the first irreversible step, usually the first product release, to form EP_2 and is obtained at a low concentration of substrate.[32] The KIE on V is determined from the enzyme-substrate complex $ES_{1,2}$ to product release to reform the free enzyme E and is obtained at high concentrations of substrate.[40] The ^{D}v

© University of Pretoria

includes all steps and therefore all steady-state distribution of enzyme forms. KIE on *v* indicates very little information regarding the mechanism of catalysis.[34] ^{D}(V/K) and ^{D}V can be obtained from the ratio of the slope and the y-axis intercept, respectively, of the reciprocal plots (Lineweaver-Burk) of the labelled and unlabelled substrate.

The relationship between the intrinsic KIE and the observed isotope effect on V/K is expressed by eqn 5.2,

$$\frac{^{D}V}{K} = \frac{^{D}k + C_f + C_r \cdot ^{D}K_{eq}}{1 + C_f + C_r} \qquad (5.2)$$

where C_f and C_r are the forward and reverse commitments to catalysis, $^{D}K_{eq}$ is the equilibrium isotope effect.[36,40] Both C_f and C_r are complex expressions and depend on the system studied and the conditions used. The C_f represents the tendency of the enzyme-substrate complex to continue forward in catalysis as opposed to diverting back to the free enzyme, whereas the C_r represents the tendency of the enzyme complex after the isotopically sensitive step to undergo reverse catalysis. For irreversible enzyme reactions the C_r is close to zero. The effect of substrate concentration on the value of the KIE is determined by the forward commitment.[40]For an ordered mechanism and high concentrations of the co-substrate, the forward commitment is large and the KIE on V_{max}/K_M is abolished whereas, at low concentrations of co-substrate, the KIE approaches the limiting value on V_{max}/K_M.[40] For a random ordered mechanism, such as for shikimate kinase, the effect of high concentration of co-substrate on V_{max}/K_M is reduced but not abolished.

5.1.4 Measuring KIEs on enzymatic reactions

The three main methods used for the analysis of KIEs on enzyme catalysis are i) direct comparison, also known as the non-competitive method, ii) internal competition method and iii) equilibrium perturbation.[32] If the labelled substrate is available in large amounts, as is often the case for deuterated substrates, and the KIE is larger than 1.05 the non-competitive method is often used. In this method two enzyme reactions are performed, one in the presence of the unlabelled substrate and the other with the labelled substrate.[40] This method is the only one that allows for the measurement of KIE on the maximal velocity and interpretation involving the rate-determining step.[42] The limitations of the non-competitive method are that isotopically pure labelled compounds (> 95%) are required, assays must be free of impurities, the exact concentration of labelled compound must be known, and precision of the rate determination is within a few percent, and is limited to of the comparison of hydrogen and deuterium.[40]

For small KIEs on V/K (i.e. up to 1.0002) and to study isotope effects of atoms present at trace levels such as tritium, ^{14}C and naturally abundant ^{13}C, ^{15}N and ^{18}O, the internal competition method is commonly used. It is the most sensitive method and overcomes the limitations of the non-competitive method such as being independent of inhibitors and labelled compounds that can occur in trace amounts.[32,43] In this method, the isotopic ratio of the substrate or product at the start of the reaction is compared to that of the substrate or product at time *t* as the reaction proceeds. Any

© University of Pretoria

deviation in the ratio between labelled and unlabelled substrate is an indication of the isotope effect.[34,40]

5.1.4.1 Absorption and fluorescence spectroscopy

Enzyme kinetics, binding assays, inhibitory studies, protein structure, conformational changes and mechanisms of enzyme catalysis have generally been studied using absorption and fluorescence spectroscopy.[44–47] These methods allow for continuous monitoring of time-dependent enzyme reactions when the product has an intense absorbance band different from that of the substrate. The measurement of KIEs using a chromophoric technique can be done through the non-competitive method. Competitive methods cannot be used as the isotope will not affect the chromophoric properties and therefore does not allow for isotopic discrimination.[35]

In most circumstances, the absorption difference between substrate and product is very small or the substrates and products don't have chromophoric properties. When an enzyme reaction that cannot be followed photometrically has a product that is a substrate or co-substrate for an enzyme that can be studied photometrically, the reactions are coupled allowing the reaction of interest to be studied by monitoring the reduction/increase in the absorbance band of the chromophoric substrate/product.[48] Sometimes one or more intermediate reactions are used to couple the reaction of interest to the chromophoric reaction to allow the non-chromophoric reaction to be monitored.[44,49] A well-known example of such a coupling reaction is catalysed by the enzyme lactose dehydrogenase where the substrate, reduced β-Nicotinamide adenine dinucleotide (NADH), has a unique absorbance band at 340 nm at which the product, oxidized β-Nicotinamide adenine dinucleotide (NAD), has no absorption.[50]

Previously the steady state kinetic parameters of shikimate kinase were obtained through coupling the reaction to that of pyruvate kinase and lactate dehydrogenase in the presence of the substrates phosphoenolpyruvate (PEP) and NADH, Figure 5.5.[11,14,15,51] The absorbance band of ATP and ADP are indistinguishable by UV spectroscopy, i.e. both occur at 260 nm. Hence, a coupling assay provided a solution to use UV spectroscopy to monitor the conversion of ATP to ADP by shikimate kinase through the indirect measurement of NADH.

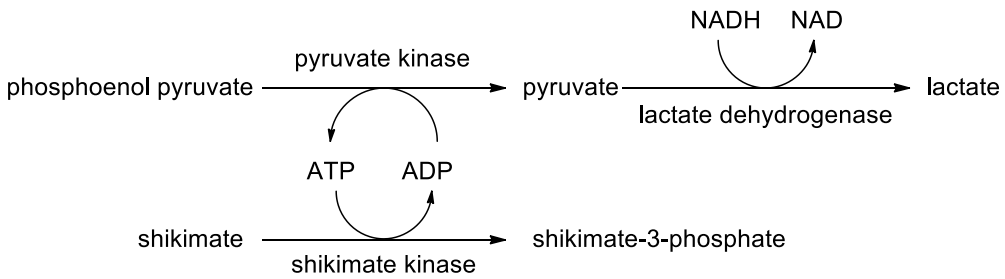

Figure 5.5: Coupled assay for monitoring the kinetics of Mt-SK via UV-spectroscopy.

The ADP produced by the reaction of shikimate kinase is used as a co-substrate for the conversion of PEP to pyruvate by pyruvate kinase. The pyruvate is then reduced to lactate by lactate

© University of Pretoria

dehydrogenase using NADH as a co-substrate which is oxidized to NAD. The Shikimate-dependent oxidation of NADH is continuously monitored by the decrease in NADH absorbance at 340 nm (ε = 6.22 × 10^3 M^{-1} cm^{-1}). The steady state kinetic parameters *of Mycobacterium tuberculosis* shikimate kinase (*Mt*-SK) obtained from previous studies are given in Table 5.1.

Table 5.1: Steady state kinetic parameters of *Mt*-SK from literature

	UV-coupled assay			LC-MS assay
	Gu et al.[14]	Rosado et al.[51]	Simithy et al.[52]	
K_{cat} (s^{-1})	44 ± 2	60 ± 8	64 ± 2	68 ± 2
			63 ± 1	65 ± 2
$K_{m(MgATP)}$ (mM)	0.083 ± 0.004	0.112 ± 0.004	0.17 ± 0.02	0.20 ± 0.01
$K_{i(MgATP)}$ (mM)	0.089 ± 0.003			
$K_{m(shikimate)}$ (mM)	0.41 ± 0.02	0.65 ± 0.028	0.51 ± 0.04	0.53 ± 0.05
$K_{i(shikimate)}$ (mM)	0.44 ± 0.02			
$K_{cat}/K_{m(MgATP)}$ ($M^{-1}·s^{-1}$)	5.3×10^5	5.4 (± 0.7) ×10^5		
$K_{cat}/K_{m(shikimate)}$ ($M^{-1}·s^{-1}$)	1.1×10^5	0.9 (± 0.1)×10^5		

The use of coupled assays can be advantageous such as when a product of the reaction of interest is a strong inhibitor of the reaction or when it is desirable to maintain a steady concentration of a reactant such as ATP.[53] In these circumstances, the use of coupled assays can remove the inhibitory product or regenerate the substrate. However, coupled assays also come with many disadvantages such as cost and unwanted side reactions. In particular, extended lag periods prevent the coupled reaction from accurately reflecting the initial rate of interest. [49,54] In addition, coupled enzymes will need to be highly active under the same conditions as the enzyme of interest and it may not be possible to optimize the buffer, pH, salt concentration, etc. for all coupled enzymes resulting in reduced activity of some.[44] Furthermore, the changes in reactants in the early stages of the reaction are smaller than the change in product formation.[53] This leads to less accurate data being obtained when monitoring the decrease in a reactant, such as in the case of measuring the decrease in the absorbance of NADH. When considering studying KIEs of the first enzymatic step in a coupled assay, the effect of the isotope on the coupling enzymes poses a serious concern.[52,55]

To avoid the use of coupling enzymes when substrates or products of enzyme reactions don't possess chromophoric properties, unnatural substrates with chromophores are synthesized substrates to allow for fluorescence to be measured. In this case, the synthesis of chromophoric substrates is laborious and the kinetic behaviour of the substrate derivative may be different from the natural substrate.[56] Another approach for monitoring enzyme reactions is to use substrates with a radioactive label, however, the availability of radioactively labelled substrates is limited and their synthesis is laborious and generates hazardous waste.[57]

5.1.4.2 Mass spectroscopy as a modern analytical technique for studying enzyme kinetics and KIEs

Modern methods with greater sensitivity that allow for direct, simple and rapid analysis of the primary enzyme reaction without the use of coupling enzymes or chemically modified substrates have grown over the years.

© University of Pretoria

Mass spectrometry and soft ionization techniques such as matrix-assisted laser desorption/ionization (MALDI) and electrospray ionisation (ESI) have been used to obtain quantitative and qualitative data for enzyme kinetics, inhibition studies, characterization of protein structures, conformational changes, protein identification, protein-ligand interactions, etc.[58–61] The use of soft ionization techniques allows for the analysis of fragile molecules and keeps the integrity of the sample.[62] MALDI produces singly charged ions, positive or negative, whereas ESI-MS produces several charged ions, positive or negative. In both techniques, the ions are accelerated and separated based on the mass-to-charge (m/z) ratio by a mass analyser.[62]

Mass spectrometry requires that there be a mass difference between the substrate and product, however, it doesn't require any modification of the native substrate or rely on chromophoric properties or coupling enzymes. MS is fast and allows for the analysis of multiple analytes during an enzyme reaction.[57] In the ESI-MS technique pre-separation of the sample is usually performed by chromatographic techniques such as high- or ultra-performance liquid chromatography (HPLC and UPLC) to achieve a greater signal-to-noise ratio and therefore increased sensitivity.[63–65] The compounds in the sample are separated based on affinity/interaction strengths with the chemical composition of the stationary phase of the chromatographic column prior to MS analysis. An example of the use of electrospray ionization coupled to liquid chromatography and mass spectrometry (ESI-LC-MS) for the study of the kinetics of *Mt*-SK has been shown to give comparable results to that of the UV-coupled assay study, Table 5.1.[52]

The downside of using ESI-MS to study enzyme kinetics without sample preparation arises from the limited choice of volatile buffers compatible with ESI-MS, such as ammonium bicarbonate, ammonium acetate or ammonium formate.[57,66,67] TRIS-HCl and phosphate buffers and NaCl and KCl salts which are generally used in enzyme assays cannot be injected directly into the UPLC-MS as it results in clogging of the ESI source and ion suppression due to cluster formation of salts and neutralization of charged analytes.[68,69] Sample preparation such as solid phase extraction, liquid-liquid extraction and LC will need to be carried out to reduce the matrix effects and build-up of the ESI-MS incompatible buffers and salts in the ESI source.[70] The inclusion of a suitable internal standard is needed for quantitative sample analysis using ESI-MS in these circumstances.[69] The use of HPLC coupled to a UV spectrometer is more acceptable for non-volatile buffers. Ambient ionization techniques do not require sample extraction, separation, or derivatization, etc. before ionization of the analyte because they cause desalting of the sample, reducing the build-up at the ESI interface, and decreasing ion suppression.[71,72] Paper spray ionization has been used to monitor the activity of aspartate aminotransferase.[72] For more details on such techniques refer to references [71], [73], [74].

Kinetics of enzyme reactions are generally studied using two methods, namely continuous or discontinuous analysis.[67,75] Continuous analysis allows for real-time monitoring of the enzyme assay in which the sample is directly injected into the ESI while the reaction is taking place in the solution.[57] No chemical quenching is required for this method. In ESI-MS real-time monitoring of an ongoing enzyme reaction has been used to study pre-steady state kinetics, identify unstable intermediates and KIEs via on-line rapid-mixing continuous flow, Figure 5.6. [43,56,58,75,76] The reaction is terminated upon nebulisation of the reaction mixture in the ESI interface. The enzyme and substrate are kept separate in two syringes which are continuously flowing by the use of a syringe/HPLC pump, mixed in the mixer chamber to initiate the reaction and flow through a capillary

© University of Pretoria

to the ESI. The time of reaction is controlled by the flow rate or the length of the capillary tube.[57] Such a technique has been used to study the kinetics of 3-deoxy-D-manno-2-octulosonate-8-phosphate synthase,[76] peptide phosphorylation by cAMP-dependent protein kinase A,[77] glutathione conjugation by glutathione S-transferase[56] and trypsin-catalysed hydrolysis of N^2-(carbobenzyloxy)-L-lysine-*p*-nitrophenyl ester.[78] A similar method known as stopped-flow ESI-MS is also available to measure fast enzyme reaction kinetics and pre-steady-state kinetics.[75,79] The KIE study on N-acetylpolyamine oxidase was determined using the competitive method with continuous flow MS with a mixture of non-deuterated *N,N'*-dibenzyl-1,4-diaminobutane (DBDB) and deuterated DBDB-d_{13} as substrate.[43] The reaction was followed by monitoring the development of the deuterated and non-deuterated products based on the mass difference, i.e. *m/z* = 267.1856 and 280.2672, respectively. The reaction was monitored via a non-competitive method as well in which no internal standard was required as isotopic substitution is expected not to alter the ionization properties of the substrate and product. This is also true for retention times in LC-MS.[35]

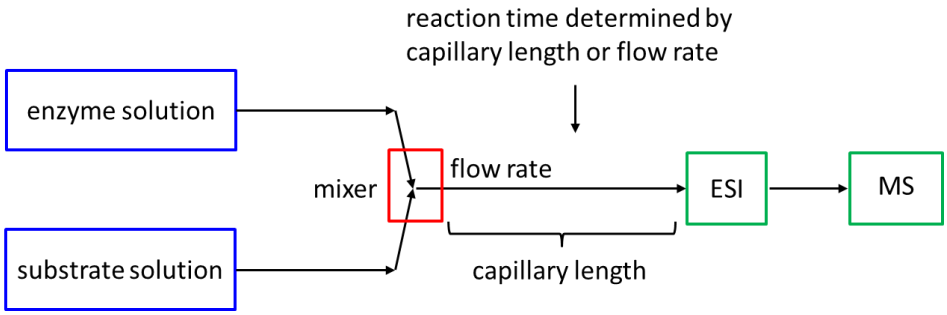

Figure 5.6: Diagram of an on-line rapid-mixing continuous flow ESI-MS set up.

Often the modification to equipment in order to achieve such experimental setups is not possible or there is limited availability of the sample and off-line methods become more attractive. One such offline technique involves the monitoring of the enzyme reaction in real-time if the reaction is slow enough to be monitored every few minutes. Direct injection of an ongoing reaction from a vial into the ESI-MS or LC-ESI-MS can be performed to monitor the decrease of the substrate and/or increase of the product.[63,80] The kinetics of the hydrolysis of dinucleotides and lactose by ribonuclease A and β-galactosidase,[63] respectively, esterase-catalysed cleavage of bis(2-pyridyl-methyl)(2-acetoxyphenyl)amine[81] and xylanase-catalysed hydrolysis of neutral underivatized xylo-oligosaccharides[82] have been obtained with such a method.

When enzyme reactions are too fast to be monitored via the above method, discontinuous assays are used whereby the reactions are quenched before ESI-MS analysis via the addition of an acid, base or organic solvent.[57,75] Such techniques have been used to study the kinetics of mycobacterial carbohydrate sulfotransferase Stf0 which catalyses the sulfuryl group transfer from 3'-phosphoadenosine-5'-phosphosulfate to trehalose[83] and glutathione conjugation by glutathione S-transferase.[56] Quenching of reactions allows for the post-reaction addition of an internal standard and therefore ensures that the enzyme reaction is not disturbed by the presence of an internal standard. A disadvantage of this technique is that chemically sensitive products may be altered upon

© University of Pretoria

quenching.[75] It is thus important to validate the choice of quenching method to prove that it does not alter the substrate and product composition. The use of rapid-mixing continuous flow ESI-MS does not have this drawback as there is no need for quenching the sample.[76]

5.1.5 The scope of this research

Previously KIEs of magnitude between 2 and 7 (showing a primary KIE) for several kinase and synthetase enzymes resulting from the deuteration of ATP at the C8 position have been reported using HPLC-UV methods, leading to the development of the push and pull mechanistic models.[28,29,84] The possibility of the involvement of the C8 proton of the adenyl moiety in the regulation of phosphoryl transfer in kinase and synthase enzymes could have valuable implications in the drug discovery field against human and animal diseases. However, the study of the KIE on ^{D}v of *Mt*-SK (or any other of the investigated enzymes) resulting from C8D-ATP has not been taken forward as one would have hoped. Hence, in our research, we aimed to investigate the C8D-ATP KIE on ^{D}V and $^{D}V/K$ of *Mt*-SK from non-competitive and competitive discontinuous enzyme assays using high resolution MS. In the presence of ATP and C8D-ATP, the enzyme produces ADP and C8D-ADP, respectively. The use of MS to study the change in ADP and C8D-ADP product formation based on the mass difference i.e. *m/z* = 428.0383 and 429.0479, respectively, provides an advantage over UV analysis for competitive assays. UV analysis cannot discriminate between the non-deuterated and deuterated forms of ADP.

5.2 Experimental details

General: The ^{1}H and ^{31}P NMR spectra were recorded at 300 and 121 MHz, respectively, with a Bruker 300 AVANCE Ultrashield Plus spectrometer equipped with a BBFP probe. All reagents for the enzyme assays were purchased from Sigma-Aldrich and the NMR solvents were purchased from Merck. Solvents for UPLC-MS were purchased from Microsep, South Africa.

Deuteration of ATP and C8D-ATP stock prep: ATP (0.127 mmol, 1 eq) was dissolved in 4.5 ml of D_2O to which solid Na (0.500 mmol, 4 eq) was added. The reaction was heated at 85 °C for 50 minutes to obtain more than 95 % deuteration at the C8 position. Deuteration was confirmed by ^{1}H NMR. Less than 3 % of ADP was formed. See Figure S4.1 in Supporting Information 4. The stock sample was adjusted to pH 7.2 with HCl.

Mass spectrometry: Analysis was performed using flow injection analysis (FIA); the flow rate was set to 0.4 ml/min and the injection volume was 5 µl. Ultra purity methanol (Romil-UpS™,Microsep, South Africa) spiked with 0.1 % formic acid (Fluka® Analytical, Sigma-Aldrich, South Africa), B2, and aqueous ammonium bicarbonate, A1, were used as elution solvents. An isotopic flow (A1:B2; 80:20 (%v/v)) was used through the entire run of 3 minutes. Compound detection was performed using a Waters® Synapt G2 high definition mass spectrometry (HDMS) system (Waters Inc., Milford, Massachusetts, USA). Samples were analysed using flow injection analysis (FIA). The system is comprised of a Waters Acquity Ultra Performance Liquid Chromatography (UPLC®) system hyphenated to a quadrupole-time-of-flight (QTOF) instrument. The system was operated with MassLynx™ (version 4.1) software (Waters Inc., Milford, Massachusetts, USA) for data acquisition and processing. An internal lock mass control standard, 2 ng/µL solution leucine enkephalin (m/z

© University of Pretoria

555.2693), was directly infused into the source through a secondary orthogonal electrospray ionisation (ESI) probe allowing intermittent sampling. The internal control was used to compensate for instrumental drift, ensuring good mass accuracy. The source conditions were as follows: the capillary voltage for ESI was 2.0 kV for positive ionisation. The source temperature was set at 120 ºC, the sampling cone voltage at 30 V, extraction cone voltage at 4.0 V and cone gas (nitrogen) flow at 10.0 L/Hr. The desolvation temperature was set at 350 °C with a gas (nitrogen) flow of 600.0 L/Hr. Mass spectral scans were collected every 0.3 seconds. The raw data was collected in the form of a centroid profile. Mass to charge ratios (*m/z*) between 50 and 1 200 Da were recorded.

ADP Standard curve: 6 assays were prepared in triplicate each containing ammonium bicarbonate (100 mM) at pH 7.5, $MgCl_2$ (7 mM), KCl (100 mM), ATP (1 mM) and shikimic acid at concentrations 0.00781, 0.0156, 0.0313, 0.0625, 0.125 and 0.250 mM. The enzyme assays were initiated by the addition of 0.101 µM *Mt*-SK. Each assay was allowed to complete at RT whereby 4 µl of 98% formic acid was added after an hour to account fully for matrix effects at the MS source. All assays were made up to a final volume of 250 µl. The shikimic acid of each assay was fully converted in which ATP was converted to ADP, resulting in 0.00781, 0.0156, 0.0313, 0.0625, 0.125 and 0.250 mM of ADP for each stock sample. Standard curves were developed with the instrument's response to the amount of ADP present in the samples. The counts of ADP over the scan range of 5-100 was taken and plotted.

Enzyme kinetics: GraphPad Prism 5 was used to fit the Michaelis-Menten parameters using non-linear regression for each enzyme assay. The *Mt*-SK enzyme was synthesized and purified via a drip column by R. Roth from the CSIR, provided to us at a concentration of 750 ng/µL (36 µM) and stored at −80 °C.

Enzyme stock preparation: Ammonium bicarbonate (1 M) at pH 7.5, $MgCl_2$ (0.08 M), KCl (1 M), ATP (0.05 M) and shikimic acid (0.12 M) were prepared using UPLC grade water as solvent. The ATP stock solution was adjusted to a pH of 7.5 with HCl. The shikimic acid, ATP and C8D-ATP stocks were aliquoted and stored at -20 °C. All other reagents were stored at 4 °C.

Enzyme assay: Simultaneous non-competitive/direct method was chosen for evaluating the kinetics and kinetic isotope effect of *Mt*-SK. The kinetic runs are performed at the same time, under the same conditions, at 25 °C, containing various concentrations of either ATP or C8D-ATP. Each assay contained ammonium bicarbonate (100 mM) at pH 7.5, $MgCl_2$ (7 mM), KCl (100 mM), shikimic acid (3 mM) and ATP or C8D-ATP at 0.0312, 0.0624, 0.125, 0.250 and 0.500 mM. All assays were made up to a final volume of 250 µl. The assays were initiated by the addition of 0.035 µM *Mt*-SK and terminated with 4 µl of formic acid after 3 minutes.

Competitive assays: Each assay contained ammonium bicarbonate (100 mM) at pH 7.5, $MgCl_2$ (7 mM), KCl (100 mM), shikimic acid (3 mM) and ATP:ATP-C8D (1:1) at 5 concentrations: 0.0156, 0.0313, 0.0625, 0.125 and 0.250 mM. The assays were initiated by the addition of 0.035 µM *Mt*-SK, run for 3 minutes at 25 °C and terminated using 4 µl of formic acid.

© University of Pretoria

5.3 Results and discussion

5.3.1 Experimental design

To study the kinetics of *Mt*-SK and the KIE experienced in the presence of C8D-ATP using high resolution MS, the buffer used for the enzyme assay was converted to an MS appropriate volatile buffer, ammonium bicarbonate, see Figure S4.2. The purpose of changing the buffer was to reduce the build-up of TRIS-HCl buffer salts at the ESI interface during multiple runs. To verify that the change of solvent did not negatively impact the enzyme performance, the enzyme assays were performed in triplicate using UV-coupling enzymes, pyruvate kinase and lactate dehydrogenase, in TRIS-HCl and ammonium bicarbonate buffer. The change in absorbance of NADH at 340 nm is monitored over time. The enzyme activity in ammonium bicarbonate was comparable to that in TRIS-HCl, which is commonly used in the kinetic studies of shikimate kinase.

To obtain the kinetics of *Mt*-SK via MS, discontinuous assays were performed in which the concentration of ATP and/or C8D-ATP was varied whereby the co-substrate, shikimic acid, concentration was in excess and constant. The reactions were initiated by the addition of 0.035 µM *Mt*-SK. Reactions were terminated after 3 minutes by the addition of 4 µl of formic acid. Samples were analysed by MS to identify and quantify the amount of the ADP and/or C8D-ADP produced via the use of a calibration curve. The mass difference between ATP (m/z = 508.0089, $[M+H]^+$), C8D-ATP (m/z = 509.0124, $[M+H]^+$), ADP (m/z = 428.0383, $[M+H]^+$) and C8D-ATP(m/z = 429.0479, $[M+H]^+$) was used to discriminate between deuterated and non-deuterated substrate and product. Furthermore, the choice of analysing the reaction with the use of adenosine groups stems from the low ionization ability of shikimic acid and S3P in negative ESI mode and the absence in positive mode.

5.3.1.1 Development of standard curve and method validation

The increase in ADP and/or C8D-ADP peak intensity in the mass spectrum was used to monitor the extent of the reaction of Mt-SK. A standard curve was developed with the instrument's response to increasing concentrations of ADP. Figure 5.7a shows the mass spectrum for a typical mixture of ADP (0.25 mM) and ATP, and Figure 5.7b shows the change in ADP peak intensity with increasing concentration. The matrix effects from the enzyme assay were taken into account by obtaining various concentrations of ADP in separate enzyme reactions in which several concentrations of shikimic acid were added, ranging from 0.00781 to 0.250 mM, in the presence of excess ATP, 1 mM. The reactions were allowed to go to completion and 4 µl of formic acid was added to each reaction to mimic the termination of the actual enzyme assays.

The counts of ADP (m/z = 428.0383) over the scan range of 5-100 was taken and plotted, Figure 5.8a, yielding a slope of 17292 ± 266 and a y-intercept of 315 ± 31 with a correlation coefficient of 0.9991. The ADP signal intensity is directly proportional to the concentration in the standard solutions. At low ADP concentrations of the standard curve, higher concentrations of ATP are present as less was converted due to the lower shikimic acid concentration. The regression line does not pass through zero as a certain amount of ATP is fragmented into ADP. The standard curve was not conducted without the presence of ATP as this won't be a true reflection of the reaction mixture since the enzyme will convert less than 10% of ATP. As the standard curve was developed under these conditions, there was no need to correct for the % of ADP fragmented from pure ATP.

© University of Pretoria

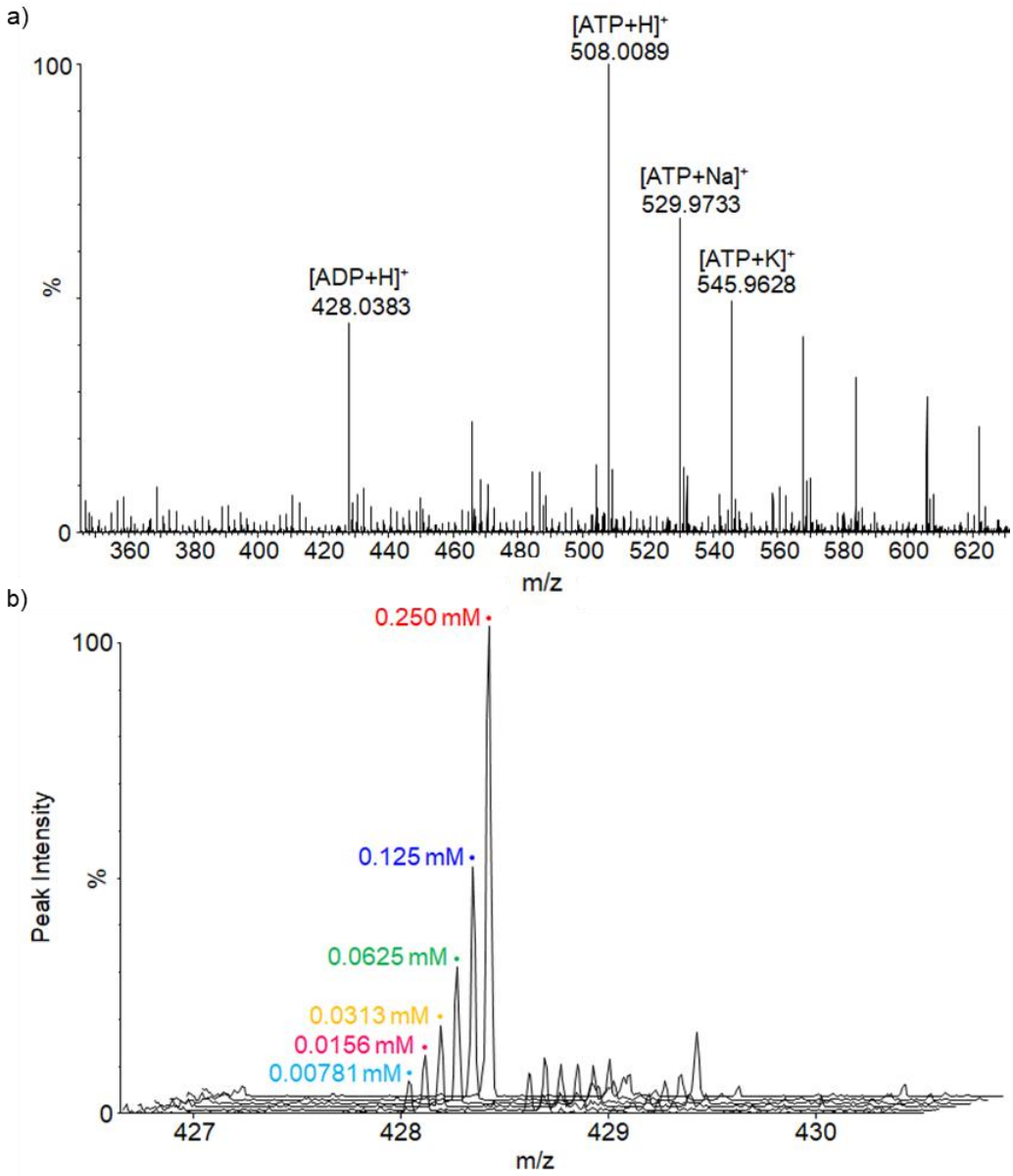

Figure 5.7: a) Mass spectrum of ADP (*m/z* = 428.0383, $[ADP+H]^+$) and ATP (*m/z* = 508.0089, $[ATP+H]^+$) with ATP sodium (*m/z* = 529.29733, $[ATP+Na]^+$) and potassium (*m/z* = 545.9628, $[ATP+K]^+$) adducts, and b) the change in ADP peak intensity with increasing concentration.

The method is validated through the limit of detection (LOD), the limit of quantification (LOQ), and precision under repeatability through triplicate injections of the same sample (standard deviation shown in Figure 5.8a) and reproducibility via interday analysis of independently prepared samples. The LOD and LOQ are calculated from the standard curve using eqn 5.3 and 5.4, respectively,

$$\mathrm{LOD} = 3 \times \left(\frac{S_y}{S}\right) \qquad (5.3)$$

© University of Pretoria

$$\mathrm{LOQ} = 10 \times \left(\frac{S_y}{S}\right) \quad (5.4)$$

where S_y is the standard error of the y-intercept of the linear fit line and S is the slope. The LOD is 5.99 × 10^{-3} mM and the LOQ of 1.82 × 10^{-2} mM. These values are well below that of the concentration range used in the study.

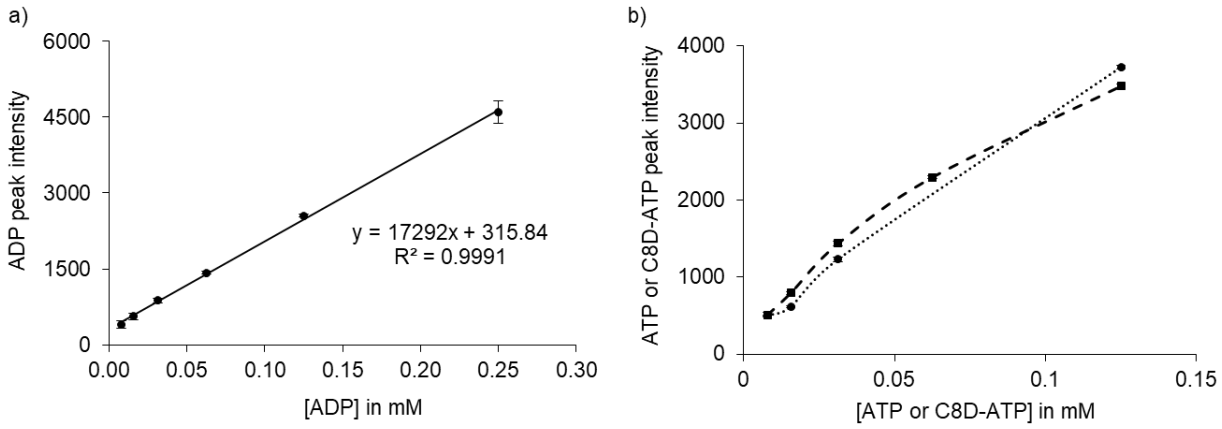

Figure 5.8: a) Standard curve obtained by measuring the ADP signal at *m/z* = 428.0383 over the scan range 1 to 100, b) instruments response to various concentrations of ATP and C8D-ATP. The counts of ATP (*m/z* = 508.0089) and C8D-ATP (5090124) over the scan range of 5-100 were used. % RSD is given for both plots.

The interday precision was determined by analysis of duplicate injections of 5 concentrations spanning the lower, mid and higher concentration range for 3 days under the same experimental conditions. The coefficient of variation (CV) is < 10 % for all concentrations tested. The 5 concentrations were freshly prepared for each interday experiment. This allows for multiple consecutive injections of samples to be performed without enormous errors occurring from signal suppression.

In order to compare the formation of ADP and C8D-ADP in the enzyme assays, the presence of the deuterium is assumed not to influence the ionization properties of the adenosine molecule (refer to Figure S4.3 for the mass spectrum of pure C8D-ATP in the assay mixture). This was tested by comparing the instrument's response to various concentrations of ATP and C8D-ATP, Figure 5.8b. It is shown that the incorporation of the deuterium at the C8 position of ATP doesn't significantly alter the ionization properties of ATP. The instrument's response for the ionization of ATP becomes suppressed and plateaus with high concentrations of ATP or C8D-ATP, rendering it less accurate to rely on the ATP and C8D-ATP for obtaining quantitative data of enzymatic kinetics.

5.3.2 Determination of *Mt*-SK kinetics and KIEs by high resolution mass spectroscopy

The concentration of *Mt*-SK to yield less than 10% conversion of the substrate (ATP) within 3 minutes was determined by performing enzyme assays at various concentrations of *Mt*-SK, Figure

© University of Pretoria

5.9a. The reactions were initiated by the addition of *Mt*-SK and allowed to react at 25 °C in which the reactions were terminated by the addition of 4 µl of formic acid. The samples were analysed using the method described above and the concentration of ADP was determined from the standard curve. The concentration used to study the enzyme kinetics of Mt-SK was chosen as 0.035 µM. Two interday triplicate *Mt*-SK enzyme assays were performed and the data fitted by non-linear regression to the Michaelis-Menten equation, eqn 5.5, in GraphPad Prism 5,

$$v_0 = \frac{V_{max}[S]}{K_M + [S]} \tag{5.5}$$

where v_0 is the reaction velocity, V_{max} is the maximum reaction velocity of *Mt*-SK, [S] is the substrate concentration and K_M is the Michaelis constant. The initial velocities were calculated using eqn 5.6,

$$v_0 = \frac{[\mathrm{ADP}]}{t_q} \tag{5.6}$$

where [ADP] is the determined concentration after quenching, and t_q is the quenching time, 3 minutes. The k_{cat} value was calculated using eqn 5.7,

$$k_{cat} = \frac{V_{max}}{[E]_t} \tag{5.7}$$

where V_{max} is the maximum reaction velocity of *Mt*-SK determined by the Michaelis-Menten equation and $[E]_t$ is the total enzyme concentration in the assay.

The resulting Michaelis-Menten plots are shown in Figure 5.9b. To investigate whether the best-fit values of the V_{max} and K_M were significantly different between the two runs, the results were compared by analysing whether a single curve better fits all data points as compared to two separate curves for each data set. Graphpad Prism 5 performs the analysis using the extra sum-of-squares F test. The null hypothesis states “one curve for all data sets” and the alternative hypothesis is “different curve for each data set”. The null hypothesis is rejected if the P-value is less than 0.05. A P value of 0.1288 was obtained and therefore the null hypothesis was not rejected. The experimentally determined kinetic parameters, from the one curve that fit both data sets, are given in Table 5.2.

Table 5.2: Kinetic parameters of *Mt*-SK in the presence of ATP and C8D-ATP

ATP			C8D-ATP		
$K_{m(ATP)}$ (mM)	V_{max} (mM/min)	k_{cat} (s^{-1})	$K_{m(C8D\text{-}ATP)}$ (mM)	V_{max} (mM/min)	k_{cat} (s^{-1})
0.17 ± 0.03	0.059 ± 0.005	28 ± 2	0.16 ± 0.04	0.040 ± 0.004	18 ± 2

© University of Pretoria

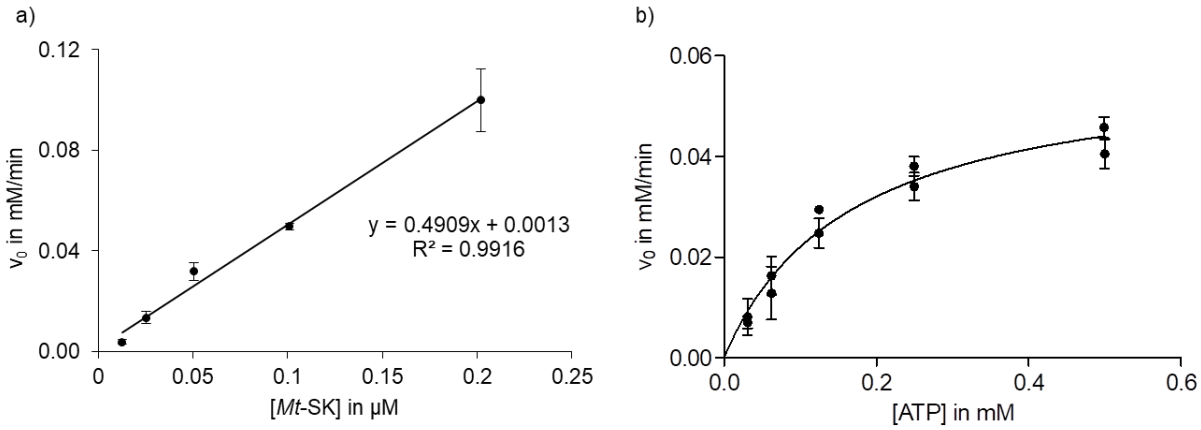

Figure 5.9: a) Linear relationship between *Mt*-SK enzymatic rate and enzyme concentration and b) Michaelis-Menten plot of the rate of reaction of *Mt*-SK at various concentrations of ATP, fitted in GraphPad Prism 5 using one curve fit for both data sets. Standard deviation is shown for each triplicate run.

KIEs on both the V and V/K can be determined with the non-competitive method whereas, with competitive methods, only the V/K KIEs can be studied. With deuterated compounds, generally one can obtain a high percentage of deuteration and hence, the non-competitive method is commonly used/favoured.

The non-competitive study of the KIE of C8D-ATP was performed in which the reactions of *Mt*-SK with ATP and C8D-ATP were conducted simultaneously, varying the concentrations of C8D-ATP and ATP while the shikimic acid concentration was kept constant at 3 mM. The reactions were initiated by the addition of 0.035 µM of *Mt*-SK enzyme and terminated after 3 minutes by the addition of 4 µl formic acid. The Michaelis-Menten plots are given in Figure 5.10 and kinetic parameters in Table 5.2.

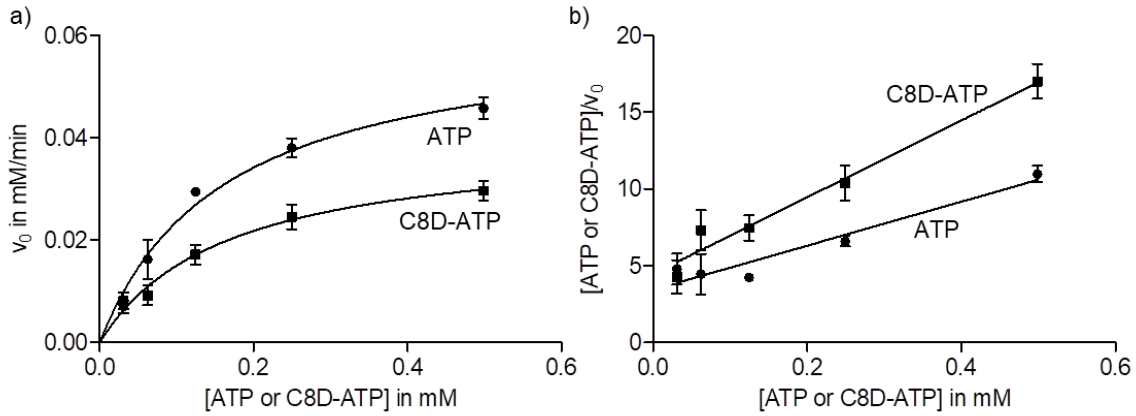

Figure 5.10: Michaelis-Menten plot of the rate of reaction of *Mt*-SK at various concentrations of ATP and C8D-ATP in a non-competitive assay. Data fitted in GraphPad Prism 5. Standard deviation is shown for each triplicate run.

© University of Pretoria

The KIE on V_{max} (^{D}V) and V/K ($^{D}V/K$) was calculated using eqn 5.8 and 5.9, respectively,

$$^{D}V = \frac{V_H}{V_D} \tag{5.8}$$

$$^{D}\frac{V}{K} = \frac{(V/K)_H}{(V/K)_D} \tag{5.9}$$

where V_H and V_D is the V_{max} in the presence of non-deuterated and deuterated ATP, respectively, and $(V/K)_H$ and $(V/K)_D$ is the V_{max}/K_M in the presence of non-deuterated and deuterated ATP.

The observed KIE on Vmax, ^{D}V, is 1.5 which is in good agreement with previously reported values of 1.3 to 2 obtained using HPLC-UV.[29] The KIE on V_{max}/K_M, the rate at which the enzyme and substrate come together to form a complex which will result in a catalytic event to produce the product, is 1.4. This is the first report of a KIE on V/K for *Mt*-SK. The fact that the KIE is present on both V and V/K indicates that the isotope effect doesn't only involve substrate binding (KIE only present on V/K) or product release (KIE only present on V). Since the value of the KIE on V is less than the generally accepted value of 2 for a primary isotope effect, it fails to indicate a C–H bond cleavage as a rate limiting step.

From these results, it is recommended that studies involving competitive assays should be conducted as the sensitivity is much greater, and more precise KIE measurements on $^{D}V/K$ can be obtained. For the success of such an experiment, both substrates, ATP and shikimic acid, will need to be at low concentrations as to not force a large forward commitment which suppresses the KIE.

This high resolution mass spectrometry method developed for the study of the kinetics of Mt-SK using ATP and C8D-ATP seems promising and the data obtained agrees with previously reported results from kinetics and KIE studies of *Mt*-SK with ATP and C8D-ATP. However, it is to be noted here that while the method showed good repeatability and precision, it is suggested that for further studies an internal standard should be used to ensure that no signal suppression occurs after extensive sets of multiple injections.

5.4 Conclusion

Over the years the development of rapid MS techniques for analysing kinetic parameters of enzymatic reactions has proved to be extremely successful. Here, the kinetic parameters and KIE of C8D-ATP for *Mt*-SK were measured using high resolution mass spectrometry and showed good agreement with previously reported data. The high sensitivity, precision and specificity of the MS-based method show promise for conducting quick analysis of kinetic data within minutes without the use of a column. The presented method can be used for quantitative data collection of enzyme assays without sample modification as long as volatile buffers are used.

© University of Pretoria

5.5 References

[1] K. M. Herrmann, in *Amin. Acids Biosynth. Genet. Regul.* (Ed.: R.L. Somerville), Addison-Wesley, **1983**, pp. 301–322.

[2] K. M. Herrmann, *Plant Cell* **1995**, *7*, 907–919.

[3] K. M. Herrmann, L. M. Weaver, *Annu. Rev. Plant Physiol. Plant Mol. Biol.* **1999**, *50*, 473–503.

[4] R. Mir, S. Jallu, T. P. Singh, *Crit. Rev. Microbiol.* **2015**, *41*, 172–189.

[5] R. Ducati, L. Basso, D. Santos, *Curr. Drug Targets* **2007**, *8*, 423–435.

[6] F. Roberts, C. W. Roberts, J. J. Johnson, D. E. Kyle, T. Krell, J. R. Coggins, G. H. Coombs, W. K. Milhous, S. Tzipori, D. J. P. Ferguson, D. Chakrabarti, R. McLeod, *Nature* **1998**, *393*, 801–805.

[7] S. A. Campbell, T. A. Richards, E. J. Mui, B. U. Samuel, J. R. Coggins, R. McLeod, C. W. Roberts, *Int. J. Parasitol.* **2004**, *34*, 5–13.

[8] M. B. Rahul Reddy, S. K. Krishnasamy, M. K. Kathiravan, *Bioorg. Chem.* **2020**, *102*, 104083.

[9] S. M. Kapnick, Y. Zhang, *Expert Opin. Drug Discov.* **2008**, *3*, 565–577.

[10] C. P. Vianna, W. F. de Azevedo, *J. Mol. Model.* **2012**, *18*, 755–764.

[11] V. Prado, E. Lence, J. A. Vallejo, A. Beceiro, P. Thompson, A. R. Hawkins, C. González-Bello, *Chem. - A Eur. J.* **2016**, *22*, 2758–2768.

[12] T. Parish, N. G. Stoker, *Microbiology* **2002**, *148*, 3069–3077.

[13] K. Chen, J. Dou, S. Tang, Y. Yang, H. Wang, H. Fang, C. Zhou, *Bioresour. Technol.* **2012**, *119*, 141–147.

[14] Y. Gu, L. Reshetnikova, Y. Li, Y. Wu, H. Yan, S. Singh, X. Ji, *J. Mol. Biol.* **2002**, *319*, 779–789.

[15] T. Krell, J. Maclean, D. J. Boam, A. Cooper, M. Resmini, K. Brocklehurst, S. M. Kelly, N. C. Price, A. J. Lapthorn, J. R. Coggins, *Protein Sci.* **2001**, *10*, 1137–1149.

[16] M. D. Hartmann, G. P. Bourenkov, A. Oberschall, N. Strizhov, H. D. Bartunik, *J. Mol. Biol.* **2006**, *364*, 411–423.

[17] I. Schlichting, J. Reinstein, *Biochemistry* **1997**, *36*, 9290–9296.

[18] M. Bellinzoni, A. Haouz, M. Graña, H. Munier-Lehmann, W. Shepard, P. M. Alzari, *Protein Sci.* **2006**, *15*, 1489–1493.

[19] M. C. Hutter, V. Helms, *Int. J. Quantum Chem.* **2003**, *95*, 479–486.

[20] L. Mao, Y. Wang, Y. Liu, X. Hu, *J. Mol. Biol.* **2004**, *336*, 787–807.

[21] M. Babor, V. Sobolev, M. Edelman, *J. Mol. Biol.* **2002**, *323*, 523–532.

[22] M. V. B. Dias, L. M. Faím, I. B. Vasconcelos, J. S. de Oliveira, L. A. Basso, D. S. Santos, W. F. de Azevedo, *Acta Crystallogr. Sect. F Struct. Biol. Cryst. Commun.* **2007**, *63*, 1–6.

[23] I. R. Vetter, A. Wittinghofer, *Q. Rev. Biophys.* **1999**, *32*, 1–56.

[24] G. E. Schulz, *Curr. Biol.* **1992**, *2*, 81.

© University of Pretoria

[25] C. Vonrhein, G. J. Schlauderer, G. E. Schulz, *Structure* **1995**, *3*, 483–490.

[26] J. E. Walker, M. Saraste, M. J. Runswick, N. J. Gay, *EMBO J.* **1982**, *1*, 945–951.

[27] J. H. Pereira, J. S. de Oliveira, F. Canduri, M. V. B. Dias, M. S. Palma, L. A. Basso, D. S. Santos, W. F. de Azevedo, *Acta Crystallogr. Sect. D Biol. Crystallogr.* **2004**, *60*, 2310–2319.

[28] C. P. Kenyon, R. L. Roth, *BMC Biochem.* **2012**, *13*, 15.

[29] C. P. Kenyon, A. Steyn, R. L. Roth, P. A. Steenkamp, T. C. Nkosi, L. C. Oldfield, *BMC Biochem.* **2011**, *12*, 36.

[30] J. R. Fox, Proton Magnetic Resonance Spectral Assignments and Deuterium Exchange Reactions in Substituted Purines, University of illinois, Urbana, IL, **1965**.

[31] D. M.-J. S. Buyens, Alkylation of Adenine: A Synthetic and Computational Study of the Reaction Mechanism, **2015**.

[32] W. W. Cleland, *Arch. Biochem. Biophys.* **2005**, *433*, 2–12.

[33] V. E. Anderson, *Curr. Opin. Struct. Biol.* **1992**, *2*, 757–764.

[34] D. B. Northrop, *Biochemistry* **1975**, *14*, 2644–2651.

[35] J. Atzrodt, V. Derdau, W. J. Kerr, M. Reid, *Angew. Chemie Int. Ed.* **2018**, *57*, 1758–1784.

[36] A. Sen, A. Kohen, *J. Phys. Org. Chem.* **2010**, *23*, 613–619.

[37] K. Francis, A. Kohen, *Perspect. Sci.* **2014**, *1*, 110–120.

[38] W. W. Cleland, *J. Biol. Chem.* **2003**, *278*, 51975–51984.

[39] M. Wolfsberg, W. A. Van Hook, P. Paneth, in *Isot. Eff.*, Springer Netherlands, Dordrecht, **2009**, pp. 343–388.

[40] D. B. Northrop, *Annu. Rev. Biochem.* **1981**, *50*, 103–131.

[41] D. B. Northrop, *J. Chem. Educ.* **1998**, *75*, 1153.

[42] D. B. Northrop, *Biochemistry* **1981**, *20*, 4056–4061.

[43] K. M. Roberts, P. F. Fitzpatrick, in *Methods Enzymol.*, **2017**, pp. 149–161.

[44] H. Bisswanger, in *Enzym. Kinet. Princ. Methods*, Wiley-VCH Verlag GmbH & Co. KGaA, Weinheim, Germany, **2017**, pp. 235–267.

[45] J. W. Donovan, in *Methods Enzymol.*, **1973**, pp. 497–525.

[46] W. Jiskoot, V. Hlady, J. J. Naleway, J. N. Herron, **1995**, pp. 1–63.

[47] L. Brand, J. R. Gohlke, *Annu. Rev. Biochem.* **1972**, *41*, 843–868.

[48] S. Y. Yang, H. Schulz, *Biochemistry* **1987**, *26*, 5579–5584.

[49] W. R. McClure, *Biochemistry* **1969**, *8*, 2782–2786.

[50] W. W. Cleland, *Anal. Biochem.* **1979**, *99*, 142–145.

© University of Pretoria

[51] L. A. Rosado, I. B. Vasconcelos, M. S. Palma, V. Frappier, R. J. Najmanovich, D. S. Santos, L. A. Basso, *PLoS One* **2013**, *8*, e61918.

[52] J. Simithy, G. Gill, Y. Wang, D. C. Goodwin, A. I. Calderón, *Anal. Chem.* **2015**, *87*, 2129–2136.

[53] A. Cornish-Bowden, *Fundamentals of Enzyme Kinetics*, Wiley-VCH, Weinheim, **2012**.

[54] M. Chaplin, *Biochem. Educ.* **1989**, *17*, 142–144.

[55] N. W. Charter, L. Kauffman, R. Singh, R. M. Eglen, *J. Biomol. Screen.* **2006**, *11*, 390–399.

[56] X. Ge, T. L. Sirich, M. K. Beyer, H. Desaire, J. A. Leary, *Anal. Chem.* **2001**, *73*, 5078–5082.

[57] A. Liesener, U. Karst, *Anal. Bioanal. Chem.* **2005**, *382*, 1451–1464.

[58] D. B. Northrop, F. B. Simpson, *Bioorg. Med. Chem.* **1997**, *5*, 641–644.

[59] H. Hernández, C. V. Robinson, *J. Biol. Chem.* **2001**, *276*, 46685–46688.

[60] K. D. Greis, *Mass Spectrom. Rev.* **2007**, *26*, 324–339.

[61] B. Bothner, R. Chavez, J. Wei, C. Strupp, Q. Phung, A. Schneemann, G. Siuzdak, *J. Biol. Chem.* **2000**, *275*, 13455–13459.

[62] N. Singhal, M. Kumar, P. K. Kanaujia, J. S. Virdi, *Front. Microbiol.* **2015**, *6*, 1–16.

[63] F. Y. L. Hsieh, X. Tong, T. Wachs, B. Ganem, J. Henion, *Anal. Biochem.* **1995**, *229*, 20–25.

[64] C. S. Ho, C. W. K. Lam, M. H. M. Chan, R. C. K. Cheung, L. K. Law, L. C. W. Lit, K. F. Ng, M. W. M. Suen, H. L. Tai, *Clin. Biochem. Rev.* **2003**, *24*, 3–12.

[65] M. Šebela, *Mass Spectrom. Rev.* **2021**, DOI 10.1002/mas.21733.

[66] M. Krappmann, T. Letzel., in *Protein Pept. Anal. by LC–MS Exp. Strateg.* (Ed.: T. Letzel), RSC Chromatography Monographs 15, Royal Society Of Chemistry, **2011**.

[67] T. Burkhardt, C. M. Kaufmann, T. Letzel, J. Grassmann, *ChemBioChem* **2015**, *16*, 1985–1992.

[68] J.-P. Antignac, K. de Wasch, F. Monteau, H. De Brabander, F. Andre, B. Le Bizec, *Anal. Chim. Acta* **2005**, *529*, 129–136.

[69] A. R. de Boer, T. Letzel, H. Lingeman, H. Irth, *Anal. Bioanal. Chem.* **2005**, *381*, 647–655.

[70] C. R. Mallet, Z. Lu, J. R. Mazzeo, *Rapid Commun. Mass Spectrom.* **2004**, *18*, 49–58.

[71] G. A. Harris, A. S. Galhena, F. M. Fernández, *Anal. Chem.* **2011**, *83*, 4508–4538.

[72] X. Yan, X. Li, C. Zhang, Y. Xu, R. G. Cooks, *J. Am. Soc. Mass Spectrom.* **2017**, *28*, 1175–1181.

[73] R. M. Alberici, R. C. Simas, G. B. Sanvido, W. Romão, P. M. Lalli, M. Benassi, I. B. S. Cunha, M. N. Eberlin, *Anal. Bioanal. Chem.* **2010**, *398*, 265–294.

[74] M.-Z. Huang, C.-H. Yuan, S.-C. Cheng, Y.-T. Cho, J. Shiea, *Annu. Rev. Anal. Chem.* **2010**, *3*, 43–65.

[75] L. Konermann, D. J. Douglas, in *Methods Enzymol.*, **2002**, pp. 50–64.

[76] Z. Li, A. K. Sau, S. Shen, C. Whitehouse, T. Baasov, K. S. Anderson, *J. Am. Chem. Soc.* **2003**,

© University of Pretoria

125, 9938–9939.

[77] M. Krappmann, A. R. de Boer, D. R. W. Kool, H. Irth, T. Letzel, *Rapid Commun. Mass Spectrom.* **2016**, *30*, 1019–1030.

[78] P. V. Attwood, M. A. Geeves, *Anal. Biochem.* **2004**, *334*, 382–389.

[79] B. M. Kolakowski, L. Konermann, *Anal. Biochem.* **2001**, *292*, 107–114.

[80] Q. Fu, J. Tang, M. Cui, Z. Zheng, Z. Liu, S. Liu, *J. Chromatogr. B* **2015**, *990*, 169–173.

[81] T. Steinkamp, A. Liesener, U. Karst, *Anal. Bioanal. Chem.* **2004**, *378*, 1124–1128.

[82] J. Jänis, P. Pulkkinen, J. Rouvinen, P. Vainiotalo, *Anal. Biochem.* **2007**, *365*, 165–173.

[83] N. Pi, M. B. Hoang, H. Gao, J. D. Mougous, C. R. Bertozzi, J. A. Leary, *Anal. Biochem.* **2005**, *341*, 94–104.

[84] C. P. Kenyon, R. L. Roth, C. W. van der Westhuyzen, C. J. Parkinson, *BMC Res. Notes* **2012**, *5*, 131.

© University of Pretoria

Chapter 6 Thesis Summary and Conclusion

6.1 Overall findings of this research

The research conducted in this thesis aimed to investigate i) the chemical behaviour of the adeninate anion in terms of its ion-pairing and self-aggregation in DMSO and the thermodynamic properties governing the regio-selectivity of alkylation and ii) develop a high resolution mass spectroscopy method for studying the kinetic isotope effect of ATP deuterated at the C8 position (C8D-ATP) on the maximal velocity V and on the specificity constant V/K of *Mycobacterium tuberculosis* shikimate kinase. The results will be summarized below in relation to the research aims and questions.

Adeninate ion-pairing. It was of interest to investigate whether or not ion-pairs exist between the adeninate anion and the Na^+ and K^+ counter ion in DMSO solution and to identify the most likely site of the coordination. The research findings indicate that the adeninate anion forms ion-pairs with Na^+ and K^+ ions in DMSO solution. The two counter ions, Na^+ and K^+, most likely coordinate either in a bidentate and/or via unidentate fashion at the N3 and N9 nitrogen atoms of the purine ring. This is proposed in the experimental study and supported by theoretical calculations using Interacting Quantum Atoms and the Reaction Energy Profile Fragment Attributed Molecular System Energy Change protocol. This is in good agreement with previous experimental and theoretical research on the ion-pairing of neutral adenine whereby bidentate coordination of K^+ at the N3 and N9 site of the N7(H) tautomer has been proposed and is more favourable than unidentate coordination at the N7 of the N9(H) tautomer.

Furthermore, the findings report that the binding of Na^+ is preferred over K^+, having the Na^+ result in highly favourable charge polarization of the adeninate anion. Additional insight was obtained through the theoretical studies which indicated an effect on the bond to the exo-cyclic amino group as a result of the coordination of the counter ion to the adeninate anion. Complexation of the ions at the N3 and N9 atoms result in the largest stabilization of the bond which in turn stabilizes the adeninate anion. The involvement of the NH_2 group upon coordination of mono and divalent metal ions to neutral adenine has been investigated previously, i.e. its mode of coordination and changes in the hybridization upon complex formation with metal ions. Hence, the chemical change experienced by the bond to the NH_2 and its effect on the remaining purine upon ion complexation could potentially be used as a tool for predicting the site of coordination.

Self-aggregation of the Na^+ and K^+ adeninate ion-pairs. We wanted to study whether the adeninate anion or its ion pairs form dimers and higher order aggregates in solution and if these aggregates differ in the non-covalent interactions compared to those of neutral adenine. Our study suggests that the adeninate Na^+ and K^+ ion-pairs form π–π stacked dimers at low concentrations. An increase in concentration leads to the formation of higher order aggregates in which it is proposed that the adeninate coordinates via the counter ion of the neighbouring ion-pair. The size of the counter ion influences how the aggregates are arranged or propagated through space. While adenine forms dimers through hydrogen-bonding and π–π stacking, the interactions between adeninate ions could be different due to the change in electron density distribution in relation to neutral adenine. However, self-aggregation is still possible even with the extra negative change in the purine ring. This is probably due to the presence of ion pairs.

© University of Pretoria

The thermodynamic properties governing the alkylation of the adeninate anion. It was of interest to examine the thermodynamic properties which control the reactivity of alkylation at the four nucleophilic nitrogen atoms of the adeninate anion. In this study, the alkylation at the N9, N3 and N7 nitrogen atoms were observed in which the thermodynamic study was only possible for the formation of N9- and N3-benzyladenine. This research suggests that the preference for alkylation at the N9 site over the N3 is due to a large entropic bottleneck of the latter pathway in which a highly ordered TS occurs. Theoretical analysis of the reaction pathways resulted in a good prediction of the N9:N3 rate constant ratio. However, the limitation of mimicking the solvent environment is noted when including the counter ion in the reaction pathway modelling. The DMSO solvent is predicted to largely influence the dissociation of the counter ion as the electrophile approaches.

Two additional findings are presented in this section of research. The first is the identification of a side reaction that depletes the adeninate starting material. This side reaction is proposed to be the Kornblum oxidation reaction. The second finding indicates the entropy-enthalpy compensation effect in the presence of 15-crown-5 ether resulting in no change in the free energy of activation relative to studies in the absence of 15-crown-5 ether.

High resolution MS method development for studying the kinetic isotope effect of C8D-ATP on V and V/K of *Mycobacterium tuberculosis* shikimate kinase. In this section of the research, we wanted to know whether the method developed is sufficiently sensitive enough and reproducible in order to give reliable results and whether or not a kinetic isotope effect exists on the V and on the V/K. In our work, a high resolution MS method has been developed to obtain quantitative data for enzyme kinetics. The validation of the method indicates good sensitivity, precision and specificity. The isotope effect of C8D-ATP on the V and V/K of *Mycobacterium tuberculosis* shikimate kinase has been studied in which a ^{D}V and $^{D}V/K$ of 1.5 and 1.4 are observed, indicating a secondary isotope effect. This is in contrast to previous research in which a primary isotope effect was predicted to occur. The adenine molecule is said to facilitate only in molecular recognition, and our study supports this.

6.2 Contribution made to the field

From the research presented in this thesis, the experimental investigation into the ion-pairing of the adeninate anion and the aggregate formation thereof has been published. This contributes towards the gap in the literature on anionic nucleobases which, along with rare tautomeric forms, can play a role in mutations and replication and translational errors. Our study provides insight into the reactivity of the molecule in relation to interactions with counter ions and aggregation. Studies of the adeninate anion which use different solvents, counter ions and investigate hetero-association with other nucleobases can be compared. The lack of literature on the change in the observable physical properties of the adeninate anion such as the chemical shifts in ^{1}H NMR spectroscopy due to a change in concentration, temperature and counter ions present made it difficult to compare our results with other studies. Thus, our research can provide a building block and reference point for future studies on the adeninate system. DMSO was used as the solvent in this research as it allows for the solubility of the adeninate salt. Many thermodynamic properties of nucleobases are reported in organic solvents that enhance the chemical property being studied. Thus, as we were investigating ion-pairing of the adeninate anion the nitrogen sites of the purine ring needed to be available for metal ion coordination. The use of water as a solvent would have competed for interaction at the

© University of Pretoria

nitrogen atoms through the formation of hydrogen bonds. Furthermore, the studies of the regio-selectivity of the adeninate anion required the use of DMSO and hence, to maintain a common solvent, DMSO was used for all studies of the adeninate anion.

The other section of research in this thesis also provides further information into the subject of the anionic nucleobases, such as the computational study of the ion-pairing and insight into the factors that potentially direct the ion coordination. The use of the REP-FAMSEC protocol has proven a very useful technique for obtaining the changes in the interactions experienced by the adeninate molecule upon complexation of a counter ion at different sites. In addition, it is shown that both the superior CCSD and the DFT level of theory are in good agreement for the in-plane metal coordinated isomers.

For the first time, we report the chemical kinetics for the alkylation of the adeninate anion. The effect of solvent and certain alkylating reagents on the regio-selectivity has been reported before, yet no thermodynamic data is available. Our research provides a base on which future studies of the thermodynamics under different conditions can be compared. In addition, the identification of the side reaction and use of a mop up base can aid in higher yields of the desired N9-alkylated adenine derivatives.

The high resolution MS method developed can allow for quick and reliable data collection of enzyme assays without sample preparation. The reported kinetic isotope effect of C8-ATP on V and V/K of *Mycobacterium tuberculosis* shikimate kinase did not indicate a primary isotope effect. This perhaps sheds some light on whether or not further studies should be conducted using more sophisticated techniques to study an intrinsic isotope effect. However, from the results, it is deemed likely that only a secondary isotope effect is present.

6.3 Limitations of the study

The research aims and questions have been addressed through this research, however, our work doesn't come without limitations. Firstly, it was impossible to obtain the free adeninate anion for the ^{1}H NMR studies. The expected change in the ^{1}H NMR chemical shifts to support the regain of electron density after the addition of the 15-crown-5 or 18-crown-6 ether to the Na^{+} and K^{+} adeninate complexes, respectively, were never observed. Hence, we could not conclude on any chemical behaviour of the free adeninate anion in solution. The free adeninate anion was only observed in the UV spectroscopy studies which allowed for much lower concentrations to be used in which the 15-crown-5 and 18-crown-6 were added in great excess. Secondly, with the concentration limit of detection in ^{1}H NMR spectroscopy, we could not obtain enough points to study the concentration and temperature dependent behaviour of the proposed π–π stacked dimers.

The experimental rates reported for the study of the alkylation of the adeninate anion were obtained via the initial rates method. The non-linear regression method for fitting experimental data is more accurate, however, the input in Origin Pro for the fit of parallel second order reactions was not available and building a model was out of the expertise of the researcher. Furthermore, the complication of including the counter ion in the theoretical modelling of the reaction pathways was reported here in which the experimental trends couldn't be well recovered due to the increase in energy required to remove the counter ion from the N3 and N9 site as the electrophile approaches.

© University of Pretoria

And lastly, the limitation of the study performed by the high performance MS method was noted around extensive consecutive injections. While the method is accurate for the set of injections used for the standard curve and the replication sets used to validate the method, the enzyme assay analysis included many more injections of the assays performed. It was considered that single suppression can occur towards the end of the experiment.

6.4 Future work

From interesting findings in the thesis and the limitations presented above, we will recommend some future research to better develop the studies covered and the data collected.

1) The NH_2 peak in the ^1H NMR spectra of the K^+ adeninate ion-pair was absent. Evidence of the appearance of the NH_2 peak is observed at very low concentrations in the presence of the 18-crown-6 ether. Further work is needed to investigate why the NH_2 peak is absent.
2) Research on obtaining and studying the concentration and temperature dependent nature of the free adeninate anion should be conducted to investigate its ability to form aggregates and the mode of aggregation.
3) ^1H NMR spectroscopy techniques with higher resolution can be used to obtain the monomer chemical shifts of the Na^+ and K^+ adeninate ion-pairs at very low concentrations. This would allow for the association constant for the proposed π–π stacked dimerization to be obtained.
4) Non-linear regression analysis of parallel second order reactions should be used in further studies to fit experimental data for the study of the alkylation of the adeninate anion to obtain more accurate rates of reaction.
5) Theoretical studies of the pathways leading to the N1-, N3-, N7- and N9-alkylated adenine with the inclusion of DMSO solvent molecules can be investigated to determine if the experimental data can be better replicated.
6) The proposed Kornblum oxidation reaction should be investigated to confirm whether or not this is indeed responsible for the protonation of the adeninate anion.
7) Future studies utilizing the high resolution MS method developed here can include an internal standard to investigate any signal suppression after extensive consecutive injections.

© University of Pretoria

List of Figures

Figure 1: Chemical structures and numbering of guanine, adenine, cytosine and thymine. 3

Figure 2.1: The configuration of the adenyl group involved in Watson-Crick, reversed Watson-Crick, Hoogsteen and reversed Hoogsteen bonding with thymine. 11

Figure 2.2: Metal coordination (M = metal ion) via the N1, N3, N9 and N7 (left to right) nitrogen atoms of the adeninate anion. IUPAC numbering of adenine purine ring shown on the first structure. 11

Figure 2.3: Hydrogen-bond π-polarization model for (a, b) Watson-Crick hydrogen bonding between adenine with a carboxylic acid and uracil, respectively and c) Hoogsteen type hydrogen bonding with uracil. Partial negative (δ-) and positive (δ+) charges are shown. 13

Figure 2.4: π-π stacking geometry of aromatic systems. 15

Figure 2.5: Concentration dependent UV absorption profile of a) Na-Ade and b) K-Ade in DMSO/H_2O (dotted lines) and anhydrous DMSO (solid lines) for the concentration range (0.05 – blue, 0.075 – red, 0.10 – green, 0.15 – pink, 0.20 – orange, in mM) and in the presence of a large excess of 15C5 (126 eq) and 18C6 (117 eq) ether, respectively (dashed black lines) are shown. Shoulder bands are indicated by red arrows. 19

Figure 2.6: Superimposed ^{1}H NMR spectra of Na-Ade (blue), K-Ade (green) and K-Ade(18C6) (black) at a) dilute concentrations of 1.44, 2.11 and 0.489 mM, respectively, with data for K-Ade(18C6) shown in the insert b) Saturated concentrations of 52.2, 84.8 and 78.7 mM, respectively, and c) ^{1}H decoupled ^{13}C NMR at the saturated concentrations, in DMSO-d_6. 21

Figure 2.7: Molecular structure of Na-Ade and XRD structure of the zigzag packing morphology of crystals obtained from DMSO-d_6 solutions, viewed along the a axis. Refer to Figure S1.13 for K-Ade data. 23

Figure 2.8: Coordination obtained from XRD of Na-Ade showing one counter ion complexed with three adenine molecules and one adenine complex with three counter ions. The numbering of specified atoms and dihedral angles relate to the geometric parameters are given in Table S1.4. Refer to Figure S1.14 for K-Ade data. 24

Figure 2.9: a): Herringbone (blue) XRD packing morphology of the K-Ade(18C6) crystal obtained from DMSO-d_6 solutions viewed along the indicated axis and b) the hydrogen bonding (red lines) and interaction with the K^+ ion at the N3 and N9 atoms (black lines). The numbering of specified atoms and dihedral angles relate to the geometric parameters are given in Table S1.4. 24

Figure 2.10: Proposed counter ion coordination between K^+ and Na^+ with the adeninate anion via the N3N9, N9 or N3 nitrogen atoms. 25

© University of Pretoria

Figure 2.11: Unlikely ion-pair interactions. Repulsion of counter ion M^+ (where $M^+ = Na^+$ or K^+) with the hydrogen on the NH_2 disfavours coordination via the N1 (M-Ade(N1)) and N7 (M-Ade(N7)) atoms. The potential cation-π interaction (M-Ade(π)) is predicted to be weaker than the cation-heteroatom interactions. 25

Figure 2.12: Graphical representation of the concentration dependent ^1H NMR chemical shift for the indicated protons of Na-Ade (blue squares), Na-Ade(15C5) (green diamonds), K-Ade (blue triangles) and K-Ade(18C6) (green circles) at the indicated concentrations (mM) in DMSO-d_6 at 320 K. Chemical shifts of Adenine purine protons are shown in black for comparison purpose. 26

Figure 2.13: Change in chemical shift of purine protons with the change in concentration for a) Na-Ade (blue lines) and K-Ade (green lines) and b) Na-Ade(15C5) (blue lines) and K-Ade(18C6) (green lines) in DMSO-d_6 at 320 K. NH_2 – squares, C8-H – circles and C2-H – triangles. The added concentration of crown ether is 2.4 times that of Na-Ade (K-Ade). Region 1 (highlighted in blue and green for Na-Ade and K-Ade, respectively) and region 2 indicates concentration dependent change in chemical shift. 27

Figure 2.14: Change in chemical shift of the CH_2 protons of 15C5 and 18C6 ether with concentration in the presence of Ade^-Na^+ and Ade^-K^+, respectively, at a 2.4-fold excess concentration of crown ether and 320 K in DMSO. 27

Figure 2.15: The change in temperature coefficients with concentration of ^1H chemical shifts of a) Na-Ade and K-Ade and b) CH_2 of 15-crown-5 ether and the 18-crown-6 ether in DMSO-d_6. NH_2 (squares), C8-H (circles) and C2-H (triangles). The shading relates to the regions defined in Figure 2.13. Refer to Figure S1.7 for the change in δ with temperature (300 K - 380 K). 29

Figure 2.16: a) Cation induced change in atomic electron density in Na-Ade and K-Ade relative to Adenine, based on the NMR chemical shifts in Table 4. Two shades of blue indicate shifts towards more positive, red towards more negative charge. Suggested structures of π-π stacked dimers with the cation b) in-plane and c) shared between the two adeninate anions, and d) in-plane hydrogen bonded dimer structures. Hydrogen bonding is indicated by red lines. 31

Figure 2.17: Hydrogen bonded aggregates of K-Ade(18C6). Hydrogen bonding is shown by red dashed line. 32

Figure 2.18: M-Ade aggregate formation via the N1 and/or the N7. 34

Figure 2.19: Van't Hoff plot of the association constant for the self-aggregation of Na-Ade (blue), Na-Ade(15C5) (red) and K-Ade (green) and the 1:1 complexation between 15C5 ether and Na^+ in DMSO-d_6 as the solvent. 35

Figure 3.1: Chelation of metal ion with the dominant forms of adenine, guanine and cytosine nucleobases. 45

© University of Pretoria

Figure 3.2: Unidentate metal ion coordination of dominant tautomeric form of adenine, uracil and thymine..... 46

Figure 3.3: Metal ion complexes with tautomeric forms of adenine. 48

Figure 3.4: Coordination of neutral, cationic and anionic Au, Au^{+}, Zn^{2+} and Cu^{+} to adenine. 49

Figure 3.5: Isomerization of $[Cp_2Mo(II)(9\text{-methyladenyl})][PF_6]$ from the bidentate coordination via the N1 and N6 (31) to the N7 and N6 (32) of adenine. 50

Figure 3.6: Bidentate metal ion complexation at the N7 and N6 atoms of adenine, where M = Rh(II), Ir(III), or Ru(II). 51

Figure 3.7: Optimized structures of Na- and K-Ade complexes at CCSD/6-311++g(d,p)/PCM(DMSO), * structure of K-Ade(π) obtained at DFT/M06-2X /6-311++g(d,p)/PCM(DMSO). 54

Figure 3.8: The numbering of the atoms of the adeninate anion. 56

Figure 3.9: Changes in the diatomic covalent bond intramolecular interactions, $\Delta \mathrm{C}-\mathrm{B}E\mathrm{intA},\mathrm{B}$, and its $\Delta V\mathrm{clA},\mathrm{B}$ and $\Delta V\mathrm{xcA},\mathrm{B}$ components. Blue and red sites indicate stabilizing and destabilizing energy terms of the adeninate anion upon coordination of Na^{+} for the Na-Ade isomers, at CCSD level of theory. 61

Figure 3.10: Changes in the diatomic covalent bond intramolecular interactions, $\Delta \mathrm{C}-\mathrm{B}E\mathrm{intA},\mathrm{B}$, and its $\Delta V\mathrm{clA},\mathrm{B}$ and $\Delta V\mathrm{xcA},\mathrm{B}$ components. Blue and red sites indicate stabilizing and destabilizing energy terms of the adeninate anion upon coordination of K^{+} for the Na-Ade isomers, at CCSD level of theory. 62

Figure 3.11: Relationship between rho (ρ) at BCP(C6,N10) and the C6–N10 bond length of the Na^{+} (blue circles), K^{+} (red circles) structural isomers and Ade^{-} (black outlined circle) at CCSD level of theory. 64

Figure 3.12: Relationship between rho (ρ) at BCP(C6,N10) and the DI(C6,N10) bond length of the Na^{+} (blue circles), K^{+} (red circles) structural isomers and Ade^{-} (black outlined circle) at CCSD level of theory. 64

Figure 3.13: Relationship between $\Delta V\mathrm{neC6},\mathrm{N10}$ (primary axis, circles) and $\Delta V\mathrm{nnC6},\mathrm{N10}$ (secondary axis, triangles) with the C6–N10 bond length of the Na^{+} (blue data points) and K^{+} (red data points) structural isomers and Ade^{-} (black outlined circle) at CCSD level of theory. 65

Figure 3.14: All individual coulombic, $V\mathrm{clA},\mathrm{Na}+$ - blue bars, and exchange-correlation, $V\mathrm{XCA},\mathrm{Na}+$ - red bars, contributions to $\mathrm{inter}E\mathrm{intNa}+,\mathrm{Ade}-$ from atom A with Na^{+}, where atom A is all atoms of the adeninate anion, for the Na-Ade isomers, at CCSD level of theory. 68

Figure 3.15: All individual coulombic, $V\mathrm{clA},\mathrm{K}+$ - blue bars, and exchange-correlation, $V\mathrm{XCA},\mathrm{K}+$ - red bars, contributions to $\mathrm{inter}E\mathrm{intK}+,\mathrm{Ade}-$ from atom A with K^{+}, where atom A is all atoms of the adeninate anion, for the K-Ade isomers, at CCSD level of theory. 69

© University of Pretoria

Figure 3.16: Orientation of the four DMSO solvent molecules for M-Ade(N3N9). 70

Figure 3.17: Optimized structures of heteroatom coordinated isomers of Na-Ade (a-e) and K-Ade (f-g) complexes with 4 explicit DMSO solvent molecules at DFT/B3LYP/6-311G++(d,p)/PCM(DMSO)... 72

Figure 3.18: Optimized structures of (N10) isomers of Na-Ade (a and b) and K-Ade (c) complexes with 4 explicit DMSO solvent molecules at DFT/B3LYP/6-311G++(d,p)/PCM(DMSO). 73

Figure 4.1: Chemical structures and numbering of guanine, adenine, cytosine and thymine. 80

Figure 4.2: S_N2 substitution reaction for the synthesis of N9-alkylated adenine. 80

Figure 4.3: S_N2 reaction mechanism. Nu− is the nucleophile and LG is the leaving group. 83

Figure 4.4: A More O'Ferrall plot for an S_N2 reaction (A) and an S_N1 reaction (B). 84

Figure 4.5: Hydrogen bond formation between chloromethyl pivalate and NH_2 of the adeninate anion. 86

Figure 4.6: Carbocation formation of benzyl halides and delocalization of the positive charge. 88

Figure 4.7: Alkylation of Na-Ade in anhydrous DMSO using benzyl bromide (1), (1-bromoethyl)benzene (2) or pentafluorobenzyl bromide (3) as the alkylating reagent. Products formed are N1-, N3-, N7- and N9-R adenine derivatives. 89

Figure 4.8: Dynamic ^{1}H NMR spectra for the alkylation of adeninate anion (40 mM) with a) benzyl bromide, b) (1-bromoethyl)benzene and c) pentafluorobenzyl bromide at 5 eq. in anhydrous DMSO-d_6. N9- and N3-R adenine alkylated derivatives are shown by the green and yellow lines, respectively. 92

Figure 4.9: Kornblum oxidation reaction involving DMSO and alkyl halides 1, 2 and 3 in the presence of a base. 94

Figure 4.10: Dynamic ^{1}H NMR spectra for the alkylation of K-Ade with a) (1-bromoethyl)benzene and b) (1-bromoethyl)benzene in the presence of 18-crown-6 ether in DMSO-d_6 at 295K. 95

Figure 4.11: Dynamic ^{1}H NMR spectra for the alkylation of adenine with benzyl chloride in the presence of a) 1 eq. BnCl and TEA, b) 8 eq. BnCl and TEA, c) 1 eq. BnCl and DBU and d) 8 eq. BnCl and DBU in anhydrous DMSO at 295 K. N9- and N3-Bn adenine alkylated derivatives are shown by the green and yellow lines, respectively. 98

Figure 4.12: The reaction profile dependency of N9-Bn and N3-Bn on the concentration of a) BnCl in the presence of BnCl:DBU 1:1 at concentrations 13.8 - yellow, 27.6 - red, 55.2 - orange, 82.8 - blue and 110 mM – green, and b) Na-Ade at concentrations 5.85 - red, 12.2 - orange, 25.0 - blue and 48.5 mM - green in DMSO-d_6 at 295 K. The corresponding log(rate) vs c) log[BnCl] in the presence of DBU (solid circles) and TEA (black outlined circles) and d) log[Na-Ade] for N9-Bn and N3-Bn in anhydrous DMSO. 99

© University of Pretoria

Figure 4.13: ^{1}H NMR of a solution of a) DBU (63.9 mM), and DBU and BnCl (65.17 mM) at b) t=0, c) t=30 minutes and d) t=24 hours..... 100

Figure 4.14: Plot of N9- and N3-Bn concentration over time during the benzylation of Na-Ade (6.65 mM) with BnCl (14.1 mM) and DBU (7.14 mM) in anhydrous DMSO-d_6 at 320 K. The average over three replicates is shown by the solid black line with error bars. 101

Figure 4.15: a) Observed rate of formation for N9- and N3-Bn in the absence (black data points) and presence (red data points) of 15C5 and b) the Eyring plots thereof in anhydrous DMSO-d_6 for the temperature range indicated, increasing in 5 K intervals. 102

Figure 4.16: $\Delta H^{\ddagger}$ vs. $T\Delta S^{\ddagger}$ enthalpy-entropy compensation plot for the formation of N9-Bn and N3-Bn in the absence and presence of 15C5 in anhydrous DMSO at 300 K..... 104

Figure 4.17: The change in measured the ratio of the rate of N9-Bn/N3-Bn with temperature in the absence (black data points) and presence (red data points) of 15C5 in anhydrous DMSO..... 105

Figure 4.18: Comparison of the curvature of the PES of two transition states reached via pathways 1 and 2.[106]..... 106

Figure 4.19: Optimized transition state structures in the absence of the Na^{+} ion (N1-Bn, N3-Bn, N7-Bn and N9-Bn). N*X*—CH_2 and CH_2—Cl bond lengths are shown in Å. 108

Figure 4.20: Optimized transition state structures in the presence of Na^{+} (N1-Bn-Na, N3-Bn-Na, N7-Bn-Na and N9-Bn-Na). N*X*—CH_2 and CH_2—Cl bond lengths are shown in Å. 109

Figure 4.21: The ΔE_{ZPVE} along the reaction path for the formation of N1-, N3-, N7- and N9-Bn in a) the absence and b) in the presence of the Na^{+} ion. 110

Figure 4.22: The ΔG along the reaction path for the formation of N1-, N3-, N7- and N9-Bn in a) the absence and b) in the presence of the Na^{+} ion. 110

Figure 4.23: a) ΔE (kJ mol^{-1}) along the reaction coordinate d(N9, Na) in Å, resulting from scanning the Na^{+} ion away from the adeninate anion of the Na-Ade(N3N9) complex, and b) optimized structures for the yellow, green and blue points shown in (a)..... 113

Figure 4.24: a) ΔE (kJ mol^{-1}) along the reaction coordinate d(N9, Na) in Å, resulting from scanning the Na^{+} ion away from the adeninate anion of the Na-Ade(N3N9)-4DMSO complex, and b) optimized structures for the yellow, green and blue points shown in (a). 114

Figure 5.1: Phosphorylation of shikimate to shikimate-3-phosphate by shikimate kinase. 121

Figure 5.2: The "push" mechanism demonstrated for shikimate kinase, adjusted from reference [28]. 122

Figure 5.3: The "pull" mechanism demonstrated for shikimate kinase, adjusted from reference [28]. 123

Figure 5.4: Range of measurable deuterium isotope effects for an ordered mechanism..... 124

© University of Pretoria

Figure 5.5: Coupled assay for monitoring the kinetics of Mt-SK via UV-spectroscopy..... 126

Figure 5.6: Diagram of an on-line rapid-mixing continuous flow ESI-MS set up. 129

Figure 5.7: a) Mass spectrum of ADP (*m/z* = 428.0383, $[ADP+H]^+$) and ATP (*m/z* = 508.0089, $[ATP+H]^+$) with ATP sodium (*m/z* = 529.29733, $[ATP+Na]^+$) and potassium (*m/z* = 545.9628, $[ATP+K]^+$) adducts, and b) the change in ADP peak intensity with increasing concentration. 133

Figure 5.8: a) Standard curve obtained by measuring the ADP signal at *m/z* = 428.0383 over the scan range 1 to 100, b) instruments response to various concentrations of ATP and C8D-ATP. The counts of ATP (*m/z* = 508.0089) and C8D-ATP (5090124) over the scan range of 5-100 were used. % RSD is given for both plots..... 134

Figure 5.9: a) Linear relationship between *Mt*-SK enzymatic rate and enzyme concentration and b) Michaelis-Menten plot of the rate of reaction of *Mt*-SK at various concentrations of ATP, fitted in GraphPad Prism 5 using one curve fit for both data sets. Standard deviation is shown for each triplicate run. 136

Figure 5.10: Michaelis-Menten plot of the rate of reaction of *Mt*-SK at various concentrations of ATP and C8D-ATP in a non-competitive assay. Data fitted in GraphPad Prism 5. Standard deviation is shown for each triplicate run. 136

© University of Pretoria

List of Tables

Table 2.1: The λ_{max} and (shoulder) bands (nm) in the UV absorption spectrum of Na- and K-Ade, Na-Ade(15C5) and K-Ade(18C6) in DMSO/H_2O and anhydrous DMSO 20

Table 2.2: ^{1}H and ^{13}C NMR chemical shifts (ppm) of adenine, Na-Ade, K-Ade and K-Ade(18C6) in DMSO-d_6 as solvent at saturated concentrations. The values in parentheses are the changes relative to free Adenine. 22

Table 2.3: Aggregation constants and thermodynamic parameters for the self-aggregation of Na-Ade, Na-Ade(15C5) and K-Ade and the association constant for the 1:1 complexation between C15C and Na^+ in DMSO-d_6 as solvent at 305 K 35

Table 3.1: Relative to the LEC, the difference in electronic energy (ΔE in kcal mol^{-1}) of Na- and K-Ade complexes 53

Table 3.2: The Energy of Formation (E_f) of Na- and K-Ade complexes (kcal mol^{-1}) 55

Table 3.3: Net atomic charge of N-atoms of free Ade^- Q(N), and the changes in charge of the N-atoms of M-Ade relative to free Ade^-, ΔQ(N), the net molecular charge of Ade^- $Q(Ade^-)$ and the change $\Delta Q(Ade^-)$,' the net atomic charge of free Na^+, ($Q(Na^+)$) and K^+ ($Q(K^+)$) and the change in charge relative to free Na^+, ($\Delta Q(Na^+)$) and K^+ ($\Delta Q(K^+)$), upon formation of Na- and K-Ade structural isomers, at CCSD level of theory (all values in *e*) 57

Table 3.4: Net atomic charge of N-atoms of free Ade^- Q(N), and the changes in charge of the N-atoms of M-Ade relative to free Ade^-, ΔQ(N), the net molecular charge of Ade^- $Q(Ade^-)$ and the change $\Delta Q(Ade^-)$,' the net atomic charge of free Na^+, ($Q(Na^+)$) and K^+ ($Q(K^+)$) and the change in charge relative to free Na^+, ($\Delta Q(Na^+)$) and K^+ ($\Delta Q(K^+)$), upon formation of Na- and K-Ade structural isomers, at the DFT/B3LYP level of theory (all values in *e*) 58

Table 3.5: Changes in the total intramolecular interaction energy of Ade^-, the covalent bond (C-B) strength including the exchange correlation and classical term components, and long-distance (L-D) interactions computed on the formation of the Na-Ade and K-Ade structural isomers at the CCSD level of theory. All values in kcal mol^{-1} 59

Table 3.6: Changes in the total intramolecular interaction energy of Ade^-, the covalent bond (C-B) strength including the exchange correlation and classical term components, and long-distance (L-D) interactions computed on the formation of the Na-Ade and K-Ade structural isomers at the DFT/B3LYP level of theory. All values in kcal mol^{-1} 60

Table 3.7: Intermolecular interaction energy and its exchange correlation and classical components for the ionic bond between Ade^- and M^+, where M^+ = Na^+ and K^+, of the Na- and K-Ade structural isomers, CCSD level of theory. All values in kcal mol^{-1} 66

© University of Pretoria

Table 3.8: Intermolecular interaction energy and its exchange correlation and classical components for the ionic bond between Ade^- and M^+, where $M^+ = Na^+$ and K^+, of the Na- and K-Ade structural isomers, DFT/B3LYP level of theory. All values in kcal mol^{-1} 67

Table 3.9: Summation of the intramolecular and intermolecular interaction energy (in kcal mol^{-1}) of the Na- and K-Ade structural isomers at CCSD level of theory 70

Table 3.10: Summation of the intramolecular and intermolecular interaction energy (in kcal mol^{-1}) of the Na- and K-Ade structural isomers at DFT/B3LYP level of theory 70

Table 3.11: Diatomic intermolecular interactions between the coordinating nitrogen atom(s) of Ade– and the counter ion, Na^+/K^+, in Na- And K-Ade-4DMSO complexes 73

Table 4.1: N9:N3:N7 product ratio (%) from the alkylation of the adeninate anion using different bases.[17] 82

Table 4.2: Dependence of the adeninate anion N9:N3:N7 product ratio on the alkylating reagent[15] 85

Table 4.3: ^1H NMR chemical shifts for N9- and N3-R adenine derivatives in anhydrous DMSO-d_6 91

Table 4.4: Proton T_1 relaxation times of Na-Ade, N9- and N3-benzyladenine in DMSO-d_6 at 295 K... 97

Table 4.5: Slope derived from the log(rate) vs log(BnCl) and log(Na-Ade) for N9-Bn and N3-Bn in anhydrous DMSO at 295 K. 97

Table 4.6: Experimental thermodynamic parameters for the formation of N9- and N3-Bn in anhydrous DMSO in the absence and presence of 15C5 103

Table 4.7: Arrhenius parameters for N9-Bn and N3-Bn 103

Table 4.8: Calculated thermodynamic parameters and rate constant for the formation of N1-, N3-, N7- and N9-Bn including all LVFs and using Truhlar's quasiharmonic approximation – values in brackets, in the absence and presence of the Na^+ ion 112

Table 5.1: Steady state kinetic parameters of *Mt*-SK from literature 127

Table 5.2: Kinetic parameters of *Mt*-SK in the presence of ATP and C8D-ATP 135

© University of Pretoria

Appendix 1

© University of Pretoria

doi.org/10.1002/cphc.202100098

Towards a Molecular Understanding of Cation-Anion Interactions and Self-aggregation of Adeninate Salts in DMSO by NMR and UV Spectroscopy and Crystallography

Dominique M. S. Buyens,[b] Lynne A. Pilcher,[b] and Emil Roduner*[a, b]

Rare anionic forms of nucleic acids play a significant biological role and lead to spontaneous mutations and replication and translational errors. There is a lack of information surrounding the stability and reactivity of these forms. Ion pairs of mono-sodium and -potassium salts of adenine exist in DMSO solution with possible cation coordination sites at the N1, N7 and N9 atoms of the purine ring. At increasing concentrations π-π stacked dimers are the predominant species of aggregates followed by higher order aggregation governed by coordination to metal cations in which the type of counter ion present has a central role in the aggregate formation.

1. Introduction

Non-covalent interactions governing the aggregation of isolated purine bases, such as hydrogen bonding and π-π stacking, have been investigated in order to gain greater understanding of their role in structure, function and stability since Watson and Crick (1953) proposed the structure of DNA. It is well known that adenine is involved in Watson-Crick[1] (WC) along with reversed WC,[2] Hoogsteen[3] (HG) and reversed HG[4] type hydrogen bonding with thymine and uracil in DNA and RNA, respectively. The self-[5–7] and hetero-association of adenine and adenine derivatives with other nucleobases[8,9] and carboxylic acids[10–12] has been extensively investigated.

The binding of alkali metal ions such as Na^+ and K^+ to nucleobases influences the structural integrity of DNA and play a role in synthesis, replication, recognition and cleavage of DNA and RNA.[13,14] Binding of metal ions can interfere with hydrogen bonding and stacking interactions between base pairs and compromise the structural stability of DNA.[15] Experimentally, the affinity for alkali metals increase in the order guanine > cytosine > adenine > thymine > uracil, following the trend of proton affinity in nucleobases.[13,16] The preferred binding sites of metal ions are the N7 in adenine, the N7 and O6 atoms in guanine, the N3 and O2 atoms in cytosine and the O4 in thymine and uracil.[13] The three dimensional folding adopted by nucleic acid repeat sequences show ion dependency[17,18] which further highlights the role and importance of monovalent metal ions in DNA structure.

The multi-site coordination and ability of nucleobases to interact non-covalently has rendered them desirable ligands in the synthesis of stable bio-metal-organic frameworks that can have structural flexibility.[19–22] Metal complexes of adenine can have mono- or bidentate coordination through different combinations of N3, N7 and N9 nitrogen atoms and its deprotonated form (adeninate anion) can be di, tri- or tetradentate, have varying coordinate combinations through the N1, N3, N7 and N9 atoms (see reference within the review[20] and reference[23]) and bridging through the N3, N7 and N9 atoms.[24]

The presence of disfavored tautomeric and anionic forms of nucleic acids can form WC-like mispairs (i.e. guanine-thymine, adenine-cytosine and guanine-uracil) that are involved in mutations and replication and translational errors.[25–28] These forms of nucleic acids are also believed to play a role in nucleic acid catalysis[29] and RNA-ligand recognition.[30] The anion forms, such as adeninate anion, features in investigations surrounding the photostability of nucleic acids in DNA[31,32] and is also used in the synthesis of N9-substituted adenines, which have important biological roles such as anti-asthmatic[33] and anti-inflammatory activity,[34] activity against diseases such as multiple sclerosis and autoimmune disease.[35]

There is a lack of information surrounding anionic forms of nucleobases and is a topic being addressed currently.[26,36] Studies involving the chemical properties of the free adeninate anion and its interactions with monovalent alkali metals are limited. In this paper the ion-pair formation of the adeninate anion with the biologically important monovalent metals, Na^+ (Na-Ade) and K^+ (K-Ade), and the self-aggregation of these ionic complexes in DMSO are investigated using NMR and UV spectroscopy as well as XRD of crystal structures. In addition, we have studied the influence of the 15-crown-5 (15C5) and 18-crown-6 (18C6) ether on the spectroscopic and crystal structures of Na-Ade and K-Ade. To this end we show that ion-pair

[a] Prof. Dr. E. Roduner
Institute of Physical Chemistry
University of Stuttgart
70569 Stuttgart, Germany
E-mail: e.roduner@ipc.uni-stuttgart.de
[b] D. M. S. Buyens, Prof. Dr. L. A. Pilcher, Prof. Dr. E. Roduner
Department of Chemistry
University of Pretoria
Pretoria 0002, Republic of South Africa

Supporting information for this article is available on the WWW under https://doi.org/10.1002/cphc.202100098

© 2021 The Authors. ChemPhysChem published by Wiley-VCH GmbH. This is an open access article under the terms of the Creative Commons Attribution License, which permits use, distribution and reproduction in any medium, provided the original work is properly cited.

© University of Pretoria
© 2021 The Authors. ChemPhysChem published by Wiley-VCH GmbH

formation exists between the adeninate anion and the counter ions even at extremely dilute concentrations and that self-aggregation of these complexes is highly influenced by the counter ion present. Furthermore, there is a possibility of complex formation between K-Ade and the 18-crown-6 ether.

2. Results and Discussion

2.1. Ion Pairing

The use of organic solvents such as DMSO, DMF, methanol etc., has an effect on the non-covalent interactions (such as hydrogen bonding, pi-pi stacking and cation binding) of nucleic acids[37] and therefore on the interactions of nucleobases as well. However, many thermodynamic properties of nucleobases are reported in organic solvents or co-solvents of water and organic solvents in order to enhance the chemical property being studied or to understand the effect of solvent.[38] It is important to note that often nucleobase derivatives are used in aqueous media due to the low solubility of free nucleobases.[39]

In order to gain an understanding of the interactions between adenine and the counter ion, the experiments are conducted in a solvent which allowed for the solubility of adenine and the adeninate salt and allows for potential ion-pairing. DMSO, which acts as a hydrogen bond acceptor only, will not form hydrogen bonds at nitrogen sites of adenine rendering these sites available for metal ion coordination. Moreover, further studies conducted of the regio-selectivity of the adeninate salt (publication in preparation) require the use of DMSO and hence, to maintain a common solvent, DMSO is used to perform these studies.

The UV studies performed showed a significant dependence on the counter ion present indicating that ion pairs exist between the adeninate anion and the Na^+/K^+ counter ion. The normalized UV absorption profiles of Na-Ade and K-Ade in anhydrous DMSO are shown in Figure 1 (UV absorbance spectra, Figure S21). The λ_{max} and shoulder bands observed are reported in Table 1. The blueshift of the λ_{max} from K-Ade (272 nm) to Na-Ade (269 nm) in DMSO is associated with the larger stabilization of the ground state of the anion by the Na^+ counter ion which has a stronger cationic field strength due to its smaller ionic radius compared to K^+.[40,41]

Water molecules should facilitate the dissociation of the counter ion from the adeninate ion pair. Studying the system with a small amount of water present (5.2% v/v H_2O) provides insight into i) how the Na- and K-Ade complexes respond to interactions with water and ii) how the M-Ade concentration dependent characteristics of the bands change (normalized UV absorption profiles in DMSO/H_2O, Figure S22). The blueshift from DMSO to DMSO/H_2O for both ionic complexes is due to the hydrogen bonding of water stabilizing the ground state of the anion. Conversely, the solvation of the adeninate anion by polar solvents stabilizes the π^* orbital, resulting in a redshift of the λ_{max} with increasing polarity and hydrogen-acceptor properties of the solvent.[42] A M-Ade concentration dependent redshift is observed in DMSO/H_2O, having the Na-Ade shift from

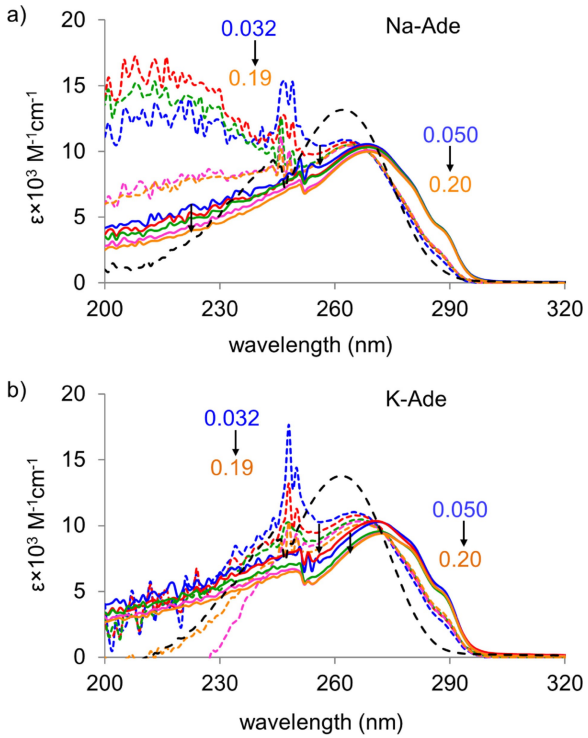

Figure 1. Concentration dependent UV absorption profile of a) Na-Ade and b) K-Ade in DMSO for the concentration range (0.05 – blue, 0.075 – red, 0.15 – green, 0.10 – pink, 0.20 – orange, in mM) and in the presence of a large excess of 15C5 (126 eq) and 18C6 (117 eq) ether, respectively (dashed black lines).

Table 1. The λ_{max} and (shoulder) bands in the UV absorption spectrum of Na- and K-Ade, Na-Ade(15C5) and K-Ade(18C6) in DMSO/H_2O and DMSO.

Solvent	λ_{max} [nm]
DMSO/H_2O + NaH	246, 250, 264→265 (278, 287)
DMSO/H_2O + KH	248, 250, 264→269 (278, 287)
DMSO + NaH	251, 254, 269 (278, 287)
DMSO + KH	251, 253, 272 (278, 287)
DMSO/H_2O + NaH + 15C5	245, 262
DMSO/H_2O + KH + 18C6	245, 262

262 to 265 nm and K-Ade shift from 264 to 269 nm, accompanied by the increase in shoulder band intensity at 278 and 287 nm, which are attributed to the presence of the cationic and anionic species.[42] These shoulder bands decrease in intensity as the concentration of Na- and K-Ade decreases as the presence of water molecules assists the dissociation of ion-pairs. In DMSO, the concentration-dependent redshift of the band around 265 nm for Na- and K-Ade is absent and the band intensity at 278 and 287 nm is larger in magnitude than in DMSO/H_2O, indicating the ion-pairs are the predominate species.

The UV spectroscopy study of Na^+ and K^+ ion complexation to the adeninate anion is conducted alongside the studies in the presence of 15C5 and 18C6 (Figure 1, dashed), respectively, in order to confirm the presence of ion-pairs. In the presence of the large excess of 15C5 and 18C6, the shoulder profile is absent and the λ_{max} blueshifts to 262 nm for both Na- and K-

© University of Pretoria
© 2021 The Authors. ChemPhysChem published by Wiley-VCH GmbH

doi.org/10.1002/cphc.202100098

Ade as the free adeninate anion is formed, thus confirming that ion-pairs exist in the absence of the crown ethers. Narrow finger like bands around the 245–250 nm region in the DMSO/H_2O spectra are ascribed to DMSO-water-metal counter ion complexes as they also appear in the cation-DMSO solutions in the absence of the adeninate anion (SI Figure S23). In the Na-Ade DMSO/H_2O UV spectra, a broad band lying below 235 nm is observed and is largely suppressed in DMSO and in the presence of 15C5 and is attributed to the population of higher lying bright $^1\pi\pi^*$ state(s) of the adeninate anion by the excitation at 220 nm.[32]

2.2. Coordination Sites of Na^+ and K^+ with Adeninate Anion

The addition of base, NaH/KH, to adenine in DMSO-d_6 results in deprotonation, shielding all the purine protons in NMR relative to the peaks of adenine as electron density is gained in the purine ring, Table 2. The Na^+ counter ion, with the larger charge/radius ratio, has stronger ion and ion-induced dipole interactions with the adeninate anion, and this is reflected in the larger deshielding of the C2-H and C8-H protons relative to K-Ade ($\Delta\delta$ of 0.11 and 0.17 ppm at dilute and 0.18 and 0.24 at saturated concentrations). The larger shielding of the C8-H is ascribed to the ring current effect (Figure S5).

The gained negative charge from deprotonation of adenine is shared on all five nitrogen atoms of the purine ring which in turn shields the neighboring carbons in the ^{13}C NMR spectra, hence the deshielding of carbons indicates which neighboring nitrogen atoms are involved in the ionic bond. In Table 2, the ^{13}C NMR chemical shifts for the imidazole ring carbons i.e. C4, C5 and C8, are deshielded relative to adenine, highlighting the 5 membered ring's involvement in the ionic bond. Moreover, the C4 and C8 are the most deshielded, suggesting the N9 as the site of coordination. The deshielding of the ^1H and ^{13}C NMR chemical shifts of K-Ade(18C6) suggests that the 18C6 ether does not remove the K^+ counter ion from K-Ade.

From ^{13}C NMR spectroscopy, the site of coordination of the counter ion with the adeninate anion cannot be determined with certainty. The crystal structures obtained of Na-Ade and K-Ade provide insight into the potential coordination sites in solution. The crystallographic information is given in Table S3 and selected geometric parameters of the crystal structure of Na-Ade are given in Table S4. The crystal system for both the Na-Ade and K-Ade display a zigzag packing morphology (Figure S16a and S17a) along the a axis in which there is a T-shape edge to face arrangement. Along the c axis, the next row of units is inverted along the b axis, cancelling the dipole moment of the units and lowering the energy. In both the Na- and K-Ade crystal structures, two DMSO-d_6 solvent molecules per Na-Ade/K-Ade are trapped within the channels formed by four Na-Ade and K-Ade (Figure S16b and S17b) units packed edge to face to form a rectangular cage. The DMSO-d_6 molecules occur in groups of two, oriented in the opposite direction to each other minimizing the steric hindrance between the methyl groups and increases contact between the O atom and the cation. The crystal packing shows that each Na^+/K^+ counter ion is coordinated to three adeninate anion molecules via the N1, N7 and N9 atoms of three purine rings (Figure 2a, Figure S18 for K-Ade). Conversely, one adeninate anion is coordinated to three Na^+ or K^+ counter ions via the N1, N7 and N9 atoms. This in agreement with previous research showing that the coordination sites of the adeninate anion are predominantly N1, N9 and N7.[24]

The crystal structure of K-Ade(18C6), Figure 2b, provides further information, showing the N3 and N9 atoms acting as a chelate in coordination with one K^+ counter ion, having the ion positioned almost equally between the N3- and the N9-atom. The K^+ ion is simultaneously interacting with one 18C6 ether molecule and one adeninate anion. The adeninate anion molecules form zigzag ribbons along the a axis (Figure S19). The K^+ and 18C6 coordination is slightly perched, with a *d* value of 0.924(8) Å (distance of K^+ from the centroid of the 18C6). A herringbone packing morphology of the K-Ade(18C6) units along the a axis is observed wherein a hydrogen-bonded network exists in which the adeninate anion molecules are linked via a mixed WC and HG type hydrogen bonding. From the same set of crystals, a second morphology is obtained, SI Figure S20, in which there is positional disorder in the system. Note that no DMSO solvent is included in the crystals in the presence of crown ether.

From the above, the N3 and N9 atoms are the most likely preferred sites of coordination in solution as the positively charged counter ion will interact with two lone pairs on either nitrogen atom. The size dependency of the counter ion for the N3–N9 coordination will favor that of the K^+ ion as it is larger in size and more suitable for the bridging between the two atoms. The Na^+ ion can chelate or coordinate via either the N9 or the N3 site. No direct evidence for cation-π interactions have been observed and the effect of the presence of the different counter ions on the ^{13}C NMR chemical shifts is too large to be due to only electrostatic interactions between the π system and the counter ion. The difference between the ^{13}C chemical shifts of K-Ade and Na-Ade range from 0.9–3.0 ppm for the imidazole ring whereas the difference between K^+ and Na^+ in a cation-π interaction with benzene is predicted to be 0.13 ppm.[43] It has been shown that compounds containing heteroatoms, such as

Table 2. ^1H and ^{13}C NMR chemical shifts (ppm) of adenine, Na-Ade, K-Ade and K-Ade(18C6) in DMSO-d_6 as solvent.

	^1H NMR chemical shifts				
	C2-H	C8-H	NH_2		
Adenine[a]	8.11	8.09	7.08		
Na-Ade[b]	7.90	7.66	5.94		
K-Ade[c]	7.72	7.42			
K-Ade(18C6)[d]	7.81	7.50			
	^{13}C NMR chemical shifts				
	C2	C4	C5	C6	C8
Adenine[a]	152.4	150.6	118.2	155.6	139.2
Na-Ade[b]	146.9	157.7	119.7	154.3	149.4
K-Ade[c]	147.9	160.7	121.7	155.0	150.5
K-Ade(18C6)[d]	147.5	161.2	121.8	154.0	151.1

[a] Adenine at 73.2 mM [b] Na-Ade at 52.2 mM, [c] K-Ade at 84.8 mM [d] K-Ade(18C6) at 78.7 mM.

© University of Pretoria
© 2021 The Authors. ChemPhysChem published by Wiley-VCH GmbH

doi.org/10.1002/cphc.202100098

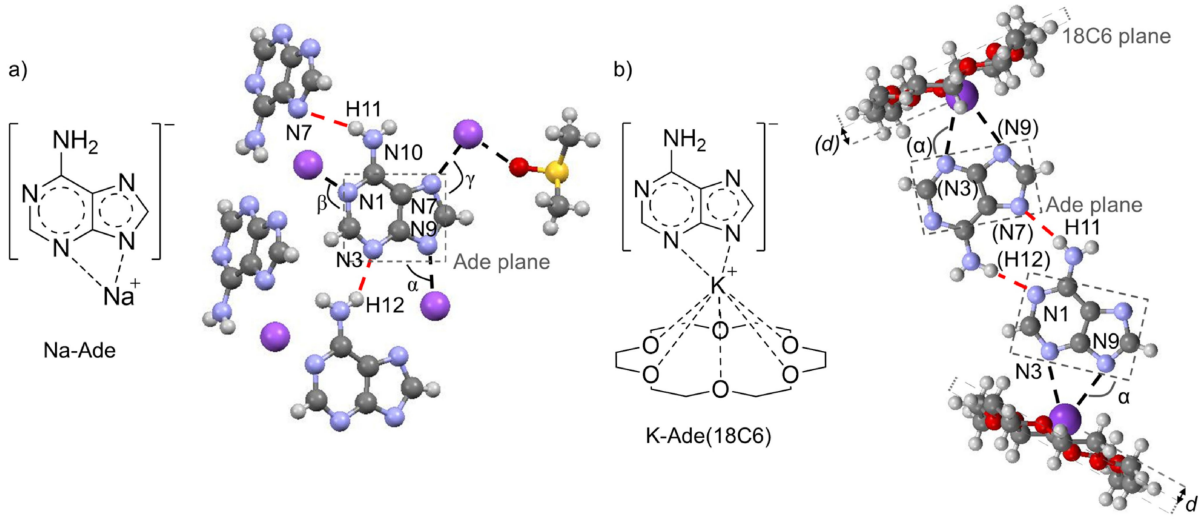

Figure 2. Molecular structure of a) Na-Ade and the Na^+ coordination obtained from single crystal XRD of Na-Ade and b) K-Ade(18C6) and the hydrogen bonding (red lines) and interaction with the K^+ ion at the N3 and N9 atoms (black lines). The numberings of specified atoms and dihedral angles for geometric parameters in Table S4, are shown.

imidazole, pyridine, aniline and imidazole have the cation interact with the heteroatom in preference to the aromatic system, with the cation-π binding being significantly low for imidazole.[44]

2.3. Concentration and ^{1}H NMR temperature coefficient of Na-Ade, K-Ade, Na-Ade(15C5) and K-Ade(18C6)

Depending on the solvent used, hydrogen bonded (chloroform as a solvent) or stacked dimers (solvents such as water or DMSO) occur upon increasing concentrations of adenine, leading to the deshielding of the NH_2 protons[45] or shielding of the purine protons,[46] respectively. The competing H···O interaction between the amino group of adenine with water has a larger interaction energy than H···N, promoting the formation of stacked dimers over hydrogen bonded dimers.[7,39] DMSO should have a similar effect due to the partial negative oxygen available for hydrogen bonding. Concentration dependent ^{1}H NMR studies were performed to investigate the ion-dependent self-aggregation of the ionic complexes (Figure S6a and b). To gain further knowledge of the influence of the cation and the effect of the potential complexation of the K-Ade with 18C6, ^{1}H NMR studies in the presence of 2.4 equivalents of 15C5 ether for Na-Ade (Na-Ade(15C5)) and 18C6 ether for K-Ade (K-Ade (18C6)), Figure S6c and d, were performed. A graphical representation of the shifts on a common axis is given in Figure S7. The change in ^{1}H NMR chemical shifts with the change in concentration ($\Delta\delta = \delta_0 - \delta_n$, where δ_0 is the chemical shift of the reference point at the lowest concentration and δ_n of higher concentration) of the ionic complexes as well as the CH_2 of the 15C5 and 18C6 are shown in Figure 3.

Temperature dependent studies were conducted over the range of concentrations used in order to investigate how increasing the temperature of the solution affects the inter-

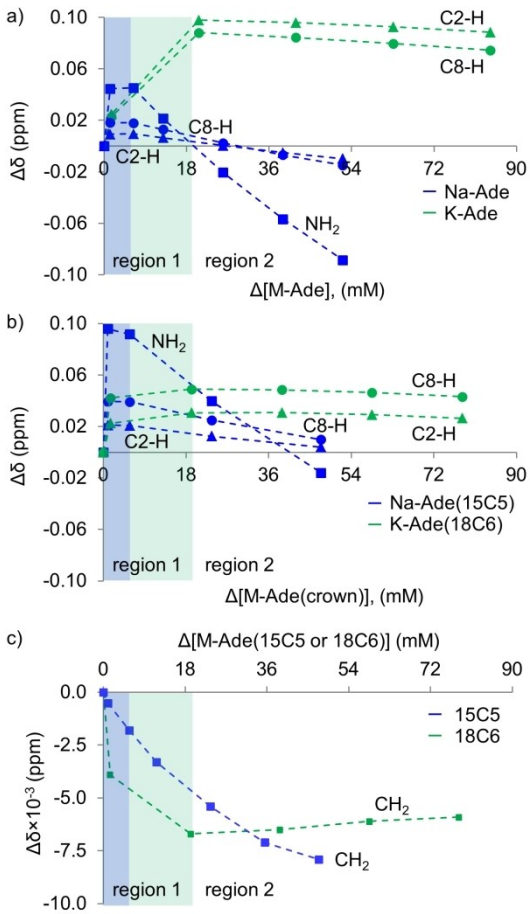

Figure 3. Change in chemical shift of purine protons with the change in concentration for a) Na-Ade and K-Ade, b) Na-Ade(15C5) and K-Ade(18C6), NH_2 – squares, C8-H – circles and C2-H – triangles, and c) the CH_2 protons of the 15C5 and 18C6 ether in the presence of Na-Ade and K-Ade, respectively. All in DMSO-d_6 at 320 K. Region 1 (highlighted in blue and green for Na-Ade and K-Ade, respectively) and region 2 indicates concentration dependent change in chemical shift.

© University of Pretoria
© 2021 The Authors. ChemPhysChem published by Wiley-VCH GmbH

actions between molecules as the distance between them is increased. Refer to Figure S9 for the change in δ with temperature (300 K–380 K). The change in chemical shift of a proton with the change in temperature gives the temperature coefficient (Δδ/ΔT) which is used to monitor hydrogen bonding and π-π stacking between molecules.[45,46] Dissociation of hydrogen bonds leads to shielding of the involved protons and therefore a negative Δδ/ΔT value. Protons exposed to solvent molecules will experience a large negative temperature dependence of the chemical shift as the hydrogen bonds with the solvent are broken. The reduction in temperature coefficient with increasing concentration indicates hydrogen bond formation shielding protons from hydrogen bonding with solvent molecules, which in turn results in a decreased dependence of the proton chemical shift with temperature.[45] For molecules in solution, as the dissociation energy of hydrogen bonds increases, the dependence of the chemical shift on temperature decreases as a larger amount of energy is needed to distort the bond.[47] The effect of temperature on stacked dimers can also be studied using Δδ/ΔT.[46] Dissociation of dimers involved in π-π stacking results in the deshielding of purine protons and hence a positive temperature coefficient (Δδ/ΔT > 0).[46] The change in the temperature coefficient with concentration is shown for the purine protons of Na-Ade and K-Ade, Figure 4a, and for the CH_2 protons of the 15C5 and 18C6 ether, Figure 4b. Refer to Figure S10 for the temperature coefficient of Na-Ade (15C5) and K-Ade(18C6).

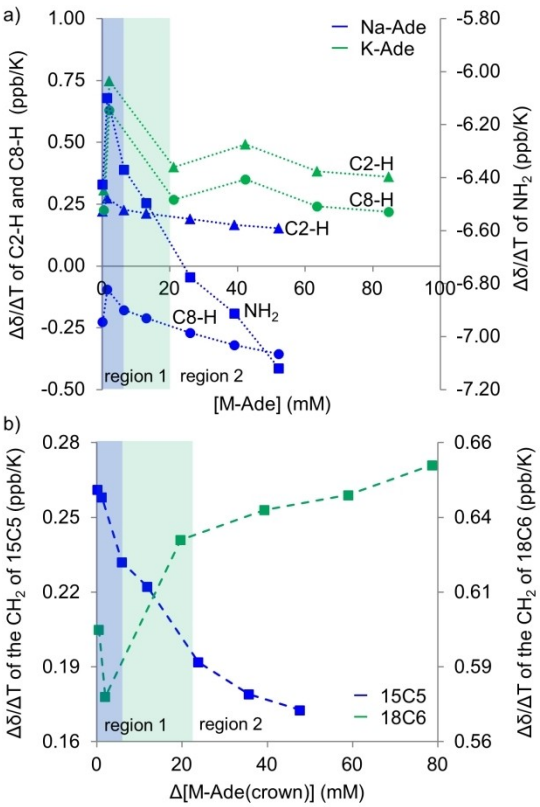

Figure 4. The change in temperature coefficients with concentration of ^{1}H chemical shifts of a) Na-Ade and K-Ade and b) CH_2 of 15-crown-5 ether and the 18-crown-6 ether in DMSO-d_6. NH_2 (squares), C8-H (circles) and C2-H (triangles). The shading relates to the regions defined in Figure 3.

2.4. Aggregation by π-π Stacking and In-Plane Dimerization

Two concentration dependent regions with opposite change in chemical shift are observed in Figure 3a, indicated as region 1 and region 2. Region 1 showed shielding of both purine protons, which indicates π-π stacking of the ionic complexes and is attributed to the ring current effect experienced by the neighboring molecule in π-π stacked dimers. The observed changes in region 1 are not explained by ion-pairing which would have caused deshielding of purine protons. Highlighting the gain and loss of electron density in the ^{13}C NMR chemical shifts of Na- and K-Ade relative to adenine, Figure 5a, it is clear that the purine ring is partially positive in the imidazole ring and negative in the pyrimidine ring. In the presence of competitive hydrogen bonding with DMSO solvent molecules, the dimerization between two M-Ade molecules would be driven by π-π stacking due to stabilizing electrostatic interactions between the oppositely charged sections of the purine

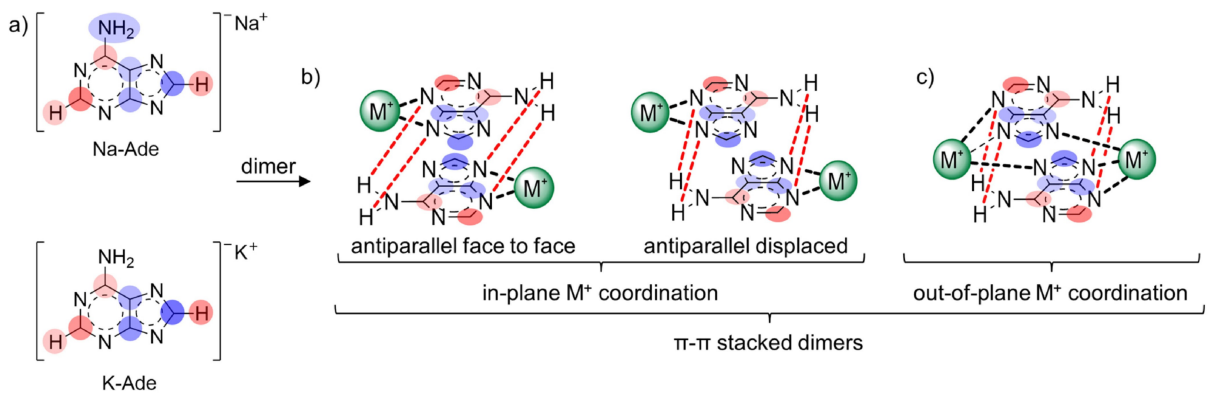

Figure 5. Cation induced change in atomic electron density in Na-Ade and K-Ade relative to adenine, based on the NMR chemical shifts in Table 2. Two shades of blue indicate shifts towards more positive, red towards more negative charge. b) Suggested structures of π-π stacked, c) proposed shift of the M^+ ion from in-plane coordination to an out-of-plane coordination in the π-π stacked dimer of M-Ade. Hydrogen bonding indicated by red lines.

© University of Pretoria
© 2021 The Authors. ChemPhysChem published by Wiley-VCH GmbH

doi.org/10.1002/cphc.202100098

ring, having the 5 membered ring of one molecule stack with the 6 membered ring of the neighboring molecule. This can occur via either antiparallel face to face or antiparallel displaced stacking, Figure 5b. Anti-parallel stacking has been suggested for deprotonated purines.[48] These stacked dimers can be further enhanced by hydrogen bonding of the NH_2 group with the N3 and N9 atom on the neighboring ring and additional stabilization can occur if the counter ion moves from in-plane to out-of-plane coordination (Figure 5c) allowing for a bridging interaction with both adeninate anion molecules, coordinating to the N3, N9 and N7 atoms. The larger sized K^+ counter ion could bridge between two neighboring molecules more readily than the smaller, more tightly bound Na^+ counter ion. In aqueous media, the self-association of nucleotide bases is driven by π-π stacking in which the association constants for nucleobases involved are in the order of purine-purine > purine-pyrimidine > pyrimidine-pyrimidine.[49] Therefore, at low concentrations, with competitive hydrogen bonding to DMSO solvent molecules, π-π stacking of the adenine salts is highly likely to be the dominant form of aggregation.

The absence of the NH_2 peak at all concentrations in the ^1H NMR of K-Ade indicates that the interaction of K^+ with the adeninate anion is different from that of Na^+. Thus, an alternative protonation state or proton exchange regime of the NH_2 group of K-Ade, either with the hydrogen bonded DMSO or neighboring adeninate molecules, could provide an explanation as to why the protons are not observed in the ^1H NMR spectra. The nuclear electric quadrupole moment of K^+ is smaller than that of Na^+, so its coupling with the hydrogen atoms is unlikely the reason for an additional relaxation. If the π-π stacked dimer does indeed occur, this phenomenon could be supported as the K^+ counter ion would be closer in the vicinity of the hydrogen atoms or shared or in a dynamic equilibrium between two adeninate anions.

The addition of 15C5 ether to Na-Ade did not result in a large difference in ^1H NMR chemical shifts concluding that it did not completely interact with the Na^+ from Na-Ade. The ability of the solvent to solvate the cation will influence the association constant for the M^+-crown formation.[50] The Na^+(15C5) complex is a perched complex allowing for the Na^+ to interact with solvent molecules.[51] Therefore, in the presence of DMSO solvent molecules and the highly competing adeninate anion, complexation between Na^+ and 15C5 ether will be significantly lowered.

The addition of 18C6 to K-Ade resulted in a reduced concentration dependence in region 1, Figure 3b, and at the very dilute concentrations of region 1, the ^1H NMR peak of the NH_2 protons became visible (Figure S4 insert). The 18C6 complexed with the K^+ forming a new complex whereby the K^+ ion is simultaneously interacting with the 18C6 and the adeninate anion. The crystal structure of K-Ade(18C6) reveals the feasibility of such an interaction and is supported by the lack of evidence for removal of the K^+ in the ^1H and ^{13}C NMR spectra (the UV data on the other hand, was obtained in dilute solutions with >100-fold excess of the crown to allow for removal of the counter ion). The K^+(18C6) complex is destabilized by the presence of the DMSO solvent molecules or any competitive complexing molecule, such as the adeninate anion, and hence the K^+ will not complex to the 18C6 ether alone. The formation of an adeninate-K^+-18C6 complex is likely to disfavor aggregation via π-π stacking. Thus, in region 1 of Figure 3b, monomers of K-Ade(18C6) complex are likely the predominant species. This would potentially allow for the NH_2 peak of K-Ade(18C6) to become visible since K^+ would not be in the vicinity of the NH_2 group such as in the proposed π-π stacked dimers. The increased shielding of the purine protons with concentration in region 1 (Figure 3b) can be linked to the gain of electron density in the purine ring as the 18C6 ether complexes with the K^+ of K-Ade, reducing the level of interaction between the adeninate anion and K^+. In-plane mixed WC-HG hydrogen bonded dimers such as those observed in the XRD crystal structure of K-Ade(18C6) might occur in region 2 (Figure 2b). Evidence of abstraction of the K^+ from the 18C6 in Figure 3c region 2, CH_2 protons become shielded as electron density is regained, suggests influence of the aggregate formation on the interaction between K^+ and 18C6 ether, resulting in partial release, Scheme 1. Upon increasing the temperature and shifting the equilibrium towards the monomer form, the 18C6 would engage in tighter binding once again as suggested by the increased temperature coefficient in Figure 4b showing increased interaction between the K^+ ions and the 18C6. The absence of the NH_2 peak at higher concentrations could be a result of imine formation involving significant dynamics of chemical shifts. From the crystal structure of K-Ade (18C6), the hydrogen bond lengths between the NH···N7 and NH···N1 differ between the linked molecules, having the latter differ quite significantly, 2.262 vs 2.160 Å, which could arise from imine formation.

2.5. Higher Order Aggregates

Apart from providing insight into the site of coordination between the counter ion and the adeninate anion, the crystal structures provide an interesting comparison and perhaps even some guidance for the aggregate structures of Na- and K-Ade

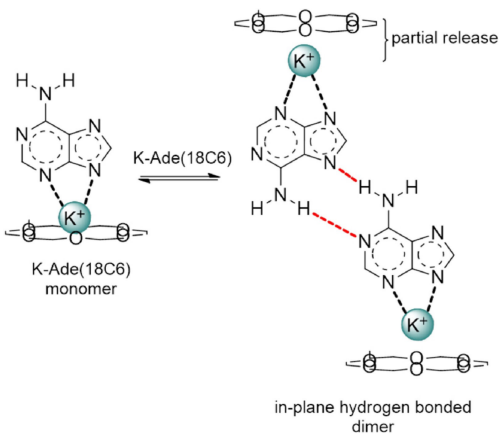

Scheme 1. Hydrogen bonded aggregates of K-Ade(18C6). Hydrogen bonding shown by red dashed line.

© University of Pretoria
© 2021 The Authors. ChemPhysChem published by Wiley-VCH GmbH

doi.org/10.1002/cphc.202100098

in solution. The Na- and K-Ade complexes in the crystal structures do not show in-plane adeninate-adeninate anion mixed WC-HG hydrogen bonded aggregates as observed in K-Ade(18C6), nor are π-π stacked aggregates evident. Instead, the Na- and K-Ade complexes are linked via the counter ions. Hydrogen bonds occur between the NH_2 of one molecule with an N3 and N7 of two neighboring molecules. This could suggest that higher order aggregate formation in region 2 of Figure 3a are governed by the complexation of M-Ade molecules via the counter ions present, Scheme 2, through the coordination of N1 or N7 to the counter ion of the neighboring M-Ade molecule. Aggregation of this type could result in the migration of the counter ion between the N3 or N9 position allowing the N9 or N3, respectively, to be available for hydrogen bonding. Dissociation of these aggregates with increased temperature would result in shielding of the NH_2 protons involved in the hydrogen bond with the N3/N9 of the neighboring molecule, and i.e. shielding of the C8-H and deshielding of the C2-H as the counter ion moves back from the N9 into the N3N9 coordination site, as observed with the temperature coefficient in Figure 4a. It has been suggested that the C8-H could be involved in hydrogen bonding with DMSO,[52] therefore, this effect has not been ruled out as additional influence on the chemical shift.

The concentration dependent change in the temperature coefficient in Figure 4a for K-Ade showed both purine protons undergo deshielding in region 2 and decreases with increasing concentration. This effect is ascribed to the temperature dependent solvent electric field effect as no explanation can be provided considering the disruption of hydrogen bonds. The cation has a peripheral solvation shell of DMSO solvent molecules which orient their dipoles towards the cation, Scheme 2. The positive charge on the cation would be partially reduced as an inflow of electron density from the partially negative O atom of DMSO will occur, weakening the ionic bond with the adeninate anion. An increase in temperature results in the disorder of these arranged DMSO molecules,[53] strengthening the ionic bond between K^+ and the adeninate anion, leading to deshielding of both purine protons. If the higher order aggregates in region 2 shield the cations from the solvent, this effect would reduce with increased concentration, which is what is observed with the reduced temperature coefficient of K-Ade. The proposed aggregate formation is one whereby one K-Ade coordinates via the N7 to the K^+ of the neighboring K-Ade molecule which then has another neighboring molecule coordinate via the N1. This type of aggregation will begin to shield the counter ion from the solvent, reducing the solvent electric field effect.

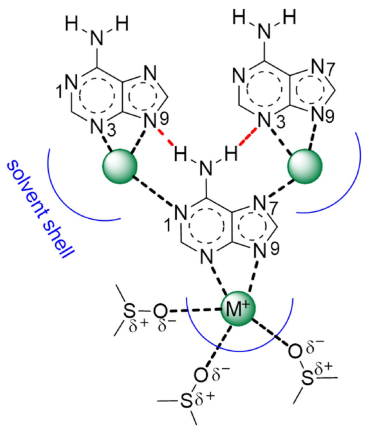

Scheme 2. M-Ade aggregate formation via the N1 and/or the N7.

The above proposed aggregate formations do not rule out the π-π stacking believed to occur at the lower concentrations of region 1 as the complexation of the ionic complexes in higher order aggregates in region 2 can disrupt the aggregation in region 1. Adenine has been reported to form trimers and higher order aggregates upon self-association.[8] Dimer formation has been observed for adenine, adenosine and adenosine monophosphate at concentrations lower than 5 mM, followed by higher order aggregation at concentrations >5 mM ascribed to the polymerization of dimers.[54] This provides confidence that dimer formation can occur at low concentrations (region 1), followed by the formation of higher order aggregates with increasing concentration (region 2).

2.6. Thermodynamics of Self-Aggregation

Two processes are possible for a single adeninate anion, the first is the ion-pairing between the adeninate anion and the counter ion Na^+/K^+ and the second is the self-aggregation of the ion pairs. It is assumed here that i) the self-complexation between free adeninate anions is negligible and ii) a significant amount of ion-pairing already exists. The concentration dependence of the chemical shifts observed in Figure 3 for Na-/K-Ade, Na-Ade(15C5) and K-Ade(18C6), is ascribed to self-aggregation and can occur via monomeric metal-adeninate (M-Ade) addition, i.e. monomer→dimer→trimer etc. The isodesmic and trimer models were used to fit the normalized ^{1}H NMR data of region 2 (refer to Table S1 in SI for *K* vlaues). In addition, the thermodynamic data for the 1:1 complexation between 15C5 ether with the Na^+ were obtained (Table S2). This was not possible for the complexation between 18C6 ether with K^+.

The van't Hoff plot for the self–aggregation of Na-Ade, Na-Ade(15C5) and K-Ade and for the 1:1 complexation between 15C5 ether and Na^+ is shown in Figure S15. The thermodynamic data are given in Table 3.

The equilibrium constants of aggregation are small and dominated by enthalpic interactions in the order of -5 kJ mol^{-1}, which compares with a weak water-amide N···H hydrogen bond and is smaller than that of the self-aggregation of 9-ethyladenine[55,56] which has an enthalpy of formation of -16.7 kJ mol^{-1} associated with more than one hydrogen bond. Cyclic dimer formation (two hydrogen bonds involved in the dimer) is largely preferred over linear dimers (one hydrogen bond).[5] Considering the above proposed ion-assisted aggregate formation, only one hydrogen bond is involved between two M-Ade molecules and it can therefore be expected that the enthalpy of formation will be about half. The gain in enthalpy is in part compensated by negative entropies of association of

© University of Pretoria
© 2021 The Authors. ChemPhysChem published by Wiley-VCH GmbH

doi.org/10.1002/cphc.202100098

Table 3. Aggregation constants and thermodynamic parameters for the self-aggregation of Na-Ade[a], Na-Ade(15C5)[a] and K-Ade[b] and the association constant for the 1:1 complexation[c] between C15C and Na^+ in DMSO-d_6 as solvent at 305 K.

Complex	K_{agg} [M^{-1}]	ΔH[d]	ΔS[e]	ΔG[d]
Na-Ade	2.4 ± 0.3	−4.7 ± 0.2	−8.0 ± 0.5	−2.2
Na-Ade(15C5)	3.0 ± 0.5 K (M^{-2})	−5.2 ± 0.5	−8.3 ± 1.6	−2.7
K-Ade	0.59 ± 0.03 K_1 (M^{-1})	−4.5 ± 0.3	−19 ± 1	+1.4
Na-Ade(15C5)	28 ± 3	−23 ± 2	−50 ± 5	−8.4

[a] Isodesmic model, [b] Trimer model, [c] 1:1 Guest-host model, [d] kJ mol^{-1}, [e] J mol^{-1} K^{-1}.

about −8 J mol^{-1} K^{-1}, which is much less than the value of −145 J mol^{-1} K^{-1} that should typically be expected for the loss of translational entropy of a Na-Ade unit due to conformational order.[57] Much of it must be compensated by a large gain in entropy of liberated solvent molecules during aggregation of Na-Ade and the gain in vibrational entropy[58] from the formed weak hydrogen bond which would result in loose NH vibration. In addition, if the π-π stacked dimer, which would have more order, is dissociated upon larger aggregate formation, this would also increase the entropy. The equilibrium of the K-Ade aggregate is slightly disfavored as seen by the slight positive ΔG.

The change in enthalpy (ΔH = −23 kJ mol^{-1}) for the 1:1 complexation between Na^+ and 15C5 ether is slightly larger than that previously reported in DMF[59] and DMSO[60] (ΔH = −20 and −15 kJ mol^{-1}, respectively) and is attributed to the use of anhydrous DMSO-d_6. The presence of water significantly reduces the binding of Na^+ to 15C5 ether.[60]

3. Conclusions

Disfavored tautomeric and anionic forms of nucleobases which have gained attention recently surround their involvement in mutations, replication, and translational errors as well as nucleic acid catalysis and RNA-ligand recognition. However, there is a lack of information surrounding the anionic forms of nucleobases such as the adeninate anion. In this paper, the ion-pairing and self-aggregation ability of the adeninate anion in DMSO are investigated using NMR and UV spectroscopy and crystallographic methods. An understanding of the variability of chemical shifts is needed in context of ongoing kinetic experiments by NMR.

The large ion-dependent difference in the UV absorbance λ_{max} from 272 nm for K-Ade to 269 nm for Na-Ade shows that ion-pairs exist between the adeninate anion and Na^+ and K^+ counter ions in DMSO at very dilute concentrations. The crystal structures obtained from the ionic complexes have the ion coordinate at the N1, N9 and N7 atoms of the purine ring. It is proposed that a chelating N3–N9 coordination is highly likely to exist in solution. The counter ions are not successfully removed by the addition of 15-crown-5 and 18-crown-6 ether from the Na- and K-Ade as no gain of electron density in the purine system was observed in the ^1H and ^{13}C NMR study. It is proposed that the addition of 18-crown-6 ether results in complex formation with the K-Ade, as indicated also by the crystal structure of K-Ade(18C6).

In the concentration dependent ^1H NMR studies, two regions with opposite chemical shift are observed which indicate two aggregation steps. The first aggregation is ascribed to dimer formation via π-π stacking as suggested by the shielding of the purine protons by the ring current of the neighboring stacked molecule. At higher concentrations, the dimer formation is followed by higher order aggregate formation of the Na- and K-Ade. The counter ion plays a role in the self-aggregation allowing for coordination to the counter ion of the neighboring Na-/K-Ade ion pairs. The size of the counter ion influences how the aggregates are arranged or propagated though space, revealing a clear difference between the Na-Ade and K-Ade forms. The assembly of the Na- and K-Ade complexes in the crystal structures does not show WC or HG type arrangement of hydrogen bonded aggregates. The possibility of weak hydrogen bond formation involving the NH_2 is indicated by the small enthalpy of formation of about −5 kJ mol^{-1}. The small decrease in entropy of about −8 J mol^{-1} K^{-1} with aggregate formation indicates that there is a gain in entropy due to either the liberation of solvent molecules, rearrangement of dimer aggregates and/or there is a gain in vibrational entropy from the formation of weak hydrogen bonds.

Theoretical studies have been conducted to investigate the proposed sites of coordination between the counter ions and the adeninate molecule (publication in progress). Current studies are underway to confirm the modes of aggregation, with this research providing a good starting point. Although these studies have been conducted in a non-aqueous environment, they provide insight into how the existence of the potential deprotonated adenine base can interact in the alkali metal ions present, having the dielectric constant of DMSO fall in between that within the DNA double helix and inside the cellular environment.[37]

The counter ion present plays an essential role in directing aggregate formation, adding new insight into how the adeninate anion interacts with neighboring molecules, and hence provides information regarding the reactivity of the systems as well as insight for the association of adenine with alkali metal counter ions which can provide stability for these forms.

Acknowledgements

The authors acknowledge the National Research Foundation for the funding of the research and Scarce Skills Doctoral Scholarships awarded (grant number 97879 to DMS B); the crystallographer at the University of Pretoria, Dr Frikkie Malan, for performing the XRD analyses; the NMR spectroscopy personal, Dr Mamoalosi Selepe, for accommodating extended use of the instrument; as well as Dr Shankara Radhakrishnan for allowing use of her UV

© University of Pretoria
© 2021 The Authors. ChemPhysChem published by Wiley-VCH GmbH

doi.org/10.1002/cphc.202100098

instrument. Open Access funding enabled and organized by Projekt DEAL.

Conflict of Interest

The authors declare no conflict of interest.

Keywords: nucleobases · aggregation · hydrogen bonding · stacking interactions · ion-pairing

[1] J. D. Watson, F. H. C. Crick, *Nature* **1953**, *171*, 737–738.
[2] J. van de Sande, N. Ramsing, M. Germann, W. Elhorst, B. Kalisch, E. von Kitzing, R. Pon, R. Clegg, T. Jovin, *Science* **1988**, *241*, 551–557.
[3] K. Hoogsteen, *Acta Crystallogr.* **1959**, *12*, 822–823.
[4] Y. K. Cheng, B. M. Pettitt, *J. Am. Chem. Soc.* **1992**, *114*, 4465–4474.
[5] Y. Kyogoku, R. C. Lord, A. Rich, *Proc. Nat. Acad. Sci.* **1967**, *57*, 250–257.
[6] A. Dunger, H.-H. Limbach, K. Weisz, *J. Am. Chem. Soc.* **2000**, *122*, 10109–10114.
[7] C. Giessner-Prettre, B. Pullman, *J. Theor. Biol.* **1970**, *27*, 87–95.
[8] L. Katz, *J. Mol. Biol.* **1969**, *44*, 279–296.
[9] J. D. Engel, P. H. Von Hippel, *Biochemistry* **1974**, *13*, 4143–4158.
[10] G. Lancelot, *J. Am. Chem. Soc.* **1977**, *99*, 7037–7042.
[11] P. Rao, S. Ghosh, U. Maitra, *J. Phys. Chem. B* **1999**, *103*, 4528–4533.
[12] E. M. Basílio Janke, H.-H. Limbach, K. Weisz, *J. Am. Chem. Soc.* **2004**, *126*, 2135–2141.
[13] B. A. Cerda, C. Wesdemiotis, *J. Am. Chem. Soc.* **1996**, *118*, 11884–11892.
[14] N. Russo, M. Toscano, A. Grand, *J. Am. Chem. Soc.* **2001**, *123*, 10272–10279.
[15] M. T. Rodgers, P. B. Armentrout, *J. Am. Chem. Soc.* **2000**, *122*, 8548–8558.
[16] F. Greco, A. Liguori, G. Sindona, N. Uccella, *J. Am. Chem. Soc.* **1990**, *112*, 9092–9096.
[17] V. M. Marathias, P. H. Bolton, *Biochemistry* **1999**, *38*, 4355–4364.
[18] S. Naskar, R. Guha, J. Müller, *Angew. Chem. Int. Ed.* **2020**, *59*, 1397–1406; *Angew. Chem.* **2020**, *132*, 1413–1423.
[19] G. Beobide, O. Castillo, J. Cepeda, A. Luque, S. Pérez-Yáñez, P. Román, J. Thomas-Gipson, *Coord. Chem. Rev.* **2013**, *257*, 2716–2736.
[20] S. L. Anderson, K. C. Stylianou, *Coord. Chem. Rev.* **2017**, *349*, 102–128.
[21] J. An, S. J. Geib, N. L. Rosi, *J. Am. Chem. Soc.* **2009**, *131*, 8376–8377.
[22] H. Cai, M. Li, X.-R. Lin, W. Chen, G.-H. Chen, X.-C. Huang, D. Li, *Angew. Chem. Int. Ed.* **2015**, *54*, 10454–10459; *Angew. Chem.* **2015**, *127*, 10600–10605.
[23] A. Gładysiak, T. N. Nguyen, S. L. Anderson, P. G. Boyd, R. G. Palgrave, J. Bacsa, B. Smit, M. J. Rosseinsky, K. C. Stylianou, *Inorg. Chem.* **2018**, *57*, 1888–1900.
[24] J. P. García-Terán, O. Castillo, A. Luque, U. García-Couceiro, P. Román, L. Lezama, *Inorg. Chem.* **2004**, *43*, 4549–4551.
[25] K. Bebenek, L. C. Pedersen, T. A. Kunkel, *Proc. Natl. Acad. Sci. USA* **2011**, *108*, 1862–1867.
[26] I. J. Kimsey, K. Petzold, B. Sathyamoorthy, Z. W. Stein, H. M. Al-Hashimi, *Nature* **2015**, *519*, 315–320.
[27] W. Wang, H. W. Hellinga, L. S. Beese, *Proc. Nat. Acad. Sci.* **2011**, *108*, 17644–17648.
[28] C. Tamm, P. Strazewski, *Angew. Chem. Int. Ed.* **1990**, *29*, 36–57; *Angew. Chem.* **1990**, *102*, 37–59.
[29] P. C. Bevilacqua, R. Yajima, *Curr. Opin. Chem. Biol.* **2006**, *10*, 455–464.
[30] V. Singh, C. S. Peng, D. Li, K. Mitra, K. J. Silvestre, A. Tokmakoff, J. M. Essigmann, *ACS Chem. Biol.* **2014**, *9*, 227–236.
[31] M. Zierhut, W. Roth, I. Fischer, *Phys. Chem. Chem. Phys.* **2004**, *6*, 5178.
[32] G. M. Roberts, H. J. B. Marroux, M. P. Grubb, M. N. R. Ashfold, A. J. Orr-Ewing, *J. Phys. Chem. A* **2014**, *118*, 11211–11225.
[33] T. J. Torphy, *Am. J. Respir. Crit. Care Med.* **1998**, *157*, 351–370.
[34] E. Boichot, J. L. Wallace, N. Germain, M. Corbel, C. Lugnier, V. Lagente, J. J. Bourguignon, *J. Pharmacol. Exp. Ther.* **2000**, *292*, 647–53.
[35] B. Bielekova, A. Lincoln, H. McFarland, R. Martin, *J. Immunol.* **2000**, *164*, 1117–1124.
[36] M. K. Mishra, S. P. Kelley, V. Smetana, D. A. Dixon, A. S. McNeill, A.-V. Mudring, R. D. Rogers, *Proc. Nat. Acad. Sci.* **2020**, *117*, 18224–18230.
[37] S. Nakano, N. Sugimoto, *Biophys. Rev. Lett.* **2016**, *8*, 11–23.
[38] H. Sapper, W. Lohmann, *Biophys. Struct. Mech.* **1978**, *4*, 327–335.
[39] P. O. P. Ts'o, I. S. Melvin, A. C. Olson, *J. Am. Chem. Soc.* **1963**, *85*, 1289–1296.
[40] H. W. Vos, H. H. Blom, N. H. Velthorst, C. MacLean, *J. Chem. Soc. Perkin Trans. 2* **1972**, *2*, 635–639.
[41] H. V. Carter, B. J. McClelland, E. Warhurst, *Trans. Faraday Soc.* **1960**, *56*, 455–458.
[42] H. H. Hammud, K. H. Bouhadir, M. S. Masoud, A. M. Ghannoum, S. A. Assi, *J. Solution Chem.* **2008**, *37*, 895–917.
[43] F. B. Sayyed, C. H. Suresh, *Chem. Phys. Lett.* **2012**, *523*, 11–14.
[44] S. Mecozzi, A. P. West, D. A. Dougherty, *Proc. Nat. Acad. Sci.* **1996**, *93*, 10566–10571.
[45] N. J. Baxter, M. P. Williamson, *J. Biomol. NMR* **1997**, *9*, 359–369.
[46] G. K. Helmkamp, N. S. Kondo, *Biochim. Biophys. Acta Nucleic Acids Protein Synth.* **1968**, *157*, 242–257.
[47] G. C. Pimentel, A. L. McClellan, *Annu. Rev. Phys. Chem.* **1971**, *22*, 347–385.
[48] W. Schimmack, H. Sapper, W. Lohmann, *Biophys. Struct. Mech.* **1975**, *1*, 311–318.
[49] P. O. P. Ts'o, *Basic Princ.* Nucleic Acid Chem., Elsevier, **1974**, p. 546.
[50] E. Karkhaneei, A. Afkhami, M. Shamsipur, *Polyhedron* **1996**, *15*, 1989–1994.
[51] M. Irandoust, H. Daraei, R. Rostamian, *Polyhedron* **2011**, *30*, 1207–1212.
[52] L. Katz, S. Penman, *J. Mol. Biol.* **1966**, *15*, 220–231.
[53] N. S. Golubev, G. S. Denisov, S. N. Smirnov, D. N. Shchepkin, H.-H. Limbach, *Zeitschrift für Phys. Chemie* **1996**, *196*, 73–84.
[54] J. Morcillo, E. Gallego, F. Peral, *J. Mol. Struct.* **1987**, *157*, 353–369.
[55] G. G. Hammes, A. C. Park, *J. Am. Chem. Soc.* **1969**, *91*, 956–961.
[56] Y. Kyogoku, R. C. Lord, A. Rich, *J. Am. Chem. Soc.* **1967**, *89*, 496–504.
[57] S. W. Benson, *Thermochemical Kinetics*, John Wiley & Sons, New York, **1976**.
[58] J. D. Dunitz, *Chem. Biol.* **1995**, *2*, 709–712.
[59] M. Jóźwiak, *J. Mol. Liq.* **2003**, *108*, 175–198.
[60] M. Jóźwiak, H. Piekarski, A. Jóźwiak, *J. Mol. Liq.* **2003**, *106*, 15–29.

Manuscript received: February 9, 2021
Revised manuscript received: March 24, 2021
Accepted manuscript online: June 21, 2021
Version of record online: August 8, 2021

© University of Pretoria
© 2021 The Authors. ChemPhysChem published by Wiley-VCH GmbH

Appendix 2

© University of Pretoria

Table of content

Supporting information – 1 pages 1 – 19

Supporting information – 2 pages 20 – 32

Supporting information – 3 pages 33 – 43

Supporting information – 4 pages 44 – 46

© University of Pretoria

Supporting Information – 1

Towards a molecular understanding of cation–anion interactions and self-aggregation of adeninate salts in DMSO by NMR and UV Spectroscopy and Crystallography

Experimental details for ^{1}H NMR studies and crystallography

Instrumentation

Purification of 18-Crown-6 via recrystallization: A mixture of 18-crown-6 and acetonitrile was heated until 18-crown-6 fully dissolved. Clear crystals formed when the heated mixture was allowed to cool to ambient temperature and left for 1 hr and then placed in the freezer for an additional hour. The crystals were filtered, washed with cold acetonitrile and vacuum dried over 24 hrs at 40 °C [1].

Preparation of adenine-salt stocks:

The sodium and potassium hydride are used as bases to avoid introduction of water into the reactions.

Preparation of Na-Ade stock: NaH (0.0688 mmol, 1.20 eq.) was added to a heterogeneous mixture of adenine (0.0574 mmol, 1 eq.) and anhydrous DMSO-d_6 (1100 µl). 7 concentrations were prepared, A (52.2), B (39.1), C (26.1), D (13.0), E (6.52), F (1.44), G (0.130).

Preparation of K-Ade stock: KH (0.121 mmol, 1.30 eq.) was added to a heterogeneous mixture of adenine (0.0932 mmol, 1 eq.) and anhydrous DMSO-d_6 (1100 µl). 6 concentrations were prepared, A (84.8), B (63.6), C (42.4), D (21.2), E (2.12), F (0.207).

Preparation of K-Ade(18C6) stock: 18-crown-6 (0.320 mmol, 2.40 eq.) was added to a solution of adenine (0.134 mmol, 1 eq.) and KH (0.160 mmol, 1.19 eq.) in anhydrous DMSO-d_6 (1632 µl). A precipitate formed which was filtered off using 25 mm hydrophilic polyamide syringe filter. From this, 6 concentrations were prepared, A (78.7), B (59.0), C (39.3), D (19.7), E (1.97), F (0.489).

Preparation of Na-Ade(15C5): 15-crown-5 (0.126 mmol, 2.40 eq.) was added to a solution of adenine (0.0523 mmol, 1 eq.) and NaH (0.0629 mmol, 1.20 eq.) in anhydrous DMSO-d_6 (1075 µl). From this, 7 concentrations were prepared, A (47.6), B (35.7), C (23.8), D (11.9), E (5.95), F (1.19), G (0.238).

Experimental details for UV spectroscopy studies:

An estimation of the percent of water in DMSO from the bottle that has been open for a period of time was calculated using an internal standard of toluic acid in non-anhydrous DMSO-d_6 that has also been open for a period of time). The percent of water in 0.5 ml of DMSO-d_6 was found to be 5.2%.

© University of Pretoria

Preparation of Na-Ade: Adenine (0.0500 mmol, 1 eq.) and NaH (0.0603 mmol, 1.20 eq.) were added to 1500 µl DMSO. From this, 12 concentrations were made: A (1.00), B (0.900), C (0.800), D (0.560), E (0.392), F (0.274), G (0.192), H (0.135), I (0.0941), J (0.0659), K (0.0461), L (0.0323) mM. These measurements were made using a 1 mm quartz cuvette. Anhydrous samples were prepared in a similar fashion in a glovebox using dried DMSO as the solvent. These sample measurements were made using a 4 mm quartz cuvette which was sealed in the glovebox. The Na-Ade(15C5) sample was prepared by addition of 126 eq of 15C5 ether to a final concentration of 0.33 mM of Na-Ade in DMSO. The measurement was done using a 1 mm quartz cuvette.

Preparation of K-Ade: Adenine (0.0500 mmol, 1 eq.) and KH (0.0605, 1.2 eq.) were added to 1000 µl DMSO. From this, 12 concentrations were made: A (1.00), B (0.900), C (0.800), D (0.560), E (0.392), F (0.274), G (0.192), H (0.135), I (0.0941), J (0.0659), K (0.0461), L (0.0323) mM. These measurements were made using a 1 mm quartz cuvette. Anhydrous samples were prepared in a similar fashion in a glovebox using dried DMSO as the solvent. These sample measurements were made using a 4 mm quartz cuvette which was sealed in the glovebox. K-Ade(18C6) sample was prepared by addition of 117 eq of 18C6 ether to a final concentration of 0.33 mM of K-Ade in DMSO. The measurement was done using a 1 mm quartz cuvette.

X-ray crystallography of Na-Ade, K-Ade and K-Ade(18C6)

Single crystal diffraction experiments of compounds Na-Ade, K-Ade and K-Ade(18C6) (morphology 2) were performed on a Rigaku XtaLAB Synergy R diffractometer, with a rotating-anode X-ray source and a HyPix CCD detector. Data reduction and absorption were carried out using the CrysAlisPro (version 1.171.40.23a) software package [2]. Single crystals of K-Ade(18C6) (morphology 1 in the main text) was analyzed using Quazar multi-layer optics monochromated Cu Kα radiation (k = 0. 1.54184 Å) on a Bruker D8 Venture kappa geometry diffractometer with duo Iµs sources, a Photon 100 CMOS detector and APEX III control software [3]. Data reduction was performed using SAINT+ [3], and the intensities were corrected for absorption using SADABS-2016 [3]. All X-ray diffraction measurements were performed at 150(1) K, using an Oxford Cryogenics Cryostat. All structures were solved by direct methods with SHELXT-2018 [4] and refined using SHELXL-2018 packages [5]. All H atoms were placed in geometrically idealised positions and constrained to ride on their parent atoms. For data collection and refinement parameters, see the Table S1.3. The X-ray crystallographic coordinates for the structures Na-Ade and K-Ade(18C6) have been deposited at the Cambridge Crystallographic Data Centre (CCDC), with deposition numbers CCDC 2055270-2055272. The X-ray crystallographic coordinates for the structure K-Ade were not submitted as the data was poor.

© University of Pretoria

HMBC NMR for characterization of proton peaks of adenine-Na, adenine-K and adenine-K 18-crown-6

Assignment of the purine protons of Na-Ade, K-Ade and K-Ade(18C6) were achieved using HMBC, Figures S1.1-S1.3.

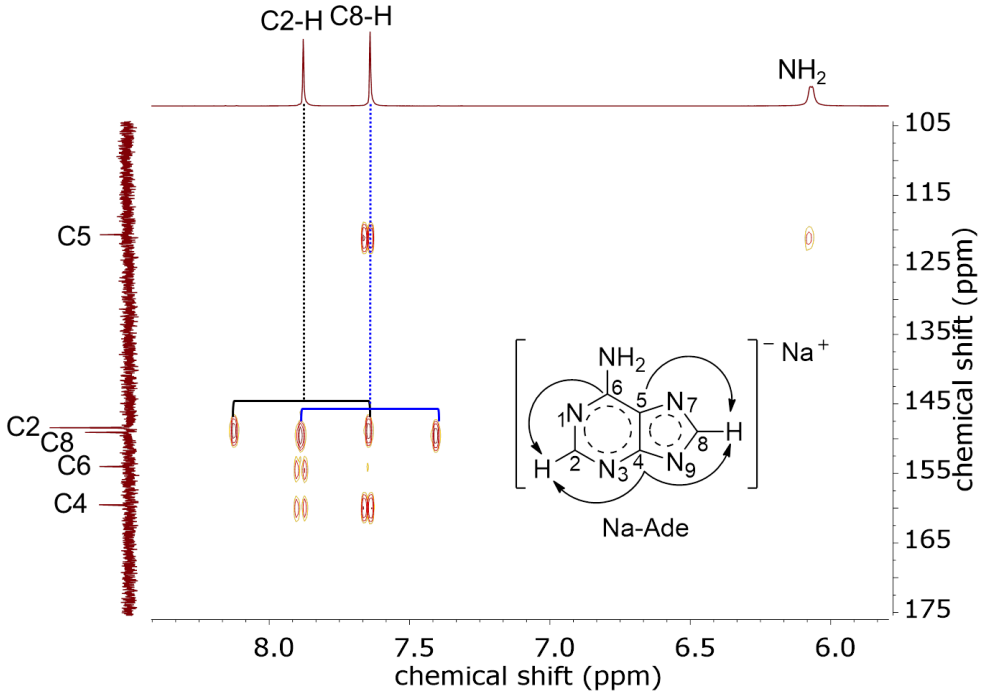

Figure S1.1: HMBC of adenine-sodium salt in DMSO-d_6. Arrows indicate the observed carbon correlation with protons 2 or more bonds away. Black and blue dotted line show hovering correlation with the directly bonded proton.

© University of Pretoria

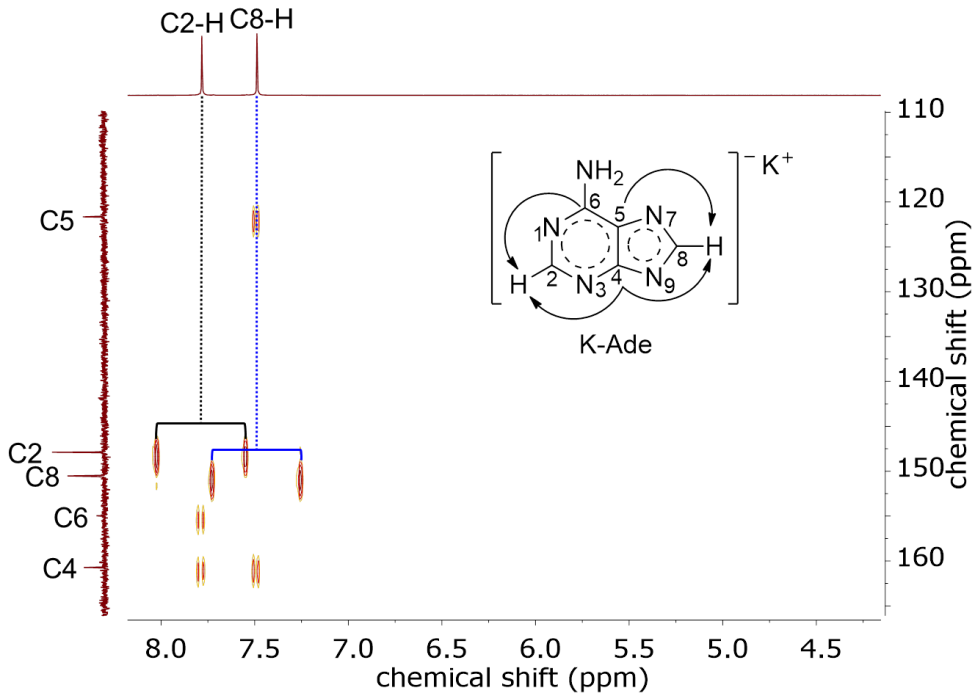

Figure S1.2: HMBC of adenine-potassium salt in DMSO-d_6. Arrows indicate the observed carbon correlation with protons 2 or more bonds away. Black and blue dotted line show hovering correlation with the directly bonded proton.

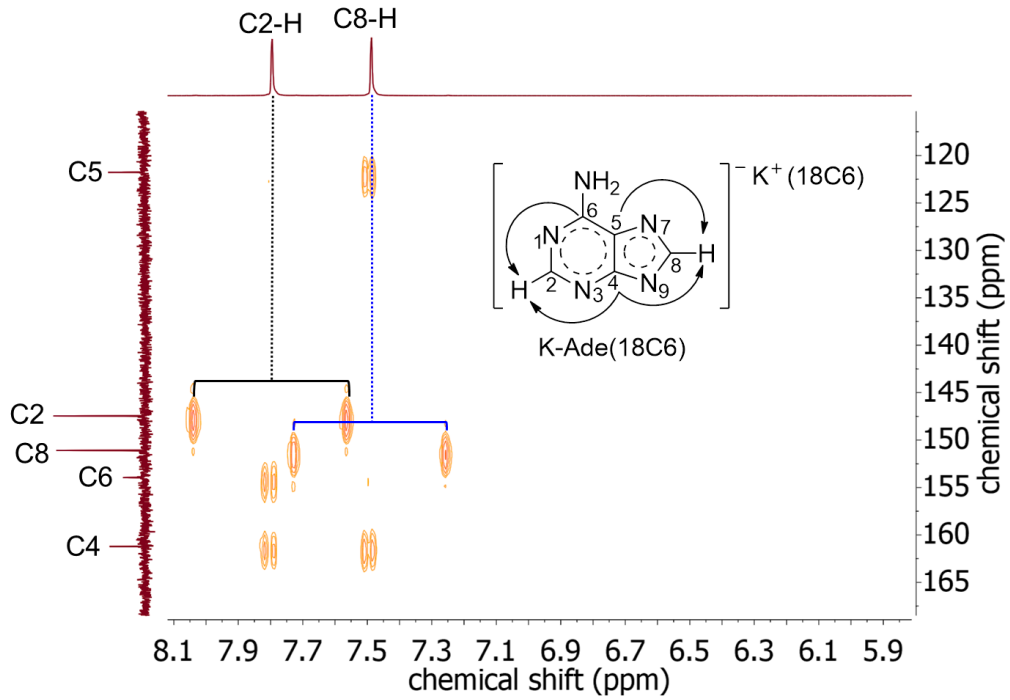

Figure S1.3: HMBC of adenine-potassium salt with 18-crown-6 in DMSO-d_6. Arrows indicate the observed carbon correlation with protons 2 or more bonds away. Black and blue dotted line show hovering correlation with the directly bonded proton.

© University of Pretoria

Coordination sites of Na^+ and K^+ with the adeninate anion

The most likely site for the metal ion coordination is the N3-N9 and N9 for K^+ and the N3-N9, N3 and N9 for the smaller Na^+ ion, Figure S1.4. The nitrogen(s) directly involved in the ionic bond will donate electron density to the counter ion, and therefore "pull" electron density from the surrounding nitrogen and carbon atoms. This effect will affect the electron density of the directly associated ring and hence decrease the effect of the ring current resulting in a lessened deshielding effect (solid arrows). The neighbouring ring will experience this affect to a smaller extent (dashed arrows).

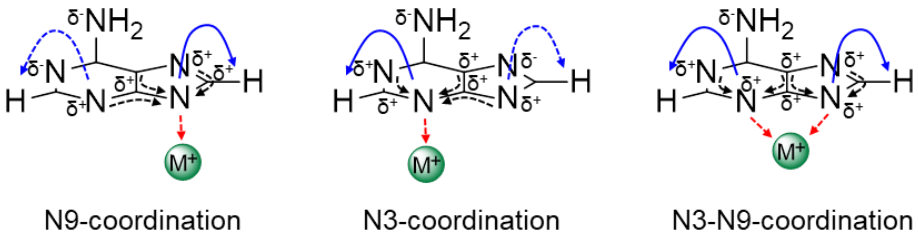

Figure S1.4: Metal ion coordinating to the N9, N3 and N3-N9

In turn, the shielding of the carbon atoms in the ^{13}C NMR will also be influenced by the coordination of the metal ion to the nitrogen atoms. The carbon atoms directly neighbouring the involved nitrogen will be more deshielded relative to adenine. The K-Ade has the C4, C5 and C8 more deshielded then the Na-Ade. This is attributed to the K^+ coordinating to the N3-N9 or N9 position. For Na-Ade, the Na^+ could coordinate either at the N3, N3-N9 or N9 atom and therefore the ^{13}C NMR will be an average between the three. As the coordination to the N3 will allow for the N7 atom to donate less electron density, the C8 and C5 will be more shielded on average.

The ^{1}H and ^{13}C NMR chemical shift positions are also influenced by the aggregation and therefore these relative shifts discussed above and the proposed reasoning is only a part of the explanation.

Concentration dependent ^{1}H NMR chemical shifts of Na-Ade, K-Ade, Na-Ade(15C5) and K-Ade(18C6)

A set of concentrations between the dilute and saturated concentration range in the NMR experiments reported in Figure 2.6 in the main text, were used to investigate the concentration dependent behaviour observed in the ^{1}H NMR spectra of Na-, K-Ade. Na-Ade(15C5) and K-Ade(18C6). The concentration dependent ^{1}H NMR spectra of Na-, K-Ade, Na-Ade(15C5) and K-Ade(18C6) are shown in Figure S1.5a-d. The concentration dependent ^{13}C NMR spectra for the reported region 2 concentration range in Figure 13a, main text, is shown in Figure S1.6a and b.

© University of Pretoria

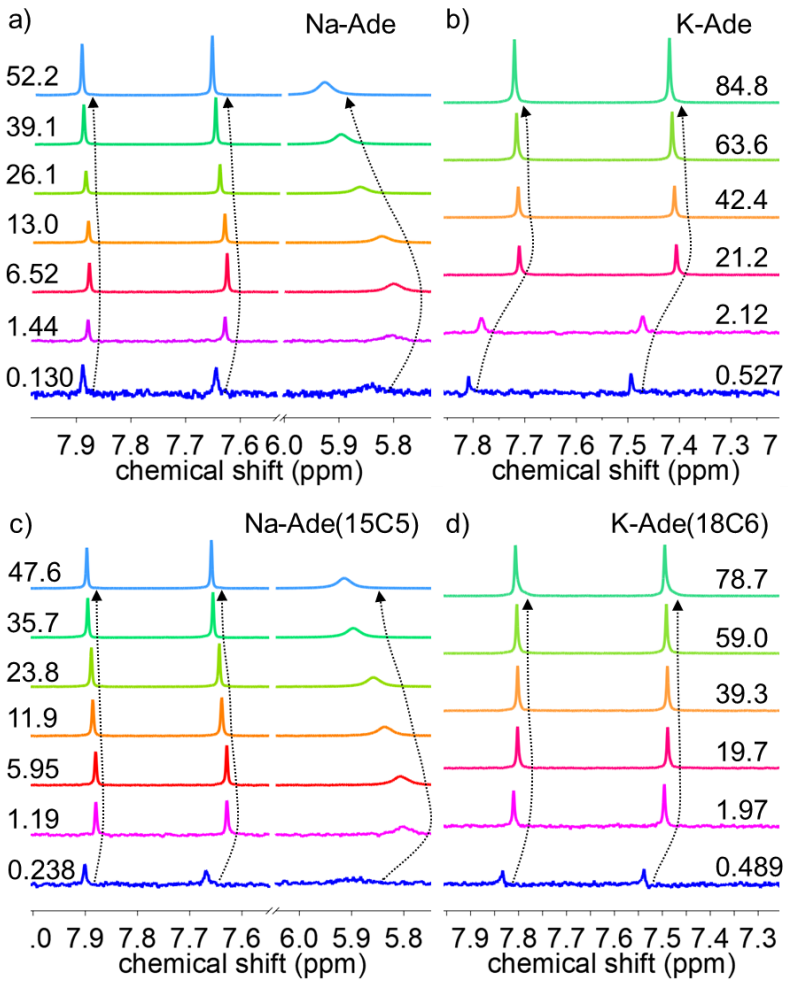

Figure S1.5: ^{1}H NMR spectra of a) Na-Ade, b) K-Ade c) Na-Ade(15C5) and d) K-Ade(18C6) at the indicated concentrations (mM) in DMSO-d_6 at 320 K. The vertical lines are drawn as a guide to the eye.

© University of Pretoria

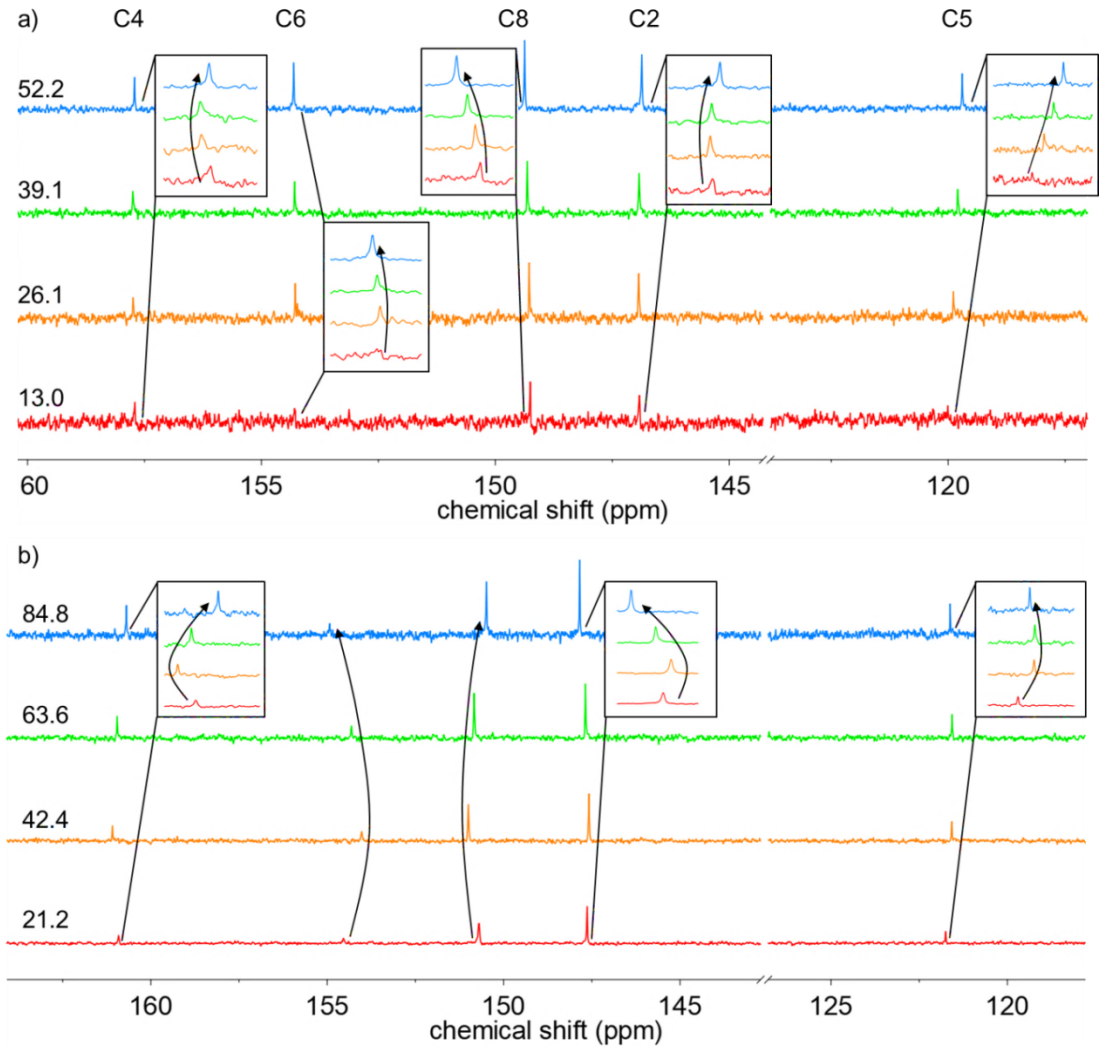

Figure S1.6 ^{13}C NMR spectra at various concentrations (indicated on the left, in mM) of a) Na-Ade and b) K-Ade, in DMSO-d_6 at ambient temperature.

^{1}H NMR temperature coefficient of Na-Ade, K-Ade, Na-Ade(15C5) and K-Ade(18C6)

Temperature dependent studies were conducted over the range of concentrations used in order to investigate how increasing the temperature of the solution effects the interactions between molecules as the distance between the molecules is increased, reducing the intermolecular interactions between them.

The change in δ with temperature ($\Delta\delta_T = \delta_{T0} - \delta_{Tn}$, where δ_{T0} is the chemical shift of the reference point at the lowest temperature and δ_{Tn} of higher temperature) at the highest concentration used for each complex for the temperature range 300 K - 380 K is shown in Figure S1.7 (the same trends are observed at all concentrations used). For both cations, the temperature effect on the purine protons in the absence and presence of the crown ether is similar. For both Na- and K-Ade complexes the C2–H proton is increasingly deshielded ($\Delta\delta < 0$) with increasing temperature as is the C8–H of K-Ade but shielding ($\Delta\delta > 0$) is observed in the case of the C8–H and NH_2 protons of Na-Ade. The deshielding of the C2–H of both the Na- and K-Ade complexes and the C8–H of K-Ade with an increase in temperature suggests an influence of the cation as the concentration dependent

© University of Pretoria

deshielding of these protons in Figure 2.13 is not reversed with increase in temperature that would have been expected with the dissociation of the aggregates.

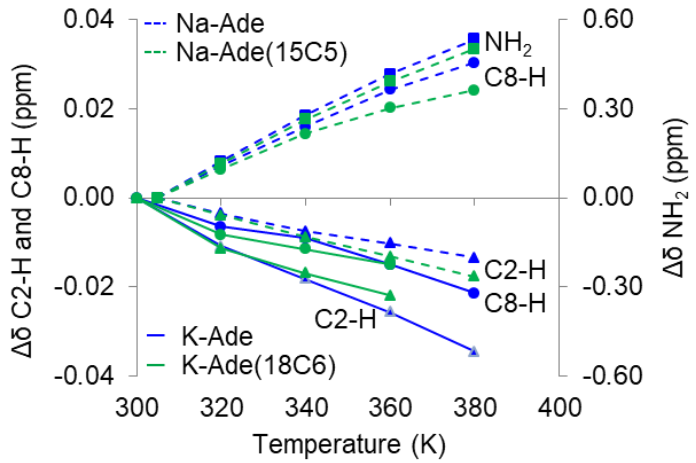

Figure S1.7: Change in ^{1}H NMR chemical shift of Na-Ade (52.2 mM), Na-Ade(15C5) (47.6 mM), K-Ade (84.8 mM) and K-Ade(18C6) (78.7 mM) at the indicated temperatures (K) in DMSO-d_6 for NH_2 (squares), C2–H (triangles) and C8–H (circles).

The change in the temperature coefficient for the purine protons of Na-Ade(15C5) and K-Ade(18C6) at various concentrations is shown in Figure S1.8. The presence of 15C5 ether resulted in a reduced temperature coefficient of the NH_2 protons in region 2 compared to Na-Ade indicating (i) shielding of these protons from the solvent or (ii) stronger hydrogen bonding involved in the aggregate formation as compared to that of the Na-Ade aggregates. The latter would suggest a difference in arrangement between the aggregated molecules of Na-Ade(15C5) and Na-Ade. For K-Ade, the presence of the 18C6 ether eliminates the difference in temperature coefficient between region 1 and 2 and there appears to be only a very slight concentration dependent change in the temperature coefficient.

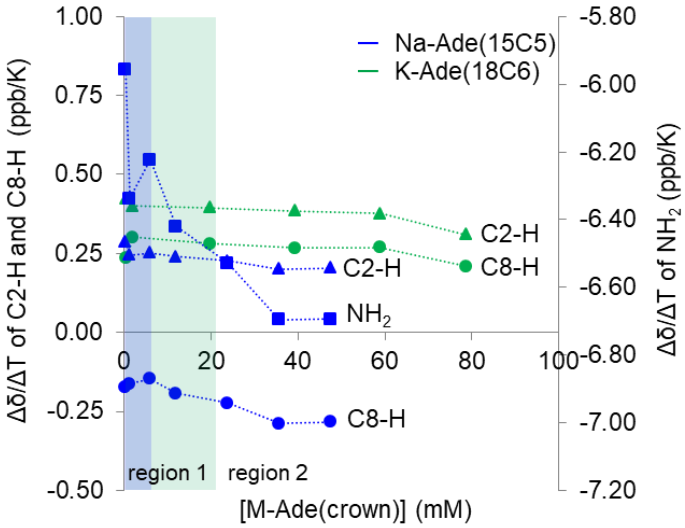

Figure S1.8: The change in temperature coefficients with concentration of ^{1}H chemical shifts for the Na-Ade(15C5) and K-Ade(18C6) in DMSO-d_6. NH_2 (squares), C8-H (circles) and C2-H (triangles).

© University of Pretoria

Fitting of thermodynamic data

The expected sigmoidal curve generally obtained during aggregation studies is not obtained in the concentration or temperature dependent studies of Na-/K-Ade, Na-Ade(15C5) and K-Ade(18C6) in DMSO-d_6 due to change in chemical shift between region 1 and 2. The limit of dilution for ^{1}H NMR detection and saturation for solubility of the complexes added additional restrictions preventing the detection of monomer- and aggregate-only chemical shifts. Data from region 2 were used to obtain an estimate of aggregation for the ionic complexes. The limited data points for all complexes from the ^{1}H NMR study for region 1 prevented modelling of the aggregation occurring at these low concentrations.

In region 2 increasing the concentration resulted in the δ for each purine proton to become deshielded as aggregates are formed. Increasing the temperature should yield less aggregates, resulting in shielding of the protons. However, the effect of temperature for a set of concentrations resulted in the δ being more deshielded, Figure S1.9.

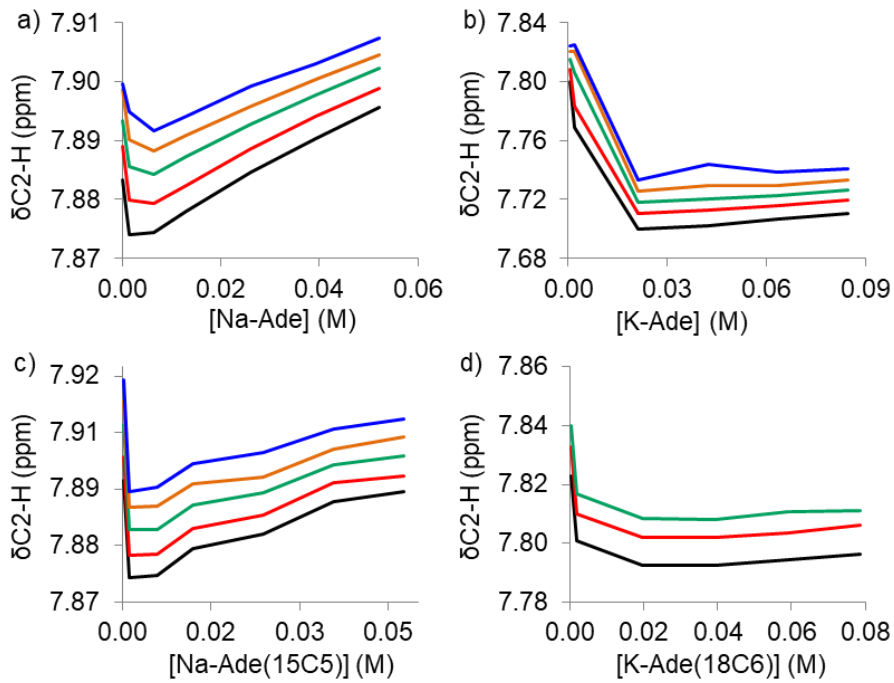

Figure S1.9: ^{1}H NMR chemical shift for the C2-H proton of a) Na-Ade, b) K-Ade, c) Na-Ade(15C5) and d) K-Ade(18C6) with an increase in concentration at 305 K (Na^+ complexes) or 300 K (K^+ complexes) (black line), 320 K (red line), 340 K (green line) 360 K (orange line) and 380 K (blue line).

The changes in chemical shifts of the purine protons with an increase in temperature were normalized, δ_N, in order to fit nonlinear NMR aggregation models. The more complex behavior of K-Ade(18C6) chemical shifts with an increase in temperature prevented model fitting, Figure S10d. The changes in chemical shift with concentration for each temperature (T) were normalized in order to obtain K_{eq} of self-aggregation in region 2 by the following method:

A normalization factor, *f*, is obtained for each T set in Figure S1.9,

© University of Pretoria

$$f = \delta_{0_T}/\delta_{0_{305}} \quad (1)$$

where δ_{0_T} is the chemical shift at the reference concentration (lowest concentration at the beginning of the linear portion of region 2) at temperature T (where T ≠ 305 or 300 K for the Na^+ and K^+ complexes, respectively, and $\delta_{0_{305}}$ is the chemical shift at the reference concentration at 305 or 300 K for the Na^+ and K^+ complexes, respectively. Reference concentrations are 6.52, 1.19, 21.2 and 19.7 mM for Na-Ade, Na-Ade(15C5), K-Ade and K-Ade(18C6), respectively.

The chemical shifts at concentrations larger than the reference concentration are normalized by the factor *f* obtained for each temperature:

$$\delta_N = \delta_T/f \quad (2)$$

The normalized δ for the C2–H protons are shown in Figure S1.10

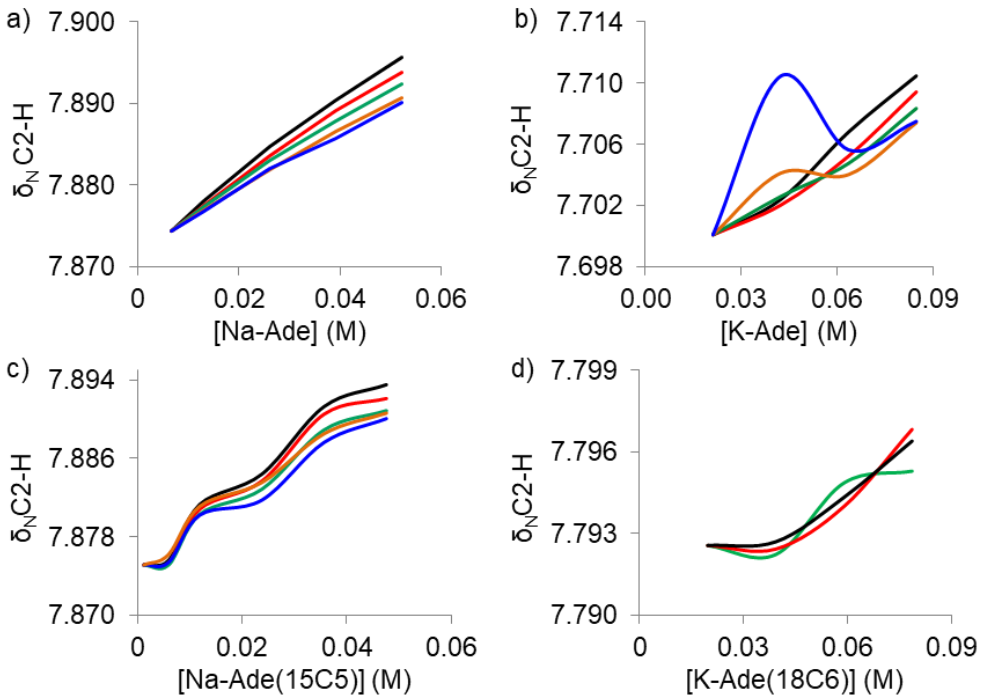

Figure S1.10: Normalized ^{1}H NMR chemical shifts for the C2-H proton of a) Na-Ade b) K-Ade, c) Na-Ade(15C5) and d) K-Ade(18C6) at black – 305 K (Na^+ complexes)/300 K (K^+ complexes), red – 320 K, green – 340 K, orange – 360 K, blue – 380 K.

In Figure S1.10b, there is a dramatic change in behavior of the K-Ade system at temperatures 360 and 380 K, indicating a change between different species in solution. This effect is not observed in the presence of the 18C6, Figure S1.10d.

© University of Pretoria

Self-aggregation studies

From the normalized chemical shifts, the isodesmic and trimer model for aggregation were fitted,

Isodesmic model:

$$\delta_{obs} = \delta_m + (\delta_a - \delta_m)\left(1 + \frac{1-\sqrt{4K_{agg}C_t+1}}{2K_{agg}C_t}\right) \quad (3)$$

where δ_{obs} is the observed chemical shift, δ_m and δ_a is the chemical shifts of the monomer and aggregate forms, K_{agg} is the aggregation constant and C_t is the total concentration of the ionic compound.

Trimer model:

$$\delta_{obs} = \delta_m + 3C_t^2K_3(\delta_t - \delta_m) \quad (4)$$

where δ_t is the chemical shifts of the trimer and K_3 is the association constant for trimer formation.

Fitting of the isodesmic and trimer model to Na-Ade, Na-Ade(15C5) and K-Ade is shown in Figure S1.11.

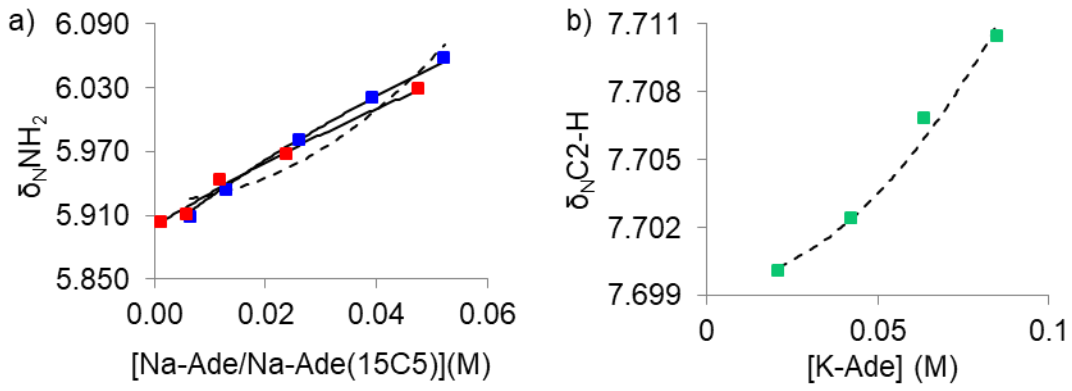

Figure S1.11: Fitting of the isodesmic (solid line) and trimer (dashed line) model to a) Na-Ade (blue squares) and Na-Ade(15C5) (red squares) for the NH_2 peaks and b) K-Ade (green squares) for the C2–H peak. Due to the extremely poor fit of the isodesmic model to K-Ade, data is not shown.

© University of Pretoria

Table S1.1: K_{eq} constants obtained for the isodesmic model for Na-Ade and Na-Ade(15C5) and the trimer model for K-Ade at the indicated temperature range in DMSO-d_6 as solvent

	Na-Ade			Na-Ade(15C5)			K-Ade	
	K_{agg} (M^{-1})						K_3 (M^{-2})	
δ_m	5.89	7.87	7.62	5.90	7.87	7.63	7.40	7.70
δ_a	7.34	8.12	8.07	7.18	8.02	7.95	8.60	8.55
	NH2	C2–H	C8–H	NH2	C2–H	C8–H	C2–H	C8–H
305 K[a]	2.82	2.30	2.20	2.59	3.50	2.79	0.61	0.60
320 K	2.61	2.10	1.93	2.32	3.19	2.43	0.53	0.54
340 K	2.33	1.96	1.76	2.00	2.91	2.06	0.49	0.50
360 K	2.10	1.78	1.55	1.94	2.70	1.91		
380 K	1.97	1.72	1.44	2.27	3.00	2.04		

[a] 300 K for K-Ade

The average of the K at a given temperature for the purine protons in Table S1.1 were used to for the van't Hoff plot.

The 1:1 complexation between 15C5 and Na^+ was modelled using the concentration dependent change in CH_2 chemical shift of the 15C5 for the temperature range 305-380 K.

$$\delta_{obs} = \frac{\delta_0 + \delta_{AB} K_1 [C_{Na^+}]}{1 + K_1 [C_{Na^+}]} \quad (5)$$

where δ_0 and δ_{AB} is the chemical shift of the uncomplexed and complexed 15C5, K_1 is the association constant of 1:1 complexation between 15C5 and Na+ and C_{Na^+} is the concentration of Na^+. The fitted 1:1 model is shown in Figure S1.12 and association constants in Table 1.2.

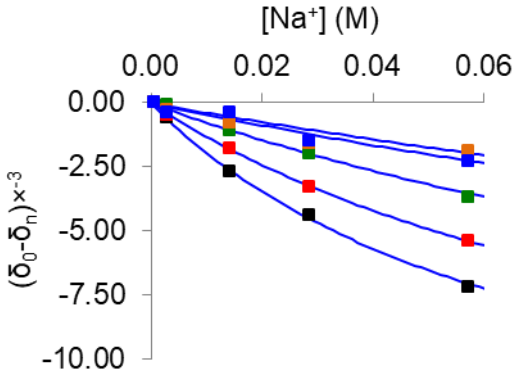

Figure S1.12: Fitting of the 1:1 model for the complexation between 15C5 and Na^+ at 305 K (black), 320 K (red), 340 K (green), 360 K (orange) and 380 K (blue)

© University of Pretoria

Table 1.2: Association constant K_1 for the 1:1 complexation of 15C5 with Na^+ in DMSO in the presence of Ade^-

Temperature (K)	K_1 (M^{-1})
δ_0	−0.04954
δ_C	−15.86
305	27.9
320	18.0
340	10.0
360	5.78
380	4.90

© University of Pretoria

Crystal structures of deprotonated adenine in the presence of sodium and potassium counter ion

Table S1.3: Structural information of the XRD crystal structure of Na-Ade, K-Ade and K-Ade(18C6) obtained in DMSO-d_6

Na-Ade	
DB05_3	Deposition Number 2055271
Space group	$P2_1/n$
Cell lengths	**a** 6.7911(2) **b** 9.1288(2) **c** 17.0758(4)
Cell angles	□ 90 □ 98.880(2) □ 90
Cell volume	1045.92
Z,Z'	**Z**: 4 **Z'**: 0
R-factor	3.69
K-Ade	
DB02	-
Space group	P $2_1/n$
Cell lengths	**a** 6.7960(6) **b** 9.1286(8) **c** 17.0547(15)
Cell angles	□ 90 □ 98.764(8) □ 90
Cell volume	1045.69
Z,Z'	**Z**: 4 **Z'**: 0
R-factor	12.36
K-Ade(18C6)	Morphology 1 (main text)
cu_DB05_0m_a	Deposition Number 2055272
Space group	$P2_1/c$
Cell lengths	**a** 19.6287(9) **b** 8.5394(4) **c** 26.1208(12)
Cell angles	□ 90 □ 93.425(2) □ 90
Cell volume	4370.48
Z,Z'	**Z**: 8 **Z'**: 0
R-factor	8.47
K-Ade(18C6)	Morphology 2
DB04	Deposition Number 2055270
Space group	P $2_1/m$
Cell lengths	**a** 7.9183(4) **b** 16.2548(4) **c** 8.8051(3)
Cell angles	□ 90 □ 111.961(5) □ 90
Cell volume	1051.07
Z,Z'	**Z**: 2 **Z'**: 0
R-factor	5.78

© University of Pretoria

Table S1.4: Selected interatomic distances [Å] and dihedral angles [degrees] in the crystal structures of Na-Ade (M = Na) and K-Ade(18C6) (M = K)

Compound	Na-Ade[a]	K-Ade(18C6)[b]
Interatomic distances		
N1-M	2.517	
N3-M	3.232	2.915(2.910)
N9-M	2.442	2.945(2.924)
N7-M	2.453	
H12-N3	2.248	
H11-N7	2.465	2.217(2.191)
H12-N1	-	2.262(2.160)
d		0.924(0.928)
Covalently bonded atoms of the adeninate anion		
N1-C2	1.351	1.345 (1.339)
C2-N3	1.317	1.320
N3-C4	1.367	1.341 (1.348)
C4-C5	1.390	1.401
C4-N9	1.366	1.369
C5-C6	1.402	1.393 (1.408)
C5-N7	1.388	1.391 (1.365)
C6-N1	1.357	1.358 (1.365)
C6-N10	1.338	1.336
N7-C8	1.336	1.341 (1.334)
C8-N9	1.349	1.344(1.361)
Solvent and 18C6 interactions		
M-O (DMSO)	2.333	-
M-O (18C6)	-	2.789-3.023 (2.830-3.021)
Dihedral angles		
H11-N10-C6-N1	0.00	-11.27(13.22)
H12-N10-C6-C5	1.16	-18.66(5.86)
α (N3C4N9M)	−17.67	-0.09(2.34)
β (H13C2N1M)	17.25	-
γ (H14C8N7M)	−4.13	-

[a] Figure 2.8 [b] Figure 2.9b

The crystal structure of K-Ade had a poor R-factor (12.36). The R-factor reveals that the structure has not fully converged. However, this should not affect the unit cell and the arrangement of the ions within the cell, and we expect the connectivity between the ions is qualitatively correct. The structure can still be used for connectivity purposes to compare with the crystal structure of Na-Ade. The crystal packing of K-Ade, Figure S1.13, displays a zigzag packing morphology.

© University of Pretoria

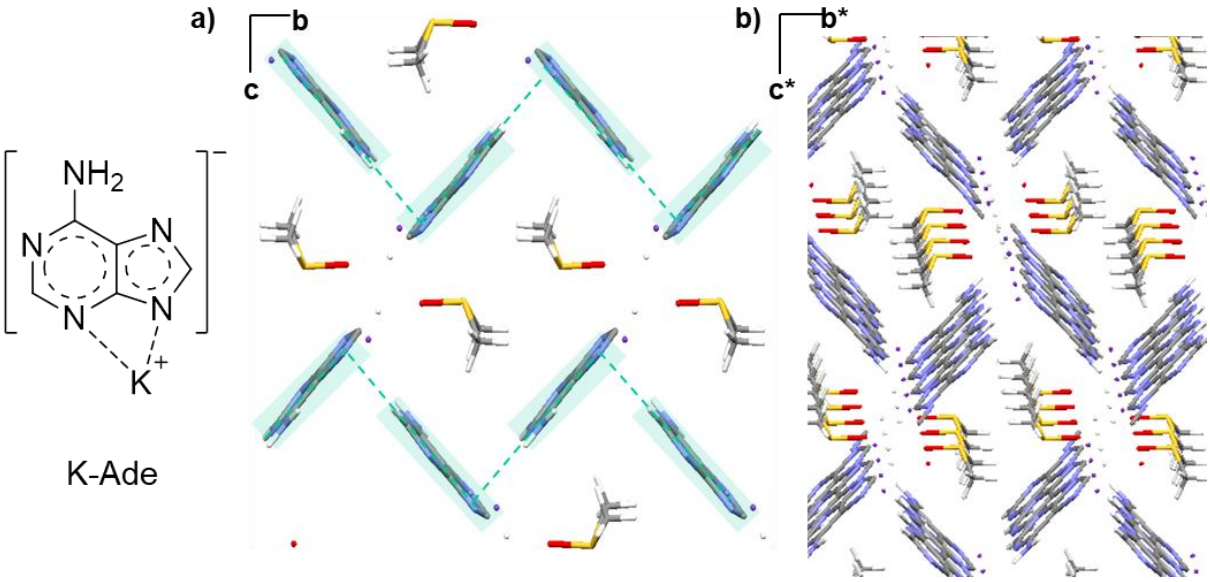

Figure S1.13: The molecular formula of K-Ade and XRD the zigzag packing morphology of crystals with included solvent molecules obtained from DMSO-d_6 solutions, viewed along the a) a axis and b) reciprocal a axis.

A closer look at the crystal packing shows that each K^+ counter ion is coordinated to three adeninate anion molecules via the N1-, N7- and N9-atoms of three purine rings of the adeninate anions (Figure S1.14).

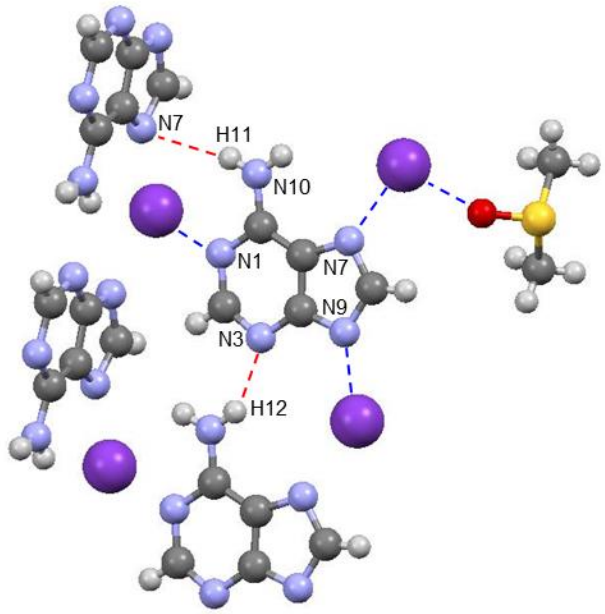

Figure S1.14: Crystal structure obtained from K-Ade showing one counter ion complexed with three adenine molecules and one adenine complexes with three counter ions.

© University of Pretoria

The second crystal morphology obtained from the K-Ade(18C6) displayed positional disorder in the system, whereby 50% of the adeninate anion molecule occupies a different position, hence resulting in the disordered adeninate anion structure. Each adenine molecule has a potassium atom complexed to the N9 and N3 nitrogen atoms of the purine ring system and the 18-crown-6. The packing lacked the hydrogen-bonded network between the adenyl moieties observed in the first morphology (Figure 2.9 of main text), and instead displayed a brick wall pattern along the a-axis (Figure S1.15a) with each K-Ade(18C6) unit inverted relative to its neighbor and a slipped stacked packing along the b axis (Figure S1.15b).

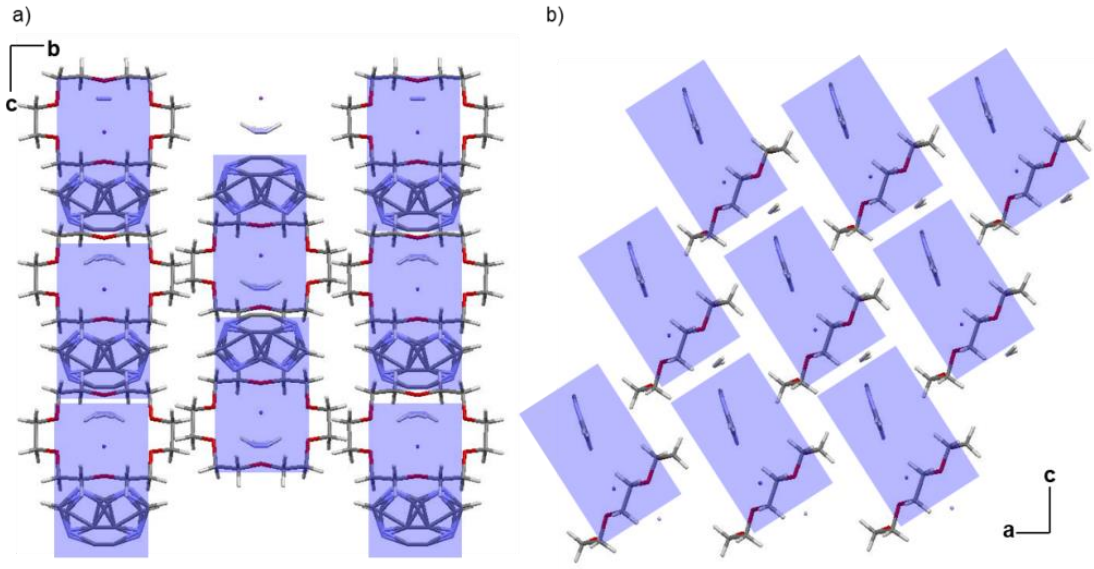

Figure S1.15: Packing of the second morphology of the adenine-potassium 18-crown-6 along the a) a and b) b axis.

© University of Pretoria

Absorption and emission spectra of adenine-Na, adenine-K, adenine-Na 15-crown-5 and adenine-K 18-crown-6

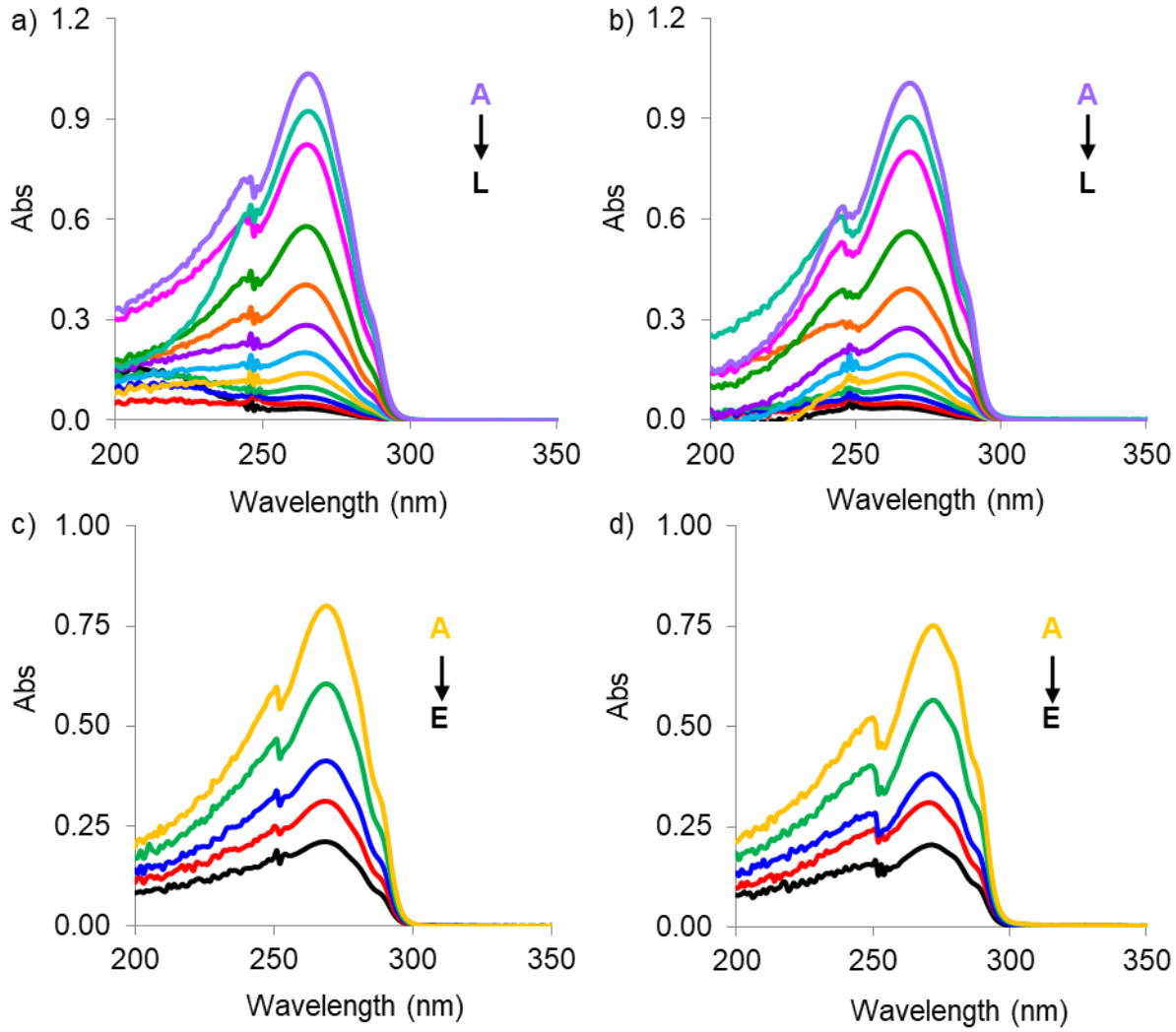

Figure S1.16: The concentration dependent UV absorption spectra of a) Na-Ade (A to H: 1.00 to 0.0323 mM) and b) K-Ade in DMSO as solvent (A to L: 1.00 to 0.0323 mM). Refer to Experimental details for UV spectroscopy studies for concentrations A to H/L. c) Na-Ade (A to E: 0.20 to 0.05 mM) and d) K-Ade (A to E: 0.20 to 0.05 mM) in anhydrous DMSO as solvent. A: 0.20, B: 0.15, C: 0.10, D: 0.075, E: 0.05 mM

The UV absorbance of KH in DMSO was run, Figure S1.17, in order to check the contribution of the hydride or free K^+ ion to the above K-Ade absorbance spectra.

© University of Pretoria

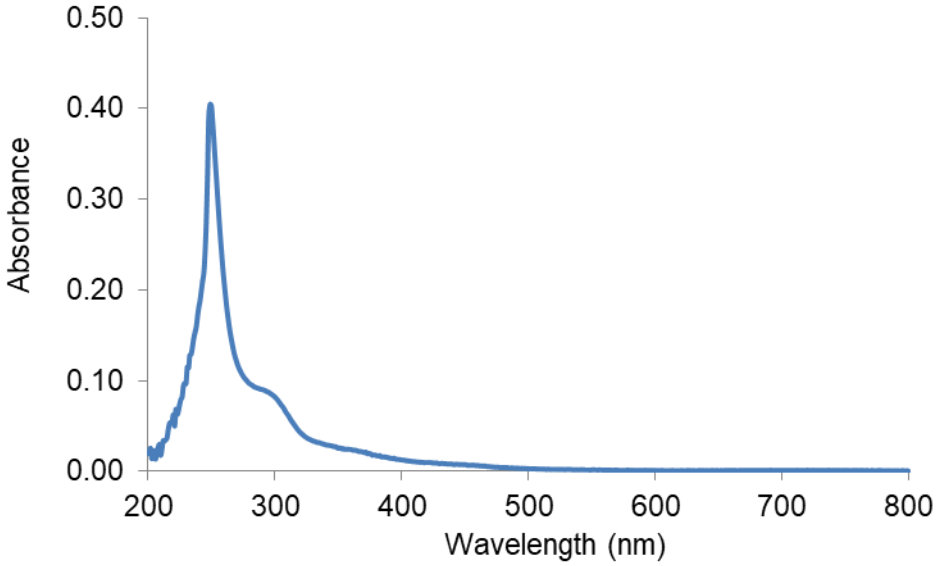

Figure S1.17: UV absorbance profile of KH (60.5 mM) in DMSO (no adenine present)

References:

[1] Organic Syntheses, Coll. Vol. 6, p.301 (1988); Vol. 57, p.30 (1977)

[2] Rigaku Oxford Diffraction, CrysAlisPro Software system, (2018).

[3] APEX3 (including SAINT and SADABS), Bruker AXS Inc., Madison, WI, 2016.

[4] Sheldrick, G. M. SHELXT – Integrated space-group and crystal structure determination, Acta Crystallogr., Sect. A: Found. Adv. 2015, 71, 3–8.

[5] Sheldrick, G. M. Crystal structure refinement with SHELXL, Acta Crystallogr., Sect. C: Struct. Chem. 2015, 71, 3–8.

© University of Pretoria

Supporting Information - 2

Towards a molecular understanding of the preferential site of coordination of sodium and potassium ions in adeninate salts in DMSO by quantum chemical studies.

Computational analysis

Table S2.1: Relative to the LEC, the difference in electronic energy (Δ*E*) and Gibbs free energy (Δ*G*), the Gibbs free energy of formation (G_f) of the Na- and K-Ade structural isomers (kcal mol^{-1})

	Na-Ade				K-Ade		
Conformer	Δ*E*	Δ*G*	G_f	Conformer	Δ*E*	Δ*G*	G_f
(N9)	0.0	0.0	-3.5	(N3N9)	0.0	0.0	-3.6
(N3N9)	0.0	0.4	-3.2	(N7)	2.2	2.3	-1.4
(N3)	0.8	0.6	-2.9	(N1)	3.3	3.5	-0.1
(N7)	1.2	1.4	-2.2	(N10)	4.4	4.2	0.6
(π)	2.2	1.5	-2.0				
(N1)	3.2	3.1	-0.39				
(N10)	5.0	5.0	1.5				

B3LYP/6-311G++(d,p)/PCM(DMSO)

© University of Pretoria

Table S2.2: Bond lengths, in Å, of the Na-Ade isomers obtained at the CCSD level of theory

	Na-Ade isomer						
Bond	(N9)	(N3N9)	(N3)	(N7)	(N1)	(N10)	(π)
N1,C6	1.34178	1.34452	1.34446	1.34072	1.34486	1.33811	1.34145
N1,C2	1.35606	1.35355	1.35253	1.35613	1.36139	1.35744	1.35712
C2,N3	1.32731	1.32875	1.32905	1.32631	1.32333	1.32721	1.32676
N3,C4	1.36209	1.36188	1.36428	1.36201	1.36465	1.36132	1.36395
C4,C5	1.40938	1.40662	1.41047	1.41199	1.41266	1.4154	1.41255
C5,C6	1.40458	1.40451	1.4034	1.40514	1.40211	1.39921	1.40391
C5,N7	1.38262	1.38305	1.38141	1.38323	1.38049	1.38048	1.3814
N7,C8	1.33964	1.34093	1.34235	1.34718	1.34277	1.34358	1.34346
C8,N9	1.36255	1.36245	1.36192	1.35374	1.36089	1.35989	1.36006
C4,N9	1.36518	1.36288	1.36062	1.36537	1.36115	1.36239	1.36353
C6,N10	1.38259	1.38022	1.38108	1.38583	1.38312	1.40223	1.38503
N10,H11	1.0114	1.01124	1.0113	1.0119	1.01123	1.01465	1.01167
N10,H12	1.01118	1.01103	1.01112	1.01097	1.01156	1.01476	1.01151
C2,H13	1.08909	1.08867	1.08879	1.08911	1.08929	1.0889	1.08932
C8,H14	1.08633	1.0861	1.08654	1.08663	1.08667	1.08677	1.08687
NX-Na	(N9) 2.41203	(N3) 2.62893	(N3) 2.45479	(N7) 2.4429	(N1) 2.49905	(N10) 2.59289	(N1) 4.47323
		(N9) 2.4781					(N3) 4.14768
							(N7) 3.94563
							(N9) 3.98487

© University of Pretoria

Table S2.3: Bond lengths, in Å, of the Na-Ade isomers obtained at the DFT/B3LYP level of theory

	Na-Ade isomer						
Bond	(N9)	(N3N9)	(N3)	(N7)	(N1)	(N10)	(π)
N1,C6	1.34562	1.3481	1.34802	1.34449	1.34556	1.33981	1.34523
N1,C2	1.34903	1.34633	1.34497	1.3487	1.35178	1.35101	1.35014
C2,N3	1.32862	1.32946	1.33074	1.32731	1.3258	1.32815	1.328
N3,C4	1.35593	1.35692	1.35967	1.35615	1.35879	1.35525	1.35928
C4,C5	1.41216	1.40839	1.41321	1.41614	1.41709	1.42031	1.4175
C5,C6	1.4034	1.40407	1.40256	1.4034	1.40159	1.3962	1.40329
C5,N7	1.3775	1.37753	1.37604	1.37929	1.37526	1.37489	1.37595
N7,C8	1.33965	1.34167	1.34331	1.34878	1.34414	1.34456	1.34445
C8,N9	1.3602	1.35972	1.35907	1.34986	1.35743	1.35717	1.35757
C4,N9	1.36418	1.36129	1.35899	1.36393	1.36132	1.361	1.36235
C6,N10	1.37061	1.36758	1.36898	1.37579	1.37366	1.39658	1.37177
N10,H11	1.00958	1.00938	1.00947	1.01057	1.00963	1.01401	1.0096
N10,H12	1.00905	1.00879	1.00895	1.00855	1.00958	1.01376	1.00914
C2,H13	1.08717	1.08651	1.08664	1.0872	1.08719	1.08687	1.08726
C8,H14	1.08356	1.08339	1.08398	1.08391	1.08425	1.08422	1.08418
NX-Na	(N9) 2.35951	(N3) 2.5114	(N3) 2.3985	(N7) 2.39149	(N1) 2.94199	(N10) 2.58135	(N1) 3.95058
		(N9) 2.45001					(N3) 3.59415
							(N7) 4.01973
							(N9) 3.81963

© University of Pretoria

Table S2.4: Bond lengths, in Å, of the K-Ade isomers obtained at the CCSD level of theory

	K-Ade isomer			
Bond	(N3N9)	(N7)	(N1)	(N10)
N1,C6	1.34366	1.34075	1.34423	1.33912
N1,C2	1.35432	1.35644	1.36009	1.35741
C2,N3	1.32797	1.3263	1.32424	1.32705
N3,C4	1.36341	1.36238	1.36429	1.36184
C4,C5	1.40858	1.41207	1.41283	1.41482
C5,C6	1.4045	1.40469	1.402	1.40015
C5,N7	1.38221	1.38294	1.38061	1.38061
N7,C8	1.34144	1.34665	1.34283	1.34351
C8,N9	1.36207	1.35516	1.36082	1.36003
C4,N9	1.36371	1.36487	1.36152	1.36237
C6,N10	1.38064	1.3861	1.38426	1.39719
N10,H11	1.01115	1.01195	1.01135	1.01365
N10,H12	1.01096	1.01108	1.01164	1.01371
C2,H13	1.08888	1.08913	1.08967	1.08897
C8,H14	1.08637	1.08701	1.08673	1.08676
NX-Na	(N3) 2.88695	(N7) 2.80654	(N1) 2.86527	(N10) 2.93894
	(N9) 2.83001			

Table S2.5 Bond lengths, in Å, of the K-Ade isomers obtained at the DFT/B3LYP level of theory

	K-Ade isomer			
Bond	(N3N9)	(N7)	(N1)	(N10)
N1,C6	1.34713	1.3443	1.34797	1.34258
N1,C2	1.34735	1.34939	1.35476	1.35095
C2,N3	1.32879	1.32755	1.32469	1.32779
N3,C4	1.35814	1.35672	1.35855	1.35603
C4,C5	1.41112	1.41612	1.41669	1.4194
C5,C6	1.40348	1.40255	1.40065	1.3983
C5,N7	1.37692	1.37804	1.37517	1.37485
N7,C8	1.34218	1.34774	1.34389	1.34433
C8,N9	1.35878	1.35185	1.35782	1.3574
C4,N9	1.36273	1.36351	1.36056	1.36082
C6,N10	1.36955	1.37654	1.37446	1.38719
N10,H11	1.00952	1.01067	1.00969	1.0122
N10,H12	1.00896	1.00923	1.00998	1.01174
C2,H13	1.08686	1.08724	1.08746	1.08696
C8,H14	1.08373	1.08426	1.0842	1.0842
NX-Na	(N3) 2.88285	(N7) 2.79304	(N1) 2.88372	(N10) 3.03404
	(N9) 2.82497			

© University of Pretoria

Table S2.6: Net atomic charge Q(A) of atoms of Ade^- and relative to Ade^- the changes in charge, ΔQ(A), upon formation of the Na- and K-Ade structural isomers, all values in e, at CCSD level of theory

	Q(A)	ΔQ(A)						
		Na-ade						
Atom A[a]	Ade^-	(N1)	(N3)	(N3N9)	(N9)	(N7)	(N10)	(π)
N3	-1.276	0.005	-0.026	-0.021	0.001	0.004	0.005	0.001
N1	-1.266	-0.017	0.006	0.010	0.004	0.003	0.001	0.001
N9	-1.248	0.005	-0.002	-0.026	-0.022	0.006	0.005	0.001
N7	-1.234	0.004	0.008	0.016	0.008	-0.020	0.004	0.001
N10	-1.147	0.000	-0.004	-0.005	-0.002	0.005	0.017	0.000
C5	0.375	0.006	0.005	0.004	0.001	-0.001	0.005	-0.002
C4	0.909	0.006	0.003	-0.005	0.002	0.005	0.012	-0.002
C6	0.979	0.000	0.005	0.010	0.008	0.005	-0.036	0.000
C8	0.982	0.002	0.002	0.012	0.012	0.010	0.003	-0.001
C2	1.090	0.001	0.012	0.012	0.004	0.005	-0.001	-0.001
H14	0.020	0.004	0.005	0.011	0.008	0.007	0.004	0.001
H13	0.024	0.004	0.008	0.010	0.004	0.004	0.005	0.001
H11	0.395	0.002	0.005	0.006	0.003	0.002	-0.001	0.001
H12	0.396	0.005	0.004	0.005	0.003	-0.002	-0.002	0.001
Total:	-1.000	0.028	0.031	0.039	0.034	0.031	0.021	0.003
		K-Ade conformers						
Atom A[a]		(N1)		(N3N9)		(N7)	(N10)	
N3		0.005	-	-0.010	-	0.003	0.005	-
N1		-0.006	-	0.007	-	0.002	0.002	-
N9		0.004	-	-0.009	-	0.004	0.005	-
N7		0.003	-	0.011	-	-0.005	0.004	-
N10		0.001	-	-0.006	-	0.005	0.013	-
C5		0.005		0.004		-0.001	0.003	
C4		0.006		-0.008		0.004	0.010	
C6		-0.003		0.009		0.002	-0.031	
C8		0.002		0.008		0.005	0.002	
C2		-0.001		0.010		0.004	-0.001	
H14		0.003		0.008		0.004	0.004	
H13		0.001		0.008		0.003	0.004	
H11		0.000		0.005		0.001	0.001	
H12		0.004		0.004		-0.003	0.000	
Total:		0.025	-	0.041	-	0.028	0.021	-

© University of Pretoria

Table S2.7: Net atomic charge Q(A) of atoms of Ade^- and relative to Ade^- the changes in charge, ΔQ(A), upon formation of the Na- and K-Ade structural isomers, all values in e, at DFT/B3LYP level of theory

	Q(A)	ΔQ(A)						
		Na-ade						
Atom A[a]	Ade^-	(N1)	(N3)	(N3N9)	(N9)	(N7)	(N10)	(π)
N3	-1.193	0.003	-0.025	-0.024	0.001	0.004	0.006	0.002
N1	-1.177	-0.014	0.006	0.010	0.005	0.004	0.002	0.002
N9	-1.166	0.003	-0.002	-0.025	-0.023	0.006	0.007	0.003
N7	-1.159	0.002	0.008	0.017	0.008	-0.019	0.006	0.003
N10	-1.105	0.001	-0.006	-0.007	-0.004	0.008	0.019	-0.004
C5	0.352	0.004	0.006	0.005	0.002	-0.003	0.006	-0.005
C4	0.838	0.002	0.002	-0.007	0.002	0.007	0.013	-0.010
C8	0.881	0.001	0.002	0.013	0.013	0.012	0.004	-0.001
C6	0.897	0.003	0.010	0.016	0.011	0.003	-0.039	0.006
C2	0.990	0.004	0.013	0.015	0.004	0.007	-0.001	0.000
H13	0.024	0.003	0.010	0.012	0.005	0.005	0.006	0.003
H14	0.024	0.002	0.005	0.012	0.009	0.009	0.005	0.003
H11	0.396	0.000	0.006	0.008	0.005	0.001	-0.003	0.003
H12	0.398	0.002	0.006	0.007	0.004	-0.004	-0.004	0.003
Total[b]:	-1.000	0.0172	0.0409	0.0513	0.0432	0.0398	0.0264	0.0064

	K-Ade conformers						
Atom A[a]	(N1)		(N3N9)		(N7)	(N10)	
N3	0.004	-	-0.009	-	0.004	0.006	-
N1	-0.004	-	0.007	-	0.003	0.002	-
N9	0.005	-	-0.008	-	0.005	0.007	-
N7	0.004	-	0.011	-	-0.004	0.006	-
N10	0.004	-	-0.005	-	0.008	0.012	-
C5	0.005		0.004		-0.002	0.002	
C4	0.005		-0.009		0.004	0.011	
C8	0.002		0.009		0.006	0.004	
C6	-0.004		0.011		0.000	-0.038	
C2	-0.001		0.011		0.004	0.000	
H13	0.003		0.008		0.004	0.006	
H14	0.003		0.008		0.006	0.005	
H11	0.000		0.006		0.000	0.001	
H12	0.003		0.005		-0.004	0.000	
Total[b]:	0.0296	-	0.0497	-	0.0362	0.0245	-

© University of Pretoria

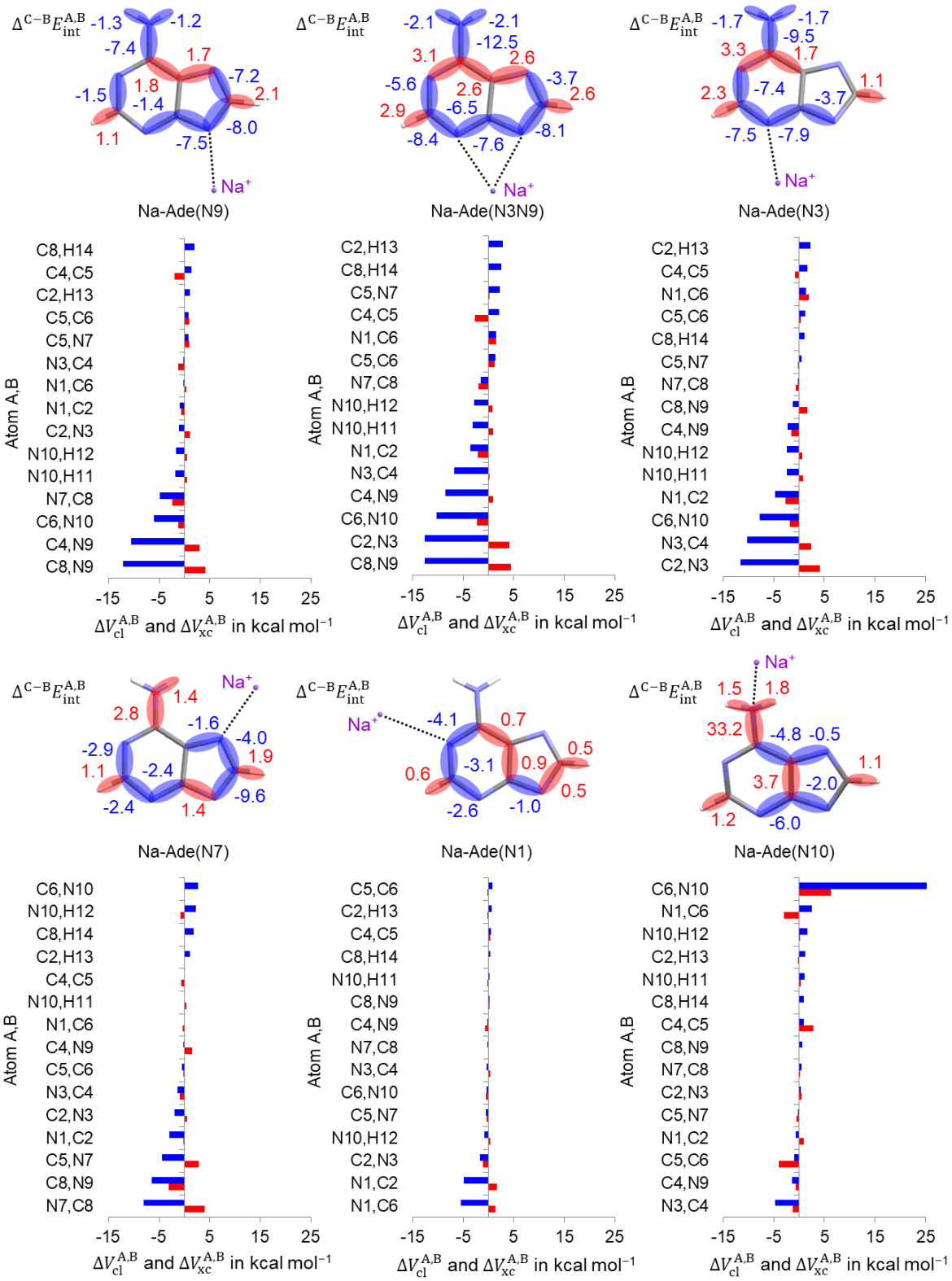

Figure S2.1: Changes in the diatomic covalent bond intramolecular interactions, $\Delta^{C-B}E_{int}^{A,B}$, and its $\Delta V_{cl}^{A,B}$ and $\Delta V_{xc}^{A,B}$ components. Blue and red sites indicate stabilizing and destabilizing energy terms of the adeninate anion upon coordination of Na^+ for the Na-Ade isomers, at DFT/B3LYP level of theory.

© University of Pretoria

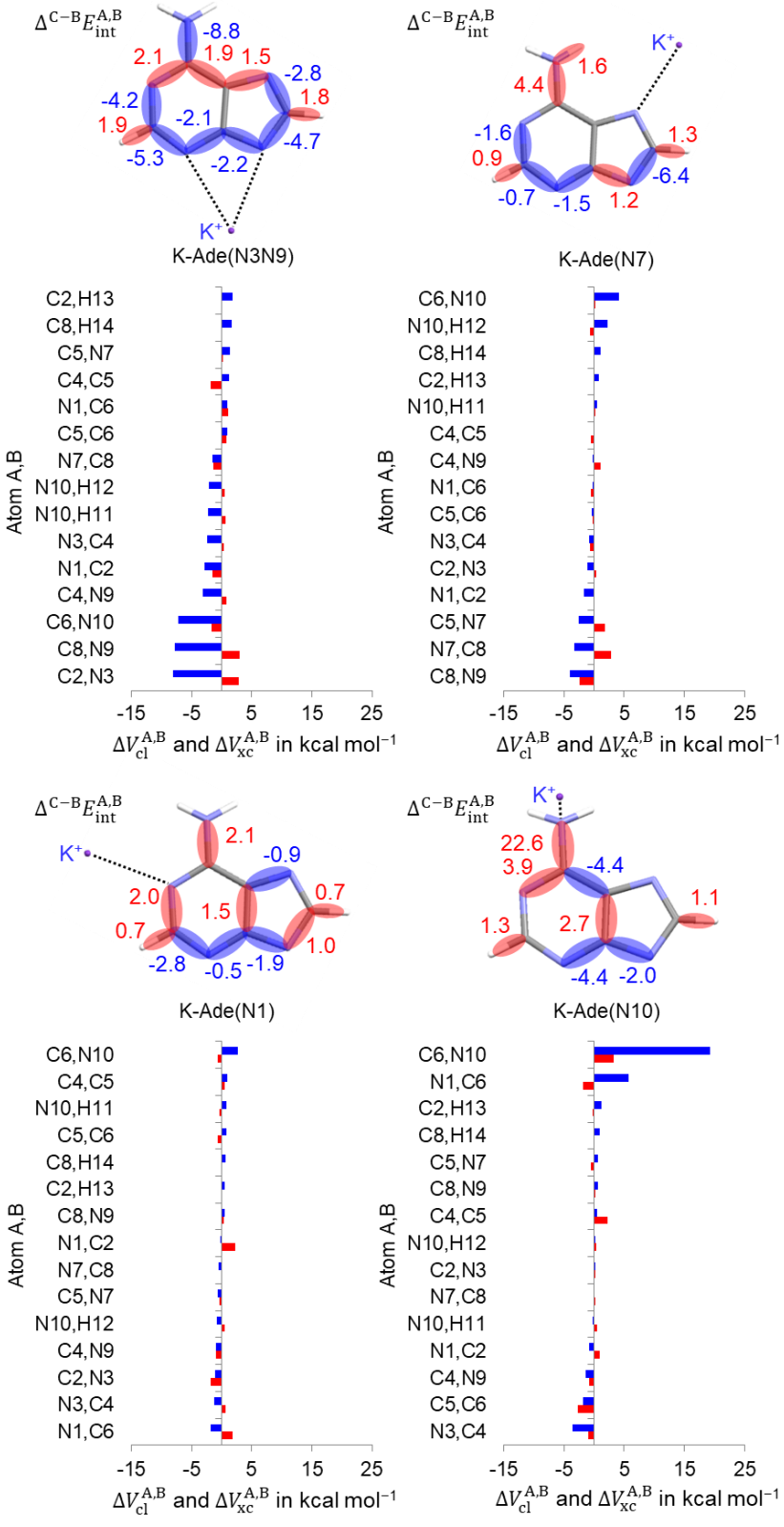

Figure S2.2: Changes in the diatomic covalent bond intramolecular interactions, $\Delta^{C-B}E_{int}^{A,B}$, and its $\Delta V_{cl}^{A,B}$ and $\Delta V_{xc}^{A,B}$ components. Blue and red sites indicate stabilizing and destabilizing energy terms of the adeninate anion upon coordination of K^+ for the Na-Ade isomers, at DFT/B3LYP level of theory.

© University of Pretoria

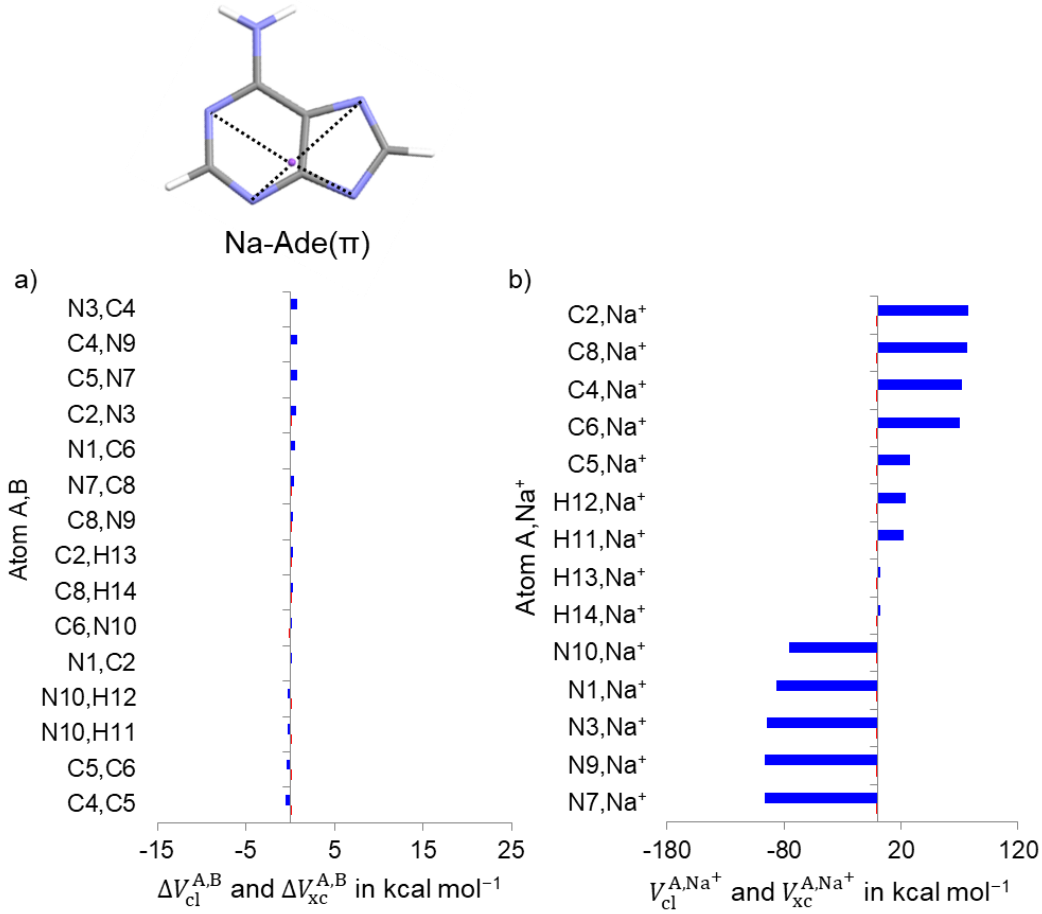

Figure S2.3: a) Changes in the diatomic covalent bond intramolecular interactions, $\Delta^{\mathrm{C-B}}E_{\mathrm{int}}^{\mathrm{A,B}}$, and its $\Delta V_{\mathrm{cl}}^{\mathrm{A,B}}$ and $\Delta V_{\mathrm{xc}}^{\mathrm{A,B}}$ components. Blue and red sites indicate stabilizing and destabilizing energy terms of the adeninate anion upon coordination of Na^+ and b) All individual coulombic, $V_{\mathrm{cl}}^{\mathrm{A,Na^+}}$ - blue bars, and exchange-correlation, $V_{\mathrm{XC}}^{\mathrm{A,Na^+}}$ - red bars, contributions to ${}_{\mathrm{inter}}E_{\mathrm{int}}^{\mathrm{Na^+,Ade^-}}$ from atom A with Na^+, where atom A is all atoms of the adeninate anion, for the Na-Ade(π) isomer, at CCSD level of theory.

© University of Pretoria

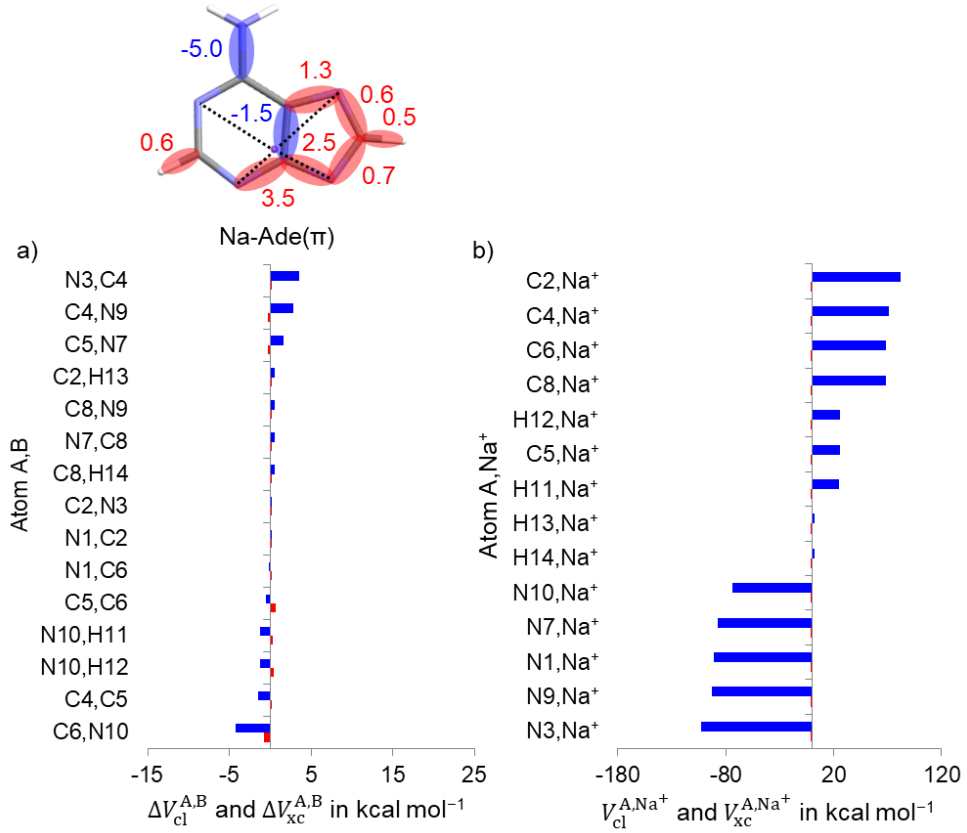

Figure S2.4: a) Changes in the diatomic covalent bond intramolecular interactions, $\Delta^{C-B}E_{int}^{A,B}$, and its $\Delta V_{cl}^{A,B}$ and $\Delta V_{xc}^{A,B}$ components. Blue and red sites indicate stabilizing and destabilizing energy terms of the adeninate anion upon coordination of Na^+ and b) All individual coulombic, V_{cl}^{A,Na^+} - blue bars, and exchange-correlation, V_{XC}^{A,Na^+} - red bars, contributions to ${}_{inter}E_{int}^{Na^+,Ade^-}$ from atom A with Na^+, where atom A is all atoms of the adeninate anion, for the Na-Ade(π) isomer, at DFT/B3LYP level of theory.

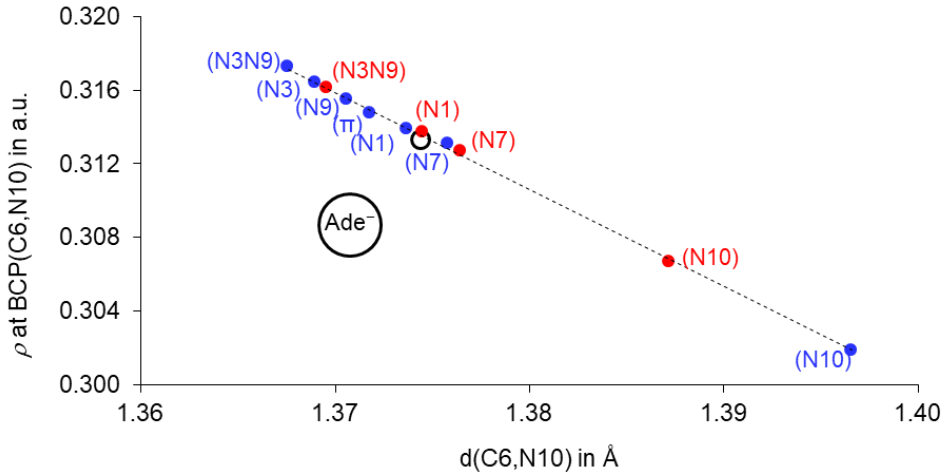

Figure S2.5: Relationship between rho (ρ) at BCP(C6,N10) and the C6–N10 bond length of the Na^+ (blue circles), K^+ (red circles) structural isomers and the free adeninate anion (black outlined circle) at DFT/B3LYP level of theory. The dashed lines show the linear relationship and the vertical dotted line is to guide the eye to the mirrored data points.

© University of Pretoria

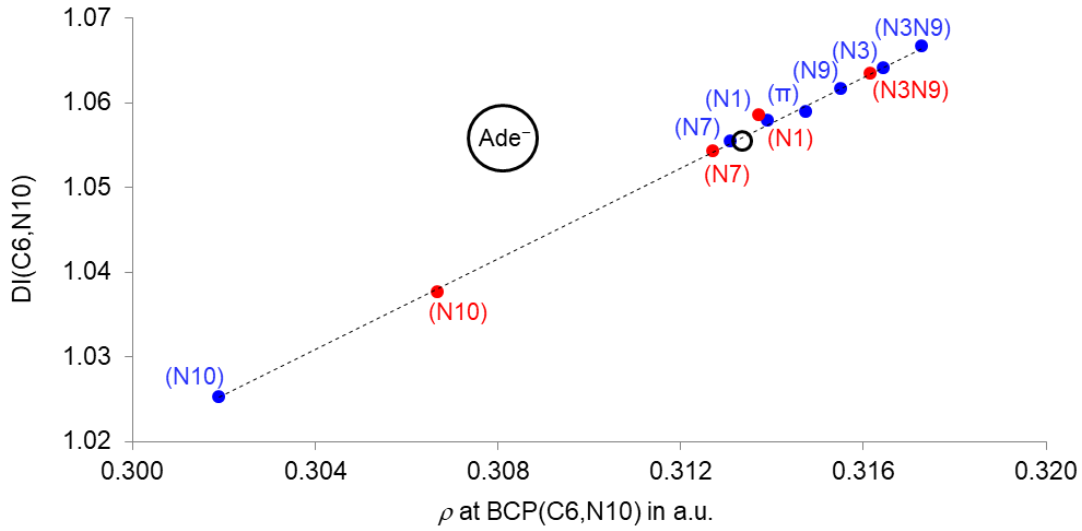

Figure S2.6: Relationship between rho (ρ) at BCP(C6,N10) and the DI(C6,N10) bond length of the Na^+ (blue circles), K^+ (red circles) structural isomers and the free adeninate anion (black outlined circle) at DFT/B3LYP level of theory.

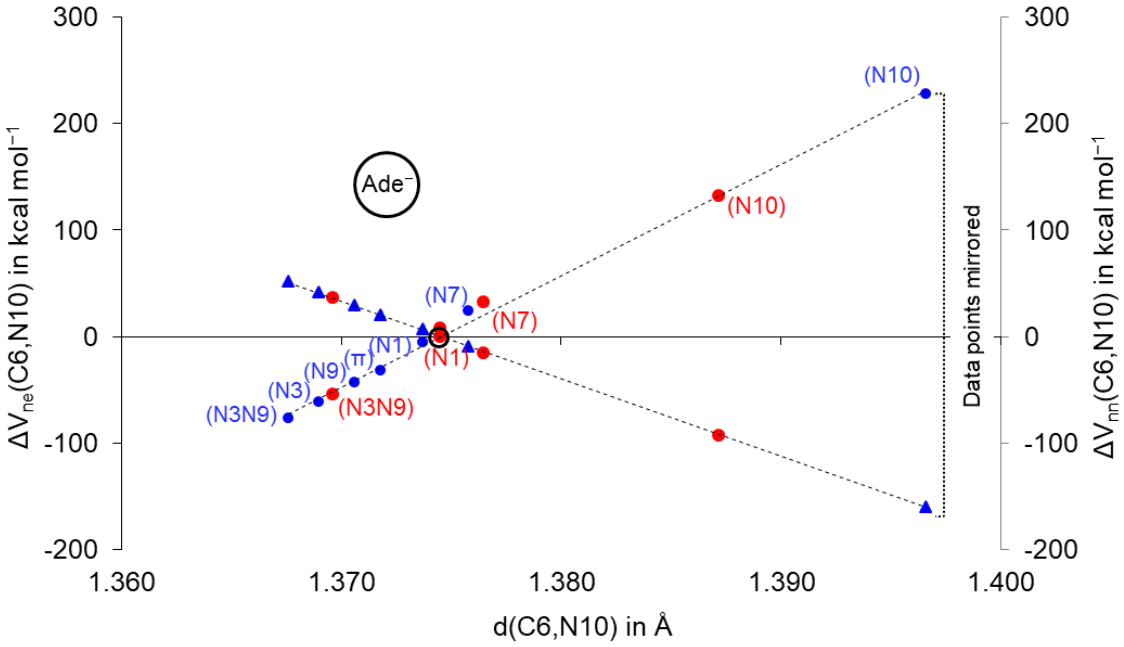

Figure S2.7: Relationship between $\Delta V_{ne}^{C6,N10}$ (primary axis, circles) and $\Delta V_{nn}^{C6,N10}$ (secondary axis, triangles) with the C6–N10 bond length of the Na^+ (blue data points) and K^+ (red data points) structural isomers and the free adeninate anion (black outlined circle) at DFT/B3LYP level of theory.

© University of Pretoria

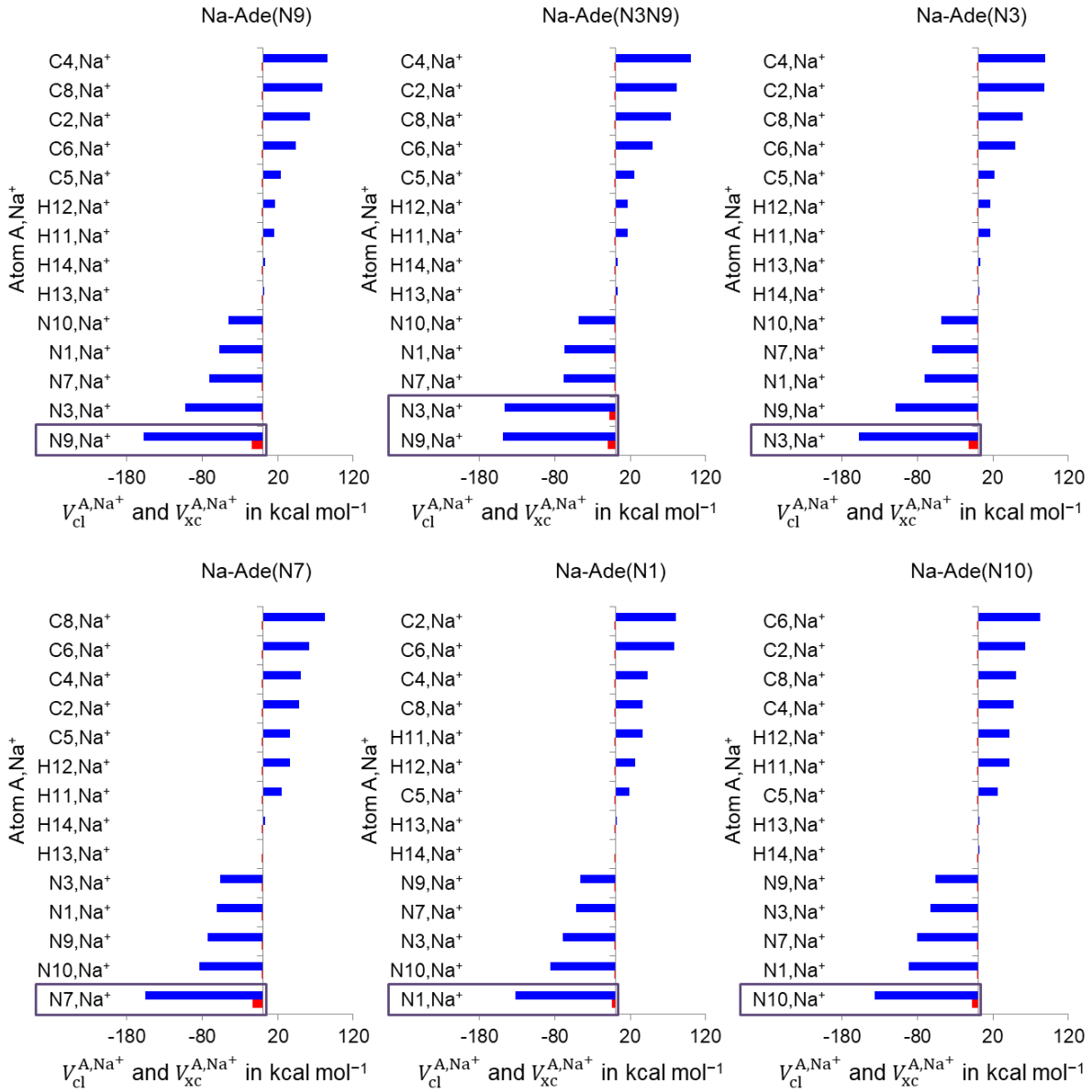

Figure S2.8: All individual coulombic, $V_{\mathrm{cl}}^{\mathrm{A,Na^+}}$ - blue bars, and exchange-correlation, $V_{\mathrm{XC}}^{\mathrm{A,Na^+}}$ - red bars, contributions to ${}_{\mathrm{inter}}E_{\mathrm{int}}^{\mathrm{Na^+,Ade^-}}$ from atom A with Na^+, where atom A is all atoms of the adeninate anion, for the Na-Ade isomers, at DFT/B3LYP level of theory.

© University of Pretoria

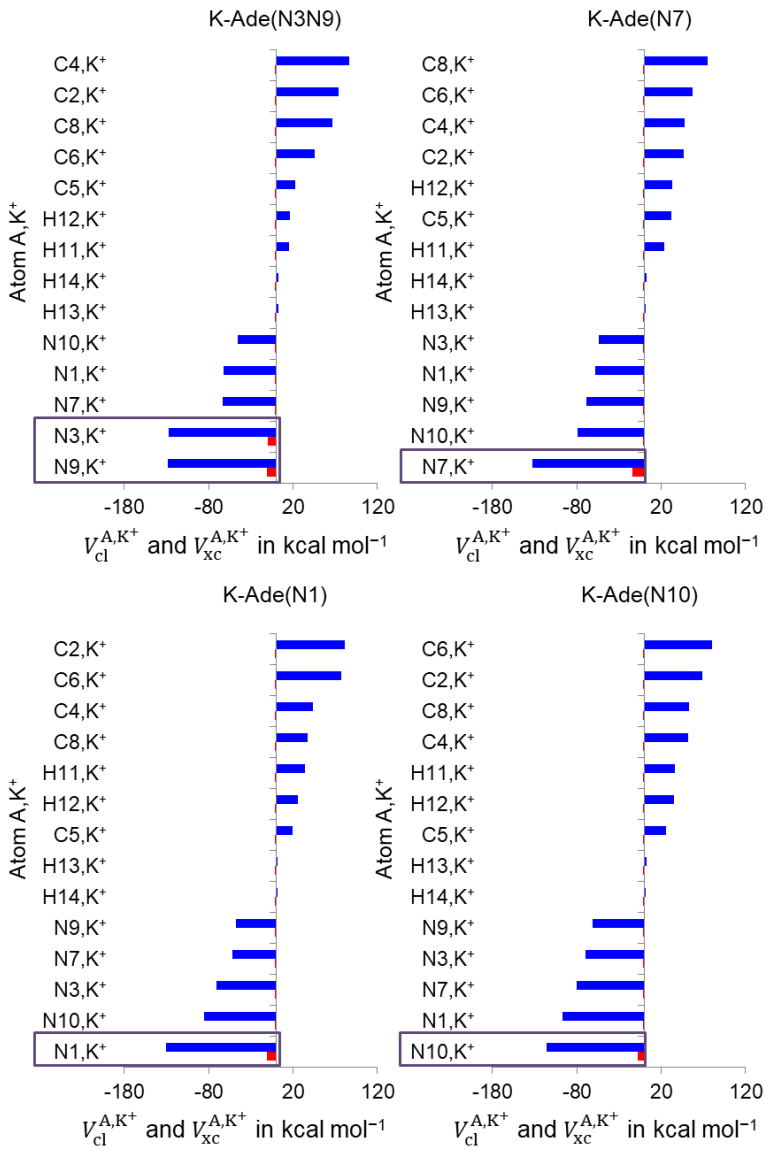

Figure S2.9: All individual coulombic, $V_{\mathrm{cl}}^{\mathrm{A,K^+}}$ - blue bars, and exchange-correlation, $V_{\mathrm{XC}}^{\mathrm{A,K^+}}$ - red bars, contributions to ${}_{\mathrm{inter}}E_{\mathrm{int}}^{\mathrm{K^+,Ade^-}}$ from atom A with K^+, where atom A is all atoms of the adeninate anion, for the K-Ade isomers, at DFT/B3LYP level of theory.

© University of Pretoria

Supporting Information - 3

Experimental and theoretical investigation into the reaction kinetics of the benzylation of sodium complexed adeninate anion in anhydrous DMSO

^{1}H NMR experimental data

The change in 1H NMR chemical shift of Na-Ade with increasing amounts of anisole is shown in Figure S3.1. There is no change in the peak positions of Na-Ade.

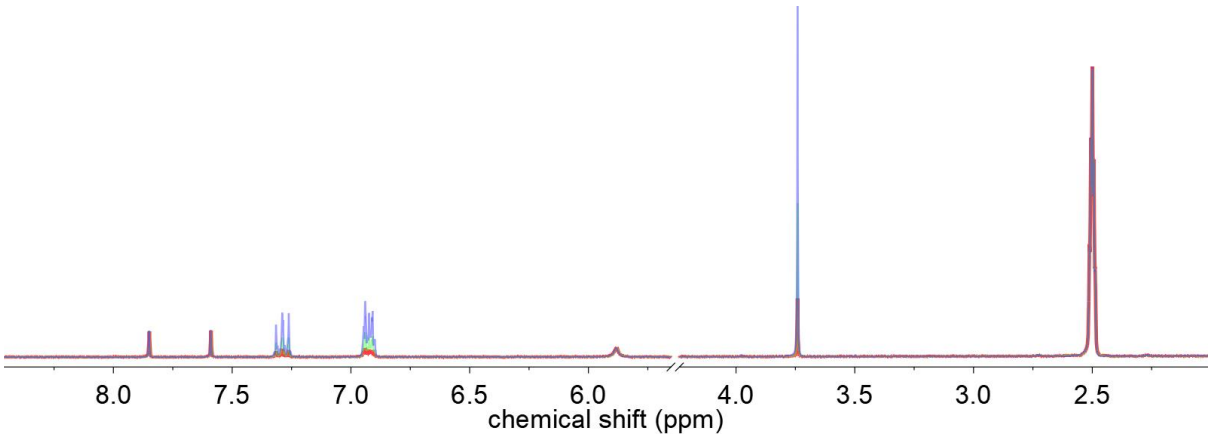

Figure S3.1: ^{1}H NMR chemical shifts for the mixture of Na-Ade and anisole in anhydrous DMSO-d_6

The aldehydes resulting from the alkylating reagents benzyl bromide and pentafluorobenzyl bromide are evident by the presence of an aldehyde peak at 10.02 and 10.14 ppm, respectively, in the ^{1}H NMR spectra (Figure S3.2a and b, respectively). The formation of methylphenyl ketone from the alkylating reagent (1-bromoethyl)benzene is observed in the ^{1}H NMR spectra from the proton peak present at 2.58 (CH_3) and benzylic protons at 7.97 and 7.95 (Figure S3.2c).

© University of Pretoria

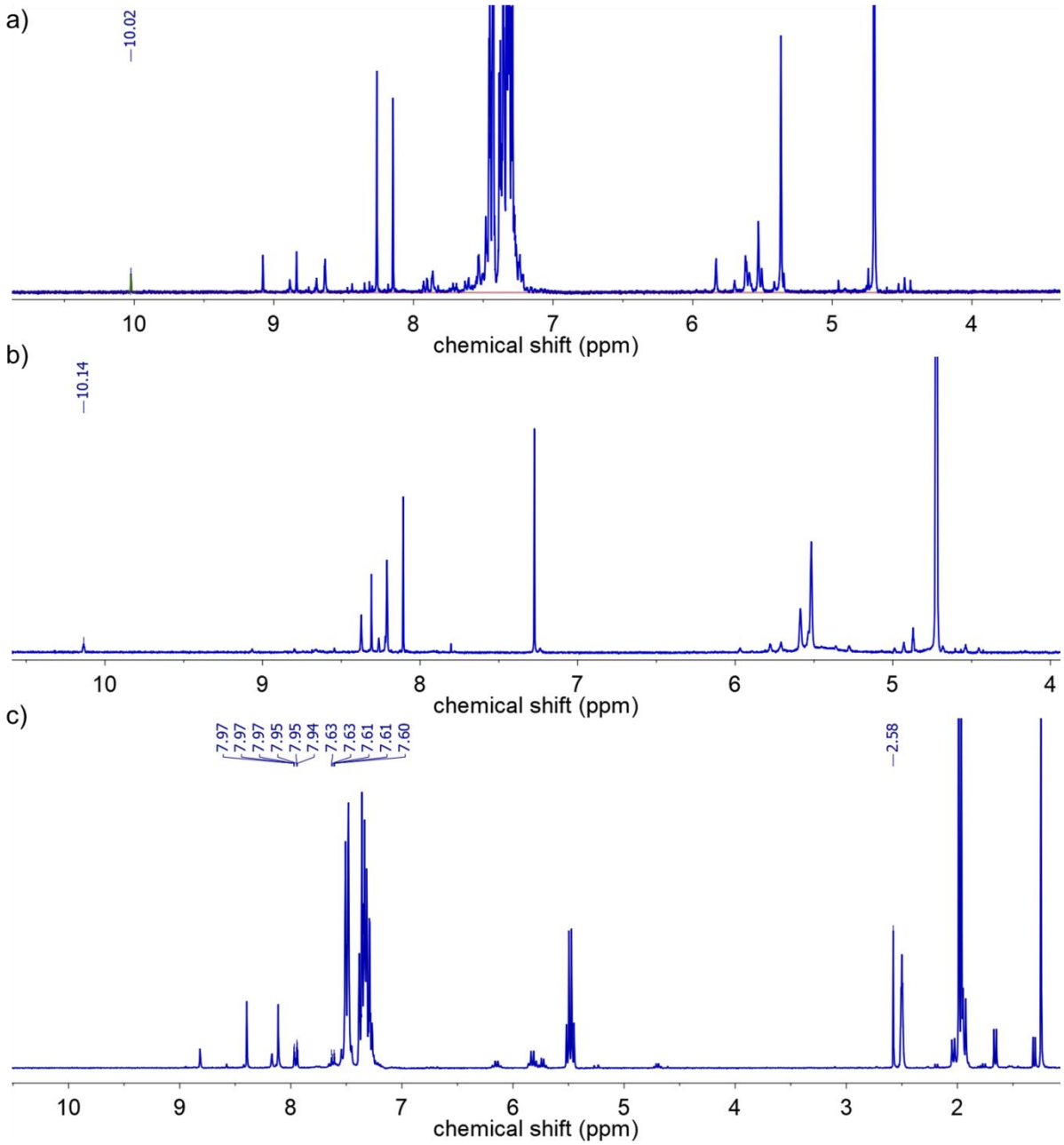

Figure S3.2: The ^{1}H NMR chemical shifts for the aldehyde compound resulting from a) benzyl bromide and b) pentafluorobenzyl bromide and the ketone from (1-bromoethyl)benzene in anhydrous DMSO-d_6

© University of Pretoria

Dynamic ^{1}H NMR spectroscopy data

The plots of the concentration of N9- and N3-Bn versus time resulting from the reaction between Na-Ade and BnCl with increasing BnCl concentration in the presence of DBU and TEA is shown in Figure S3.3 and Figure S3.4, respectively. The initial rates (Table S3.1) are measured using the slope of the linear portion of the plots, indicated by the solid black lines.

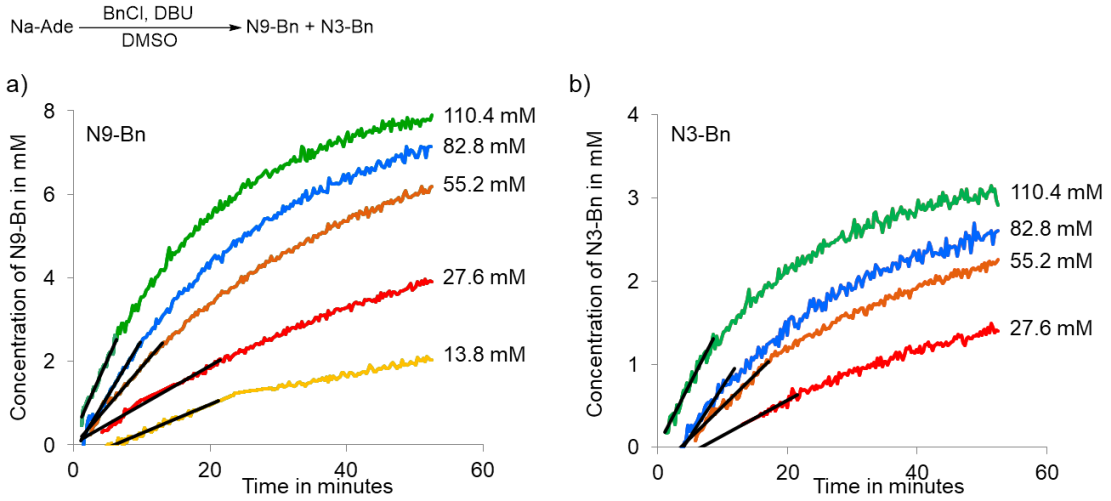

Figure S3.3: Plot of a) N9- and b) N3-Bn concentration over time during the benzylation of Na-Ade in the presence of DBU with increasing benzyl chloride concentrations in anhydrous DMSO. Regions used for initial rates are indicated by the black and orange slopes for the N9- and N3-Bn, respectively.

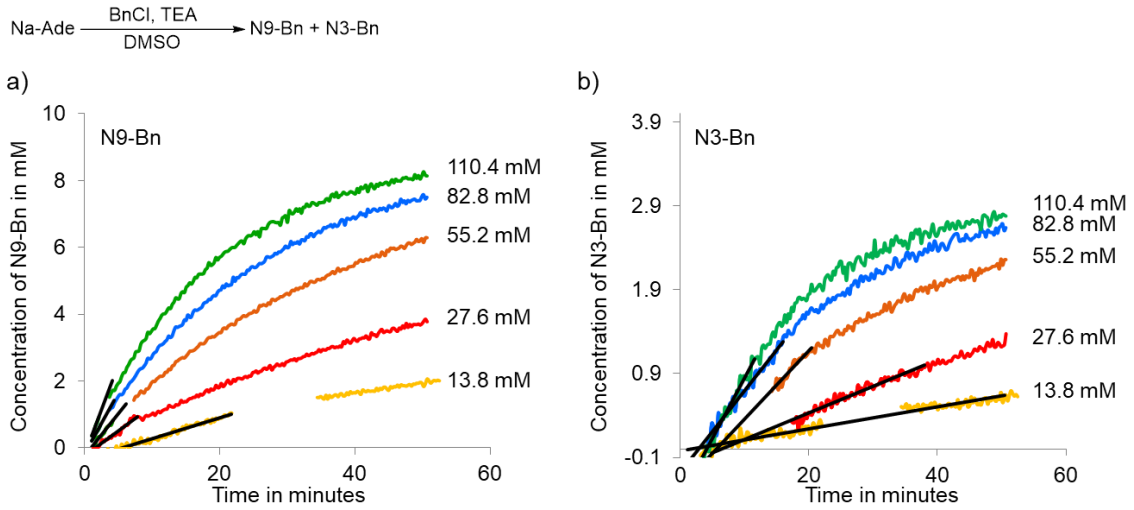

Figure S3.4: Plot of a) N9- and b) N3-Bn concentration over time during the benzylation of Na-Ade in the presence of TEA with increasing benzyl chloride concentrations in anhydrous DMSO. Regions used for initial rates are indicated by the black slopes.

© University of Pretoria

Table S3.1: Initial rates for the formation of N9- and N3-Bn in the presence of DBU and TEA with increasing benzyl chloride concentrations in anhydrous DMSO

	rate, mM s^{-1}			
	N9-Bn		N3-Bn	
conc BnCl	DBU	TEA	DBU	TEA
13.8	7.12×10^{-4}	7.39×10^{-4}	2.44×10^{-4}	2.31×10^{-4}
27.6	1.42×10^{-3}	1.38×10^{-3}	5.84×10^{-4}	5.30×10^{-4}
55.2	2.95×10^{-3}	3.16×10^{-3}	1.04×10^{-3}	9.91×10^{-4}
82.8	4.10×10^{-3}	4.35×10^{-3}	1.67×10^{-3}	1.63×10^{-3}
110.4	6.04×10^{-3}	5.97×10^{-3}	2.35×10^{-3}	2.40×10^{-3}

The plots of the concentration of N9- and N3-Bn versus time resulting from the reaction between Na-Ade and BnCl with increasing Na-Ade concentration in the presence of TEA is shown in Figure S3.5, respectively. The initial rates (Table S3.2) are measured using the slope of the linear portion of the plots, indicated by the solid black lines.

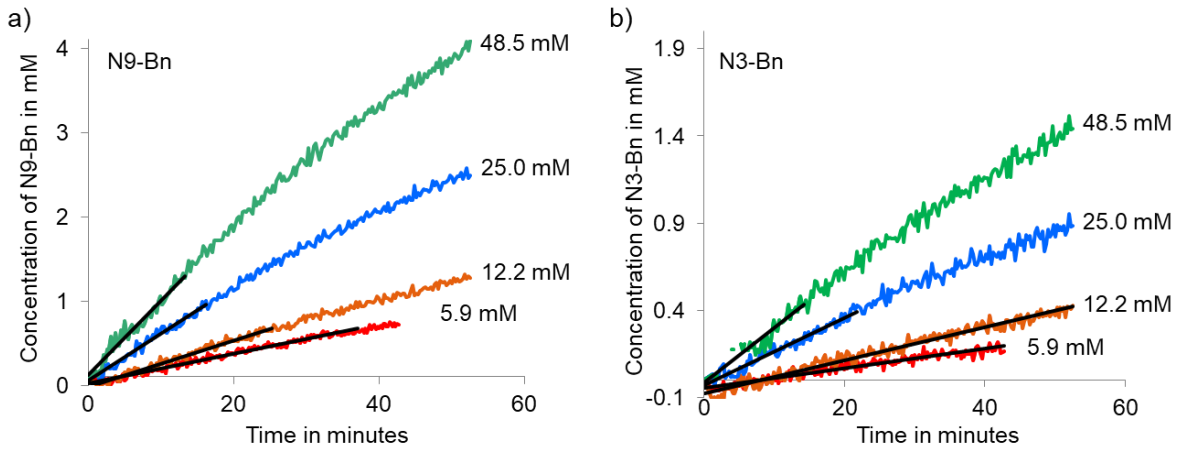

Figure S3.5: Plot of a) N9- and b) N3-Bn concentration over time during the benzylation of Na-Ade in the presence of TEA with increasing Na-Ade concentrations in anhydrous DMSO. Regions used for initial rates are indicated by the black slopes.

Table S3.2: Initial rates for the formation of N9- and N3-Bn in the presence of TEA with increasing Na-Ade concentrations in anhydrous DMSO

	rate, mM s^{-1}	
Na-Ade	N9-Bn	N3-Bn
5.9	2.30×10^{-4}	8.27×10^{-4}
12.2	4.58×10^{-4}	1.61×10^{-4}
25.0	9.04×10^{-4}	3.27×10^{-4}
48.5	1.51×10^{-3}	4.94×10^{-4}

© University of Pretoria

The initial rates plots for the formation of N9- and N3-Bn with increasing temperature are shown in Figure S3.6 and are given in Table S3.3. The Arrhenius plot is shown in Figure S3.7.

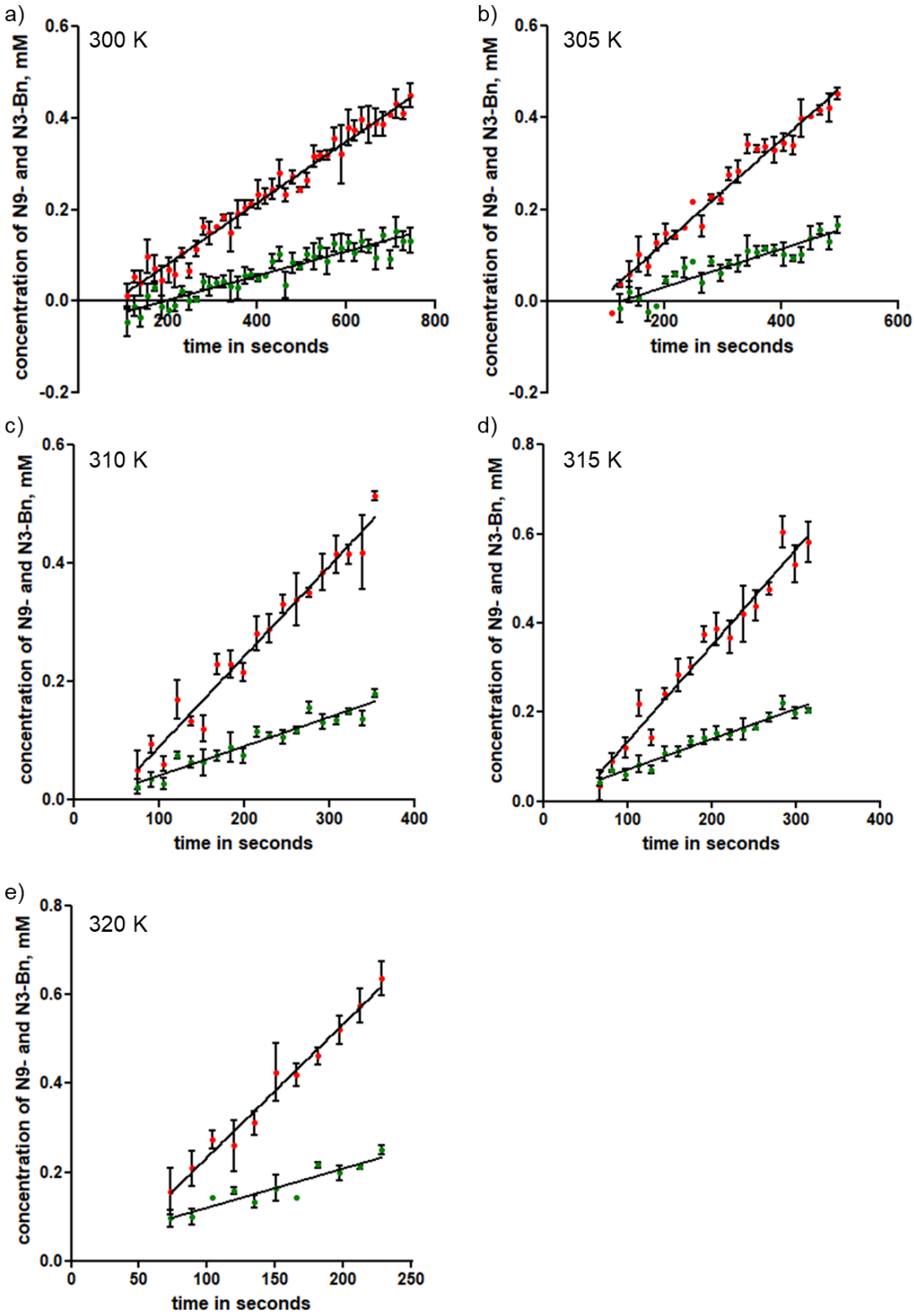

Figure S3.6: Plot of concentration versus time for the initial rate region during the benzylation of Na-Ade in the presence of DBU with increasing temperature a) 300 K, b) 305 K, c) 310 K, d) 315 K and e) 320 K for N9-Bn (red data points) and N3-Bn (green data points) in anhydrous DMSO

© University of Pretoria

Table S3.3: Initial rates and rate constant, *k*, for the formation of N9- and N3-Bn in the presence of DBU with increasing temperature in anhydrous DMSO

	N9-Bn		N3-Bn	
Temperature (K)	rate, mM s^{-1}	*k*, M^{-1} s^{-1}	rate, mM s^{-1}	*k*, M^{-1} s^{-1}
300	$6.68 \times 10^{-4} \pm 0.2$	7.13×10^{-3}	$2.66 \times 10^{-4} \pm 0.2$	2.84×10^{-3}
305	$1.12 \times 10^{-3} \pm 0.04$	1.20×10^{-2}	$4.15 \times 10^{-4} \pm 0.3$	4.43×10^{-3}
310	$1.53 \times 10^{-3} \pm 0.07$	1.63×10^{-2}	$4.95 \times 10^{-4} \pm 0.3$	5.28×10^{-3}
315	$2.16 \times 10^{-3} \pm 0.1$	2.30×10^{-2}	$6.83 \times 10^{-4} \pm 0.4$	7.29×10^{-3}
320	$3.01 \times 10^{-3} \pm 0.2$	3.21×10^{-2}	$8.83 \times 10^{-4} \pm 1.0$	9.42×10^{-3}

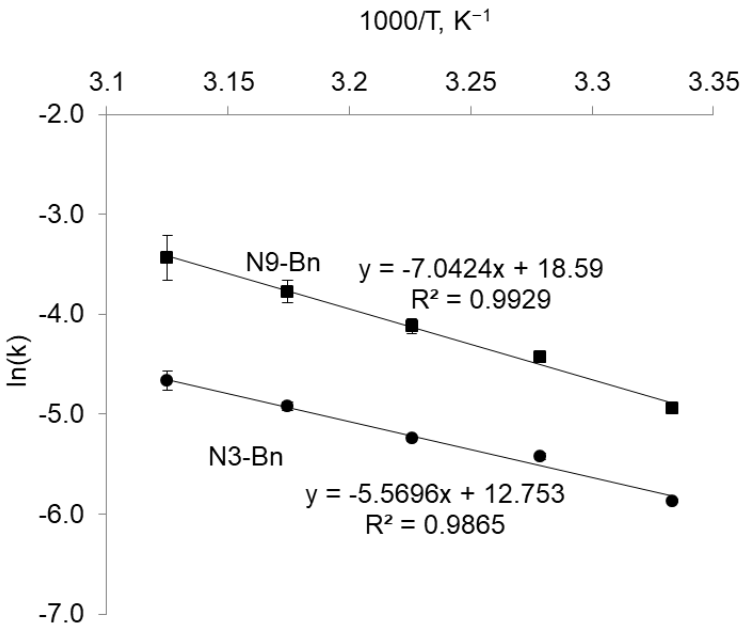

Figure S3.7: Arrhenius plot for N9- (squares) and N3-Bn (circles) in the presence of DBU in anhydrous DMSO

The initial rates plots for the formation of N9- and N3-Bn with increasing temperature in the presence of 15-crown-5 ether are shown in Figure S3.8 and are given in Table S3.4. The Arrhenius plot is shown in Figure S3.9.

© University of Pretoria

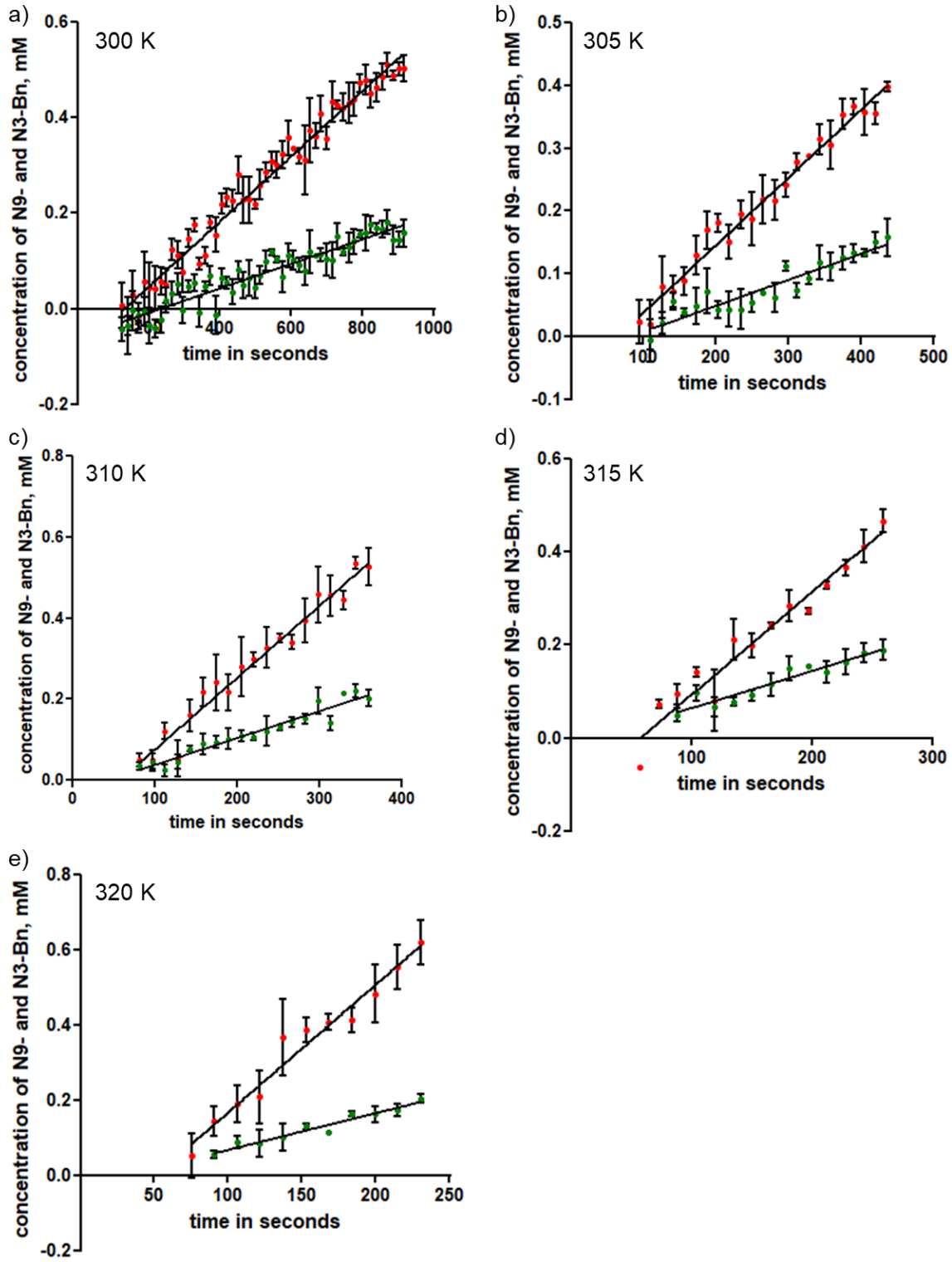

Figure S3.8: Plot of concentration versus time for the initial rate region during the benzylation of Na-Ade in the presence of DBU and 15-crown-5 ether with increasing temperature a) 300 K, b) 305 K, c) 310 K, d) 315 K and e) 320 K for N9-Bn (red data points) and N3-Bn (green data points) in anhydrous DMSO

© University of Pretoria

Table S3.4: Initial rates and rate constant, *k*, for the formation of N9- and N3-Bn in the presence of DBU and 15-crown-5 ether with increasing temperature in anhydrous DMSO

	N9-Bn		N3-Bn	
Temperature (K)	rate, mM s^{-1}	*k*, M^{-1} s^{-1}	rate, mM s^{-1}	*k*, M^{-1} s^{-1}
300	$6.84 \times 10^{-4} \pm 0.2$	7.30×10^{-3}	$2.58 \times 10^{-4} \pm 0.1$	2.75×10^{-3}
305	$1.08 \times 10^{-3} \pm 0.05$	1.15×10^{-2}	$4.15 \times 10^{-4} \pm 0.4$	4.43×10^{-3}
310	$1.77 \times 10^{-3} \pm 0.1$	1.89×10^{-2}	$6.64 \times 10^{-4} \pm 0.5$	7.08×10^{-3}
315	$2.21 \times 10^{-3} \pm 0.1$	2.36×10^{-2}	$7.98 \times 10^{-4} \pm 1.0$	8.51×10^{-3}
320	$3.41 \times 10^{-3} \pm 0.3$	3.63×10^{-2}	$9.80 \times 10^{-4} \pm 1.2$	1.05×10^{-2}

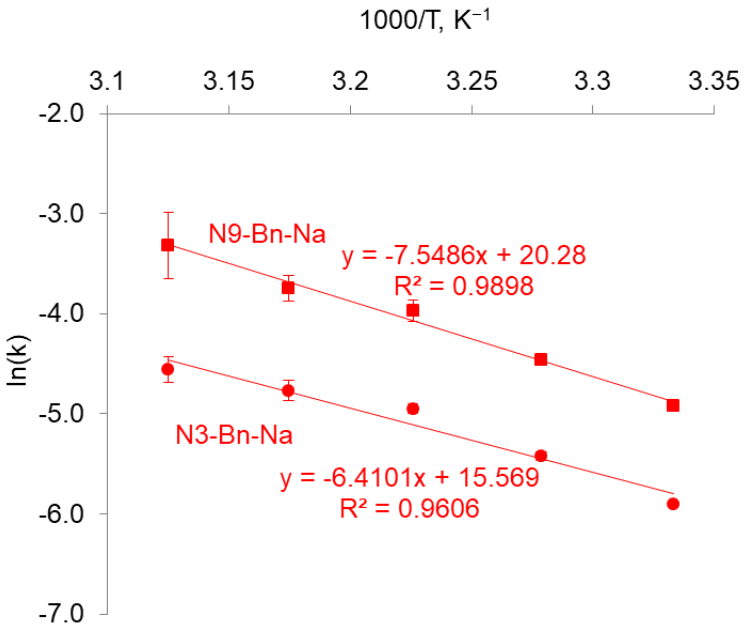

Figure S3.9: Arrhenius plot for N9- (squares) and N3-Bn (circles) in the presence of DBU and 15-crown-5 ether in anhydrous DMSO

© University of Pretoria

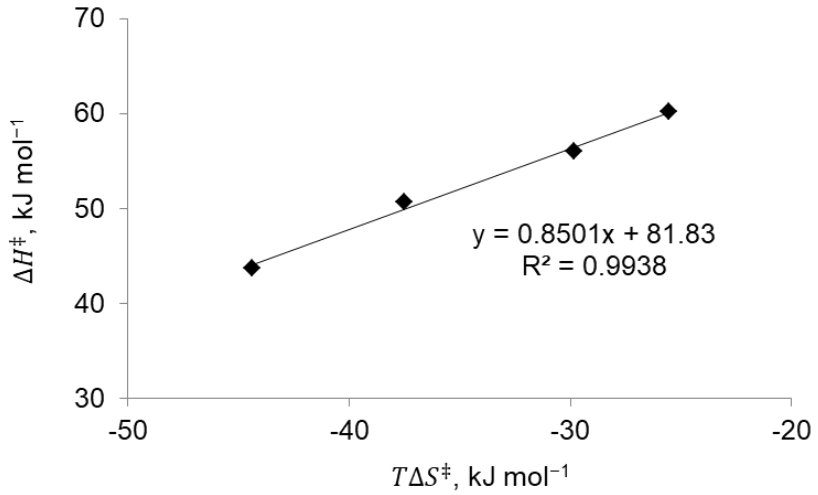

Figure S3.10: $\Delta \boldsymbol{H}^{\ddagger}$ vs. $\boldsymbol{T}\Delta \boldsymbol{S}^{\ddagger}$ enthalpy-entropy compensation plot for formation of N9-Bn and N3-Bn in the absence and presence of 15C5 in anhydrous DMSO at 300 K

Computational modelling

A pre-reactive complex is formed from the optimization of Ade^- and BnCl placed arbitrarily at a distance of 4 Å between the $\underline{C}H_2$ of BnCl and the reactive nitrogen atom i.e. N1, N3, N7 and N9 for the N1-, N3-, N7- and N9-Bn pathway respectively. From the pre-reactive complex, the two molecules were scanned along the reaction coordinate (decreasing the distance between the electrophilic $\underline{C}H_2$ carbon on the BnCl and the reactive nitrogen of the adeninate anion by 0.1 Å increments), through a TS to the final product of each pathway. The resulting change in electronic energy along the reaction coordinate is shown in Figure S3.11.

© University of Pretoria

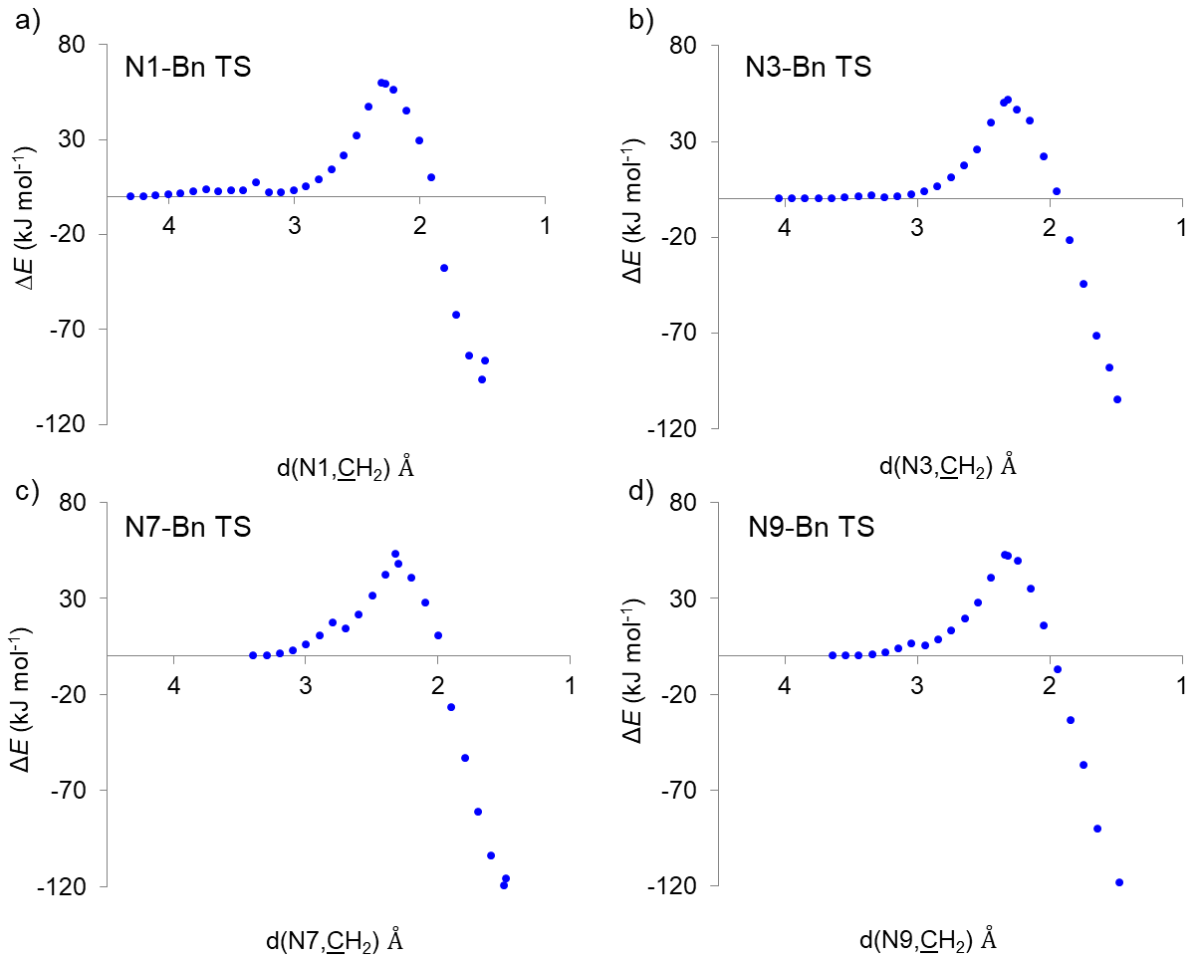

Figure S3.11: Change in electronic energy (Δ*E*) along the reaction coordinate for the scan between Ade and BnCl for the a) N1-, b) N3-, c) N7- and d) N9-Bn pathway

A pre-reactive complex is formed from the optimization of Na-Ade and BnCl placed arbitrarily at a distance of 4 Å between the $\underline{C}H_2$ of BnCl and the reactive nitrogen atom i.e. N1, N3, N7 and N9 for the Na-N1-, Na-N3-, Na-N7- and Na-N9-Bn pathway respectively. From the pre-reactive complex, the two molecules were scanned along the reaction coordinate (decreasing the distance between the electrophilic $\underline{C}H_2$ carbon on the BnCl and the reactive nitrogen of the adeninate anion by 0.1 Å increments), through a TS to the final product of each pathway. The resulting change in electronic energy along the reaction coordinate is shown in Figure S3.12.

© University of Pretoria

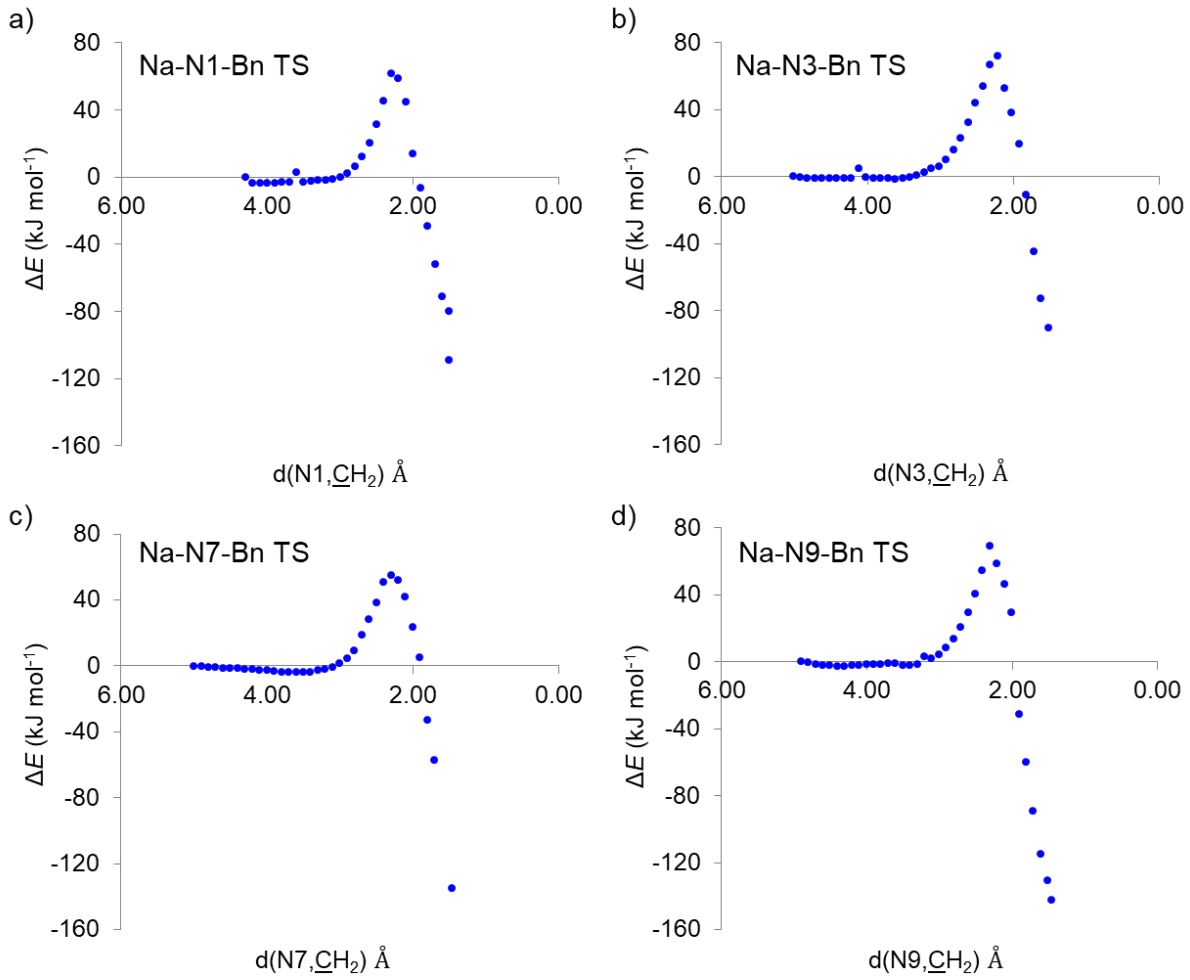

Figure S3.12: Change in electronic energy (Δ*E*) along the reaction coordinate for the scan between Na-Ade(N3N9) and BnCl for the a) Na-N1-, b) Na-N3-, c) Na-N7- and d) Na-N9-Bn pathway

© University of Pretoria

Supporting Information - 4

The study of the kinetic isotope effect of ATP-C8D on shikimate kinase through high resolution mass spectrometry

Deuteration of ATP

The deuteration of ATP was determined by monitoring the disappearance of the C8-H peak at 8.47 ppm of ATP in the ^{1}H NMR spectrum, Figure S4.1. Small amount of ADP was present after 95% of the ATP was deuterated. The ADP was identified by the singlet peaks at 8.41 and 8.06 ppm corresponding to the C8-H and C2-H of ADP, respectively, and the doublet at 6.11 ppm.

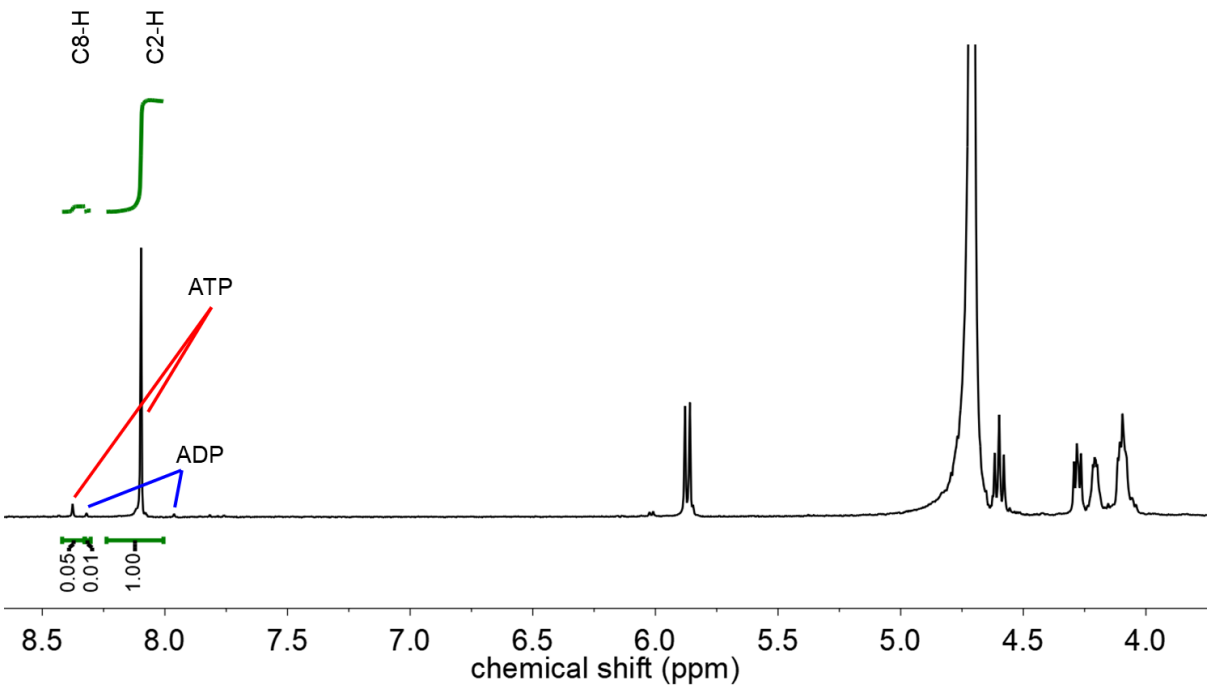

Figure S4.1: ^{1}H NMR of deuterated ATP in D_2O

C8D-ATP: ^{1}H NMR (300 MHz, D_2O, 25 °C) δ 8.19 (s, 1H, C2-H), 5.96 (d, *J* = 5.9 Hz, 1H, CH), 4.69 (t, *J* = 5.6 Hz, 1H, CH), 4.37 (dd, *J* = 5.3, 3.4 Hz, 1H, CH), 4.32-4.26 (m, 1H, CH), 4.19 (m, 1H, CH_2). ^{31}P NMR (121 MHz, D_2O, 25 °C) δ −5.46 (d, *J* = 19.4 Hz, γ-PO_4), −10.77 (d, *J* = 18.5 Hz, α-PO_4), −21.19 (t, *J* = 19.1 Hz, β-PO_4)

© University of Pretoria

Change from TRIS to ammonium bicarbonate

Enzyme assays were completed in triplicate under identical conditions using either TRIS-HCL (100 mM, pH 7.82) or ammonium bicarbonate (100 mM, pH 7.86) at 25 °C. Assays were monitored every 10 seconds by detecting the decrease in NADH at 340 nm.

Enzyme assay contained PK/LDH (42 U/ml), ATP (1.0 mM), SA (3.0 mM), buffer (100 mM), KCl (100 mM), NADH (0.2 mM), PEP (1.5 mM), $MgCl_2$ (7 mM). The enzyme assay was initiated by addition of *Mt*-SK (0.914 µg/ml). NADH concentration in assay was confirmed to be 0.20 mM using a control.

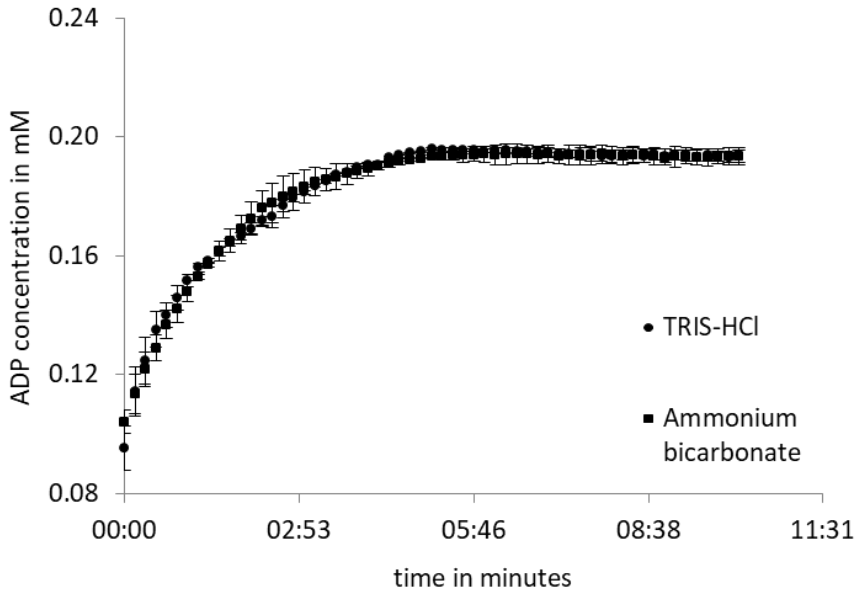

Figure S4.2: ADP formed during the course of the reaction of Mt-SK with ATP and shikimic acid in the presence of TRIS-HCl buffer (circles) and ammonium bicarbonate (squares)

© University of Pretoria

Mass spectroscopy

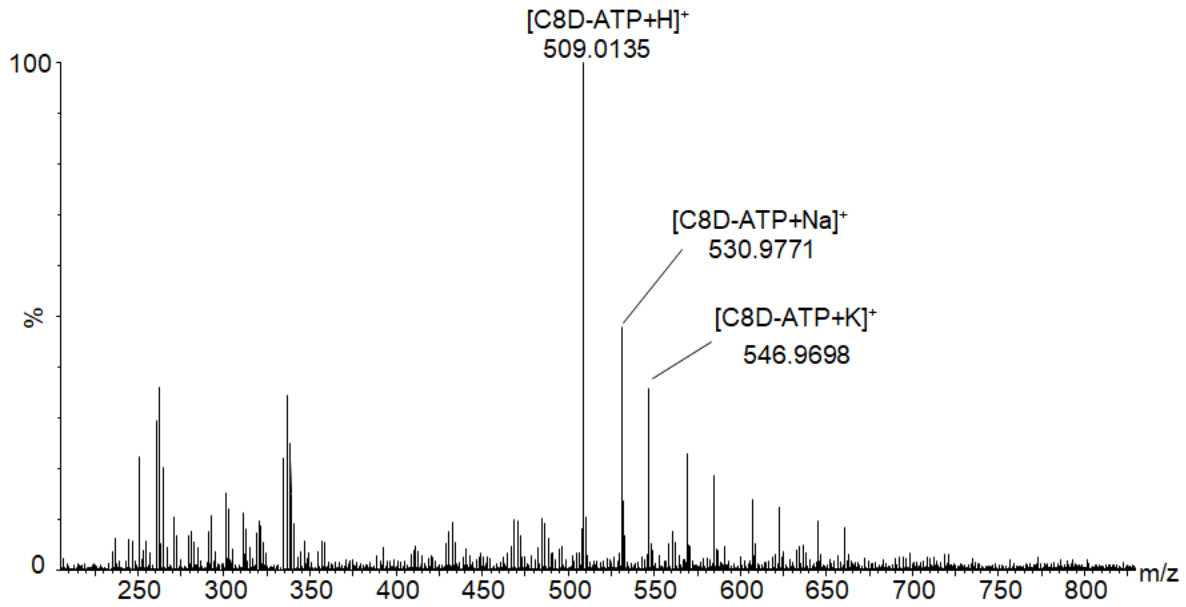

Figure S4.3: Mass spectrum of C8D-ATP (*m/z* = 509.0135, $[C8D\text{-}ATP+H]^+$) with C8D-ATP sodium (*m/z* = 530.9771, $[C8D\text{-}ATP+Na]^+$) and potassium (*m/z* = 546.9698, $[C8D\text{-}ATP+K]^+$) adducts

© University of Pretoria